

5-2010

## Experimental and numerical analysis of structures with bolted joints subjected to impact load

Kumarswamy K. Nakalswamy  
*University of Nevada, Las Vegas*

Follow this and additional works at: <https://digitalscholarship.unlv.edu/thesesdissertations>



Part of the [Mechanical Engineering Commons](#)

---

### Repository Citation

Nakalswamy, Kumarswamy K., "Experimental and numerical analysis of structures with bolted joints subjected to impact load" (2010). *UNLV Theses, Dissertations, Professional Papers, and Capstones*. 227. <http://dx.doi.org/10.34917/1445308>

This Dissertation is protected by copyright and/or related rights. It has been brought to you by Digital Scholarship@UNLV with permission from the rights-holder(s). You are free to use this Dissertation in any way that is permitted by the copyright and related rights legislation that applies to your use. For other uses you need to obtain permission from the rights-holder(s) directly, unless additional rights are indicated by a Creative Commons license in the record and/or on the work itself.

This Dissertation has been accepted for inclusion in UNLV Theses, Dissertations, Professional Papers, and Capstones by an authorized administrator of Digital Scholarship@UNLV. For more information, please contact [digitalscholarship@unlv.edu](mailto:digitalscholarship@unlv.edu).

EXPERIMENTAL AND NUMERICAL ANALYSIS OF STRUCTURES WITH  
BOLTED JOINTS SUBJECTED TO IMPACT LOAD

by

Kumarswamy, Karpanan Nakalswamy

Bachelor of Engineering in Mechanical Engineering  
Kuvempu University, Karnataka, India  
Nov 2001

Master of Science in Mechanical Engineering  
University of Nevada Las Vegas, Las Vegas  
May 2005

A dissertation submitted in partial fulfillment  
of the requirements for the

**Doctor of Philosophy Degree in Mechanical Engineering**  
**Department of Mechanical Engineering**  
**Howard R. Hughes College of Engineering**

**Graduate College**  
**University of Nevada, Las Vegas**  
**May 2010**

Copyright by Kumarswamy, Karpanan Nakalswamy 2010  
All Rights Reserved



**THE GRADUATE COLLEGE**

We recommend that the dissertation prepared under our supervision by

**Kumarswamy, Karpanan Nakalswamy**

entitled

**Experimental and Numerical Analysis of Structures with Bolted Joints  
Subjected to Impact Load**

be accepted in partial fulfillment of the requirements for the degree of

**Doctor of Philosophy in Mechanical Engineering**

Brendan O'Toole, Committee Chair

Woosoon Yim, Committee Member

Mohamed Trabia, Committee Member

Daniel Cook, Committee Member

Samman Ladkany, Graduate Faculty Representative

Ronald Smith, Ph. D., Vice President for Research and Graduate Studies  
and Dean of the Graduate College

**May 2010**

## ABSTRACT

### **Experimental and Numerical Analysis of Structures with Bolted Joints Subjected to Impact Load**

by

Kumarswamy Karpanan Nakalswamy

Dr. Brendan J. O'Toole, Examination Committee Chair  
Associate Professor of Mechanical Engineering  
University of Nevada, Las Vegas

The aim of this study is to analyze the transient behavior of structures with bolted joints subjected to impact or shock loads using experimental methods and Finite Element Analysis (FEA). Various factors that affect the response of the bolted joint structures for shock loading were studied, such as damping, preload, intensity of impact load and type of FE modeling. The objective of this work was to develop computational modeling procedures that provide structural analysts an improved physics-based shock model for combat vehicles focusing mainly on shock transmission across bolted joints. There is only a limited amount of published literature describing the proper method for analyzing the transient shock propagation across bolted connections for high impact loading. The initial case study focused on a simple cantilever beam with bolted lap joint subjected to relatively low levels of impact force. The second case study used a flat plate bolted to a hat-section and the third structure evaluated was two hat sections bolted together. These simple configurations are representative of structures found in many military ground vehicles that can be subjected to transient impact and blast loads. These structures were subjected to low impact loading (non destructive) using impact hammers and high impact loading (destructive) using an air gun and their responses were measured using

accelerometers. LS-DYNA FE solver was used to simulate the shock propagation in bolted structures.

For all the bolted structures, the modal analysis was performed both experimentally and numerically. The results were in excellent agreement for lower modes and small deviation in higher modes. Secondly, the time history response of experimental and FE analysis are compared. Normalized Root Mean Square Deviation (NRMSD) criterion was used to compare the experimental and FE result. A full detailed FE model and a simplified FE model of the bolted structures were developed for impact analysis and their prediction were compared with the experimental results. In all the cases, the detailed FE model with 3-D solid elements showed good agreement with the experimental results. The simplified FE model with shell elements (bolts were not modeled) predicted higher magnitudes in the acceleration values. Addition of damping in the simplified FE model reduced the higher magnitudes in the predicted response and the results were in good agreement with the experiment. The simplified FE model developed for bolted joint structure in this report reduced the CPU time by one order (30 hours to 3.5 hours) and can be practically implemented in the full vehicle FE model for crash or blast analysis.

## TABLE OF CONTENTS

ABSTRACT.....	iii
TABLE OF CONTENTS.....	v
LIST OF FIGURES.....	vii
LIST OF TABLES.....	xi
ACKNOWLEDGMENTS.....	xii
CHAPTER 1 INTRODUCTION.....	1
1.1 Background.....	1
1.2 Literature review.....	4
1.3 Dissertation objectives.....	14
CHAPTER 2 DESCRIPTION OF EXPERIMENTAL SETUP.....	18
2.1 Introduction.....	18
2.2 Experimental setup for low impact test.....	18
2.3 Repeatability and consistency test.....	23
2.4 Preload on the bolt.....	29
CHAPTER 3 ANALYSIS OF CANTILEVER BEAM FOR IMPACT LOADING.....	34
3.1 Background.....	34
3.2 Experimental and finite element analysis of cantilever beam.....	34
3.3 Fundamental natural frequency of cantilever beam by analytical method.....	41
3.4 Experimental and finite element simulation of cantilever beam with bolted joint.....	45
3.5 FE simulation of impact analysis of the cantilever beam with bolted joint.....	54
3.6 Parametric study of the FE model.....	64
3.6.1 Damping in the FE model.....	64
3.6.2 Mass proportional damping.....	65
3.6.3 Stiffness proportional damping.....	69
3.7 Element formulation.....	71
3.8 Preload (pre-stress) modeling for explicit analysis.....	74
3.8.1 Applying force on the bolt and nut.....	75
3.8.2 Applying force on the bolt shank.....	77
3.8.3 Modeling interference fit between nut and plate.....	77
3.8.4 Applying thermal gradient on the bolt shank.....	78

3.8.5	Using INITIAL_STRESS_SOLID card in LS-DYNA.....	84
3.8.6	Using INITIAL_STRESS_SECTION card in LS-DYNA.....	85
3.9	Experimental measurement of damping factors .....	87
3.10	Summary of results .....	93
CHAPTER 4 LOW IMPACT ANALYSIS ON HAT SECTION AND FLAT PLATE.....		95
4.1	Experimental setup and procedure.....	97
4.2	Experimental and FE modal analysis of the bolted hat-plate section .....	100
4.3	Effect of impact hammer striking head on the transient response of structure .....	105
4.4	Transient analysis of bolted hat-plate section subjected to impact load.....	107
4.4.1	Response of bolted hat-plate structure to low force impact loading.....	107
4.5	Summary of results .....	111
CHAPTER 5 IMPACT ANALYSIS USING AIR GUN.....		112
5.1	Introduction.....	112
5.2	Design of air gun experiment for high impact loading.....	114
5.3	Air gun experiment procedure .....	120
5.4	Design and analysis of catch tube .....	124
5.5	Calibration of air gun experiment.....	130
5.5.1	Analytical slug velocity calculation.....	130
5.5.2	Slug velocity verification using high speed camera .....	132
5.6	High impact analysis of bolted structures using air gun .....	135
5.6.1	Repeatability of the air gun experiment.....	135
5.6.2	FE analysis of medium impact loading on the hat-plate structure.....	139
5.6.3	Response of hat-plate structure to high force impact loading.....	151
5.7	Response of bolted two-hat structure to high force impact loading: FE analysis and experiments .....	156
5.8	Summary of results .....	163
CHAPTER 6 CONCLUSIONS AND FUTURE WORK.....		164
APPENDIX-A.....		168
REFERENCES:.....		170
VITA.....		178



## LIST OF FIGURES

Figure 1.1	Typical army combat vehicles.....	5
Figure 1.2	FE Analysis of Ford truck subjected to mine blast.....	6
Figure 1.3	Resultant acceleration plot on cabin of Ford truck subjected to mine blast...	7
Figure 1.4	Frontal crash of Econoline van.....	7
Figure 1.5	Acceleration plot on dashboard and rear door of Ford Econoline van subjected to frontal crash .....	8
Figure 2.1	Diagram of the lap joint cantilever beam with constraints, loading point and sensor location (Front and top View).....	20
Figure 2.2	Cantilever beam with lap joint, support and accelerometers.....	21
Figure 2.3	Experimental setup for impact loading on the bolted cantilever beam .....	21
Figure 2.4	Instrumented impact hammer .....	22
Figure 2.5	PCB accelerometer .....	22
Figure 2.6	Impact hammer striking the cantilever beam .....	24
Figure 2.7	Repeatability test - Force curve from impact hammer .....	25
Figure 2.8	FFT of the cantilever beam response for the repeatability test .....	25
Figure 2.9	Time history response of the cantilever beam for the repeatability test.....	26
Figure 2.10	Time history response of the cantilever beam for the repeatability test-Cutout .....	26
Figure 2.11	Consistency test showing two accelerometers placed side by side .....	27
Figure 2.12	Time History response of two accelerometers during consistency test.....	28
Figure 2.13	Time History response of two accelerometers during consistency test- Cutout.....	28
Figure 2.14	Force diagram for a typical bolted joint .....	30
Figure 2.15	Time history response of the bolted cantilever beam for three pre-torque levels .....	32
Figure 2.16	Cutout of the time history curves .....	33
Figure 2.17	FFT of the time history plots for three pre-torque test cases.....	33
Figure 3.1	Monolithic cantilever beam.....	37
Figure 3.2	FFT of the experimental time history curve .....	38
Figure 3.3	Solid and shell element FE model of cantilever beam .....	39
Figure 3.4	Mode shape and natural frequencies of the cantilever beam using FE model with solid elements and six elements through the thickness of the beam....	43
Figure 3.5	Natural frequency of cantilever beam from experiment and FEA .....	45
Figure 3.6	Experimental set-up for impact analysis on cantilever beam with bolted joint .....	48
Figure 3.7	FFT of the cantilever beam with and without bolted joint .....	48
Figure 3.8	FE Model-1 Simplified FE model with shell elements and no bolted joint in the model (Top and Front View) .....	49
Figure 3.9	FE Model-2, simplified solid FE model of cantilever beam with no preload .....	50
Figure 3.10	FE Model-3, solid FE model of cantilever beam with preload on bolt and all contacts defined .....	51

Figure 3.11	Mode shape and Natural frequencies of the cantilever beam with bolted lap joint using FE Model-2 .....	52
Figure 3.12	Natural frequency of the cantilever beam from experiment and FEA .....	54
Figure 3.13	Experimental impact force curve used in FEA as input .....	57
Figure 3.14	FFT from the experiment and FEA Model-1 (A1).....	57
Figure 3.15	Experimental and FE Model-1, Time history response at point A1 and A2	58
Figure 3.16	Energy plots for FE Model-1.....	59
Figure 3.17	FFT from experiment and FE Model-2 (A1).....	59
Figure 3.18	Experimental and FE Model-2 Time history response at points A1 and A2	60
Figure 3.19	Energy plots for FE Model-2.....	61
Figure 3.20	Experimental and FE Model-3 time history response at points A1 and A2	61
Figure 3.21	Experimental and FE Model-3 time history response at points A1 and A2	62
Figure 3.22	Relation between damping ratio and frequency for Rayleigh damping .....	65
Figure 3.23	Influence of mass proportional damping at point A2 acceleration using FE model-1 .....	67
Figure 3.24	Cutout of the acceleration curves for mass proportional damping using FE model-1 .....	68
Figure 3.25	Influence of mass proportional damping at point A2 displacement using FE model-1 .....	68
Figure 3.26	Influence of stiffness proportional damping ( $\beta$ ) at point A2 acceleration using FE model-1 .....	69
Figure 3.27	Cutout of the acceleration curves for stiffness proportional damping ( $\beta$ ) using FE model-1 .....	70
Figure 3.28	FFT for various stiffness proportional damping ( $\beta$ ) at point A2 using FE mode-1 .....	70
Figure 3.29	Under and fully integration points on the shell element.....	71
Figure 3.30	Comparison of fully integrated and constant stress element formulation for the shell element FE model-1 .....	73
Figure 3.31	Bolt assembly of the cantilever beam (FE model-3) with preload force applied.....	76
Figure 3.32	Bolt assembly of the cantilever beam with pre-stress .....	76
Figure 3.33	Bolt assembly with split bolt shank and pre-stress.....	77
Figure 3.34	Bolt assembly of the cantilever beam (FE model-3) with interference fit ..	78
Figure 3.35	Three beams with thermal material at the center.....	79
Figure 3.36	Two Temperature curve for defining preload in the beam.....	81
Figure 3.37	Constant Von-Misses stress in the beam due to thermal gradient.....	81
Figure 3.38	Constant stress on the beam during the transient explicit analysis .....	82
Figure 3.39	Bolt assembly with thermal gradient on the bolt shank .....	83
Figure 3.40	Pre-stress on the bolt assembly by thermal gradient .....	83
Figure 3.41	Bolt assembly with pre-stress using INITIAL_STRESS_SOLID card.....	84
Figure 3.42	Bolt assembly with vectors for defining pre-stress .....	86
Figure 3.43	Force (preload) on the bolt shank for 34 Nm pre-torque.....	87
Figure 3.44	Half-power bandwidth method [60] .....	89
Figure 3.45	FFT from the experiment.....	89
Figure 3.46	Half bandwidth method applied to first natural frequency of the cantilever beam.....	90

Figure 3.47	Model-1, Time history response with SPD 6.5% (0.065)	91
Figure 3.48	Model-2, Time history response with SPD 6.5% (0.065)	92
Figure 4.1	Bolted hat-plate structure configuration	96
Figure 4.2	Hat section configuration	97
Figure 4.3	Experimental set-up for axial loading on the bolt assembly	99
Figure 4.4	Location of impact force and acceleration measurement - The Force is applied in the y-direction, acceleration 1 is measured in the x-direction and acceleration 2 is measured in the y-direction	99
Figure 4.5	Experimental setup for impact analysis on bolted hat-plate structure	100
Figure 4.6	Typical impact force measured from the instrumented impact hammer	101
Figure 4.7	FFT of the hat and plate structure	102
Figure 4.8	Mode shape and natural frequencies of the bolted hat-plate structure	103
Figure 4.9	Force curve from impact hammer for hard, medium and soft striking head	106
Figure 4.10	Time history response from impact hammer for hard, medium and soft striking head	106
Figure 4.11	Solid element FE model of bolted hat-plate structure	108
Figure 4.12	Detailed view of bolt assembly in the hat-plate structure	108
Figure 4.13	FFT of experiment and FEA	109
Figure 4.14	Experimental and FE time history response for bolted hat-plate structure for low impact loading	110
Figure 5.1	Block diagram of air gun experimental set up	115
Figure 5.2	A-frame used in the air gun experiment	115
Figure 5.3	Air gun barrel and the I-Beam	117
Figure 5.4	Pressure tank and barrel of the air-gun test	118
Figure 5.5	Catch tube	118
Figure 5.6	Diagram of slug impacting the hat-plate structure	119
Figure 5.7	Aluminum slug used in the air gun experiment	119
Figure 5.8	Bolted hat-plate structure with load cell and accelerometer	121
Figure 5.9	Bolted two-hat sections used in high impact loading experiment	122
Figure 5.10	Load cell and accelerometer specification	122
Figure 5.11	High speed camera image of slug impacting the two-hat structure (64.33 ms and 68.66 ms)	123
Figure 5.12	High speed camera image of slug and catch tube	126
Figure 5.13	Deformed catch tube from the slug impact	126
Figure 5.14	FE model of slug and the catch tube (initial design)	127
Figure 5.15	Deformed catch tube from FE analysis	127
Figure 5.16	Final design of catch-tube with six L-clamps	128
Figure 5.17	Velocity of slug and catch tube predicted by LS-DYNA FE analysis	128
Figure 5.18	Displacement of slug and catch tube predicted by LS-DYNA FE analysis	129
Figure 5.19	Analytical velocity of catch tube and slug for various 'e' values	129
Figure 5.20	Diagram showing initial and final position of slug in the barrel	130
Figure 5.21	Theoretical velocity of slug with & without friction and velocity of slug obtained from the high-speed camera	132

Figure 5.22	Images of slug and catch tube from high-speed camera to calculate the velocity of slug (1.66 ms, 2.0 ms and 2.33 ms) .....	134
Figure 5.23	Experimental set-up of high impact loading on the hat-plate structure (Acceleration is measured in the arrow direction).....	137
Figure 5.24	Impact force repeatability for the slug velocity of 24 m/s.....	137
Figure 5.25	Acceleration repeatability on the hat structure.....	138
Figure 5.26	Acceleration repeatability on the plate structure.....	138
Figure 5.27	FFT of hat structure response from low and medium impact loading .....	139
Figure 5.28	FE model-1 of bolted hat-plate structure and slug with solid elements ....	141
Figure 5.29	FE model-2 of hat-plate structure with shell elements and rivets .....	142
Figure 5.30	Impact force plots from experiment and FEA for velocity of 9 m/s slug..	143
Figure 5.31	Impact force plots from experiment and FEA for velocity of 24 m/s slug	144
Figure 5.32	Impact force plots from experiment and FEA for velocity of 34 m/s slug	144
Figure 5.33	Hat-plate structure showing impact point and accelerometer locations....	146
Figure 5.34	FFT of the experiment and FE model-1 for medium force impact loading .....	147
Figure 5.35	Acceleration on hat (Acc-1) and plate (Acc-2) structure for 24 m/s slug impact (medium force impact load).....	148
Figure 5.36	FFT of the experiment and FE model-2 for medium force impact loading .....	149
Figure 5.37	Acceleration on hat (Acc-1) and plate (Acc-2) plate structure for 24 m/s slug impact (medium force impact load) .....	150
Figure 5.38	Experimental and FE model-2 showing deformed hat structure for slug impacting at velocity of 68 m/s.....	153
Figure 5.39	Plastic strain contours on FE model-2 for slug impacting at velocity of 68 m/s.....	154
Figure 5.40	FE model-2 impact force curve for 68 m/s slug impact velocity .....	154
Figure 5.41	FFT from experiment and FE model-2 for slug velocity of 68 m/s .....	155
Figure 5.42	Acceleration plots on hat structure for slug impacting at 68 m/s .....	155
Figure 5.43	High impact loading experimental set-up for two hat structure .....	158
Figure 5.44	High speed camera image showing slug impacting the structure (4.33 ms after impact) .....	159
Figure 5.45	Impact force from FE Model-2 for slug impacting at velocity of 24 and 34 m/s on two-hat structure.....	159
Figure 5.46	Experiment and FE Model-2 showing deformed shape of two-hat structure for slug impacting at 34 m/s (front view) .....	160
Figure 5.47	Experiment and FE Model-2 showing deformed shape of two-hat structure for slug impacting at 34 m/s (side view).....	160
Figure 5.48	FFT from experiment and FE model-2 for slug velocity of 34 m/s .....	161
Figure 5.49	Experimental and FE Model-2 results of top hat structure for slug impacting at 34 m/s velocity .....	161
Figure 5.50	Experimental and FE Model-2 results of bottom hat structure for slug impacting at 34 m/s velocity .....	162

## LIST OF TABLES

Table 3-1	Mechanical properties of 1045 steel [54] .....	36
Table 3-2	Description of FE model .....	39
Table 3-3	Natural frequency of the cantilever beam from experiment and FEA .....	44
Table 3-4	Natural frequency of the cantilever beam from experiment and FEA .....	53
Table 3-5	NRMSD between experiment and FE model transient results.....	63
Table 3-6	NRMSD between experiment and FE model transient results.....	93
Table 4-1	Natural frequencies of the hat-plate structure from experimental modal analysis.....	104
Table 4-2	NRMSD between experiment and FE model transient results.....	111
Table 5-1	NRMSD between experiment and FE Model 1 &2.....	151
Table 5-2	NRMSD between Experiment and FE Model-2 for slug impacting at 68 m/s velocity.....	156
Table 5-3	NRMSD between the experiment and FE mode-2 for two hat structure ...	162

## ACKNOWLEDGMENTS

I would like to thank Dr. Brendan O’Toole for his invaluable help, constant guidance and wide counseling extended by them toward successful completion of my research work. I have enjoyed my time working under Dr. O’Toole because of the range of projects he involved me in.

I would like to thank my committee members, Dr. Ladkany, Dr. Yim, Dr. Cook and Dr. Trabia, for their direct and indirect contribution throughout this investigation. I would also like to thank Masoud, Kamal, Vikram, Qin Lee, Sachiko, Trevor, and Dr. Joon Lee.

Finally I would like to thank my sister Lokeshwari, for her support, advice, and motivation through my college career.

# CHAPTER 1

## INTRODUCTION

### 1.1 Background

The bolted joint is a common type of fastener in army vehicles and plays a very important role in maintaining the structural integrity of a combat vehicle. The combat vehicle may be subjected to various kinds of loading in combat. Some of the important transient shock loading on the vehicle can be initiated by mine blast, projectile impact or frontal crash. To understand the response of the vehicle to these shock / impact loads, and simulate these phenomenon using numerical methods, it is important to understand the behavior of a bolted joint structure during shock or impact loading. Shock transfer performance of joints has substantial influence on the dynamics of assembled structures as they induce a large amount of damping into the structure. Study of high shock transmission through the bolted joint components of the combat vehicle is of particular interest to the army. In this report, high shock or impact loading refers to impact load acting on a structure, which can damage or deform the structure or bolt assembly. The low shock loading refers to impact loads usually induced by instrumented impact hammer on the structure and doesn't damage the structure.

Mechanical joints, especially fasteners have a complex nonlinear behavior. The non-linearity may arise from the material, geometry or by the contacts in the joints. When the vehicle trips a land mine or is subjected to any high shock / impact loading, there is a need to guarantee the survivability or minimize the damage caused to both the primary and secondary electronic systems present inside the combat vehicle. Another area of concern is to reduce or damp the shock transmission to the driver and commander in the

vehicle, caused by a projectile impact. For an armored vehicle, there is an immediate need to develop methodologies for constructing predictive models of structures with bolted joints and shock based dynamic response analysis in order to ensure the safety of critical equipment, hardware, and personnel.

The finite element method has been very useful in the simulation of mechanical joint behavior. Even this method has limitations in simulating the dynamic response. This study investigates the dynamic response of the structure with bolted joint and suggests different ways to simulate the response using commercial FE software LS-Dyna [1,2]. The finite element method (FEM) is a mathematical method to solve differential equation via a piecewise polynomial interpolation scheme. FEM evaluates a differential equation by using a number of polynomial curves to follow the shape of the underlying and more complex differential curve. Each polynomial in the solution can be represented by a number of points and so FEM evaluates the solution at the points only. These points are known as nodes. FEM uses Non-Variational, Variational or Residual methods to evaluate the values at nodes. Finite element analysis (FEA) is an implementation of FEM to solve a certain type of problem. FEM uses piecewise polynomial solution to solve the differential equation, while applying the specifics of element formulation is FEA. The element formulation may be plane 2D element or 3D Hexahedral element. Structural engineers working in the aerospace industry pioneered FEA during the 1950's and 1960's. Since then it has been widely used for modeling and simulation of linear and nonlinear problems in structural analysis, fluid flow, heat transfer, and fracture mechanics.



The shock propagation in the bolted structures is a complex phenomenon and involves short duration transient loading, contacts, large displacement and large strain of the structure and bolt assembly. Therefore to handle all these issues, the explicit FE analysis was used in simulating shock propagation in bolted structures.

Figure 1.1 is a typical military combat vehicle used by US army. These military vehicles must be capable of sustained operation in the face of mechanical shocks due to projectile or other impacts. Almost all of the joints in these vehicles are either welded or bolted. The important joints in these vehicles; between chassis and the top part, engine to chassis, axle and chassis, and wheels to axle are all bolted joints. Apart from these important joints, hundreds of bolts are used in these vehicles to connect and assemble various parts. Explicit FE analysis can be used to simulate the shock-loading phenomenon on these vehicles.

Figure 1.2 and Figure 1.3 are the LS-DYNA FE models of the Ford truck and Ford Econoline Van. The Ford truck in Figure 1.2 was subjected to 10 Kg of TNT explosives under the front wheel, which represent the vehicle tripping a land mine. The FE models of vehicles are available at National Crash Analysis Center, and are modified to include blast load. The response of the truck cabin to the blast is shown in Figure 1.3. This plot is the resultant acceleration on the dashboard where the electronics will be mounted. Figure 1.4 is the frontal crash of the Econoline van, at a speed of 30-miles/hour. The frontal crash produces a high shock in the vehicle and is shown in Figure 1.5. These FE models are similar to army vehicle FE models and can be used to study the blast loading on bolted joints. In any FE vehicle model, it is impossible to model all the bolted connections with complete detail because of computational limitations. Except few bolts,

none of the bolts in the vehicle are modeled in these vehicle FE models. Therefore it is necessary to develop a method or technique to accurately represent the bolt assemblies in vehicle FE models. For this, it is important to understand the physical mechanism of shock transfer through bolted connections, so that simplified, but accurate modeling methods can be incorporated into large vehicle design models.

This dissertation focuses on developing and understanding of shock propagation through a bolted structure that is typical to a variety of military vehicle structures (Figure 1.1). There are many parameters to choose or ignore when it comes to building a FE model for the simulation. Picking the right parameters leads to a reliable simulation, and it is impossible to get an exact match between any simulation or analysis and experimental data. The aim of this work is to determine a satisfactory method for analyzing shock propagation across bolted joints and to provide experimental guidelines for verifying the analysis procedures.

## 1.2 Literature review

Combat vehicles are at great risk when they are subjected to projectile hits or to mine blasts. Sensitive equipment present inside the combat vehicles is most vulnerable to ballistic shocks and mine blasts. Shock propagation from the impact region to the vital locations where the sensitive components are present may lead to damage or misalignment, which might result in malfunctioning, and reduction of vehicle performance. These shocks may also kill or injure the driver and commander inside the vehicle. Extensive research is in progress to analyze the dynamic response of complex structures involving assemblies, such as a combat vehicle, as the study helps in

understanding and evaluating the structural integrity of such structures when they are subjected to transient loading [3]

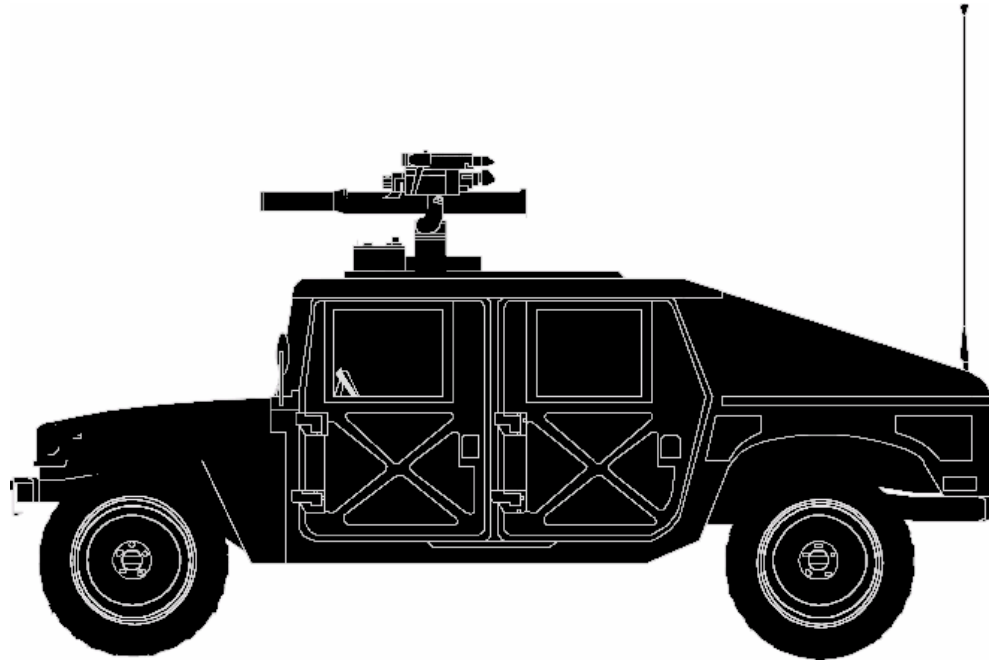


Figure 1.1 Typical army combat vehicles<sup>1</sup>

---

<sup>1</sup>[http://www.mgaresearch.com/MGA\\_Blog/wpadmin/images/military\\_army\\_vehicle\\_hummer\\_02.png](http://www.mgaresearch.com/MGA_Blog/wpadmin/images/military_army_vehicle_hummer_02.png)  
[http://www.armyvehicles.dk/images/merc270gdircon\\_2.jpg](http://www.armyvehicles.dk/images/merc270gdircon_2.jpg)

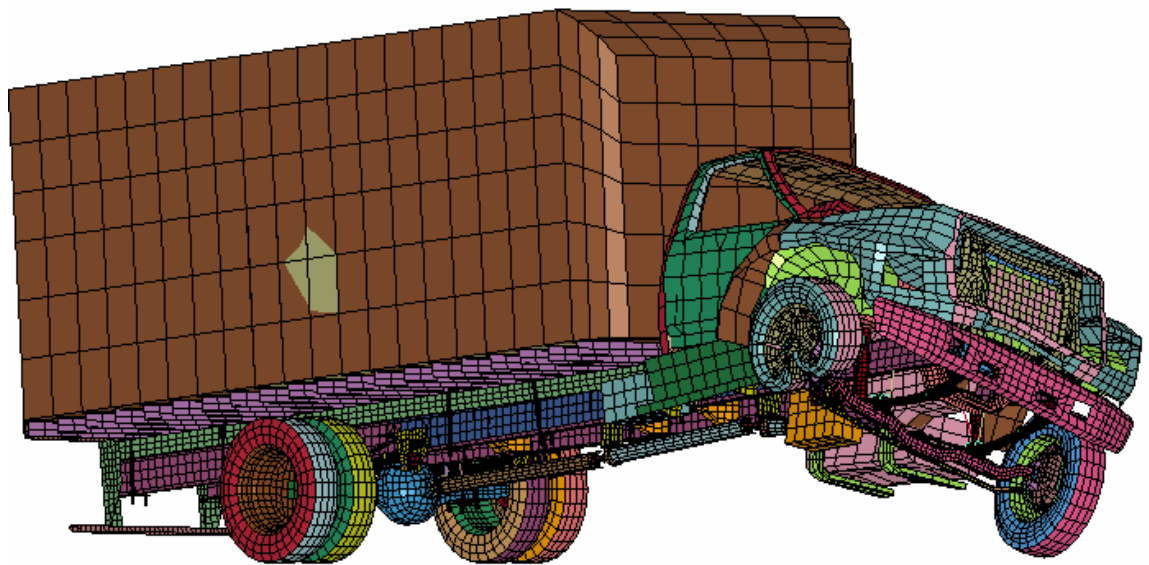
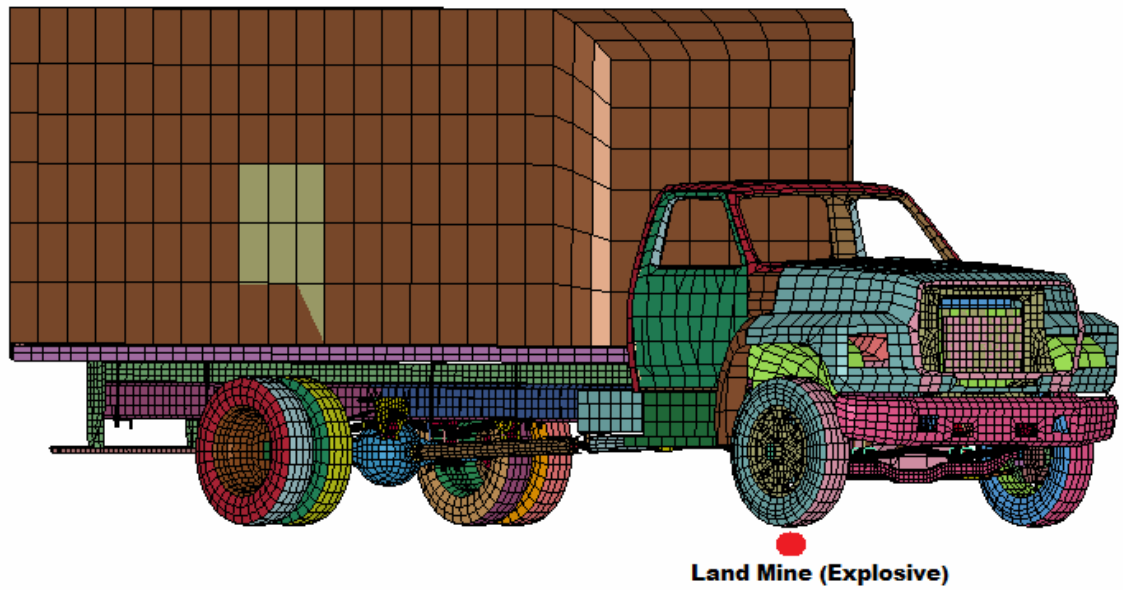


Figure 1.2 FE Analysis of Ford truck subjected to mine blast<sup>2</sup>

---

<sup>2</sup> Basic LS-DYNA FE models were obtained from National Crash Analysis Center

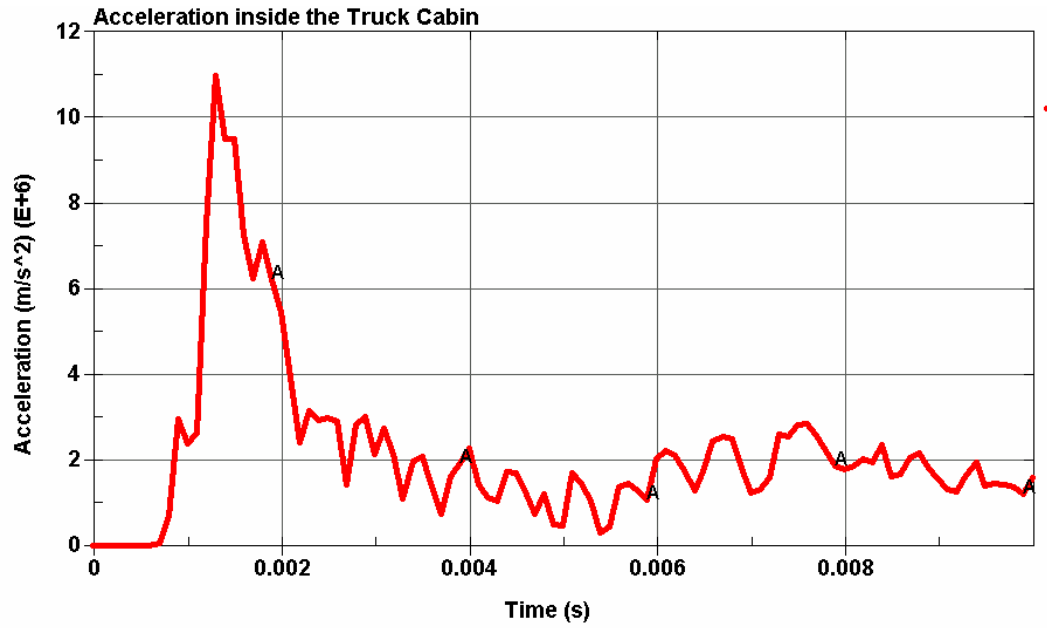


Figure 1.3 Resultant acceleration plot on cabin of Ford truck subjected to mine blast

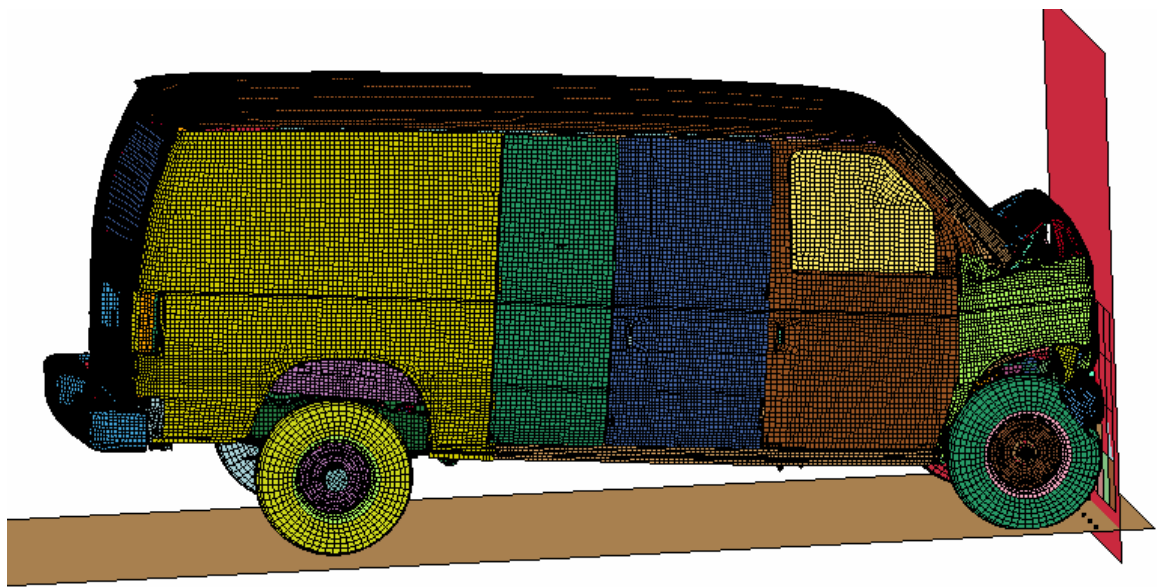


Figure 1.4 Frontal crash of Econoline van<sup>3</sup>

<sup>3</sup> Basic LS-DYNA FE models were obtained from National Crash Analysis Center

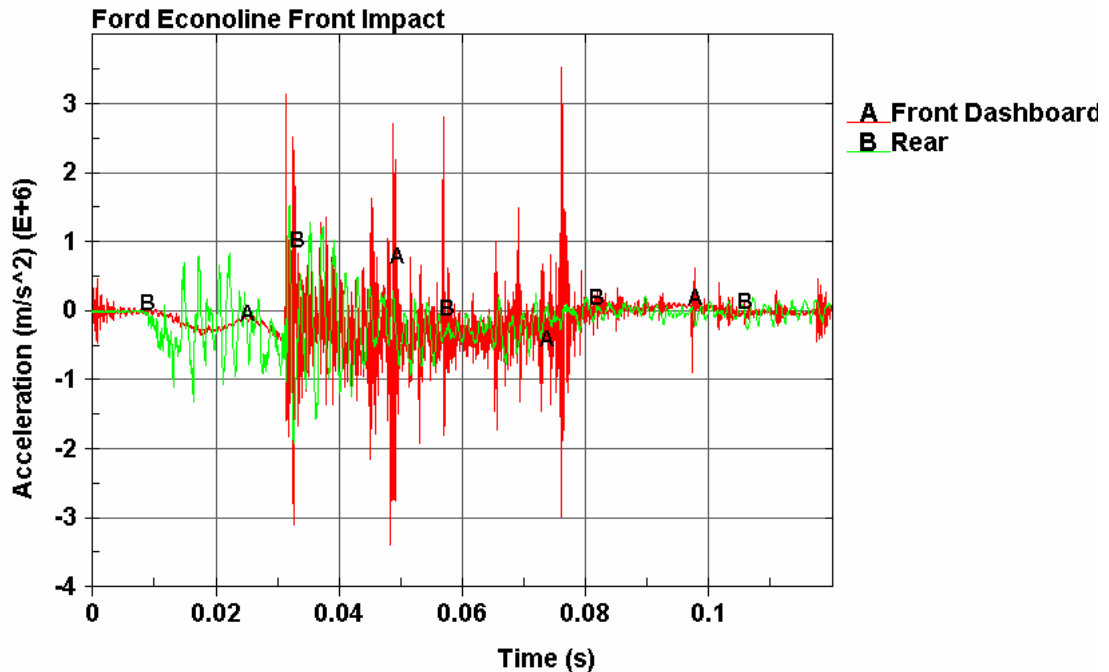


Figure 1.5 Acceleration plot on dashboard and rear door of Ford Econoline van subjected to frontal crash

Study of shock transmission through the various jointed (both mechanical and adhesive) components of the combat vehicle is of particular interest to the Army. There is a need to guarantee the survivability and minimize the damage caused to both the primary and secondary electronic systems present inside the combat vehicle. The complex behavior of bolted joints plays an important role in the overall dynamic characteristics of structures such as natural frequencies, mode shapes, and non-linear response characteristics to the external excitations. The joint represents a discontinuity in the structure and results in high stresses that often initiate structural failure [4].

Bolted joints appear to be simple and are the most widely used fastener, but their modeling and their effects on structural dynamics are not yet fully understood. There are a number of journal papers, which discuss the static / quasistatic loading on the bolted joints [5-8]. These papers study the failure mode and load deformation behavior of bolted

connections on various structures. Little work has been published on the study of shock propagation in bolted joints (especially high impact loading).

Doppala [9] studied the shock propagation in the adhesive and bolted steel structures subjected to low impact loading. He compared experimental and FE transient analysis results and showed that the explicit LS-DYNA solver can predict the shock propagation in bolted joints with marginal error. Feghhi [10] also studied shock propagation in bolted structures and discussed several error analysis techniques to compare two time signals. Mattern and Schweizerhof [11] studied shock wave propagation in T-shaped spot-welded structures impacted by a rigid ball, which includes both experimental and numerical simulation. In this work, commercial FE code LS-Dyna was used to simulate different models and evaluate the influence of several modeling modifications and of other simulation parameters. Semke et al. [12] has studied the dynamic structural response of piping systems with the bolted flange. Experimental and numerical results are presented and show excellent correlation. The experimental procedure utilizes an accelerometer to gather the dynamic response output of the piping system due to an impulse. The resonant frequencies are determined using a Fast Fourier Transform (FFT) method. The dynamic effects of a bolted flange and gasket on a piping system are critical in their use and has been demonstrated that the finite element method can simulate the response of an overhanging beam with a varying mid span. Kwon et al. [13] studied FE analysis of bolted structures for static and dynamic loading. They developed three kinds of models for structures with bolted joints: detailed model, practical model and simple model. Based on the applications, one of these models can be selected for stress analysis. Pratt and Pardoen [14] developed non-linear finite element models that predict the load-elongation

behavior of single and dual-bolted conical head bolted lap joints and compared predictions with experimental test data. The model load-elongation predictions are in excellent agreement with experimental results.

Detailed finite element models have been developed to establish an understanding of the slip-stick mechanism in the contact areas of the bolted joints [15]. Reid and Hiser [16] have done the detailed modeling of bolted joints with slippage to study the roadside structures. They studied discrete-spring based clamping model with rigid parts and stress based clamping model with deformable elements to determine joint slippage behavior. Force-deflection curves from simulation compared fairly well with the experiment results. Kim et al. [17] developed four kinds of finite element models for the structure with bolted joint; a solid bolt model, a coupled bolt model, a spider bolt model and a no-bolt model. Among these models the solid bolt model, which is modeled using 3-D solid elements predicted the stresses in the structure very close to experimental results. A detailed FE analysis of nut and bolt interaction was developed by Englund [18] to investigate the effects of sliding, friction and yielding in bolted connection. The stresses in the bolt and nut thread are compared with experimental stress values.

Bolted or riveted joints are the primary source of damping in the structure, because of the friction in the contact area [19]. Friction in bolted joints is one of the sources of energy dissipation in mechanical systems [20 21]. The finite element models are constructed in a nonlinear framework to simulate the energy dissipation through joints [22]. Sandia National Laboratory also has an extensive research program for investigating energy dissipation due to micro-slip in bolted joints [23]. Wentzel [24] discusses various methods to model the frictional joints in dynamically loaded structures. The nonlinear



transfer behavior of the frictional interfaces often provides the dominant damping mechanism in jointed structure. They play an important role in the vibration properties of the structure [25]. Wentzel and Olsson [26] used FE analysis to study the frictional and plastic dissipation in joints. Coulomb friction was incorporated in their FE model and the force displacement plots matched with experimental results. Damping in a structure is a complex phenomenon and bolted joints are the main source of damping in a structure. Damping is classified as internal damping (material), structural damping (joints and interfaces) and fluid damping (fluid-structure interface)[27]. Damping in the explicit FE analysis may be applied at both the material and system levels [28]. Material level damping is due to plastic deformation of the material, visco elastic energy dissipation or by the application of a factor proportional to mass and /or stiffness terms, known as Rayleigh damping. System level damping can be applied in the explicit FE code by using discrete viscous damper between two nodes. Segalman [29] discuss in detail the modeling of joint friction in dynamic analysis of structures. The calculation of damping ratio matrix for multiple degree of freedom systems can be solved by complex Eigenvalue analysis. A simple perturbation matrix method can be used to find the relation between the mode number and its damping ratio [30].

The strength and stiffness of the bolted structure depends on the preload of the bolt. The preload or pre-stressing might affect the dynamic behavior of bolted joints. The preload will increase the stiffness of the structure especially in higher mode natural frequency. Most of the research in the modeling of preload has been done for fatigue or cyclic loading. These kinds of loads are usually in the category of the static loading, but because of the importance of these parameters, it is useful to mention them in dynamic

response of the joints. Duffey, Lewis and Bowers [31] present two types of pulse-loaded vessel closers to determine the influence of bolt preload on the peak response of closure and bolting system. Esmalizedeh et al. [32] investigated the effect of bolt pre-stress on the maximum bolt displacement and stress. The loading initially peaked, for exponentially decaying internal pressure pulse acting on the bolted closure. Kerekes [33] used a simple beam model of the screw with fatigue loading to show the damage vulnerability of pre-stressed screws on the flange plate. In all of these studies there is no well-defined procedure to apply the preload in the finite element model. Schiffner [34] showed the simulation of pre-stressed screw joints in complex structures such as flywheel using truss and beam elements instead of 3-D volume elements. Park et al., [35] discussed preloading of core bolt of a vehicle rubber mount, which is subjected to impact. Here the bolt is preloaded by applying force directly on the bolt shank. The disadvantage of this method of applying preload is that, the preload force will not be constant throughout the explicit analysis. Initially there will be a transient part for the preload. O'Toole et al. [36] showed several different preload modeling procedures for dynamic finite element analysis and made recommendations on the most suitable methods. Szwedowicz et al. [37] presented the modal analysis of a pinned-clamped beam for three different magnitudes. They have determined that even for fine mechanical fit with the maximum bolt clearance up to 5  $\mu\text{m}$ , the analytical and numerical Eigen-frequencies above the 2nd mode show discrepancies with the measured results.

Different methods have been employed to determine the dynamic response of complex jointed structures. Studying the natural frequencies, modal behavior and damping of a structure, which constitute its dynamic characterization, gives us a better

understanding of the dynamics of a structure and its reliability [38]. The dynamic analysis results can be either viewed in time domain or in frequency domain. The time domain shows the changes that occur in time, whereas the frequency domain provides information about the frequency content of a measurement [39]. The Frequency Response Function (FRF), which is obtained from Fast Fourier transform (FFT) of the time domain data, is the widely used method for determining the natural frequencies and mode shapes of a structure [40]. The peaks in the FFT curve give the natural frequencies of a structure [41]. Responses measured from impulsive loading (like blast or impact) are typically accelerations, velocities and displacements at the crucial locations on the structure. While comparing the finite element results with the results obtained from experiments, one of these parameters is considered [42]. Accelerometers are widely used in measuring the dynamic response (acceleration) of the structures. Even velocity can be measured using laser vibrometry [43] as a dynamic response of the structure. This technique is a non-contact method and is more accurate in measuring the dynamic response than using accelerometers.

A few simplified finite element models for bolted joints are developed [44-46] which can predict the dynamic response for a particular application. Adoption of this type of analysis early in the design phase can influence decisions that improve the structural performance. Crash modeling and simulation is one of the subjects that finite element analysis has been employed to obtain the dynamic response of the whole structure, including joints. A truck impacting a guardrail system is one of the examples of these crash analyses. In this study a spring has been used to simulate component crashworthiness behavior, like the bolted connection between the rail and block-out.

Ouyang [47] conducted experimental and theoretical studies of a bolted joint for dynamic torsional load. He used Jenkins element in his model to represent the bolt assembly and showed that the Jenkins element can represent the friction in the joint very well. Hartwigsen [48] et al. used two structures with bolted lap joint to study the non-linear effects. They are beam with bolted joint in its center and a frame with bolted joint in one of its members. He also used monolithic and jointed structures with identical geometrical and material properties, so that the effect of the joint on the dynamics can be checked. Y. Songa, [49] has developed an Adjusted Iwan Beam Element (AIBE), which can simulate the non-linear dynamic behavior of bolted joints in beam structures. The same element was used to replicate the effects of bolted joints on a vibrating frame; the attempt was to simulate the hysteretic behavior of bolted joints in the frame. The simulated and experimental impulsive acceleration responses had good agreement validating the efficacy of the AIBE. This element shows its compatibility with the finite element two-dimensional linear elastic beams and is, thus, easily used. There are a number of factors, which can affect the FE analysis responses of a bolted structure. McCarthy [50] shows the number of integration points on the elements, type of analysis, contact modeling etc. have significant effect on the stress analysis of bolted structures subjected to static load.

### 1.3 Dissertation objectives

The aim of this project is to study the structures with bolted joints subjected to shock or impact loading, experimentally and numerically. It is important to understand the physical mechanism of shock transfer through bolted connections, so that simplified, but accurate FE modeling methods can be incorporated into large vehicle design models.

This dissertation focuses on understanding the shock propagation through bolted structures that is typical to a variety of military vehicle structures.

The shock loading may arise from direct impact on the structure or by a blast load. The structures used in this study were subjected to low and high impact loading. An instrumented impact hammer was used to induce low impact loading and an air gun launched slug was used for the high impact loading on the bolted structures. The low impact-loading test does not cause yielding or permanent damage on the structure or bolt. Parametric study of factors affecting the transient FE response of the bolted structure was conducted. Mesh density, element type, element formulation, damping, contacts, preloading effect, type of preload modeling, and friction modeling are some of the factors that influence the FE results were studied in the parametric study. The high impact-loading test induces permanent deformation in the structure and the bolt and this damage may be similar to the actual damage during mine blast. The experimental and FE analysis knowledge accumulated during the low impact-loading test was used to model the high impact loading successfully. The final objective of this project was to develop a simplified FE model of the bolted structure. This model can predict the shock loading response with good accuracy, use minimum amount of CPU time, simple to model and can be implemented in the vehicle FE model.

The best way to understand the bolted joints was to study the shock propagation in simple structures such as a cantilever beam with bolted joints. Chapter 2 gives the experimental procedure for low impact loading on a cantilever beam with bolted joint. Also the deterministic nature of the impact experiment is explained in this chapter. Experimental and FE analysis of low impact loading on the cantilever beam is given in

Chapter 3. FE parametric study of all the factors affecting the transient response of the cantilever beam is given in this chapter. Six preload modeling techniques for explicit FE analysis are discussed. A more complex, bolted hat-plate structure was used in low impact loading test and is discussed in Chapter 4. The bolted hat-plate structure is a representative of structures found in many military ground vehicles that can be subjected to transient loads such as blasts. Impact loads to this structure cause axial, bending and/or shear shock loading through bolted connections. The bolted hat section and plate structure was selected for study based on numerous discussions with structural dynamic research staff at the U.S. Army Research Laboratory (ARL). Design and experimental procedure for conducting high impact loading on the bolted structure using air gun and slug is given in Chapter 5. Also procedures for calibrating the air gun using thermodynamic-dynamic equations and high-speed camera are discussed. A simplified LS-DYNA FE model of bolted structure, for transient analysis was developed and its response is compared with experimental results.

Here is the step-by-step procedure to study the shock propagation in bolted joint for low or high impact loading test.

1. Perform the impact experiments on the structures with the bolted joints and measure the force (force vs. time) and acceleration (Time history response).
2. Perform Fast Fourier Transform (FFT) on the experimental results and calculate the natural frequency of the structure.
3. Demonstrate that this experiment can be computationally simulated using a detailed LS-DYNA analysis (Modal and Transient analysis).
4. Compare the experimental and simulation results.

5. Develop a simplified LS-DYNA FE model of the bolted joint to simulate the experiment with good accuracy.

## CHAPTER 2

### DESCRIPTION OF EXPERIMENTAL SETUP

#### 2.1 Introduction

Understanding the response of the bolted joint structures to shock / impact is crucial for simulating the vehicles subjected to blast. This is because the vehicle may house thousands of bolts and other kinds of joints. To analyze the bolted joints, many simple structures with bolted joints were used in this project. One of the common types of bolted joints used in the vehicle is the lap joint, which can take axial, shear, bending or combination loads. This chapter explains the experimental setup for studying shock propagation in a simplified bolted joint structure such as cantilever beam with bolted lap joint. This simplified structure was useful in studying in detail, the response of bolted joints subjected to shock / impact. Accelerometers were used to capture the response of the structure for impact loading. The impact / shock on the bolted structure were generated by the instrumented impact hammers (low impact) and firing aluminum slug (high impact) using air gun. The impact experiments are transient in nature and therefore the measured response (acceleration) will be a function of time. The impact experiment happens in very short duration of time (in milliseconds) and therefore the instruments used in the experiments should be able to capture the response with good accuracy.

#### 2.2 Experimental setup for low impact test

The first step in conducting any complicated experiment is to start with a simplified form of the experiment. In this chapter the simplified form of experimental setup and procedure is explained for studying the response of the bolted joints to shock. The simplified form of experiment is the low impact test (no failure or damage of the



structure or bolted joint) on a cantilever beam with bolted lap joints. The low impact test setup consists of bolted structure, instrumented impact hammer, cables, accelerometers, oscilloscope and signal conditioners.

A schematic of the bolted structure used in the experiment is shown in Figure 2.1. The structure consists of a slender clamped cantilever beam of length 0.73 m and the cross section 5.080 cm x 0.635 cm (2" x 0.25"). The cantilever beam is made of two steel plates (1040 steel), which forms a lap joint using two bolts as shown in Figure 2.1. The bolts were M8 size and the steel washers (8 cm inner diameter) were used between the bolt assembly and plate. Calibrated Torque wrenches were used to tighten the bolts to the required preload. One end of the beam is fixed to a rigid support as shown in Figure 2.2. The excitation, an impact loading is applied on the cantilever beam near the support using an instrumented impact hammer. Two piezoelectric accelerometers were glued on the cantilever beam- one near the fixed support (A1) and other at the end of the cantilever beam (A2), following the manufacturer recommended mounting procedures.

The experimental setup and the procedure are shown in Figure 2.3. Steel tip was used in the instrumented impact hammer to strike the cantilever beam is shown in Figure 2.4. The PCB Model 352C22 accelerometers (Figure 2.5) were used to measure the acceleration on the cantilever beam. These accelerometers are glued to the cantilever beam using wax adhesive. The impact hammer was connected to the Dytran 4103C signal conditioner and the accelerometer was connected to the PCB signal Conditioner (Model: 482A21) as shown in Figure 2.3. Both signal conditioners were connected to DL 750 oscilloscope. The sensitivity of the accelerometer and impact hammer is  $0.956\text{-mv/m/s}^2$  and  $0.23\text{-mv/N}$  respectively. When the impact hammer strikes the cantilever beam, the

impact hammer and the accelerometers generate voltage proportional to the excitation of the impact force. The oscilloscope reads the voltage from the transducers via signal conditioners during the experiment, and the results were saved on an external memory drive. The impact hammer and accelerometer data were recorded at a sampling rate of 500,000 samples/second. The high sampling rate ensures the capture of high frequency response from the accelerometers [51].

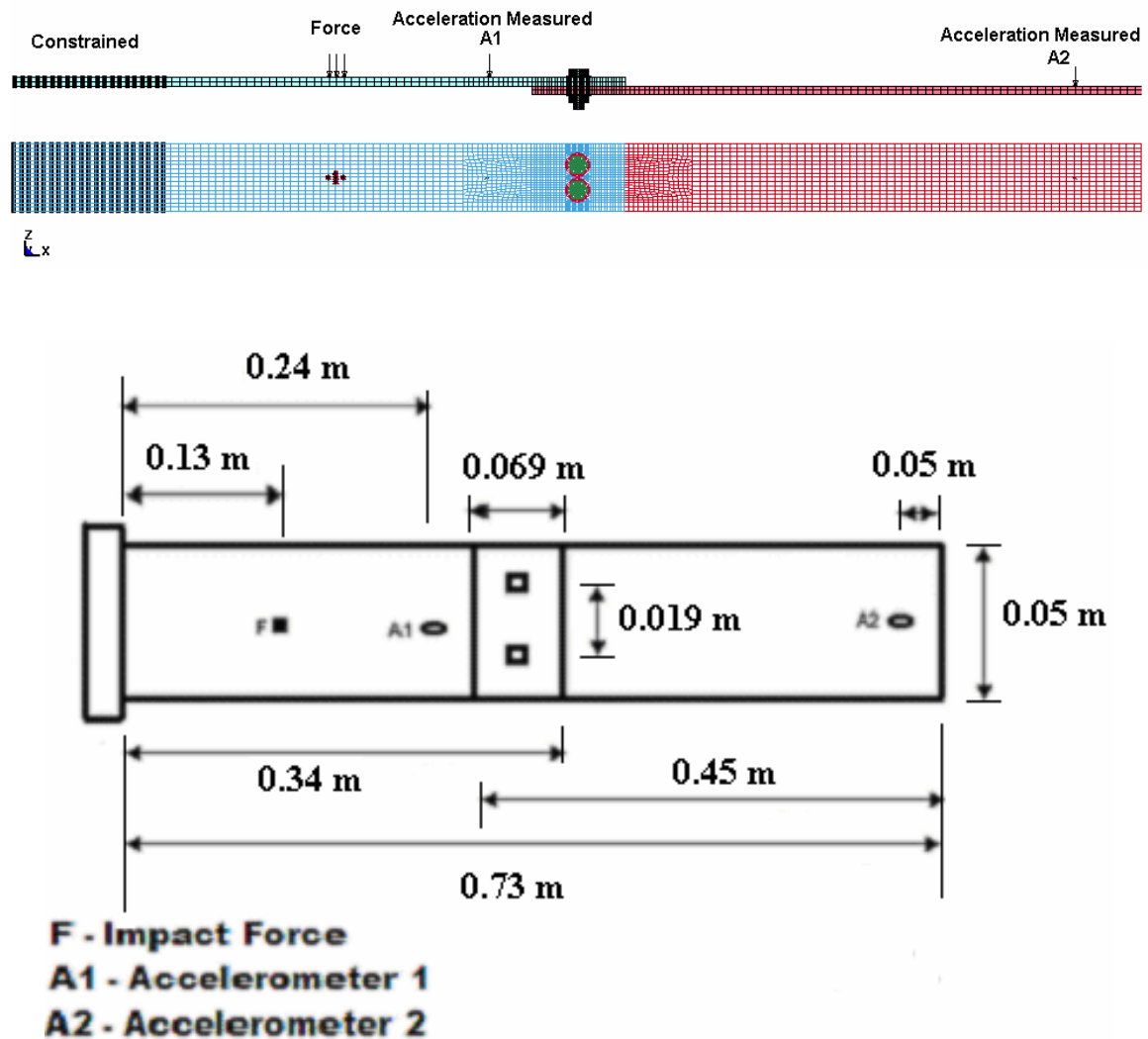


Figure 2.1 Diagram of the lap joint cantilever beam with constraints, loading point and sensor location (Front and top View)



Figure 2.2 Cantilever beam with lap joint, support and accelerometers

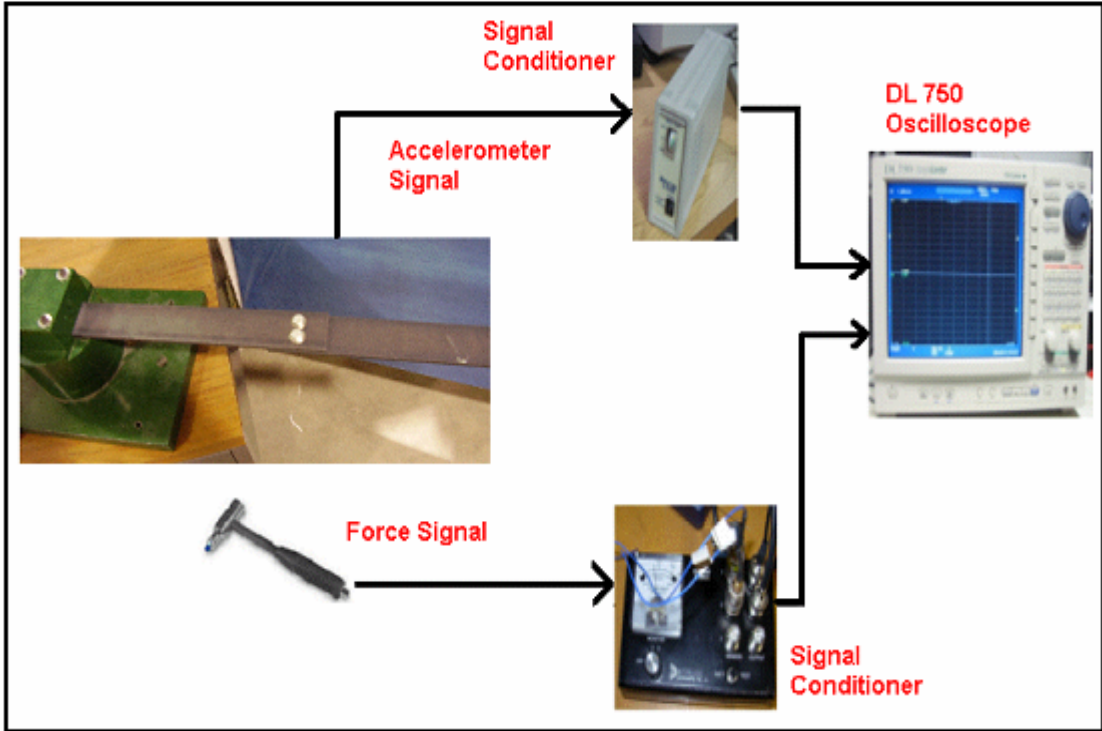


Figure 2.3 Experimental setup for impact loading on the bolted cantilever beam



Figure 2.4 Instrumented impact hammer

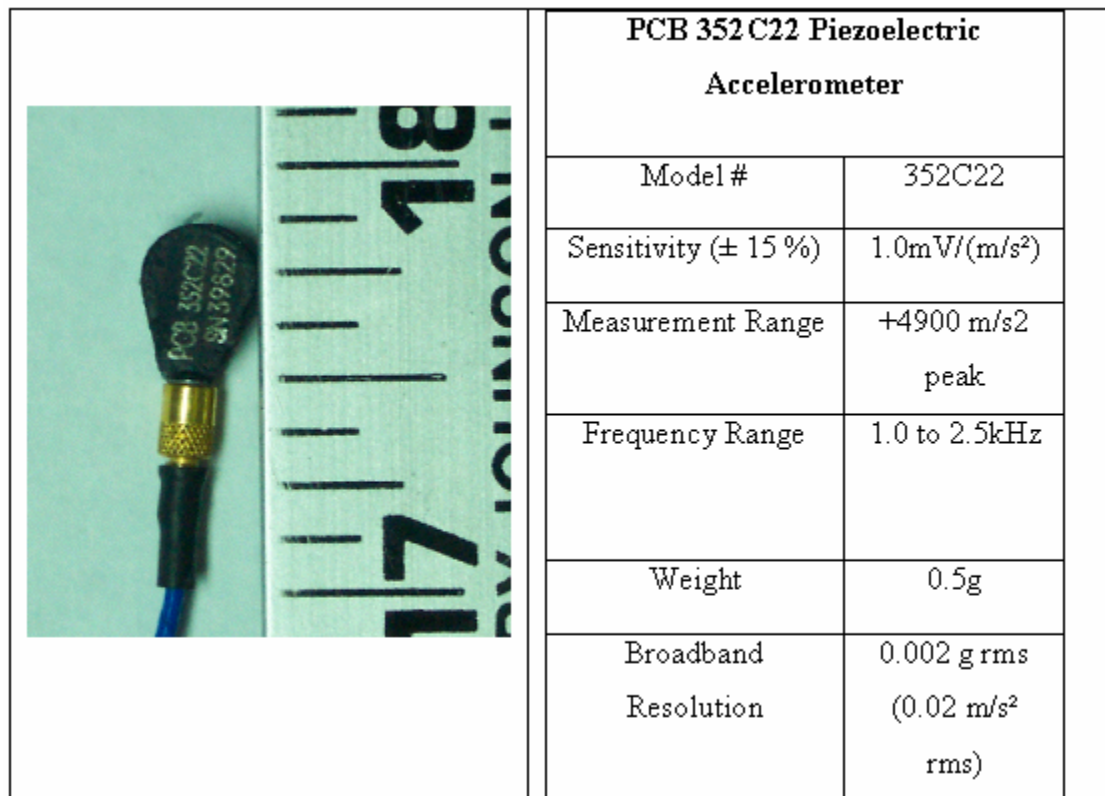


Figure 2.5 PCB accelerometer

### 2.3 Repeatability and consistency test

The impact test described in the previous section on the bolted structure is a transient phenomenon and the response can be non-linear, deterministic, or random. “If an experiment producing specific data of interest can be repeated many times with identical results (within limits of experimental error), then the data can generally be considered deterministic. Otherwise the data is random” [52]. If the impact test is random then it is impossible to simulate these results using any numerical methods. To confirm the deterministic nature of the impact test on the cantilever beam repeatability test was conducted. Also the consistency test was conducted to check the consistency in the two accelerometers used.

The repeatability test ensures that the test being conducted is deterministic in nature and the results from the experiment were not random. To conduct the repeatability test first a known peak force was selected. In this case, a peak force of 900 N was considered and the impact test on the bolted cantilever beam was repeated to get the same impact peak force. The striking of the impact hammer on the cantilever beam is done with a slight tapping motion of the hand as shown in Figure 2.6. As no mechanism was used to strike the impact hammer on the cantilever beam, it may take several attempts to get the required force level. The repeated (identical) force curves of 900 N (peak force) are shown in Figure 2.7. There are three spikes in the force curves recorded from the impact hammer. The first spike is the actual impact of the hammer with the cantilever beam. The other two spikes are the multiple impacts due to the rebounding of the slender cantilever beam. The acceleration was recorded on the cantilever beam during both the cases and is shown in the Figure 2.9. Using MATLAB, the Fast Fourier Transform (FFT) of the Time

history response (Figure 2.8) was generated for both the test cases. The FFT gives the response in frequency domain and the peaks in the FFT are the natural frequency of the cantilever beam. The response (output) of the cantilever beam is identical when the similar force (input) was used. The two curves in the Figure 2.9 are identical and have the same magnitude and frequency. The Time History responses were filtered at 6 KHz, based on the highest frequency excited in the structure. The filtering of the time history signal will remove the high frequency noise generated by the instruments. Figure 2.10 shows the cutout of the time history curve showing only a few milliseconds from 0.04 s to 0.06 s. This figure shows in detail, that both the responses are identical. This concludes that the procedure and the experimental set-up for conducting impact experiment on the bolted cantilever beam is deterministic and the response measured are not random, when the impact load is low (no permanent deformation or yielding of the structure and bolted joint).



Figure 2.6 Impact hammer striking the cantilever beam

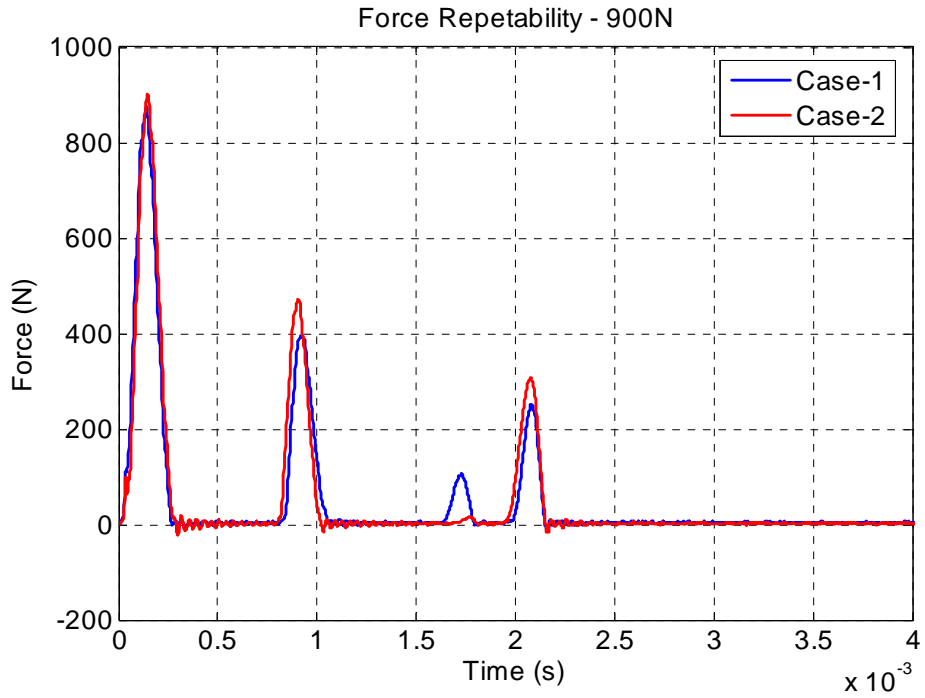


Figure 2.7 Repeatability test - Force curve from impact hammer

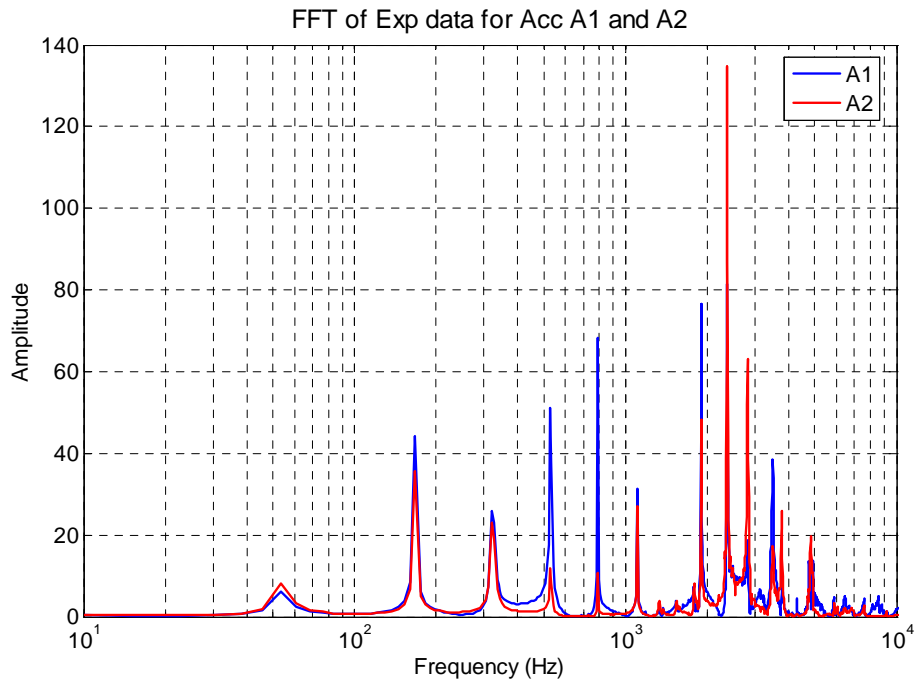


Figure 2.8 FFT of the cantilever beam response for the repeatability test

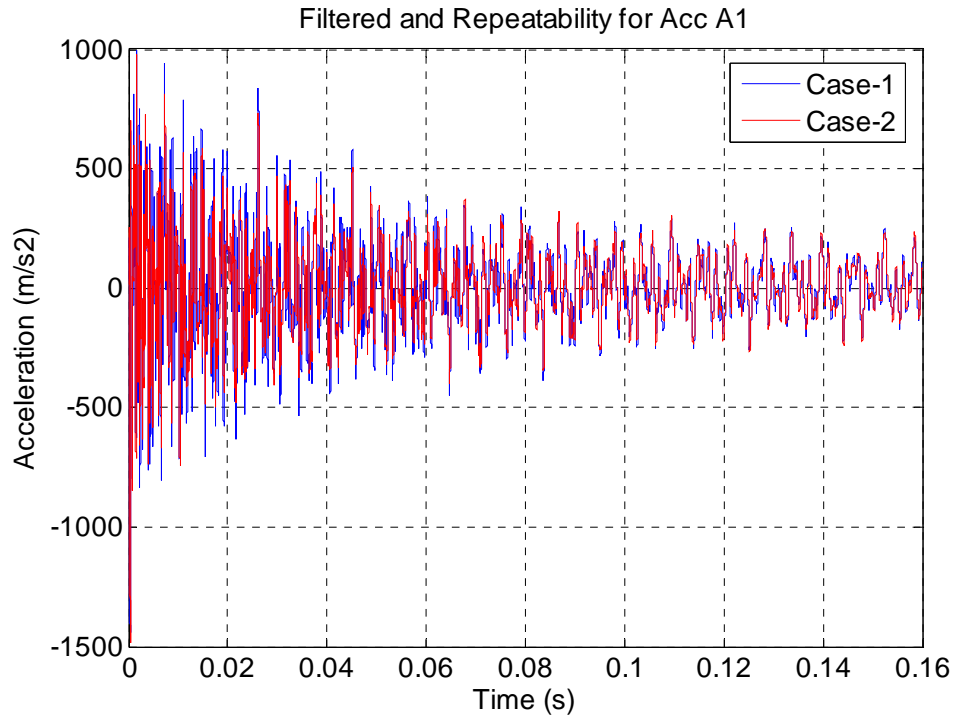


Figure 2.9 Time history response of the cantilever beam for the repeatability test

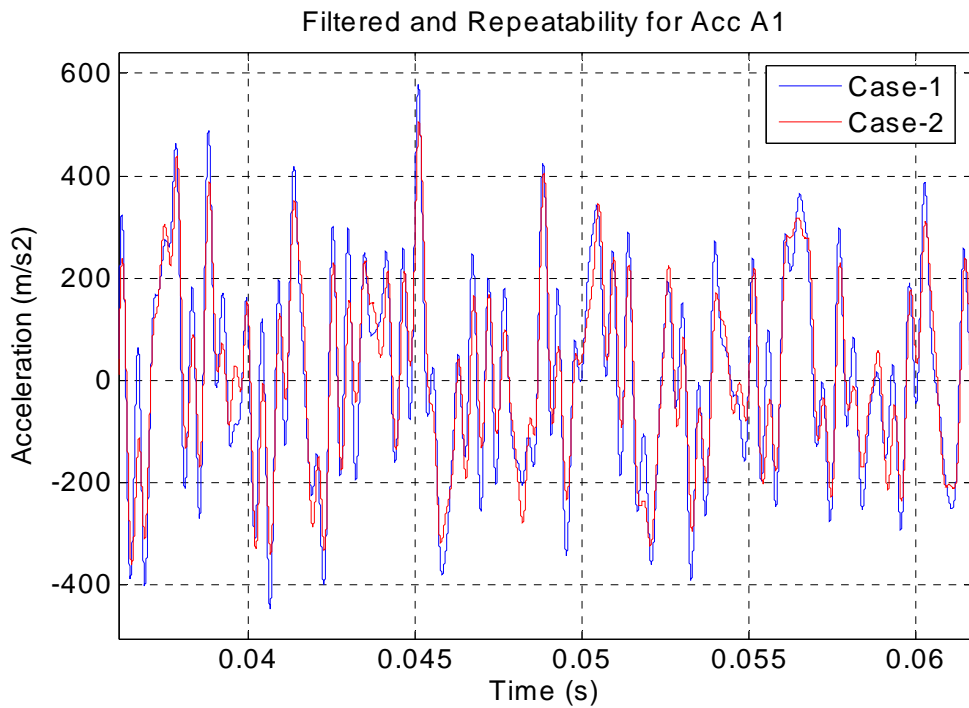


Figure 2.10 Time history response of the cantilever beam for the repeatability test-Cutout



The sensitivity of the accelerometers used in this experiments were calibrated using pulse software and hand held calibrator. Another way of testing (calibrating) the accelerometers, is to place two accelerometers next to each other and when excited, theoretically they should produce identical (consistent) results The consistency test set-up is shown in Figure 2.11, where two accelerometers are placed next to each other on the cantilever beam to measure the acceleration. The impact test is conducted as mentioned above and the response of both the accelerometers was recorded and is shown in Figure 2.12. The response of both the accelerometers is identical and Figure 2.13 shows the cutout of the time history curve. This figure shows the response of both the accelerometers has identical magnitude and phase or frequency. The repeatability and consistency test confirmed that the experiment being conducted is deterministic and the instruments used in the experiment produce consistent results.

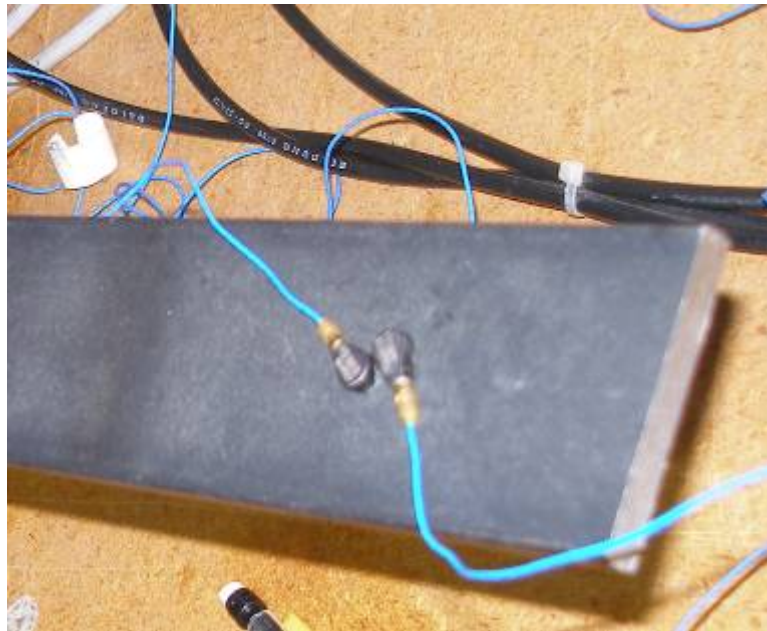


Figure 2.11 Consistency test showing two accelerometers placed side by side

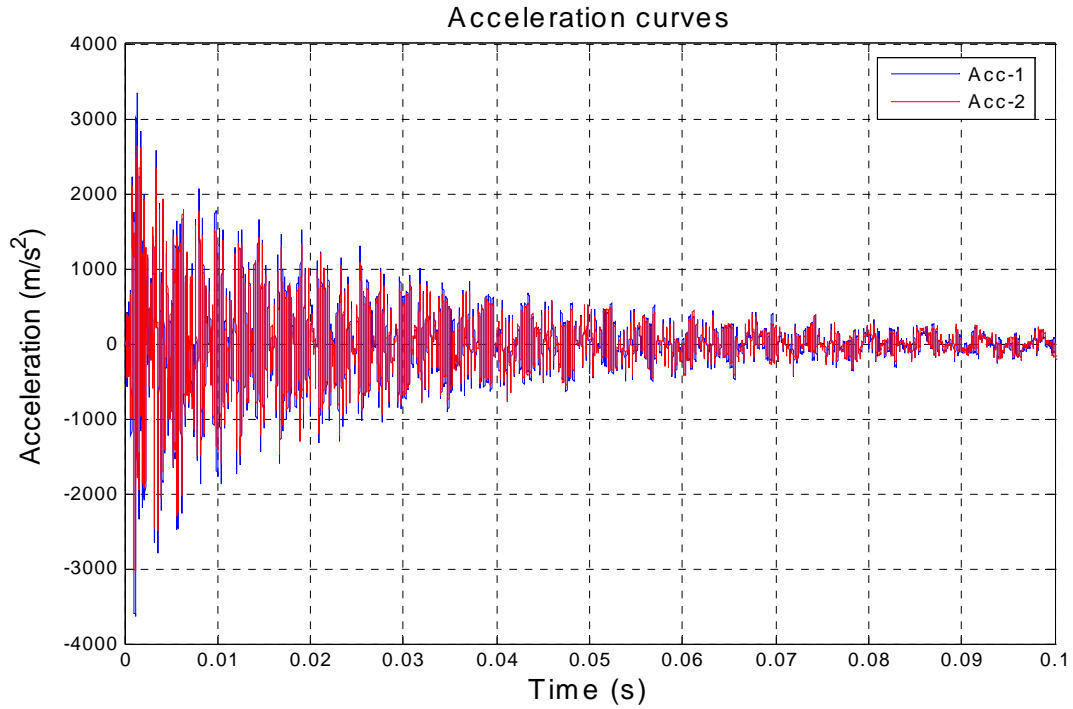


Figure 2.12 Time History response of two accelerometers during consistency test

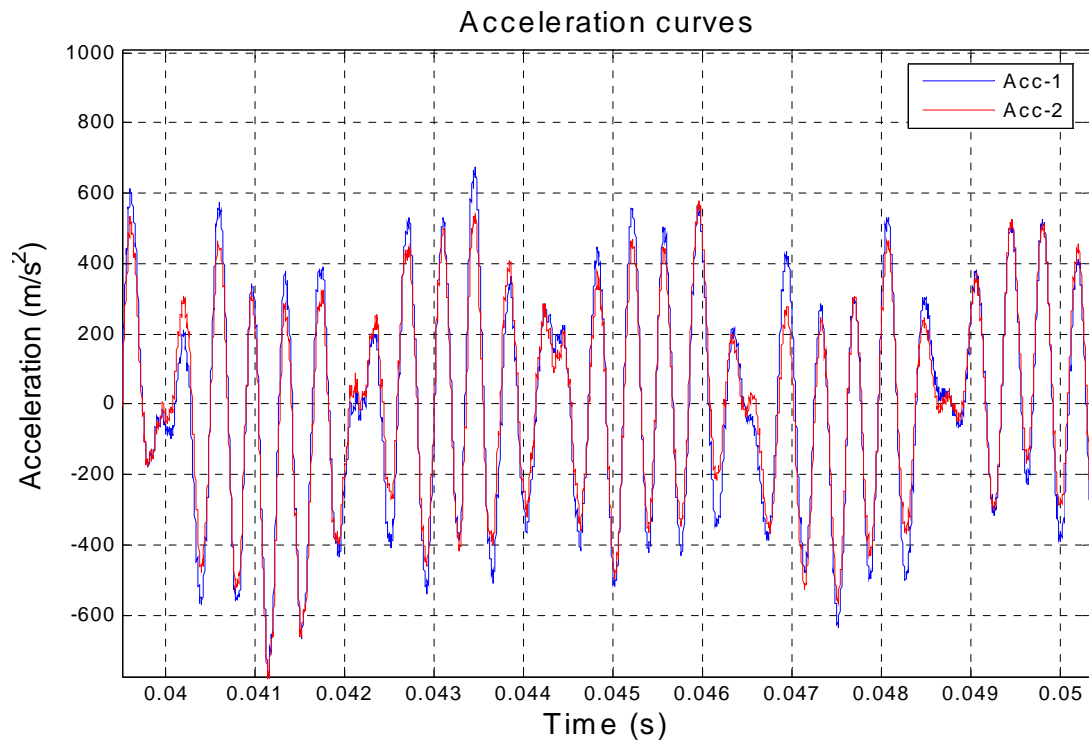
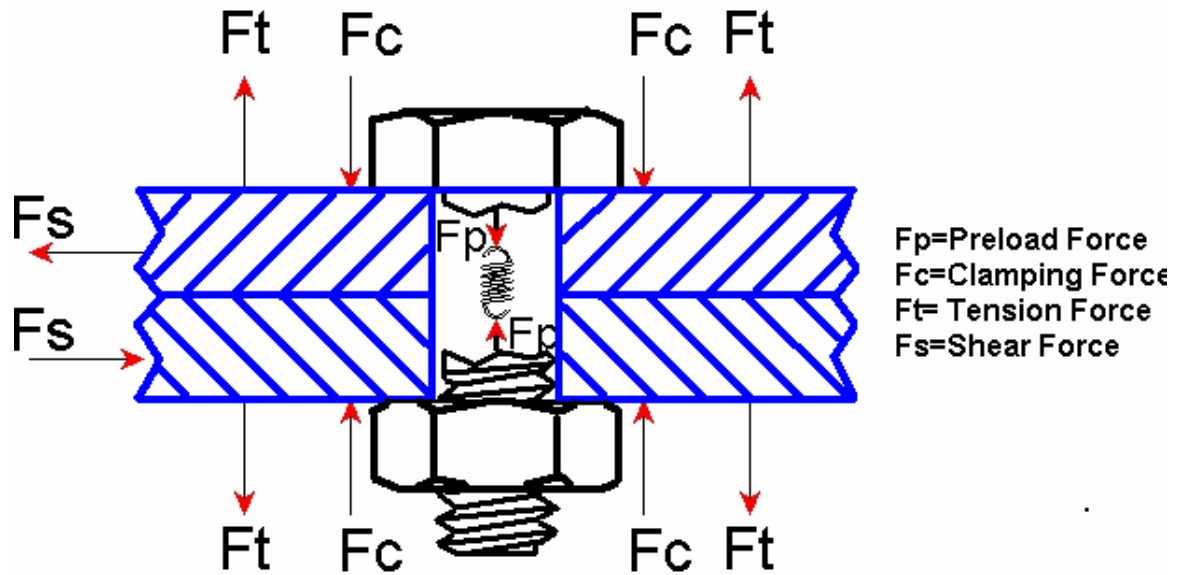


Figure 2.13 Time History response of two accelerometers during consistency test-Cutout

## 2.4 Preload on the bolt

The most common reason why bolted joints fail is due to the bolt failing to provide sufficient preload to prevent the external applied forces overcoming the clamp force acting between the joint faces. A fully tightened bolt can survive in an application where an untightened or loose bolts, would fail in a matter of seconds. Bolt-nut assemblies should be ideally tightened to produce an initial tensile force, which is also known as preload on bolt. Therefore preload or the torque used to tighten the bolted joints is an important factor that affects the response of the structure subjected to static or dynamic load. Bolts can be compared to springs in tension as shown in Figure 2.14. Rotating the bolt, which in turn stretches the spring, generates the preload force. The more the bolt is rotated, the more it stretches and generates more preload or tension. The clamping force,  $F_c$ , is the difference between the preload force and the tension force,  $F_t$ , on the joint. The clamping force is what holds the parts together, i.e.,:  $F_c = F_p - F_t$ .

Bolted joints can be loaded with shear force, tension force or a combination of both. In a joint loaded in tension the joint separating forces are opposed by the preload force on the bolt. The ultimate strength of the joint is limited by the strength of the bolt. Nevertheless, the higher the preload force the better the joint, because it will prevent the assembled parts from moving and the joint from loosening. A highly preloaded joint is also more resistant to static, cycling and shock loads. In general, the preload force determines the strength of the joint. Joints are stronger and more fatigue resistant with greater preload force. As the strength of the bolted joints is mainly dependent on the preload force, the preload has a significant effect on the response of the bolted joint to dynamic or shock loads.



**Bolts act like a spring to clamp the parts**

Figure 2.14 Force diagram for a typical bolted joint

The bolt preload is also measured in terms of “proof load”, which is the maximum tensile force that does not produce a normally measurable permanent set. Usually the proof load will be a little less than the yield strength of the material.

The initial tension can be calculated by the following equation [53]:

$$F = K \times A \times S$$

where

F = Initial tension

K = Constant ranging from 0.75 to 1.0

A = Tensile stress area

S = Proof strength.

Another important equation, which relates the tightening torque or pre-torque to the initial tension, is

$$T = K \times F \times D$$

where

T = Pre-torque

F = Preload or Pre-force

D = Nominal diameter of the thread.

Bolt preload is an important factor that affects the strength and response of the structure. To understand the effects of bolt preload on the dynamic response of structure, the bolted joint in the cantilever beam was tested for three pre-torques. The pre-torque is applied on the bolted joint using a torque wrench. The torque wrench has an adjustable knob and by setting this knob the torque wrench can precisely apply a specific torque on the bolted joint. The impact experiment (explained in the previous section) was conducted on the cantilever beam with bolted lap joint structure for three pre-torques of 21 Nm, 34 Nm and 47 Nm. The tightening force (preload) on the bolt shank, caused by these pre-torques is 13.12 kN, 21.2 kN and 29.35 kN respectively. The average axial tensile stress on the bolt shank caused by the pre-torque is 260.0 MPa, 422.0 MPa and 586.0 MPa respectively. These stresses are below the yield stress (600.00 MPa) of the bolt material and there was no yielding or damage to the bolt thread.

Figure 2.15 shows the time history response of the bolted cantilever lap joint beam for the three pre-torques of 21 Nm, 34 Nm, and 47 Nm. The impact force (peak force is 1500 kN) due to impact hammer striking the cantilever beam for the three cases was same. The response of the cantilever beam looks identical for all the three preload cases

(Figure 2.15), but the Figure 2.16 shows the cutout region of the time history response from 2ms to 3ms. In this figure the green curve, which corresponds to the pre-torque of 47 Nm, shows higher frequency excitation in the cantilever beam. This infers that the higher pre-torque in the structure makes the structure stiffer. Figure 2.17 shows the FFT of the time history curves in the frequency domain. At lower frequencies, the peaks in all the three cases have the same value, which corresponds to the natural frequency of the structure. At the higher frequencies (above 6000 Hz) the peaks in the green curve move towards the right when compared with the corresponding peaks in red and blue curves. This suggests that the natural frequency of the bolted structure for the higher Eigenmodes depend on the bolt pre-torque.

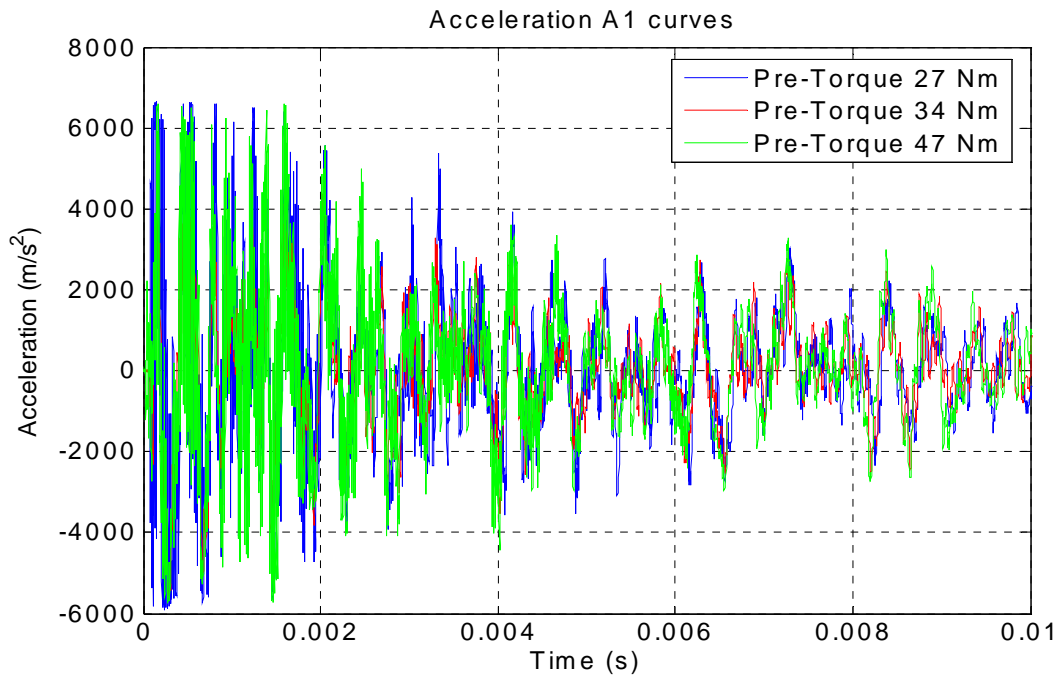


Figure 2.15 Time history response of the bolted cantilever beam for three pre-torque levels

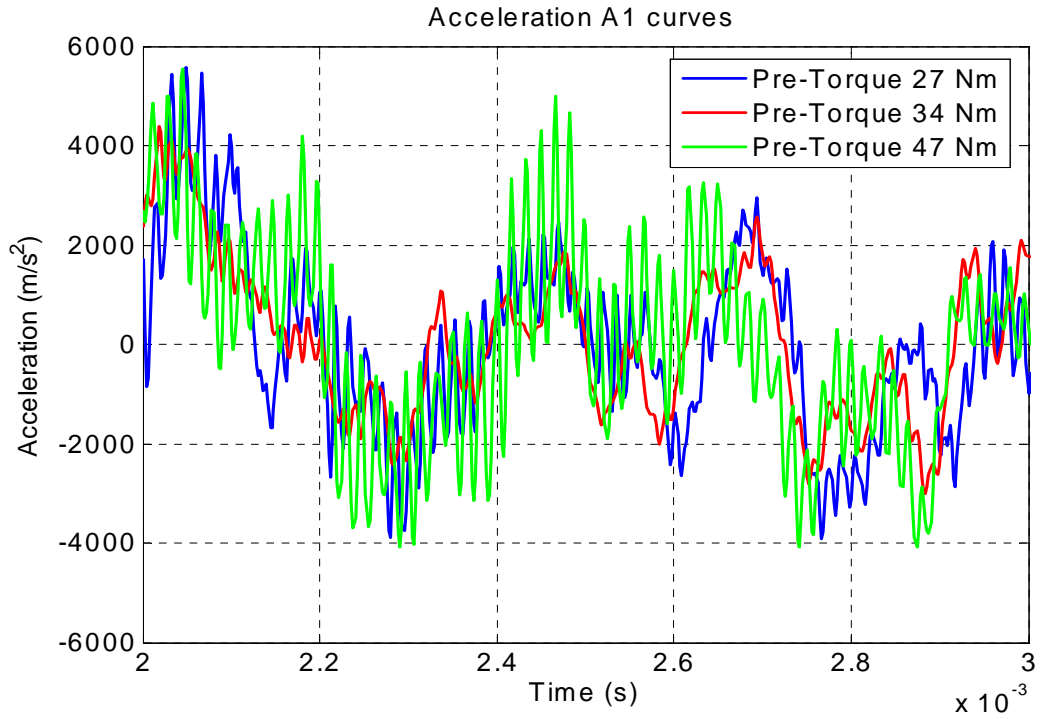


Figure 2.16 Cutout of the time history curves

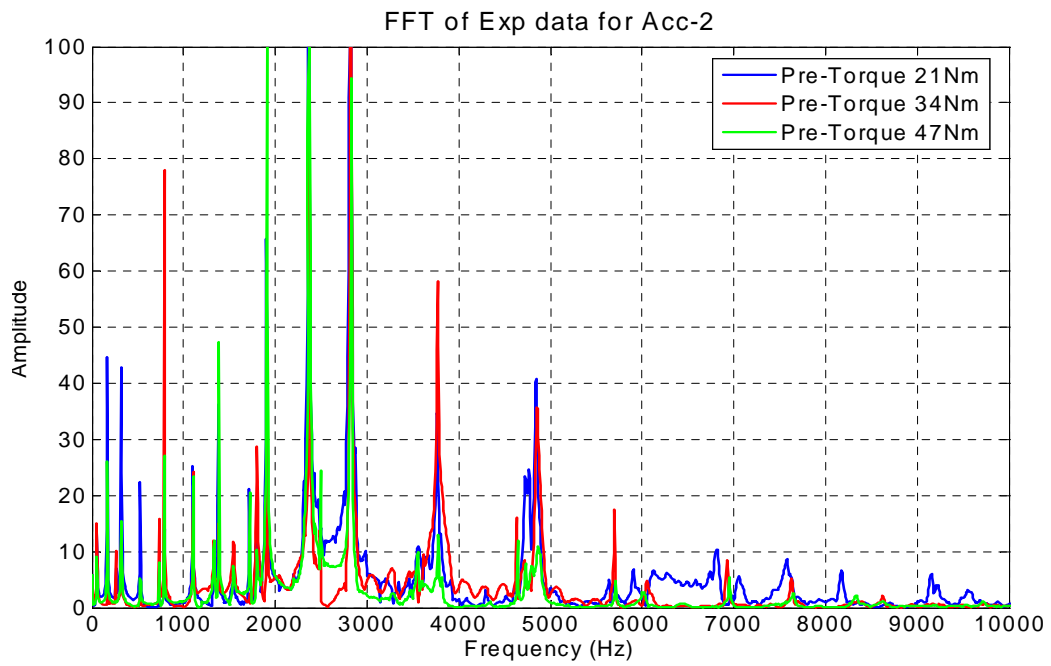


Figure 2.17 FFT of the time history plots for three pre-torque test cases

## CHAPTER 3

### ANALYSIS OF CANTILEVER BEAM FOR IMPACT LOADING

#### 3.1 Background

Although bolted joints are integral parts of army vehicles, their modeling and their effects on the structural dynamics are not yet fully understood. This is a big drawback in predicting the bolted joint response using numerical methods. Among all the numeric methods, FE analysis are commonly used in simulating vehicle crash or blast analysis. In this report, finite element analysis (FEA) was used to simulate the experimental impact analysis on the cantilever beam with bolted lap joint. As this is an impact analysis, wave propagation in the structure is important, and therefore the explicit FE method was used during the simulation. ALTAIR HyperMesh was used as the pre-processor to create and mesh the 3-D models of impact testing setup. Non-Linear commercial FE code LS-DYNA v971 [1, 2] was used to simulate the impact analysis on the cantilever beam with bolted lap joint. LS-POST, Altair Hyper View and MATLAB were used for post-processing the results from the simulation. Both modal analysis and transient analysis were solved using LS-DYNA solver. The FE modal analysis uses implicit solver and the FE transient analysis uses explicit solver.

#### 3.2 Experimental and finite element analysis of cantilever beam

The main objective of this research is to study the effects of the bolted joints on the overall structural dynamics of the structure and simulate the response of the bolted joint using FE analysis. The best way to approach this problem is to select simple structures for studying the effects of local bolted joint on the dynamics. Also for comparison purposes, in addition to bolted joint structure, a structure having similar identical



geometry and material properties to the jointed structure, but with no joint interface (monolithic structure) was used. Therefore under identical forcing and boundary conditions, subtraction of the dynamics of the jointed and monolithic structures will provide the effect of the joint on the dynamics.

Two types of cantilever beam configurations were used to study the shock response of the bolted structure. These two sets of cantilever beams were identical in size, shape, material and boundary conditions. The only difference between the two beams is that, one beam is monolithic (no joints) and the other beam is a bolted lap joint as shown in Figure 3.1 and Figure 3.6 respectively. The monolithic cantilever beam is a simple structure without any joints and is easy to simulate whereas the cantilever beam with bolted joint is complex because of the non-linearity from the joint. First the impact experiment was conducted and the response of the cantilever beam was recorded. Then using FE analysis, the impact experiment was simulated and compared with the experimental values. Doing this, gives a better understanding of the nature of bolted joints.

The procedure for performing the impact experiment on the cantilever beam is explained in chapter 2. Figure 3.1 shows the monolithic cantilever beam (no joints) with impact point and the accelerometer position. The cantilever beam is 0.73 m in length, and 5.080 cm x 0.635 cm (2"x 1/4") cross-section. The beam is made of 1040 steel, and is clamped at one end. Instrumented impact hammer was used to excite the cantilever beam and the accelerometers were used to capture the response of the beam. Figure 3.2 shows the FFT of the experimental time history curves of the monolithic cantilever beam. The peaks in the plot represent the natural frequency of the monolithic cantilever beam. The

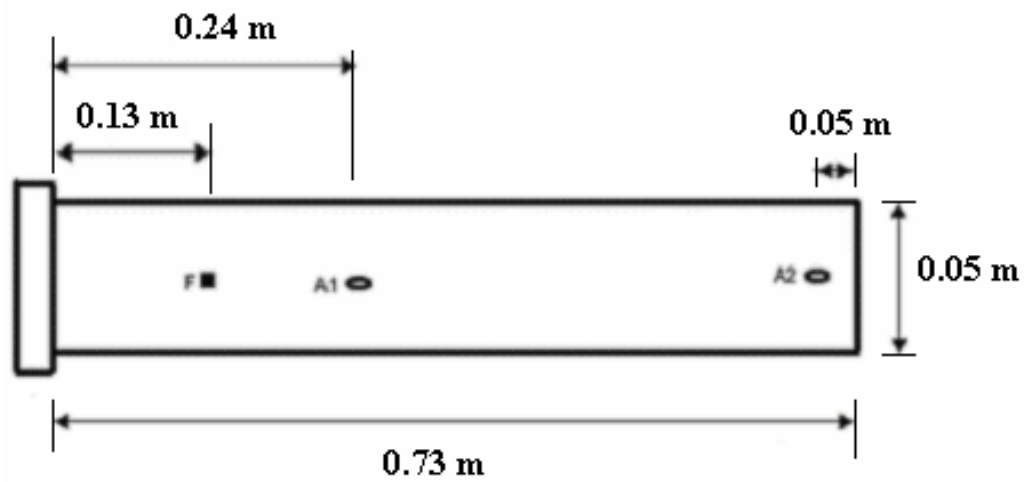
corresponding values in the abscissa are the natural frequency of the beam. The fundamental frequency of the cantilever beam is 61 Hz.

Altair HyperMesh was used for modeling and meshing the FE model of the cantilever beam. Modal analysis was carried out on the monolithic cantilever beam using LS-DYNA implicit solver. When single precision was used during modal analysis in LS-DYNA, it gave erroneous natural frequency values. By using double precision in LS-DYNA implicit solver, this error was solved. It is always recommended to use double precision in LS-DYNA, especially with implicit solver.

Using consistent unit system is very important in dynamic analysis. SI unit system was used in all the experiment and the FE analysis. The unit system used should always satisfy Newton's second law,  $F = m \times a$ . The material properties of 1045 steel used in the FE analysis are tabulated in the Table-3.1.

Table 3-1 Mechanical properties of 1045 steel [54]

Properties	Symbol	Units
Density	$\rho$	7810 kg/m <sup>3</sup>
Modulus of Elasticity	E	201 x 10 <sup>9</sup> N/m <sup>2</sup>
Poisson's ratio	$\nu$	0.3
Yield strength	$\sigma_y$	507 x 10 <sup>6</sup> N/m <sup>2</sup>
Tangent Modulus	$E_T$	3.35 x 10 <sup>9</sup> N/m <sup>2</sup>



**F - Impact Force**  
**A1 - Accelerometer 1**  
**A2 - Accelerometer 2**

Figure 3.1 Monolithic cantilever beam

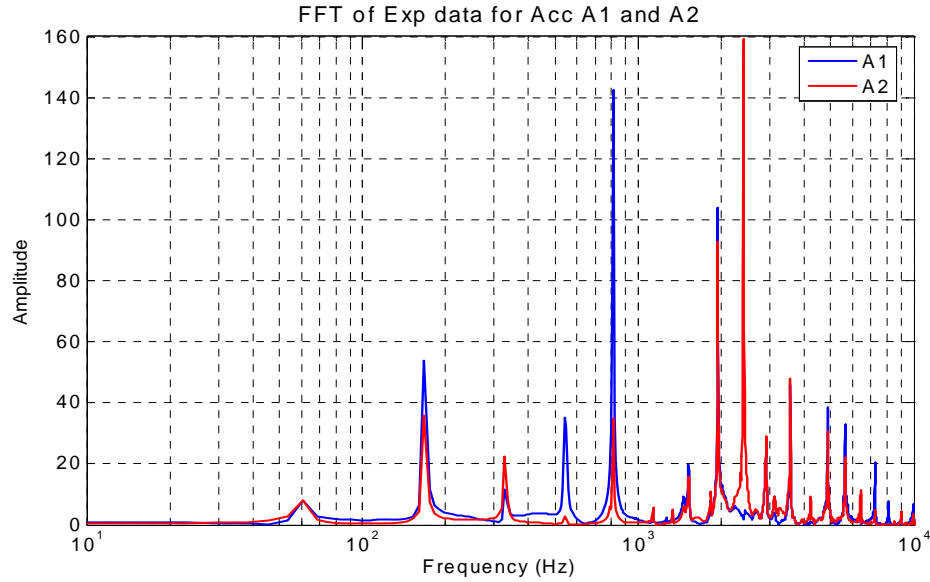


Figure 3.2 FFT of the experimental time history curve

The FE model of the cantilever beam was built and meshed using Altair HyperMesh. Shell or solid elements can be used in the FE model. The type and number of elements in the FE model has a significant effect on the response. Six different FE models were developed to study the modal analysis of monolithic cantilever beam. Three of the FE models used linear solid elements and these models had two, four and six elements along the thickness of the cantilever beam as shown in Figure 3.3. In all three solid element FE models, the number of elements on the plane of the cantilever beam was the same. Also three linear shell element models were developed. The mesh density in the first shell FE model was coarse and the second FE model was developed from splitting elements in the first model. Splitting the element creates additional three elements. This gives a medium mesh density FE model. Splitting the elements in the medium mesh density FE model generated the third FE model, which had a fine mesh density. Table 3.2 gives a summary of elements and nodes in each FE model.

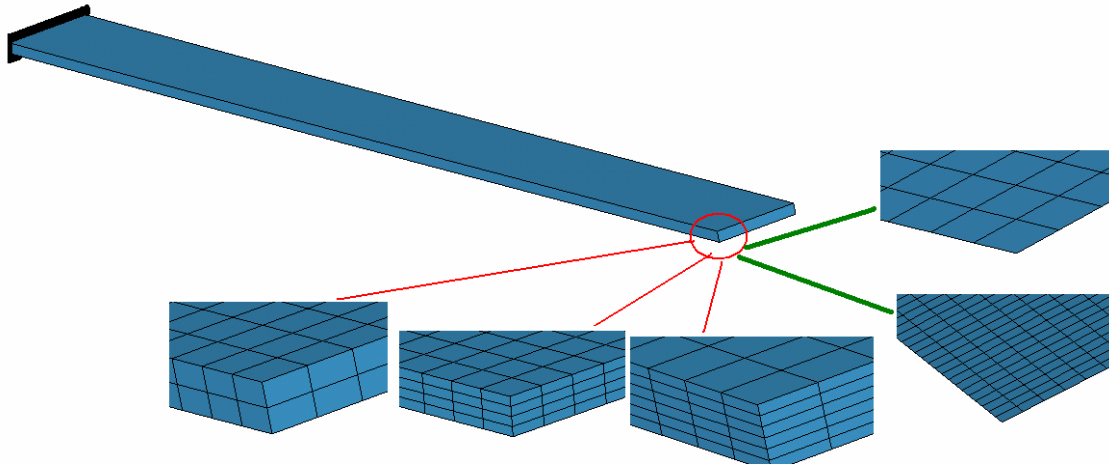


Figure 3.3 Solid and shell element FE model of cantilever beam

Table 3-2 Description of FE model

FE Model		Total Nodes	Total Elements
Solid Elements (No. of elements through the thickness)	2	3051	1792
	4	5085	3584
	6	7119	5376
Shell Elements (Mesh Density)	Coarse	1017	896
	Medium	3825	3584
	Fine	14,817	14,336

Modal analysis determines the vibration characteristics such as natural frequency and mode shapes of a structure. Mode shape and natural frequency are the important parameters in the design of a structure subjected to dynamic loading. Also modal analysis serves as the starting point for another more detailed dynamic analysis. The response of any structure subjected to the impact analysis depends on the natural frequency of the structure. Therefore it is crucial to check the natural frequency of the structure while

doing transient or dynamic FE analysis. Therefore the first step in any transient FE analysis is to compare the experimental and FE modal analysis results. In the experimental modal analysis, the structure was excited by a transient load (impulse), and the response of the structure is captured using accelerometers. FFT of the transient acceleration curves gives the natural frequency of the structure as shown in Figure 3.2. The frequency value corresponding to spikes in the FFT plots are the natural frequency of the structure.

The FE modal analysis is an Eigenvalue problem, which solves the undamped equation of motion [57].

$$[\mathbf{K}]\{\varphi_i\} = \omega_i^2[\mathbf{M}]\{\varphi_i\}$$

where

$[\mathbf{K}]$  = Stiffness matrix

$\{\varphi_i\}$  = Mode shape vector

$\omega_i$  = Eigenvalue

$[\mathbf{M}]$  = Mass matrix

The Eigenvalues and the Eigenvectors, which come from solving the above equation, represent the frequencies and the corresponding mode shapes. LS-DYNA solver uses implicit method to solve the Eigenvalue problem. Figure 3.4 shows the FE modal analysis of the monolithic cantilever beam and the first eight mode shapes along with the frequency values. The FE modal analysis predicts all the mode shapes and the frequencies: axial, bending and torsion mode. The experimental modal analysis results are tabulated in Table 3.3 along with FE modal analysis results. In the experimental modal analysis, predominantly the bending modes were excited because the impact load was applied perpendicular to the plane (bending load) of the beam. The peaks in Figure 3.2 are predominantly bending mode frequencies. Totally six FE models were used for

studying modal analysis as shown in Figure 3.3. The frequencies predicted from these six FE models are tabulated in Table 3.3. Figure 3.5 shows the bar chart of the monolithic cantilever beam natural frequencies from the experiment and all the FE models. The FE modal analysis of the model with two solid elements along the thickness predicted lower frequency values compared to experimental values. All the FE models use under-integration as a quadrature rule to calculate the stiffness matrix coefficients  $K_{ij}$ , except the case 3, which uses full integration quadrature rule. This FE model predicts higher frequency values compared to experimental values and under-integration FE model for each mode as shown in Figure 3.5. The frequency values predicted from remaining FE model where in good agreement with the experiment.

### 3.3 Fundamental natural frequency of cantilever beam by analytical method

The equation of motion for the forced lateral vibration of a non-uniform beam is given by:

$$\frac{\partial^2}{\partial x^2} \left[ EI(x) \frac{\partial^2 w}{\partial x^2}(x, t) \right] + \rho A(x) \frac{\partial^2 w}{\partial x^2}(x, t) = f(x, t)$$

where

$E = \text{Elastic Modulus}$

$I = \text{Moment of Inertia}$

$w = \text{Lateral displacement}$

$\rho = \text{Mass density}$

$A = \text{Area of cross - section of beam}$

For a uniform beam and free vibration, the equation of motion is

$$\left[ c^2 \frac{\partial^4 w}{\partial x^4}(x, t) \right] + \frac{\partial^2 w}{\partial x^2}(x, t) = 0$$

where

$$c = \sqrt{\frac{EI}{\rho A}}$$

This fourth order PDE can be solved using separation of variables method by substituting

$$w(x, t) = W(x)T(t)$$

This results in two ordinary differential equations:

$$\frac{d^4 W(x)}{dx^4} - \beta^4 W(x) = 0$$

$$\frac{d^2 T(t)}{dt^2} - \omega^2 T(t) = 0$$

where

$$\beta^4 = \frac{\omega^2}{c^2} = \frac{\rho A \omega^2}{EI}$$

Therefore

$$W(x) = C_1 (\cos \beta x + \cosh \beta x) + C_2 (\cos \beta x - \cosh \beta x) \\ + C_3 (\sin \beta x + \sinh \beta x) + C_4 (\sin \beta x - \sinh \beta x)$$

where  $C_1, C_2, C_3,$  and  $C_4$  are constants and can be found from the boundary conditions.

The natural frequency of the beam are computed as

$$\omega = \beta^2 \sqrt{\frac{EI}{\rho A}} = (\beta l)^2 \sqrt{\frac{EI}{\rho A l^4}}$$

For cantilever beam, the boundary conditions are

$$\text{Fixed End: } w = 0, \frac{\partial w}{\partial x} = 0$$

$$\text{Free End: } EI \frac{\partial^2 w}{\partial x^2} = 0, \frac{\partial}{\partial x} \left( EI \frac{\partial^2 w}{\partial x^2} \right) = 0$$

Substituting the boundary conditions results in

$$W_n(x) = C_n [\sin \beta_n x - \sinh \beta_n x - \alpha_n (\cos \beta_n x - \cosh \beta_n x)]$$

where

$$\alpha_n = \left( \frac{\sin \beta_n l + \sinh \beta_n l}{\cos \beta_n l + \cosh \beta_n l} \right)$$

$$\cos \beta_n l \cdot \cosh \beta_n l = -1$$

$$\omega = \beta^2 \sqrt{\frac{EI}{\rho A}} = (\beta l)^2 \sqrt{\frac{EI}{\rho A l^4}}$$

$$\omega = 1.875^2 \sqrt{\frac{210e9 \times 0.05 \times 0.0605^3}{7810 \times 0.05 \times 0.0605 \times 12 \times 0.73^4}} = 61.4 \text{ Hz}$$



The analytical and experimental fundamental natural frequency of the cantilever beam is 61 Hz.

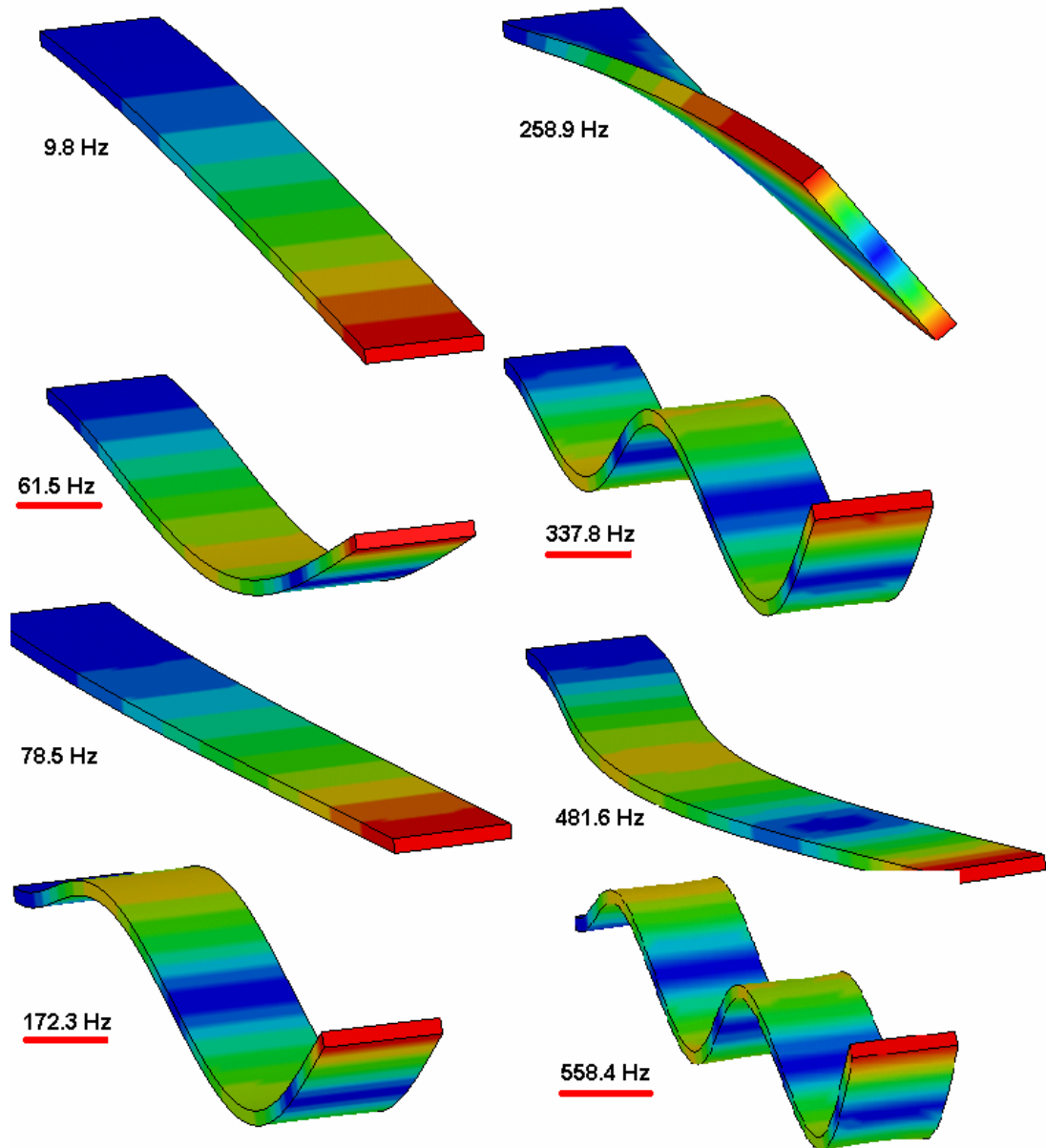


Figure 3.4 Mode shape and natural frequencies of the cantilever beam using FE model with solid elements and six elements through the thickness of the beam

Table 3-3 Natural frequency of the cantilever beam from experiment and FEA

Mode	Natural frequency of the cantilever beam excited in the impact experiment							
	Experi- ment	Solid Element FE Model Number of Elements along the Thickness				Shell Element FE Model Mesh Density		
		2	4	4*	6	Coarse	Medium	Fine
1	61	55	61	74	62	62	62	62
2	168	154	170	207	172	175	175	175
3	328	301	332	405	338	342	342	342
4	542	498	549	669	558	566	566	566
5	816	744	821	998	834	846	846	845
6	1137	1040	1147	1316	1165	1182	1181	1181
7	1335	1306	1306	1393	1306	1333	1349	1353
8	1518	1385	1527	1772	1552	1575	1573	1573
9	1945	1779	1961	2375	1993	2024	2021	2021
10	2411	2222	2449	2470	2452	2449	2470	2478
11	2914	2641	2902	3059	2948	3017	3055	3065
12	3571	3162	3474	3679	3529	3614	3661	3672
13	4227	3857	4230	5009	4298	4380	4367	4364
14	4868	4266	4685	5093	4759	4878	4945	4962
15	5646	5462	5676	6480	5766	5889	5865	5859
16	6416	5886	6474	7264	6576	6489	6693	6685

\* Fully Integrated Element Formulation

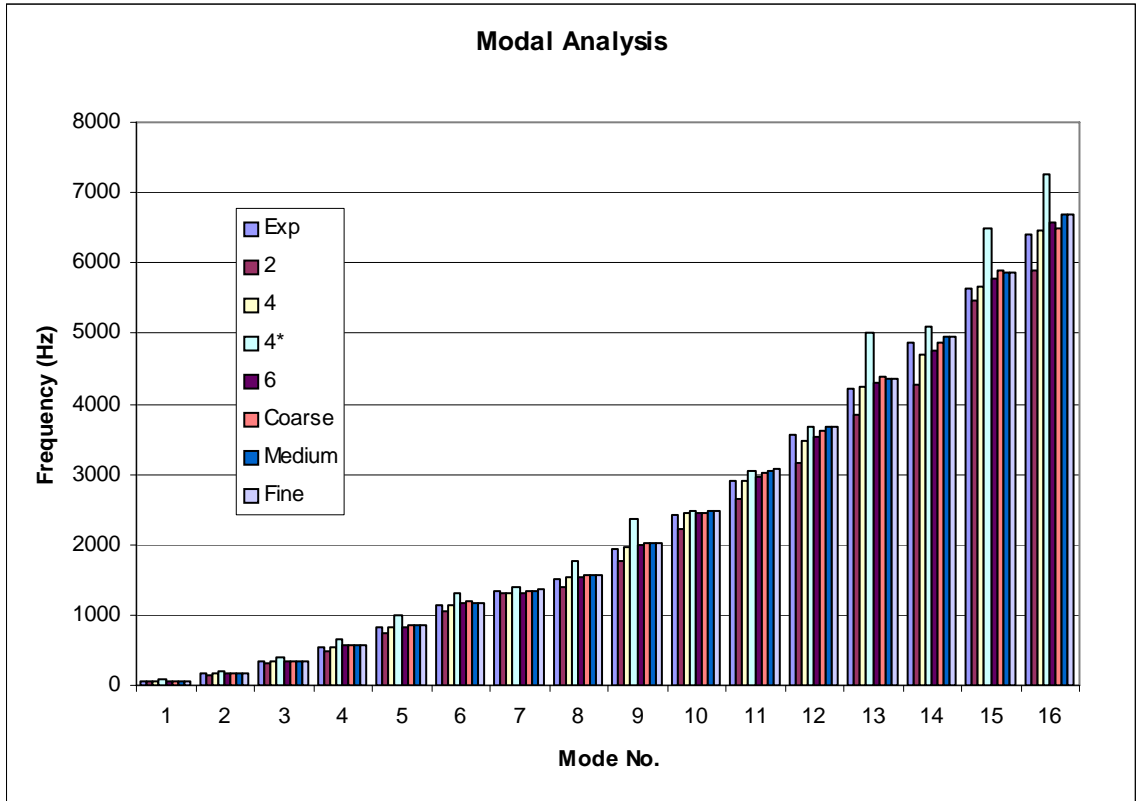


Figure 3.5 Natural frequency of cantilever beam from experiment and FEA

### 3.4 Experimental and finite element simulation of cantilever beam with bolted joint

It is very important to understand the bolted joints in any structure, because the joints have a substantial effect in the dynamic response of the structure. Most of the damping in a structure comes from bolted joints. Beards [55] showed that damping in joints is much larger than the material damping. Newmark [56] showed viscous damping levels for bolted steel structures in elastic range (5 to 7) and plastic range (10 to 15)

A cantilever beam with bolted lap joint was used to study the response of bolted joints to impact loading. The understanding of this simple bolted structure subjected to impact loading helps in modeling more complex bolted structures. Also studying two

similar structures, one with bolted joint and the other with no bolted joint helps in understanding the contribution of bolted joint in the structure, especially for transient analysis. In the previous section, a monolithic cantilever beam was analyzed in detail using experimental and FE modal analysis. In this section, a similar cantilever beam, but with bolted joint will be analyzed for both modal and transient analysis. Figure 3.6 shows the bolted cantilever beam with lap joint, along with impact hammer and accelerometers. The experimental procedure for impact analysis on this structure is explained in detail in Chapter 2. Figure 3.7 shows the experimental modal analysis result (FFT) of the monolithic cantilever beam and a similar cantilever beam with bolted joint. The first fundamental natural frequency is 61 Hz and 53.4 Hz for monolithic and jointed cantilever beam. But the remaining excited natural frequencies are almost identical. After 6000 Hz, there are no significant natural frequencies excited for the bolted cantilever beam, but the monolithic cantilever beam shows two prominent natural frequencies after 6000 Hz.

From the FE analysis of the monolithic cantilever beam, it was concluded that the solid FE model with four layers along the thickness of the beam will be sufficient to capture the dynamic response and will be practical to implement. Three kinds of FE models were developed to simulate the dynamic response of the cantilever beam with bolted lap joint. The FE models were generated in HyperMesh and the LS-DYNA was used as the solver. The first FE model (Model-1) is a simple shell element model (medium mesh density) with tied contacts as shown in Figure 3.8. The shell elements used in Model-1 are structural plain stress and linear elements. These elements are defined by four-nodes and have six degrees of freedom at each node. Bolts are not modeled in this FE model, but instead tied contact was used to join the two beams. In the

tied contact, true thickness for shell elements is activated. This makes the master and slave part of the contact to stay at their true mean position as shown in Figure 3.8. Figure 3.9 shows the second kind of FE model (Model-2), used to simulate the impact analysis on the cantilever beam with bolted lap joint. This model uses 3-D structural solid element for meshing cantilever beam, bolt and nut assembly. These solid elements are eight-node and have three degrees of freedom at each node. Four layers of solid elements are used along the thickness of the cantilever beam. No contacts were modeled between the beams in the lap joint and between bolt assembly and beam. All the nodes near the contacts were merged or connected. This makes the FE model simple to solve and the non-linearity arising from the contacts is eliminated. Also the preload on the bolt caused by pre-torque was not modeled. Again this simplifies the FE model. The third FE model (Model-3) is shown in Figure 3.10. This FE model represents the experimental cantilever beam with bolted joint in every detail, which includes preload on the bolt, and contacts with friction. The contacts are defined between the two beams at the lap joint and also between the bolt assembly and the beam. The contact surfaces for master and slave were defined using set-segment option and the bolt preload was defined using the thermal gradient method in LS-DYNA. The preload modeling for the explicit FE analysis is discussed in detail in a later section. Four layers of elements were used through the thickness of the cantilever beam. This FE model allows for slippage in the bolted lap joint.



Figure 3.6 Experimental set-up for impact analysis on cantilever beam with bolted joint

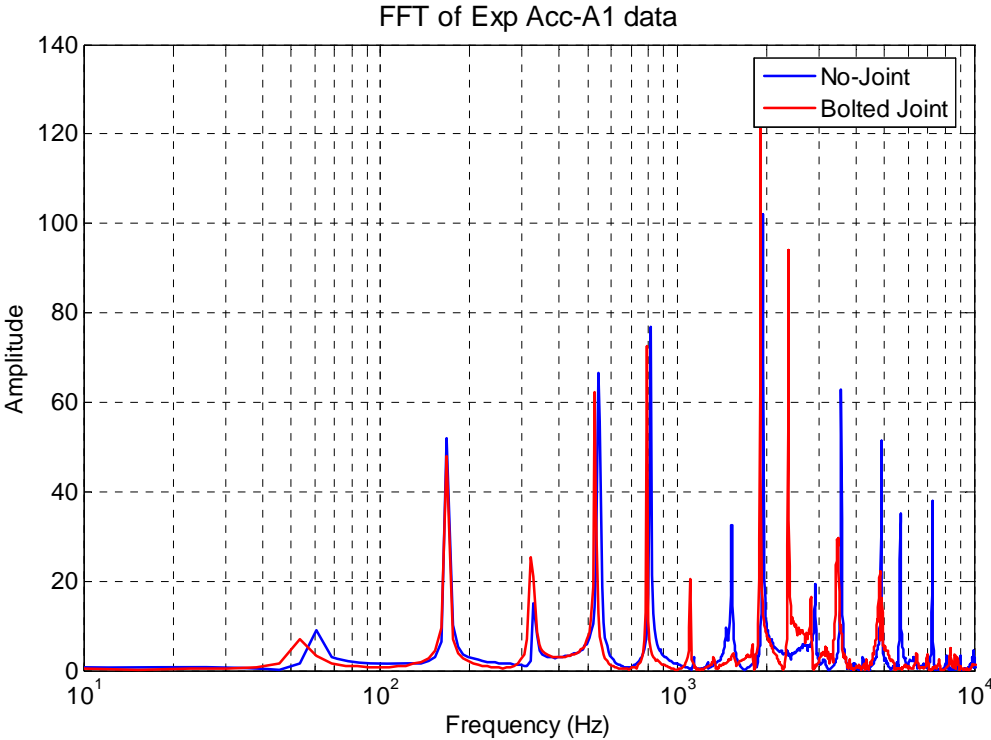
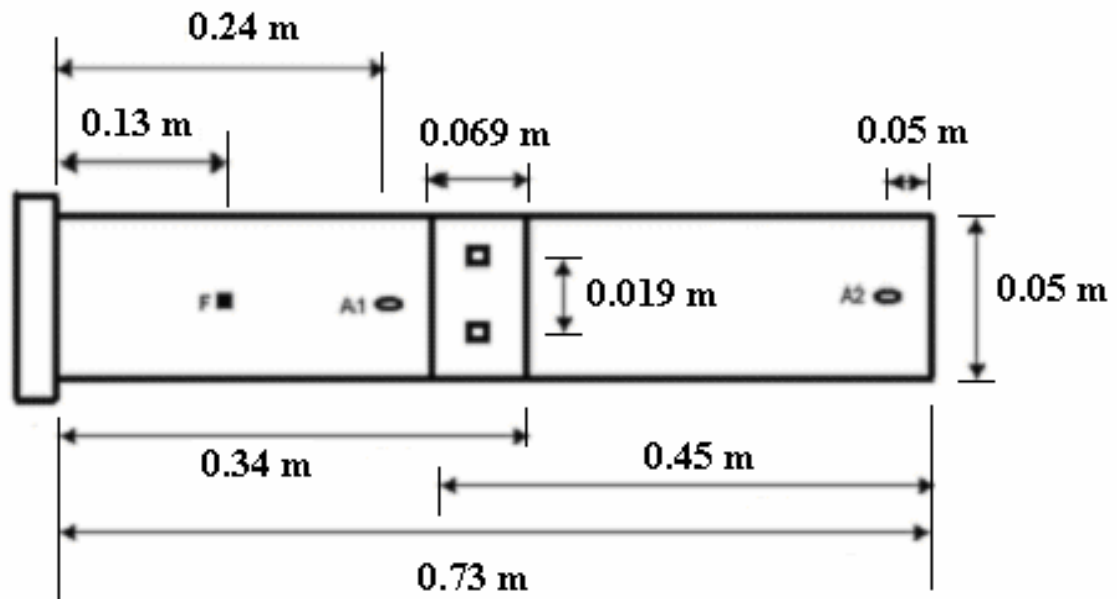


Figure 3.7 FFT of the cantilever beam with and without bolted joint



**F - Impact Force**  
**A1 - Accelerometer 1**  
**A2 - Accelerometer 2**

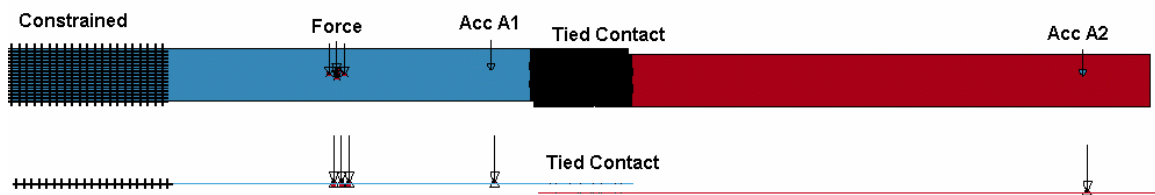


Figure 3.8 FE Model-1 Simplified FE model with shell elements and no bolted joint in the model (Top and Front View)

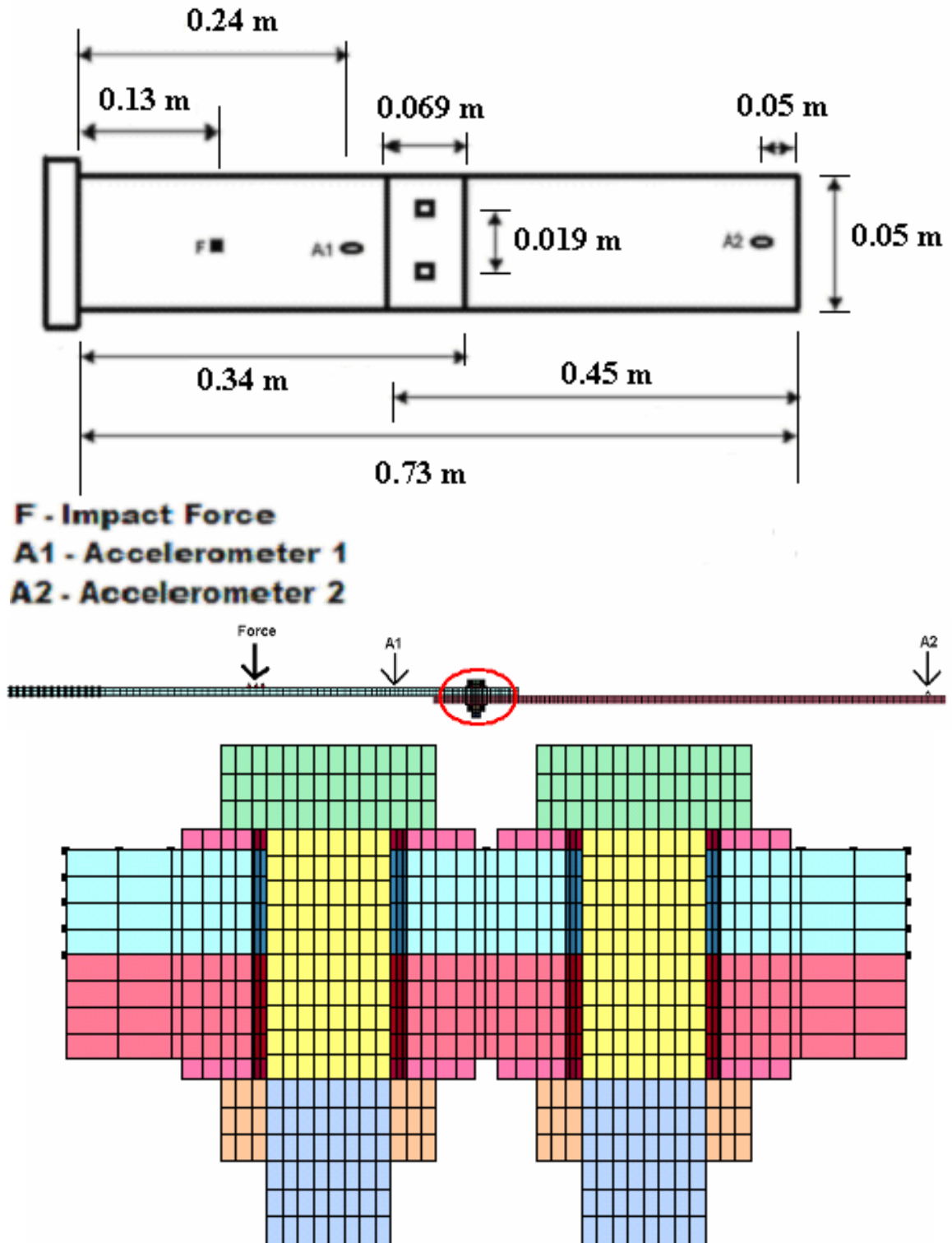


Figure 3.9 FE Model-2, simplified solid FE model of cantilever beam with no preload



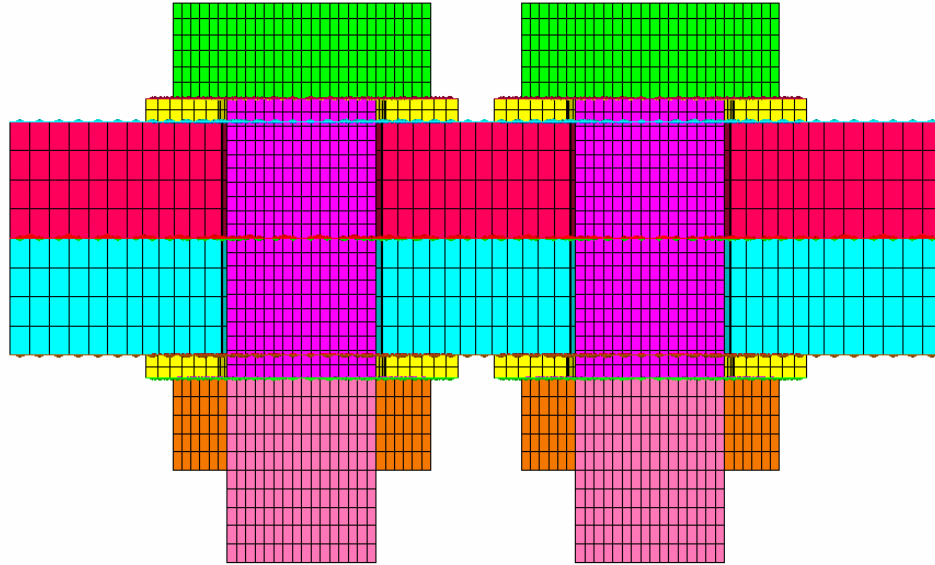


Figure 3.10 FE Model-3, solid FE model of cantilever beam with preload on bolt and all contacts defined

LS-DYNA implicit solver was used for modal analysis of the cantilever beam with bolted joints. Figure 3.11 shows the first eight-mode shape and frequencies predicted by FE Model-2. The mode shapes of cantilever beam with bolted lap joint (Figure 3.11) are similar to mode shape of monolithic cantilever beam (Figure 3.4). The FE modal analysis predicts all the mode shapes and the frequencies: axial, bending and torsion mode. The experimental modal analysis results are tabulated in Table 3.4 along with FE modal analysis results. Figure 3.12 shows the bar chart of the natural frequencies of cantilever beam with bolted joint, no joint and the three FE models. The natural frequencies of monolithic and jointed cantilever beam are similar at lower modes, except first, but at the higher modes the cantilever beam with bolted joint shows lower frequency values. Also for the same input force, some of the modes are not excited for bolted beam (Mode: 8, 12, 14, 16). The frequency values predicted by the FE modal analysis are higher than the natural frequencies predicted from experiment.

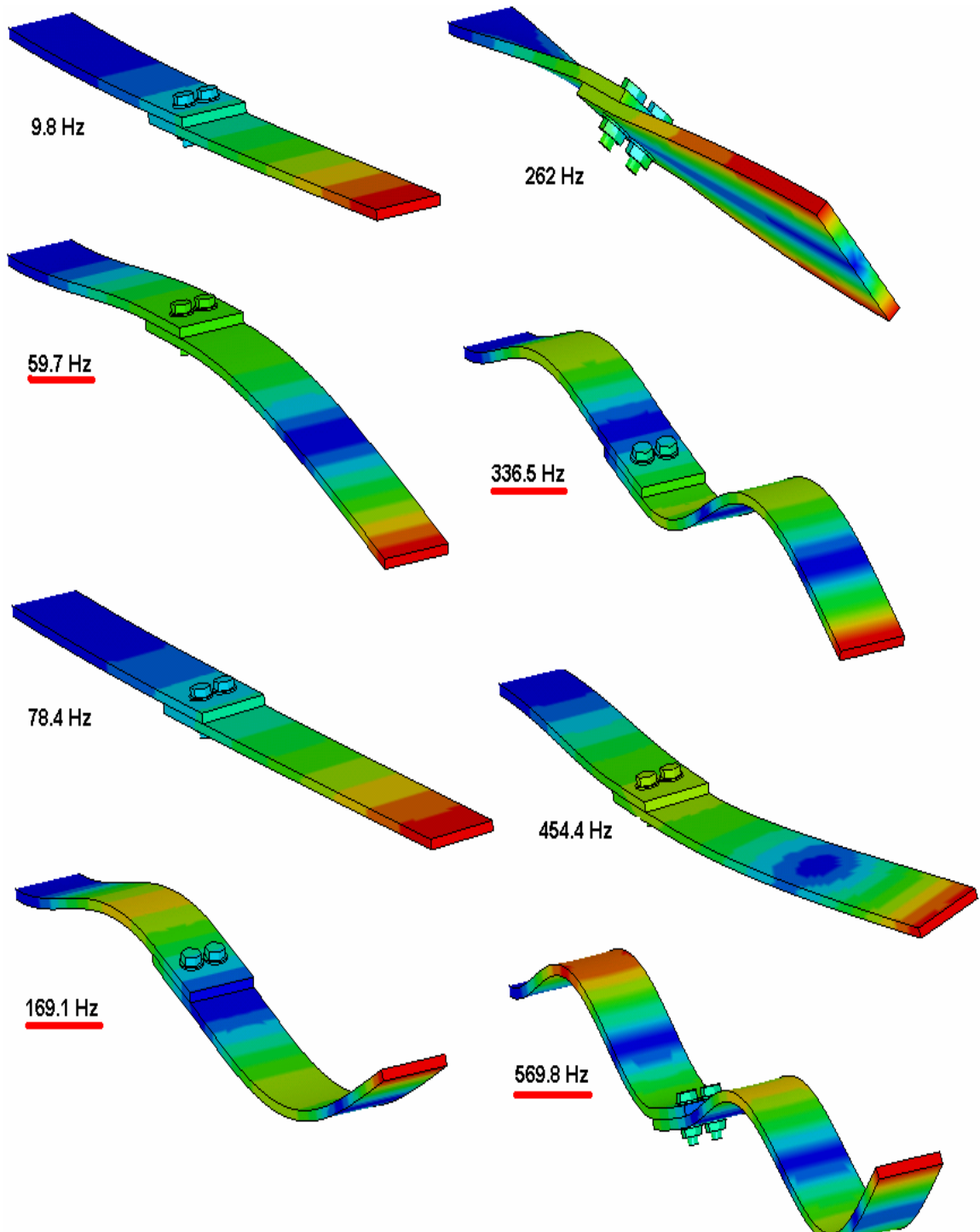


Figure 3.11 Mode shape and Natural frequencies of the cantilever beam with bolted lap joint using FE Model-2

Table 3-4 Natural frequency of the cantilever beam from experiment and FEA

Mode	Natural Frequency of Cantilever Beam From Experiment and FEA				
	Experiment		FEA		
	No-Joint Monolithic beam	Bolted Lap Joint	FE Model-1	FE Model-2	FE Model-3
1	61	53	60	60	60
2	168	168	172	169	171
3	328	320	338	337	339
4	542	526	559	570	576
5	816	794	836	814	821
6	1137	1106	1178	1219	1229
7	1335	1335	1414	1443	1455
8	1518		1549	1488	1506
9	1945	1907	2018	2077	2090
10	2411	2373	2503	2540	2548
11	2914	2823	3039	3057	3091
12	3571		3635	3612	3623
13	4227	3487	4366	4566	4616
14	4868		4891	4807	4850
15	5646	4837	5801	5886	5936
16	6416		6678	6796	6813

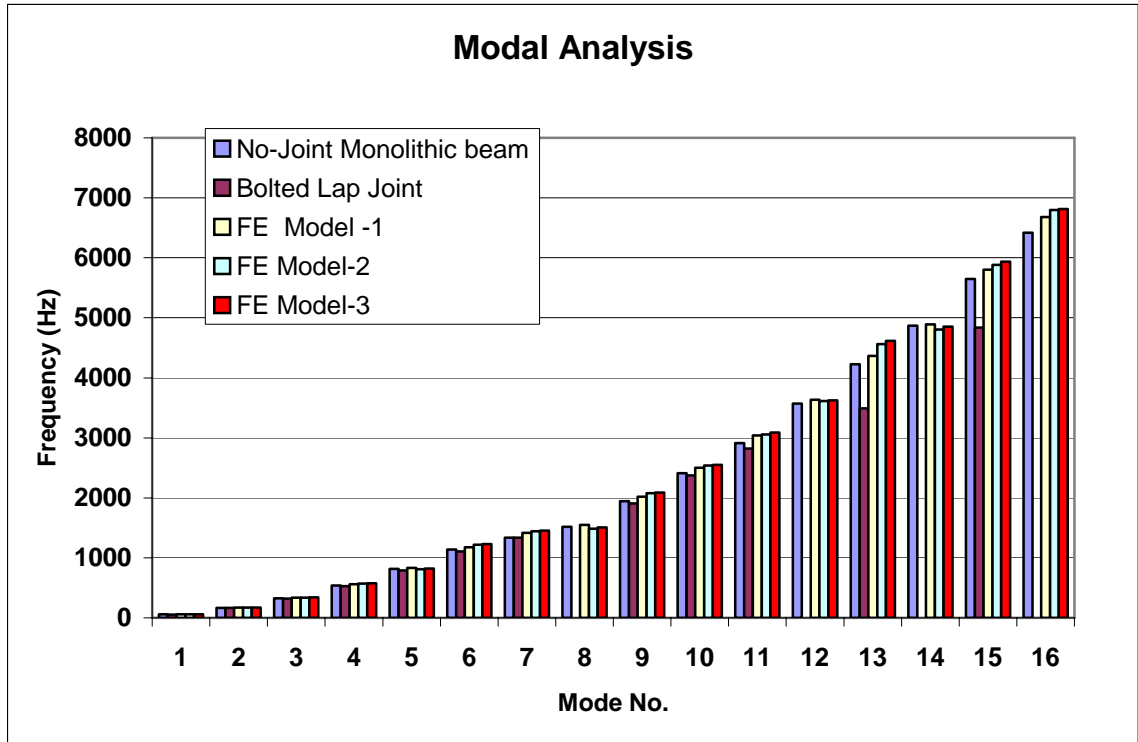


Figure 3.12 Natural frequency of the cantilever beam from experiment and FEA

### 3.5 FE simulation of impact analysis of the cantilever beam with bolted joint

The three FE models (Model 1, 2, 3) described in the previous sections were used to simulate the impact analysis on the cantilever beam with bolted joint. The procedure for experimental impact analysis on the bolted cantilever beam is explained in the previous chapter. The input force for the FE model was the force curve obtained from the experiment (by instrumented impact hammer). The oscilloscope records the force curve (Force time history), when the impact hammer strikes the beam. The force curve (Peak force –1680 N) from the experiment is shown in Figure 3.13, was used as input force in all the three FE models. The acceleration is measured at two points on the cantilever beam as shown in the Figure 3.8. The point ‘A1’ is before the joint (near fixed end of the

beam) and point 'A2' is after the joint (near free end of the beam). The force is applied on five nodes in the FE model so that it represents the actual area of the impact hammer tip.

Figure 3.14 is the Fast Fourier Transform (FFT) plot of the experimental and FE Model-1 time history response. The peaks in this plot are the natural frequencies of the bolted cantilever beam predicted from experiment and FE Model-1. The frequencies predicted from FE Model-1 are exhibiting higher magnitudes compared to experimental prediction especially at higher frequency ( $> 2000$  Hz). Damping was not included in the FE Model-1 and this is the reason for high magnitude response. Figure 3.15 is the acceleration plots (Time history response) from the simulation (Model-1) and is compared with the experiment. The acceleration values from the simulation show higher magnitude than the experiment values. The higher magnitude in the acceleration values in the FE simulation (FE Model-1) is because of the absence of inbuilt damping in the material model of the LS-DYNA solver. In the actual experiment, the bolted structure may dissipate energy by structural (joints) and material damping. Total energy (TE), kinetic energy (KE), internal energy (IE), and hourglass energy (HG) for the FE Model-1 is shown in Figure 3.16. The KE and IE energy remains steady through out the simulation, which indicates that the damping energy is zero. Even though the experimental response of the cantilever beam showed decay in the response, the FE response showed no decay. This concludes that the external damping should be included in the FE model. The FE Model-2 predicted similar high magnitude time history response as shown in Figure 3.17 to Figure 3.19. FE Model-3 with preload, contacts and friction showed very high magnitude time history response compared to experimental results as

shown in Figure 3.20 and Figure 3.21. The preload, contacts and the friction in the FE model didn't damp the response of the cantilever beam. The preload modeling in the FE analysis induces high frequency noises and these noises add to the beam response. The preload induced noises may not be significant in the high impact structural response

Normalized root mean square deviation (NRMSD) was used to quantify the experimental and FE results. Root mean square deviation (RMSD) is a frequently used measure of the differences between values predicted by a model and the values actually observed from the thing being modeled or estimated. RMSD is a good measure of accuracy. These individual differences are also called residuals, and the RMSD serves to aggregate them into a single predictive measure [57]. The NRMSD is the RMSD divided by the range of observed values.

$$RMSD = \sqrt{\frac{\sum_{i=1}^n (x_i - a_i)^2}{n}}$$

$$NRMSD = \frac{RMSE}{(x, a)_{\max} - (x, a)_{\min}}$$

where

$x = \text{Experimental Acceleration}$

$a = \text{FEA Acceleration}$

$n = \text{Number of points}$

Table 3-5 shows the NRMSD values for all the three FE models from the experimental results. The deviation of FE Model-1 time history response from experiment is 0.15 (A-1) and 0.17 (A-2) and whereas for FE Model-2 the deviation is 0.15 (A-1) and 0.19 (A-2). The FE Model-3 results show higher deviation from the experiment (0.21 and 0.24).

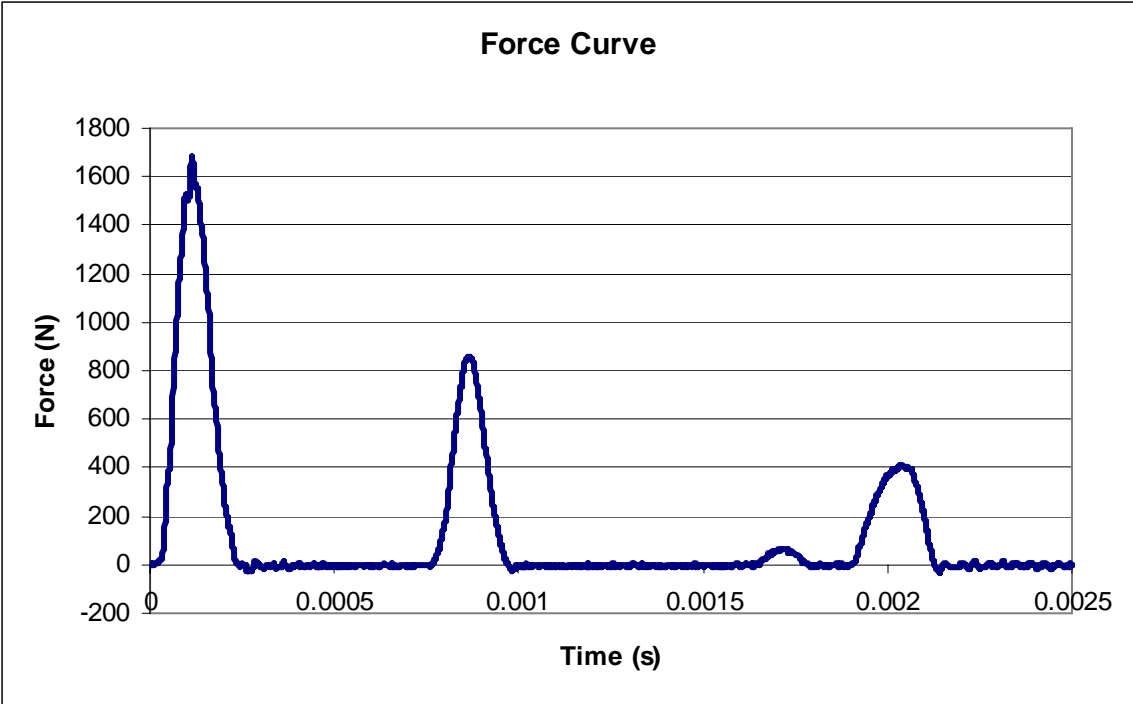


Figure 3.13 Experimental impact force curve used in FEA as input

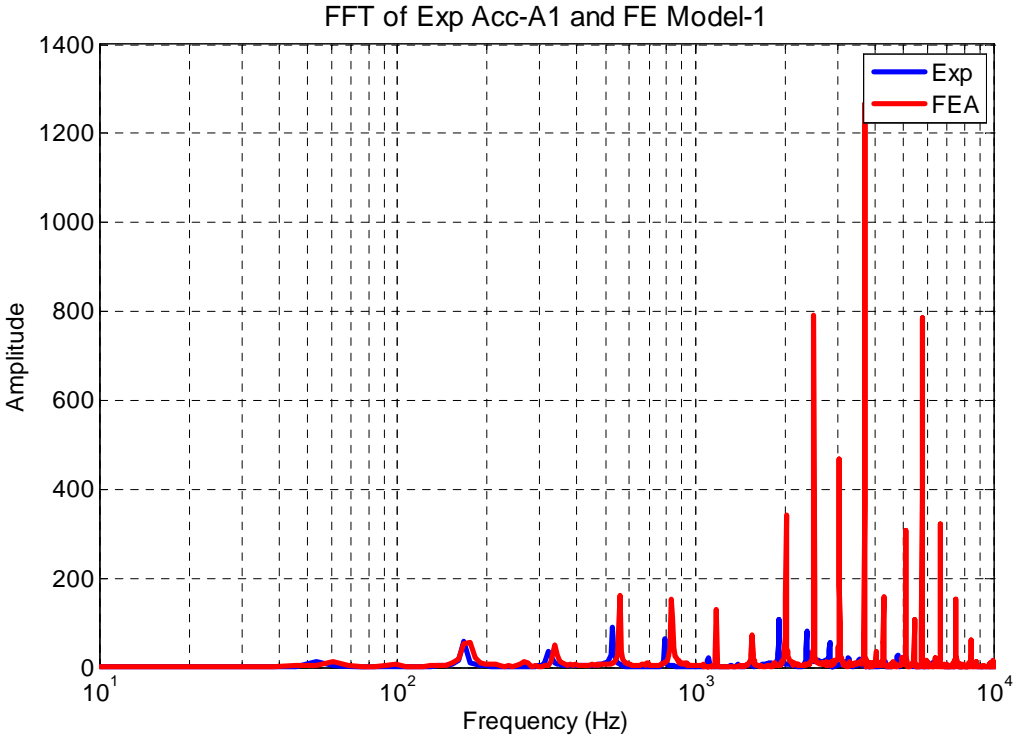


Figure 3.14 FFT from the experiment and FEA Model-1 (A1)

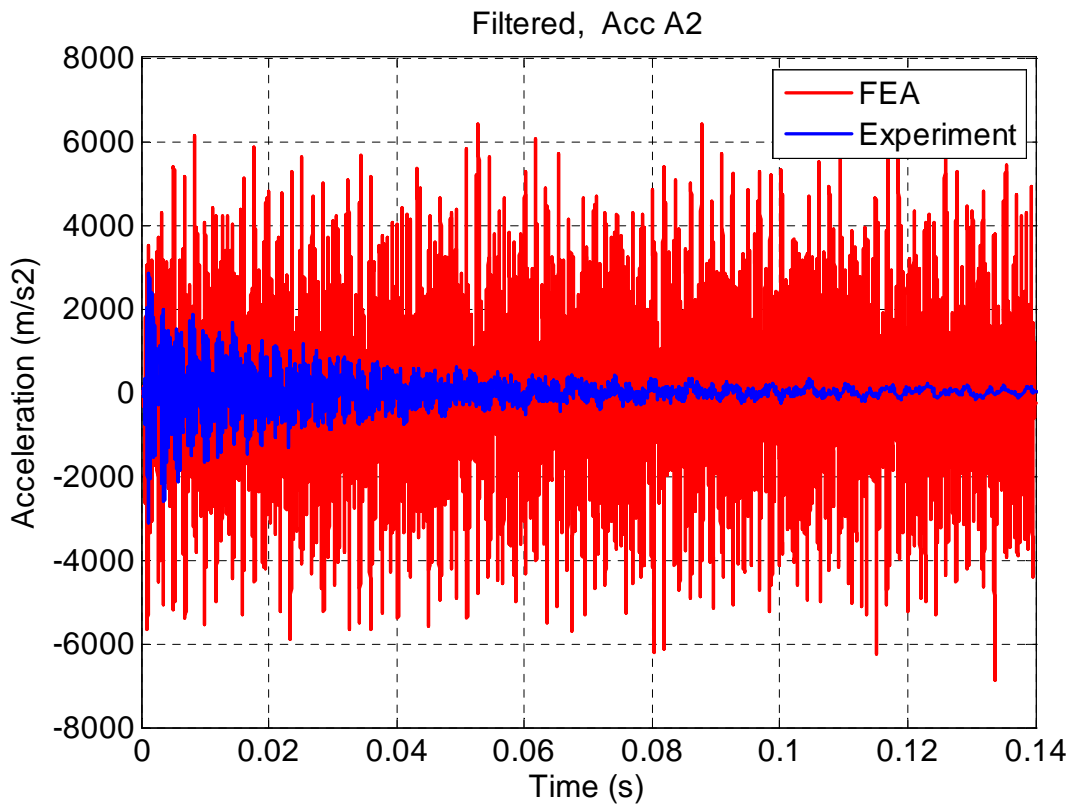
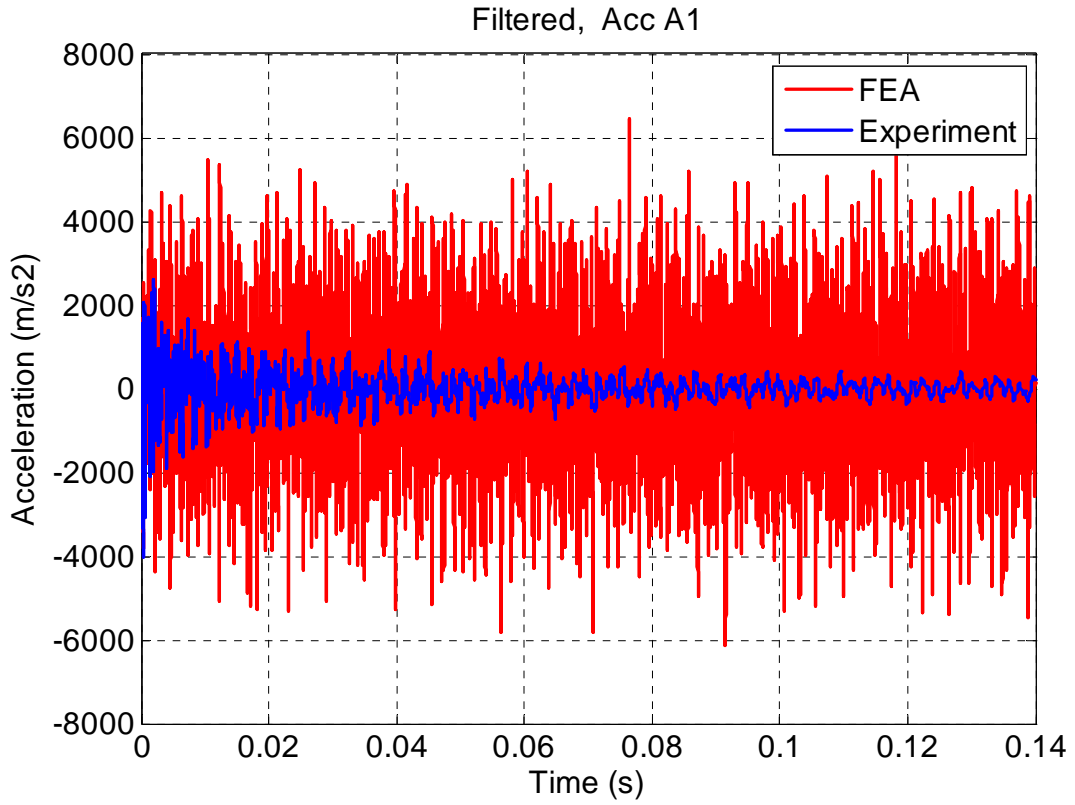


Figure 3.15 Experimental and FE Model-1, Time history response at point A1 and A2



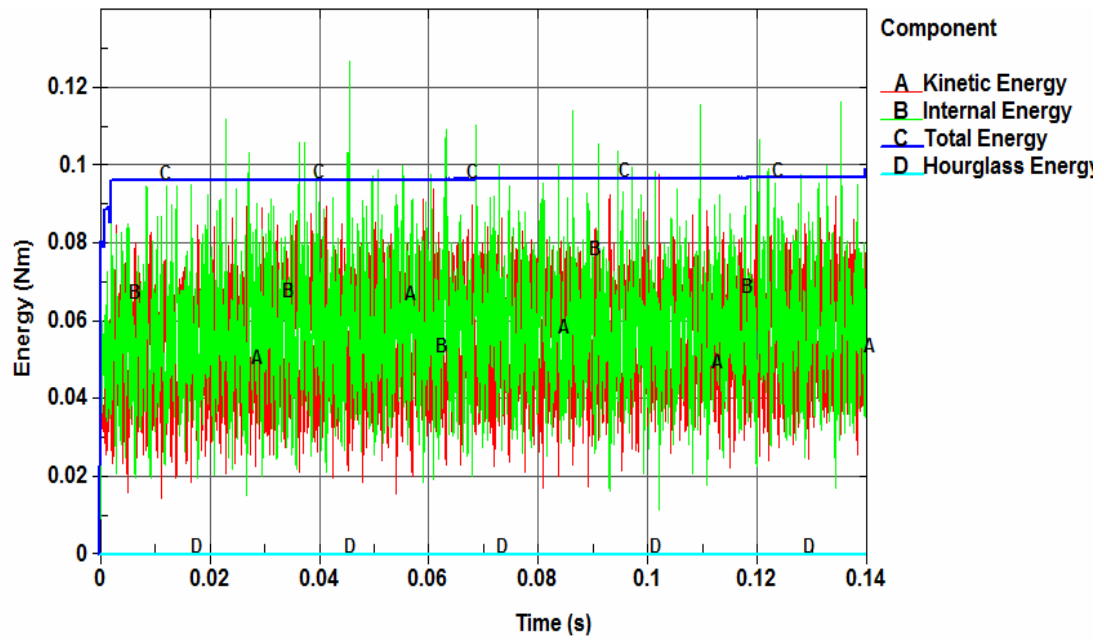


Figure 3.16 Energy plots for FE Model-1

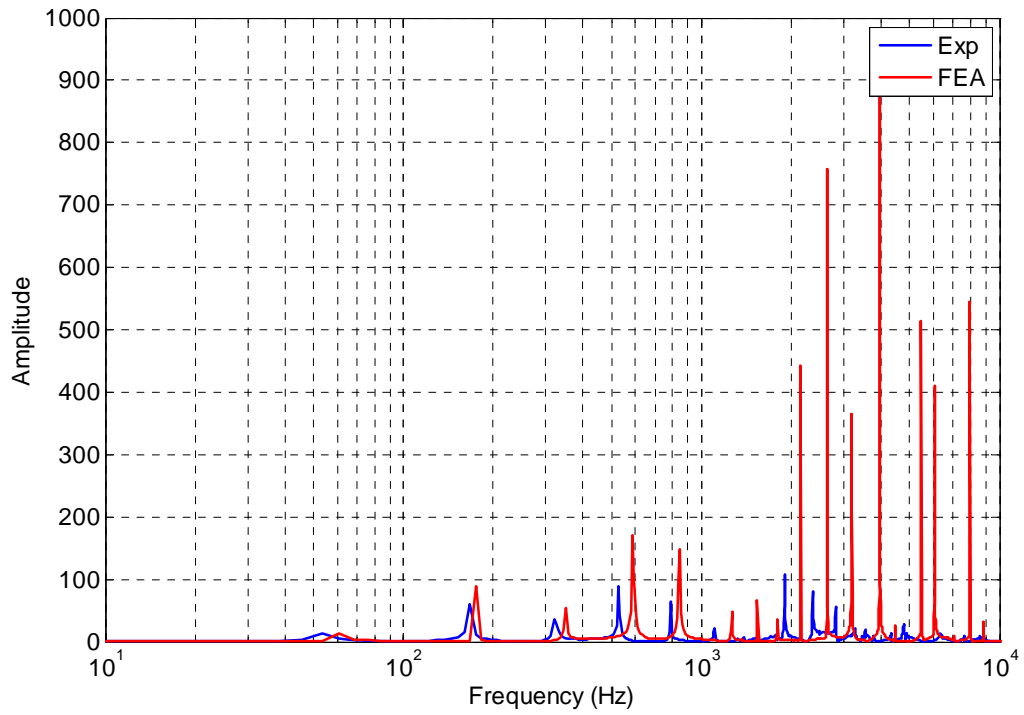


Figure 3.17 FFT from experiment and FE Model-2 (A1)

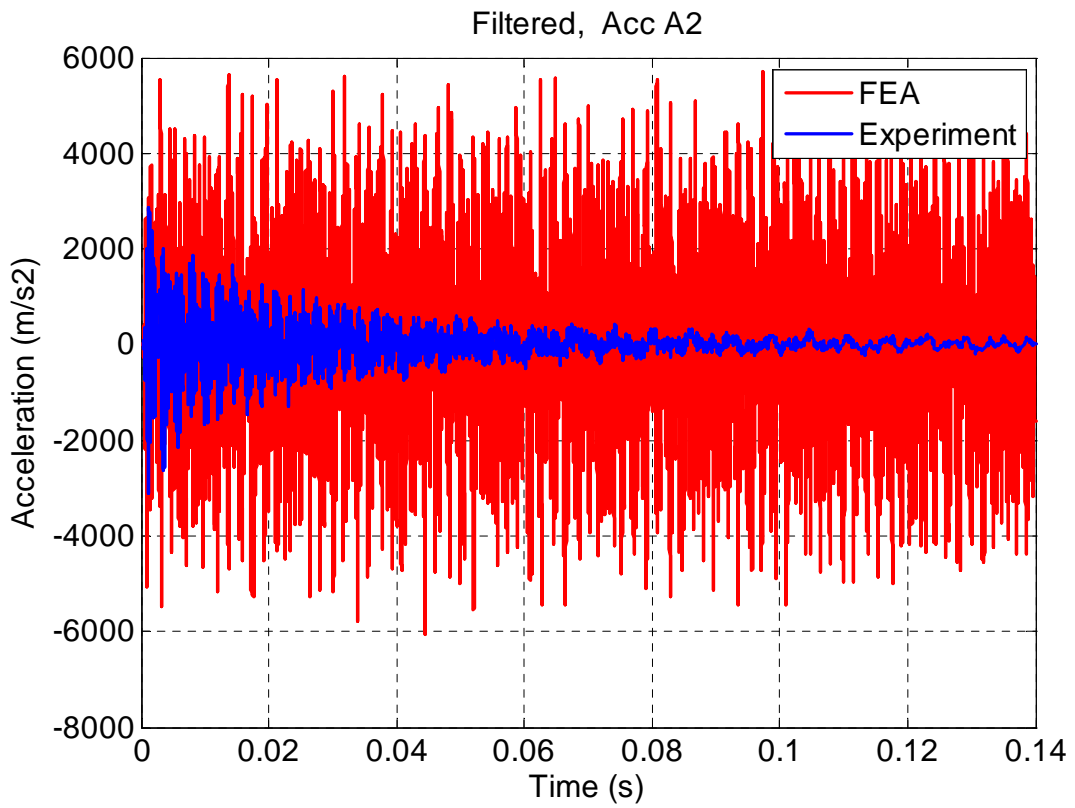
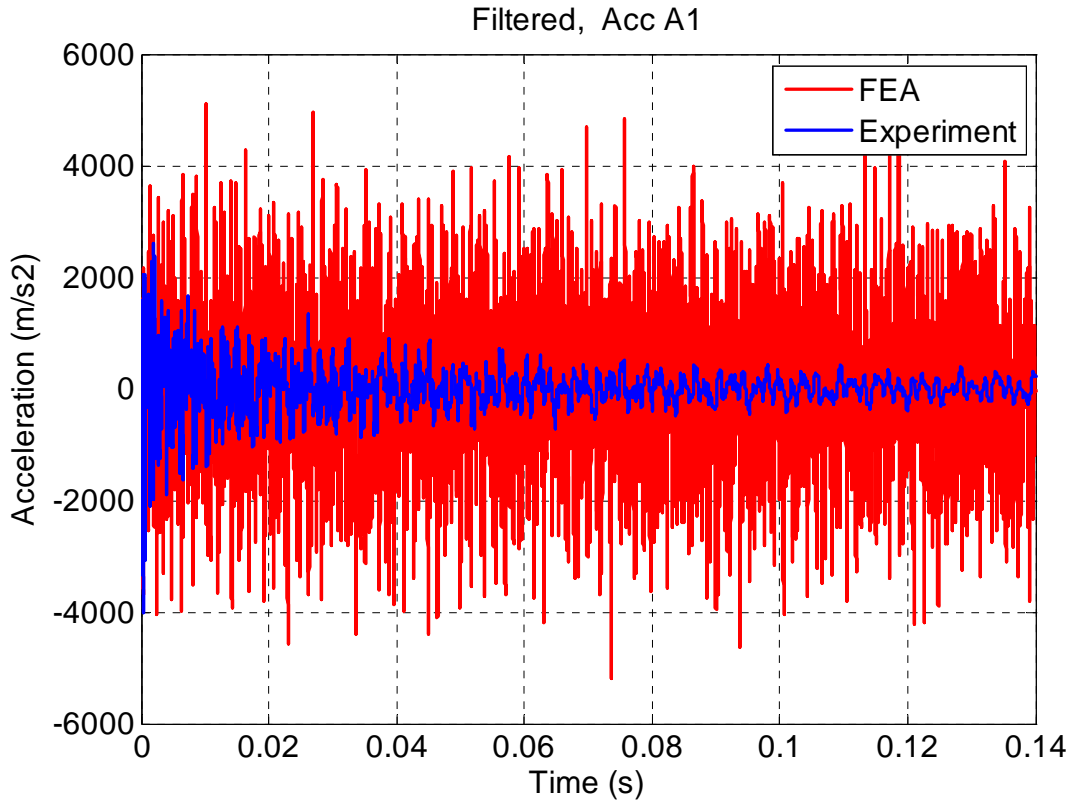


Figure 3.18 Experimental and FE Model-2 Time history response at points A1 and A2

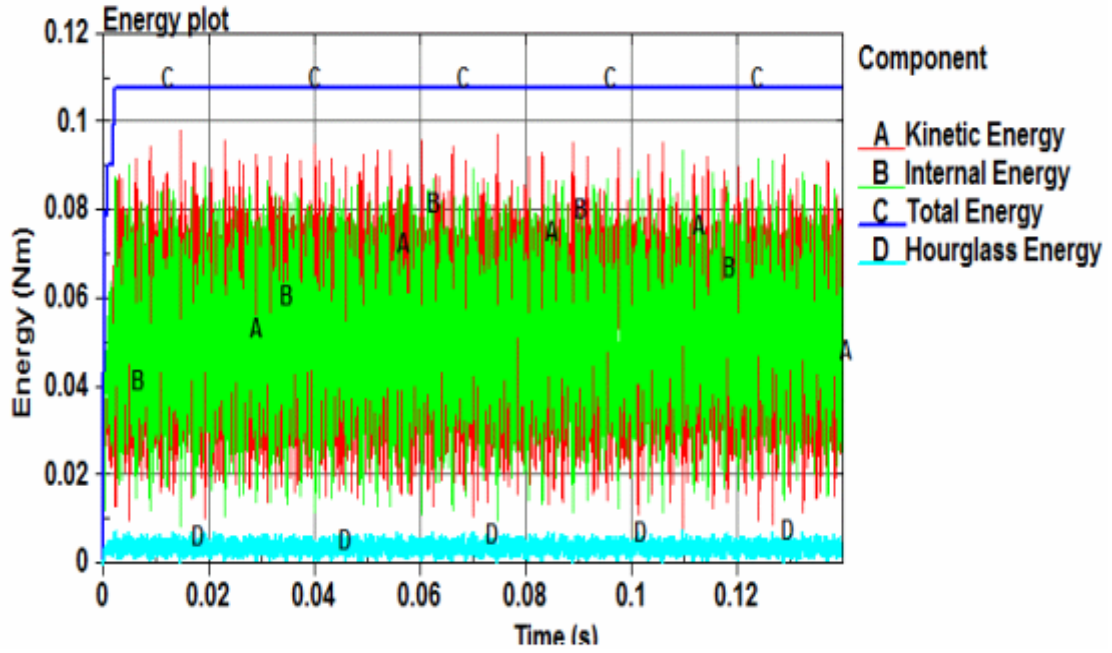


Figure 3.19 Energy plots for FE Model-2

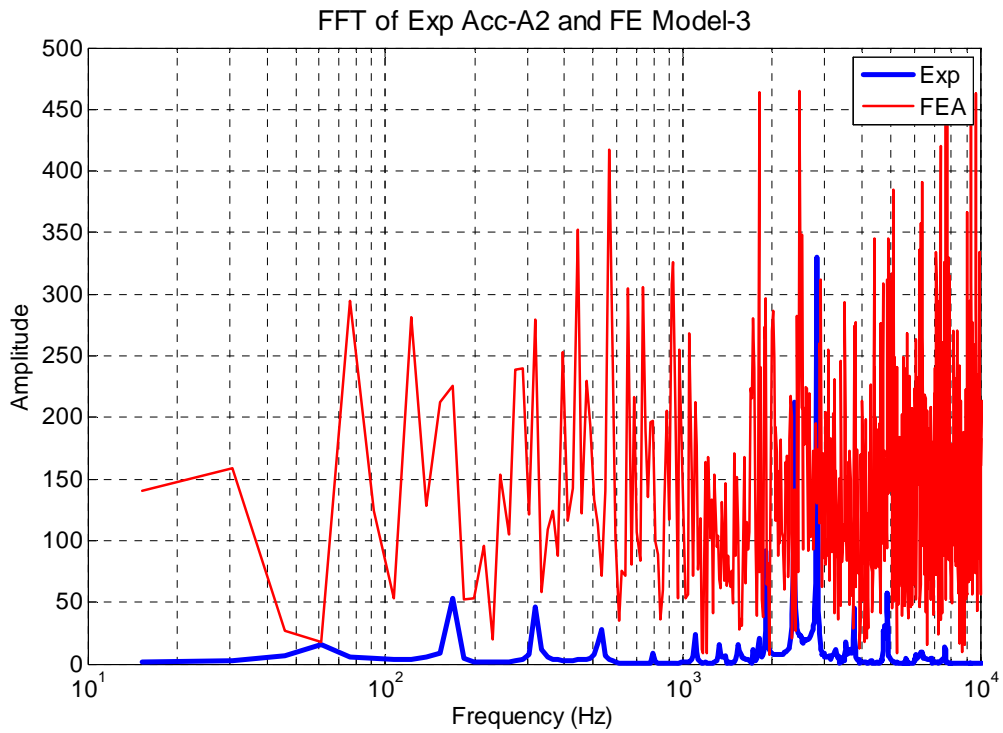


Figure 3.20 Experimental and FE Model-3 time history response at points A1 and A2

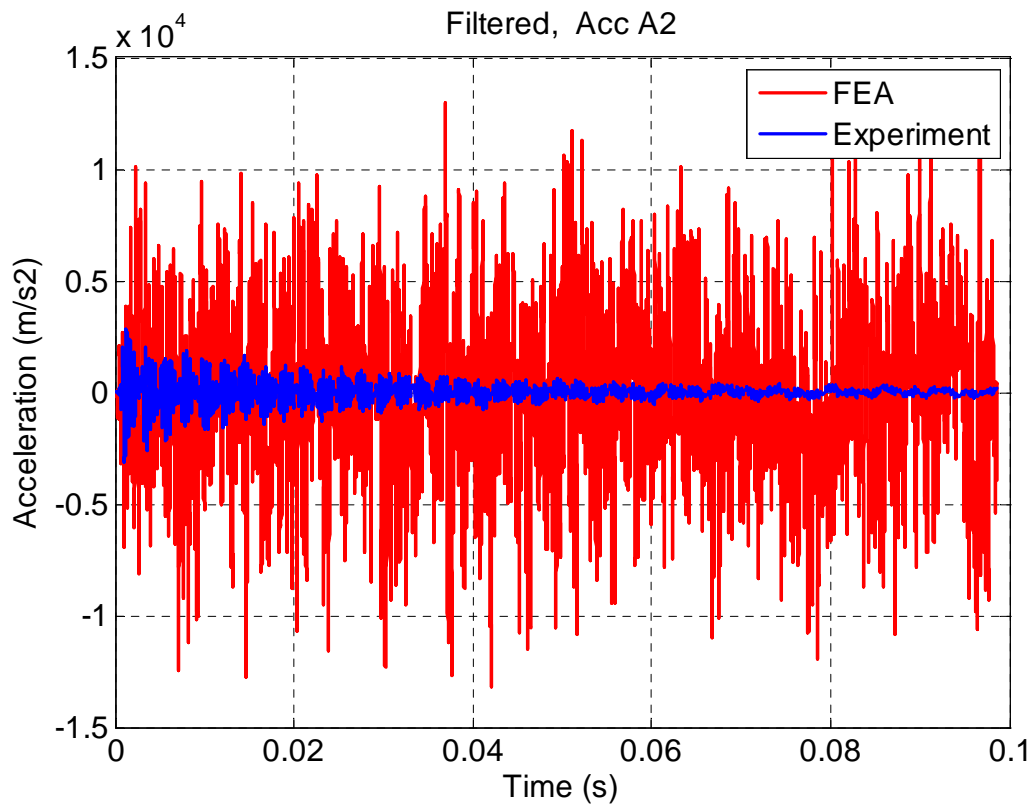
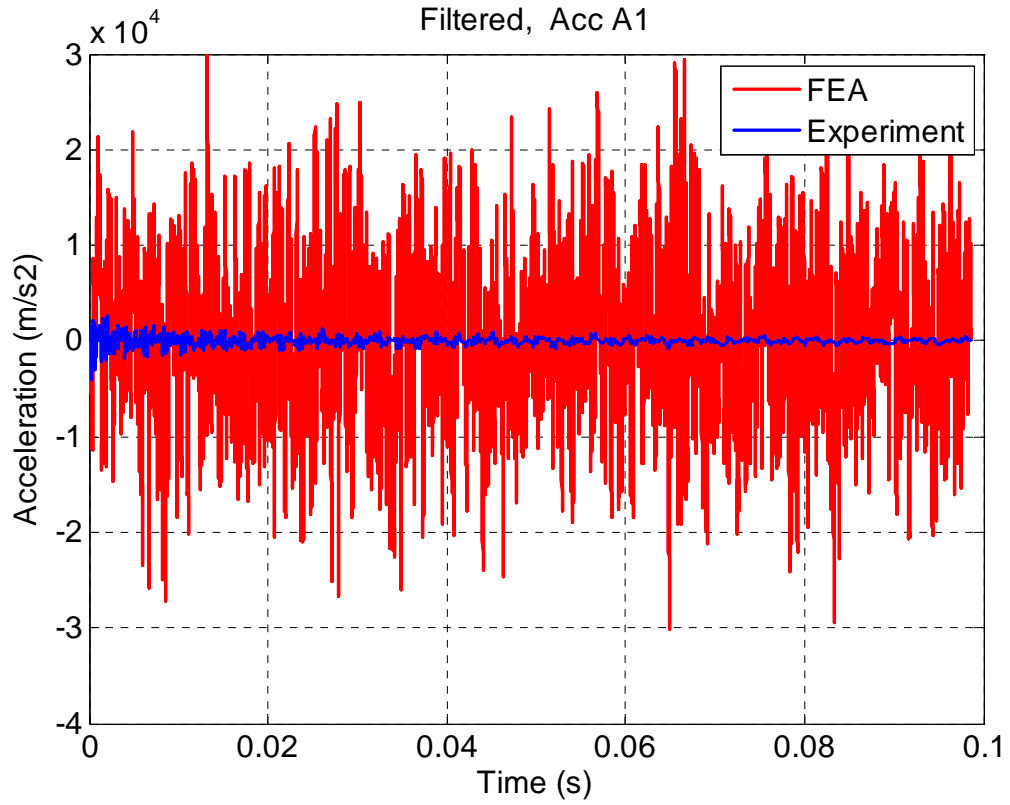


Figure 3.21 Experimental and FE Model-3 time history response at points A1 and A2

Table 3-5 NRMSD between experiment and FE model transient results

Normalized Root Mean Square deviation between Experiment and FE results		
FE Model	Experiment	
	Acceleration (A1)	Acceleration (A2)
FE Model-1	0.15	0.17
FE Model-2	0.15	0.19
FE Model-3	0.21	0.24

All the three FE models predicted high magnitude response when used for impact analysis. The main reason for high magnitude prediction by the FE models is because of the absence of the damping in the material models of the LS-DYNA solver. Even though the FE Model-3 was more accurate and realistic model with all the details defined, it didn't yield the best results. Along with the damping, there may be other factors, which can influence the FE results in the transient analysis. There is a need to understand each of these factors to accurately simulate the FE model. Some of the factors, which affect the FE results, are: Mesh density in the FE model, element type used (shell or solid), damping in the FE model, element formulation, Preload on bolt and Type of preload modeling. The effects of each of these factors will be studied in detail in the next section.

## 3.6 Parametric study of the FE model

### 3.6.1 Damping in the FE model

In all three FE models studied in the previous section, the acceleration curves from the FE simulation had higher magnitude and higher frequency than the corresponding experimental results. The loss of energy in the experiment is due to the system damping, which is mainly by the dissipation of energy at the joints and the material damping. These phenomena were not included explicitly in the FE model. The material models used in the LS-DYNA don't support any kind of material damping. Therefore the damping in the FE simulation needs to be externally defined. The FE model describes all kinds of material damping using Rayleigh damping. The Rayleigh damping defines the damping matrix C has

$$C = \alpha M + \beta K$$

where,

$\alpha, \beta$  = Mass and Stiffness Damping factor

M = Mass matrix

K = Stiffness matrix.

Therefore the damping matrix will be the linear combination of mass and stiffness matrices. While defining the damping matrix C, either M or K matrix can be used individually or a combination of both. The Rayleigh damping equation can also be written in terms of damping ratio ( $\xi$ ) as

$$\xi = \frac{\alpha}{2\omega} + \frac{\beta\omega}{2}$$

By assuming  $\beta=0$  in the damping ratio equation we get  $\xi = \frac{\alpha}{2\omega}$  and similarly assuming  $\alpha=0$ , we get  $\xi = \frac{\beta\omega}{2}$ . These expressions show that for mass proportional damping, the damping ratio is inversely proportional to the frequency while for stiffness proportional damping it is directly in proportion with the frequency [58]. Figure 3.22 shows the relation between the damping ratio and the frequency for Rayleigh damping.

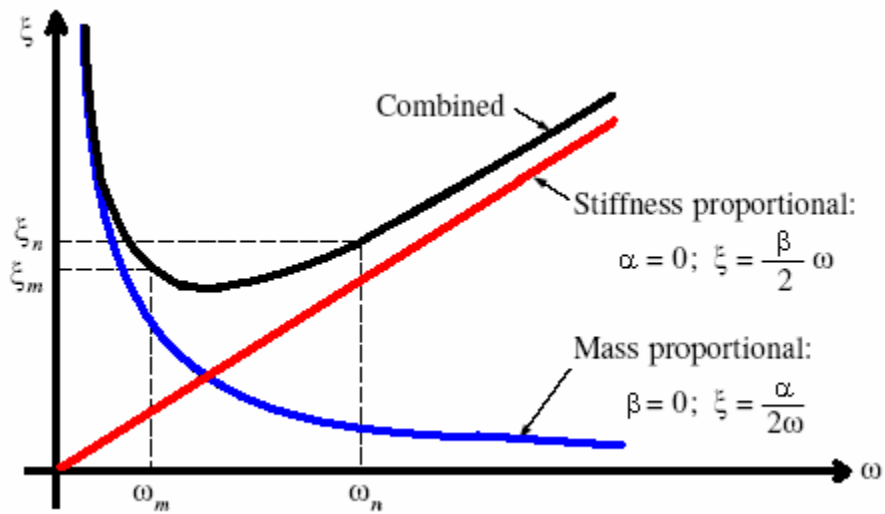


Figure 3.22 Relation between damping ratio and frequency for Rayleigh damping

### 3.6.2 Mass proportional damping

Mass proportional damping will damp both the rigid body motion and the vibration in the lower frequency range. The mass proportional damping can be used for the whole structure or for a certain part of the structure. Also it is possible to choose different damping coefficient for different parts in a same structure. When mass proportional is used in the equation of motion, the acceleration is computed as [1,2]

$$a^n = M^{-1} (P^n - F^n - F_{damp}^n)$$

$$F_{damp}^n = D_s m v$$

$$D_s = 2\omega_{\min}$$

where,

$M$  = Diagonal mass matrix

$P^n$  = External load vector

$F^n$  = Internal load vector

$F^n_{\text{damp}}$  = Force vector due to system damping

$D_s$  = Damping constant for the system which corresponds to critical damping

$\omega_{\min}$  = Fundamental natural frequency of the structure

The fundamental frequency of the structure can be determined from an Eigenvalue analysis or from the undamped transient analysis.

The response of the cantilever beam FE Model-1 for various mass proportional damping value is studied. Figure 3.23 shows the response of the FE analysis (FE Model-1) of the cantilever beam with bolted joint with different mass proportional damping factor. In LS-DYNA, the mass proportional damping factor ( $\alpha$ ) is defined as  $D_s$ , which is defined in terms of fundamental natural frequency and not as damping factor. The best mass proportional damping (MPD) factor is the critical damping factor for the lowest frequency mode of interest. Therefore the lowest natural frequency is defined for  $D_s$  ( $\alpha$ ). Three cases of MPD factor are studied using FE model-1 ( $D_s = 0, 10, 100$ ). For a mass proportional damping factor ( $D_s$ ) of 100, the magnitude of the acceleration reduced drastically and is close to zero from 0.06 seconds onwards. Figure 3.24 is the cutout of the acceleration plots from time 0.01 s to 0.02 s. When the mass proportional damping is added in the FE model, only the magnitude of the acceleration is reduced but the high frequency contents are not removed. Figure 3.25 shows the displacement plots for



damping factor of 100, 10 and no damping. As the damping factor increases, the magnitude of the displacement decreases and for the damping factor of 100 the cantilever beam is under damped and is very close to critically damped. The displacement curve for damping factor of 100 makes just one oscillation and it reaches the steady state as shown in Figure 3.25.

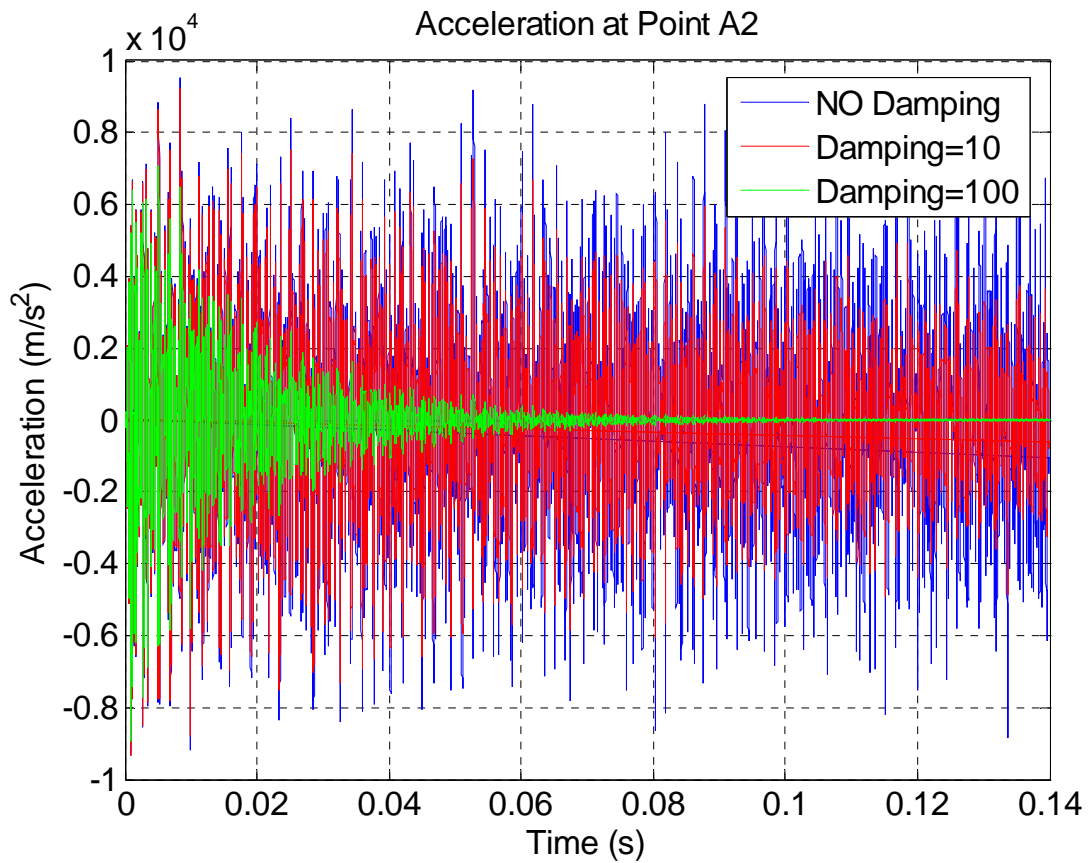


Figure 3.23 Influence of mass proportional damping at point A2 acceleration using FE model-1

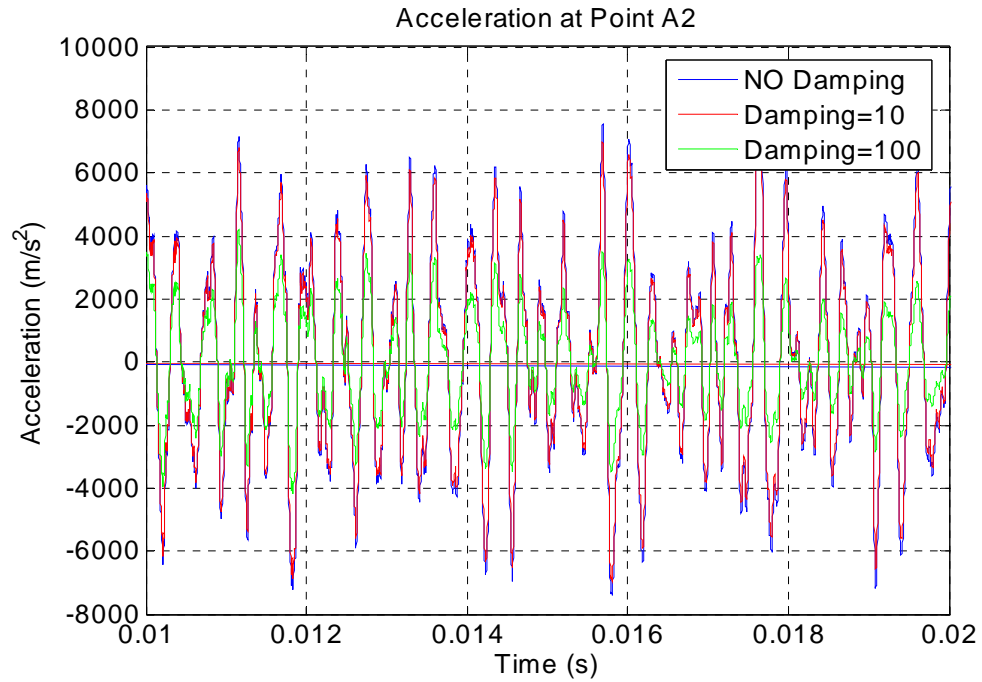


Figure 3.24 Cutout of the acceleration curves for mass proportional damping using FE model-1

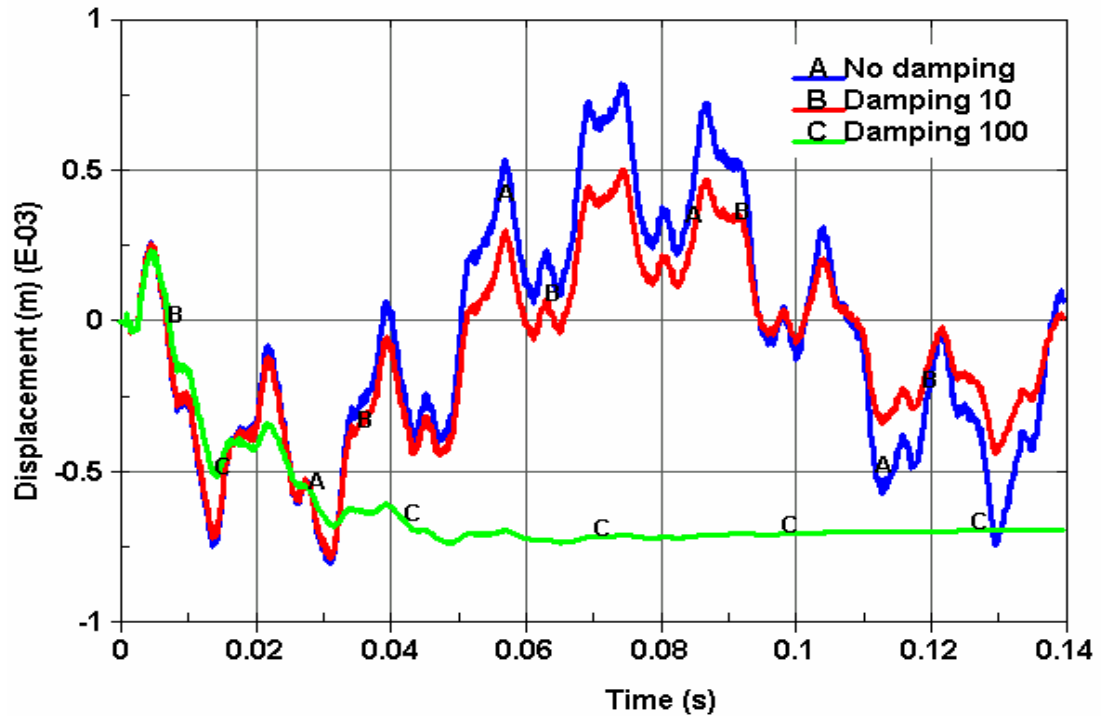


Figure 3.25 Influence of mass proportional damping at point A2 displacement using FE model-1

### 3.6.3 Stiffness proportional damping

Stiffness proportional damping (SPD) is effective for damping high frequencies and is orthogonal to rigid body motion. A Rayleigh damping factor ( $\beta$ ) for stiffness weighted damping of 0.1 to 0.25 are recommended [1, 2]. These values correspond to the 10% to 25% of damping in the high frequency domain. In LS-DYNA, the SPD factor ( $\beta$ ) is defined as 0.1 and 0.25 for 10% and 25% damping respectively. Also for higher values of damping factors the explicit time step needs to decrease significantly. Figure 3.26 shows the acceleration plots of the cantilever beam with bolted joint using shell elements (FE Model-1) for various damping factor. These plots correspond to 10% and 25% damping factor and are compared to results with no damping in the FE model. Figure 3.27 is the cutout of the acceleration plot and from this plot it is clear that the stiffness proportional damping, damps the high frequency contents in the time history. Fast Fourier Transform (FFT) of the acceleration curve is shown in Figure 3.24. Here it is clearly visible that the stiffness weighted damping, damps the higher frequencies.

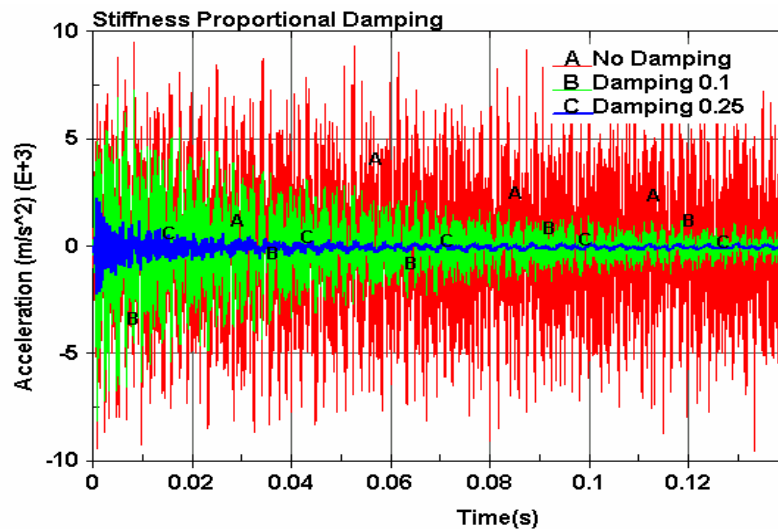


Figure 3.26 Influence of stiffness proportional damping ( $\beta$ ) at point A2 acceleration using FE model-1

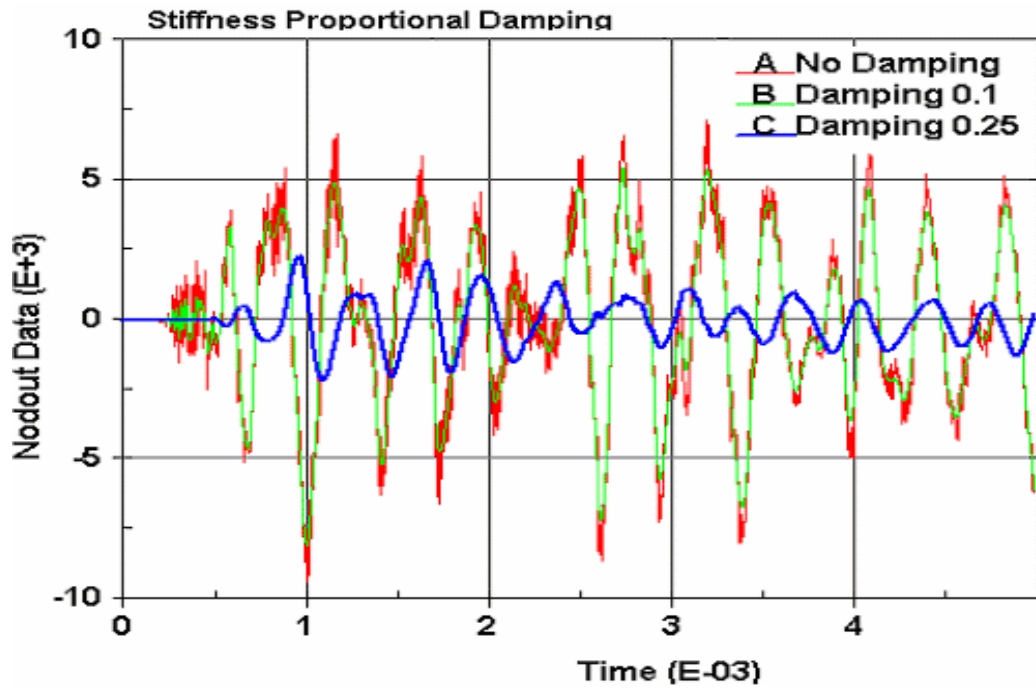


Figure 3.27 Cutout of the acceleration curves for stiffness proportional damping ( $\beta$ ) using FE model-1

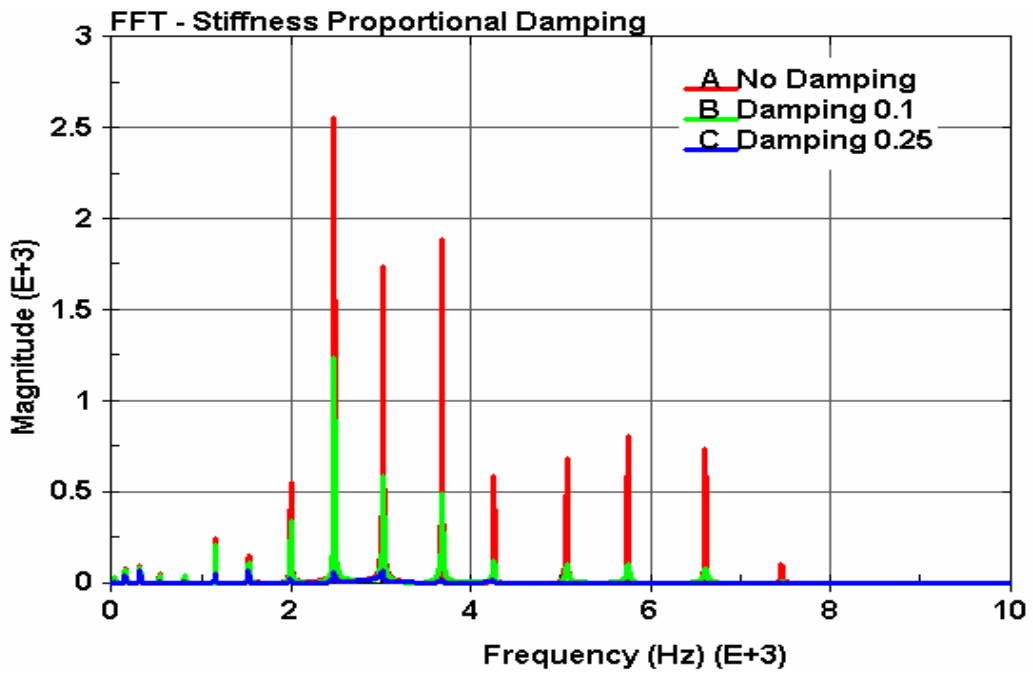


Figure 3.28 FFT for various stiffness proportional damping ( $\beta$ ) at point A2 using FE mode-1

### 3.7 Element formulation

Element formulation in Finite element analysis is an important factor that can influence the simulation results considerably. Also the run time and the efficiency of the computation are based on the element formulation. Figure 3.29 shows the number of integration points used for the under-integration (reduced) and fully integration shell element. The four-node plane element uses, 1-point and  $2 \times 2$  gauss quadrature rule for under-integration and fully integration respectively. Accuracy of integration can be increased, by using more integration points but more points may not increase the accuracy of the computed FE results. FE results may become more accurate if the order of quadrature is reduced [59]. The under-integration formulation (low order quadrature rule) may allow elements to have one or more spurious (hourglass) mode. The hourglass mode can be avoided by using fully integrated elements.

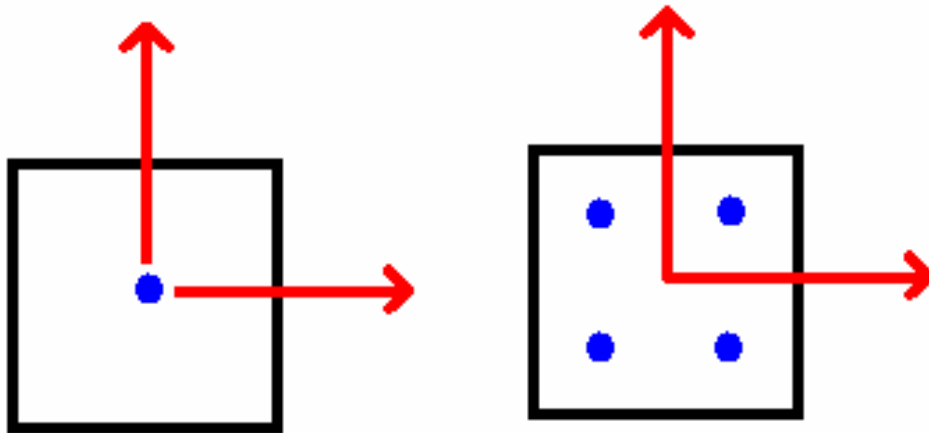


Figure 3.29 Under and fully integration points on the shell element

In order to investigate the influence of the element formulation on the simulation results, both the standard element formulation (Under integrated Belytschko-Tsay, Type-

2) and the fully integrated element formulation (Type-16) were used with shell element FE Model-1 of the cantilever beam with bolted joint. The FE model used for both the element formulation was identical and nothing was changed in the FE model except the element formulation. This will ensure that the differences in the results can be associated exclusively to the element formulation.

Figure 3.30 is the acceleration plot from the shell FE Model-1 with fully integrated (Type-16) and under-integrated (Belytschko-Tsay Type-2) element formulations. Both frequencies and magnitude of the time history response are similar for the fully integrated element formulation and the under-integrated element formulation with hourglass control. The fully integrated element takes about three times the computation time of under integrated elements. Based on the above results the fully integrated element formulation can be avoided in the transient analysis and the under-integration element formulation can be used with hourglass control. The under-integrated element formulation induces numerical damping by increasing the hourglass energy, which damp the response of the structure. This can be avoided by adding hourglass control in the explicit FE analysis. The hourglass deformation modes are orthogonal to the strain calculations, work done by the hourglass resistance is neglected in the energy equation [1, 2]. The Flanagan-Belytschko hourglass control method resists components of the velocity field that are not part of a fully linear field, which is also known as hourglass velocity field. With these vectors they resist the hourglass velocity deformations.

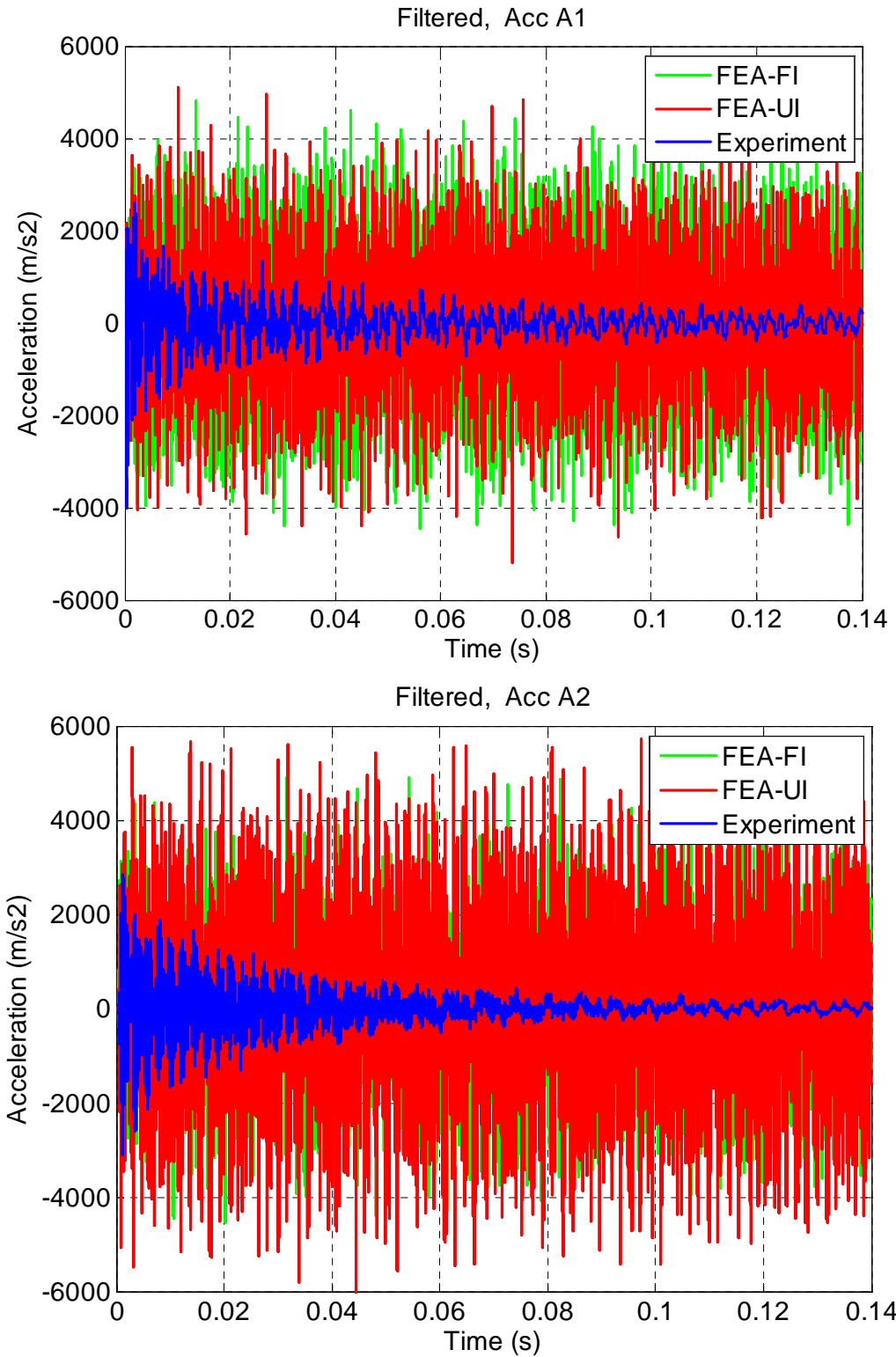


Figure 3.30 Comparison of fully integrated and constant stress element formulation for the shell element FE model-1

### 3.8 Preload (pre-stress) modeling for explicit analysis

Modeling pre-stress on the bolted joints in LS-DYNA can be done in several ways. Six pre-stress modeling techniques are discussed in this chapter for explicit FE analysis. These techniques can be used in other applications to preload or pre-stress the structures. These techniques are

- Applying force on the bolt and nut
- Applying force on the bolt shank
- Modeling interference fit between nut and plate
- Applying thermal gradient on the bolt shank
- Using INITIAL\_STRESS\_SOLID card in LS-DYNA
- Using INITIAL\_STRESS\_SECTION card in LS-DYNA

Dynamic relaxation (DR) is a damping technique in LS-DYNA. The DR damps the initial kinetic energy generated during the pre-stressing of the structure. Dynamic relaxation allows an explicit solver to conduct a static analysis by increasing the damping until the kinetic energy drops to zero [1, 2]. When an implicit solver is used to provide the preload, a slightly different approach is taken, in that the stress initialization is based on a prescribed geometry (i.e., the nodal displacement results from the implicit solution). In this latter case, the explicit solver only uses 101 time steps to apply the preload. In the former case, the solver will check the kinetic energy every 250 cycles (by default) until the kinetic energy from the applied preload is dissipated. Dynamic relaxation is activated by the SIDR variable in DEFINE\_CURVE card. Dynamic relaxation cannot damp all the initial kinetic energy from the preload. Therefore external damping needs to be introduced in the FE model to completely damp any unwanted energy.



### 3.8.1 Applying force on the bolt and nut

LS-DYNA solver has two analysis techniques to solve dynamic problems – Implicit and Explicit analysis. When the loading is not periodic or is suddenly applied we seek the transient response, which is also known as response history [59]. Solution requires that the differential equation of motion be integrated in time. If loading excites only a few of the lowest frequencies and response must be calculated over a time span equal to several multiples of the longest period of vibration, as in the case for earthquake loading, an implicit method of direct integration can be used. If loading excites many frequencies and response must be calculated for no more than a few multiples of the longest periods, as in the case for impact loading, explicit direct integration may be used.

The LS-DYNA card, CONTROL\_IMPLICIT\_GENERAL has an option of switching from implicit to explicit analysis or vice versa. The preload force is applied on the bolt and nut during implicit analysis and then the LS-DYNA solver is switched to explicit analysis for transient impact analysis. The preload force is applied on the bolt and nut of the cantilever beam FE Model-3 as shown in Figure 3.31. The preload force is applied on the nodes along the axial direction of the bolt. The preload force increases linearly to reach final preload value for 1 millisecond and then is constant throughout the simulation. The constant force gives the required preload in bolted joint. By varying this force the required preload on the bolt shank can be obtained. The pre-stress on the bolt is proportional to applied force. The pre-load is applied on the bolt and nut during implicit analysis. The force applied on bolt and nut during implicit analysis is continued in explicit analysis. Figure 3.32 shows the cross section of bolt assembly with preload. There is a uniform stress along the bolt shank.

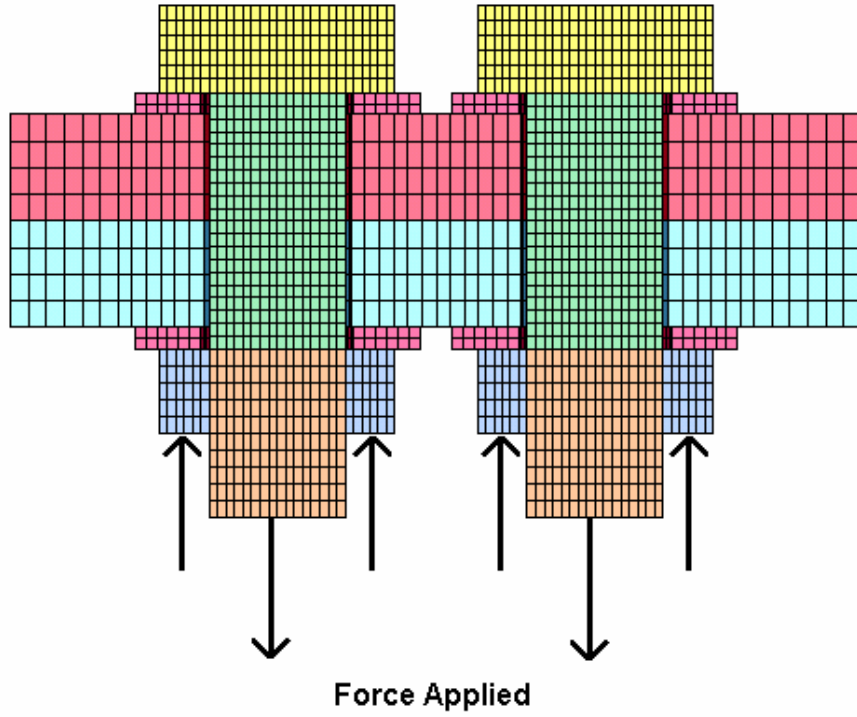


Figure 3.31 Bolt assembly of the cantilever beam (FE model-3) with preload force applied

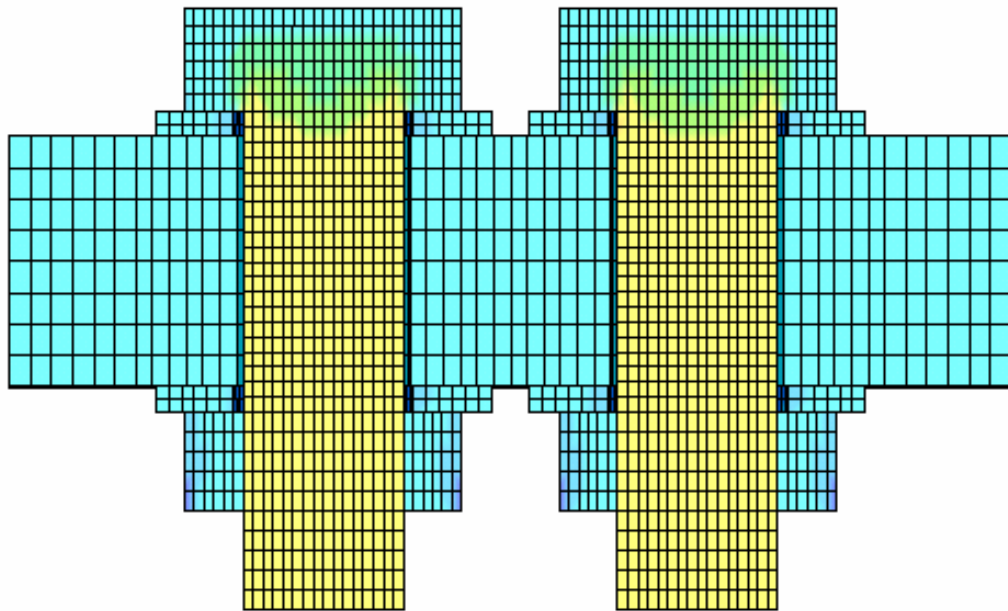


Figure 3.32 Bolt assembly of the cantilever beam with pre-stress

### 3.8.2 Applying force on the bolt shank

This method is similar to the previous method and the only difference is that instead of applying force on the bolt end and nut, here the bolt shank is split at the center and the force is applied on the split face as shown in Figure 3.33. The force applied on the two faces of the shank is equal and opposite. In this FE model, there is no continuity in the bolt shank.

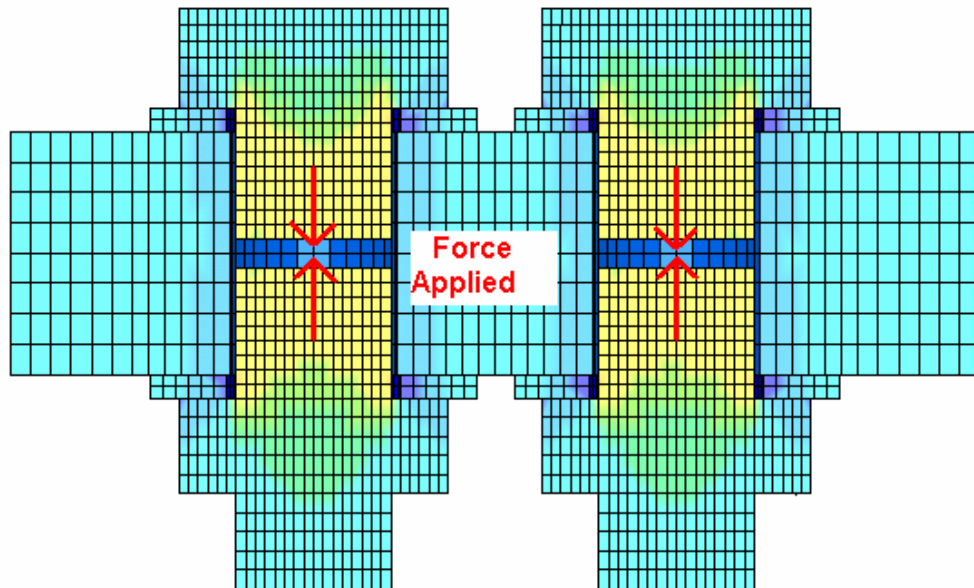


Figure 3.33 Bolt assembly with split bolt shank and pre-stress

### 3.8.3 Modeling interference fit between nut and plate

This is another easy way of defining the pre-load in the bolted joint for the explicit FE analysis. Here the bolt head and nut are modeled in such ways that, the bolt head mesh initially penetrates into the washer mesh as shown in Figure 3.34. \*CONTACT\_SURFACE\_TO\_SURFACE\_INTERFERENCE card is defined between

the penetrating meshes. This type of contact is used for defining interference fit between parts. When LS-DYNA starts solving this problem, it recognizes the penetration between parts and separates the bolt head and nut from the washer. This separation (elongation of bolt) induces the required preload in the bolt assembly. The elongation of the bolt (preload) during the explicit analysis is proportional to the depth of penetration. This method also uses the implicit analysis for initial elongation of bolt and explicit solver to continue transient impact analysis. Dynamic relaxation needs to be used for this problem to eliminate the induced initial kinetic energy.

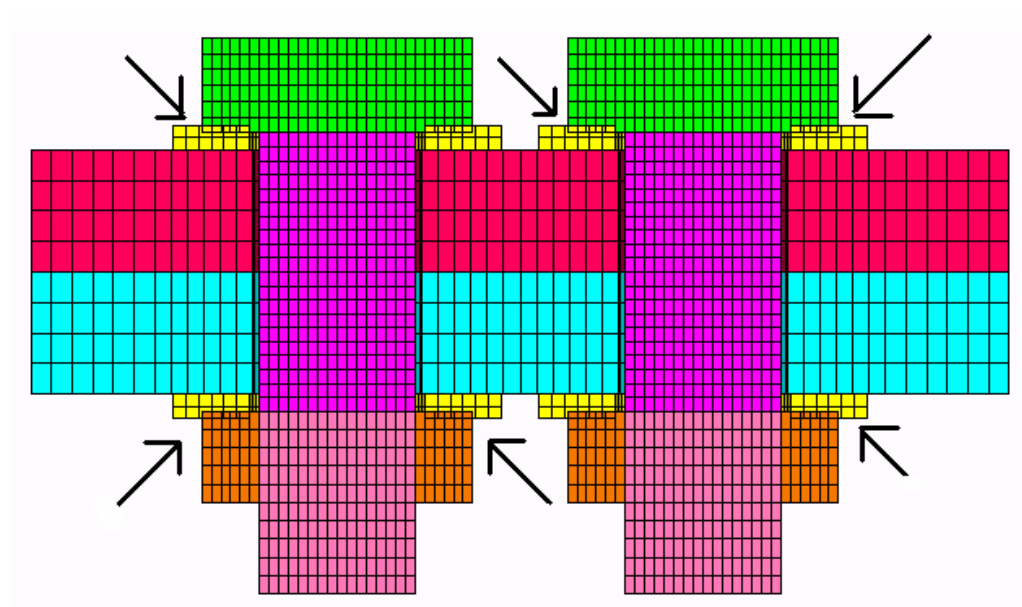


Figure 3.34 Bolt assembly of the cantilever beam (FE model-3) with interference fit

#### 3.8.4 Applying thermal gradient on the bolt shank

This is the widely used technique for modeling pre-load in static FE analysis and this technique is altered to suit for explicit FE analysis. This technique is better understood by

considering a simple statically indeterminate beam as shown in Figure 3.35. This beam is divided into three parts. The part-1 and part-3 are made of same material and part-2 is made of thermal material. The two ends of the beam are constrained which makes it as a statically indeterminate problem. The thermal stress is induced only in statically indeterminate structure when the temperature is varied. If the ends of the beam are not constrained then it becomes statically determinate problem and when the thermal gradient is applied in the beam, only thermal strains are induced and not the thermal stress (preload).

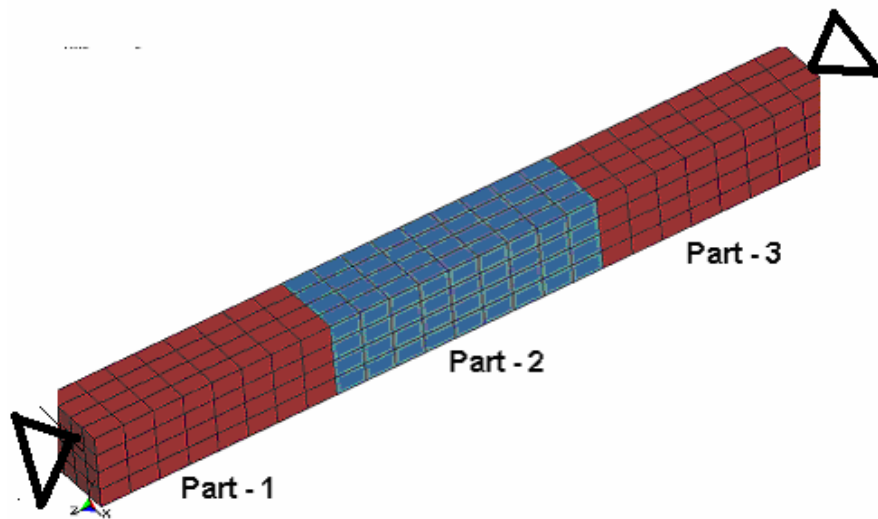


Figure 3.35 Three beams with thermal material at the center

Thermal strain is calculated by the following equation.

$$\varepsilon = \alpha \Delta T$$

Thermal stress is calculated as

$$\sigma = E \varepsilon = E \alpha \Delta T$$

where

$E$  = Elastic modulus

$\varepsilon$  = Strain

$\alpha$  = Thermal expansion coefficient

$\sigma$  = Thermal stress

$\Delta T$  = Temperature gradient

In the above equation ‘E’ and ‘ $\Delta T$ ’ are constant. Therefore the thermal stress (preload) is proportional to the temperature gradient. To model the pre-load in the beam (Figure 3.35), the temperature of the Part-2 is decreased from the reference temperature i.e., the part-2 is made to shrink. The shrinking of part-2 induces the tensile stress in the beam. The LS-DYNA material card MAT\_ELASTIC\_PLASTIC\_THERMAL is used for defining the temperature dependent material property for part-2 in the beam. Along with this card, LOAD\_THERMAL\_LOAD\_CURVE is used for defining the temperature vs. time curve. Two temperature vs. time curves need to be defined for the above LS-DYNA card. One curve is used for Dynamic Relaxation, where the temperature is increased from reference temperature to the maximum temperature. The other curve will have a constant maximum temperature. These two curves are shown in Figure 3.36.

Dynamic relaxation is carried out before the explicit analysis in LS-DYNA. During Dynamic relaxation the temperature is applied on the part-2 linearly and the kinetic energy induced due to the deformation of the beam is dampened. After dynamic relaxation the explicit analysis is carried out. Figure 3.37 shows the Von-mises stress on the beam during the explicit analysis. Figure 3.38 shows the stress vs. time plot for three elements on the beam. During the explicit analysis, at time  $t = 0$ , the maximum stress has been reached on the beam and the stress on the beam remains constant through out the simulation.

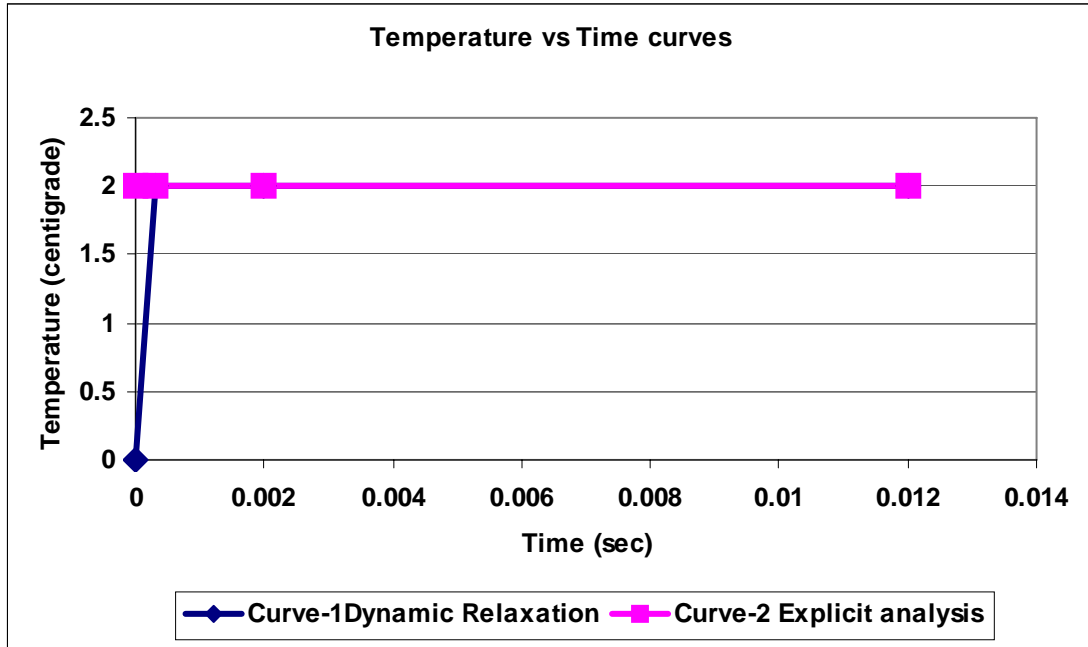


Figure 3.36 Two Temperature curve for defining preload in the beam

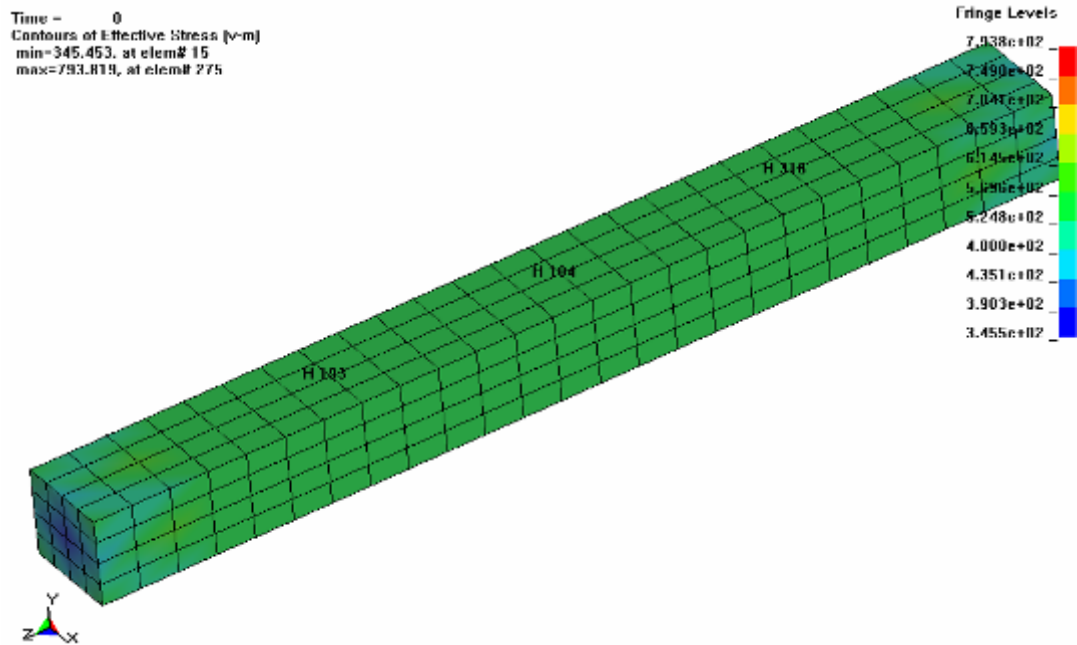


Figure 3.37 Constant Von-Misses stress in the beam due to thermal gradient

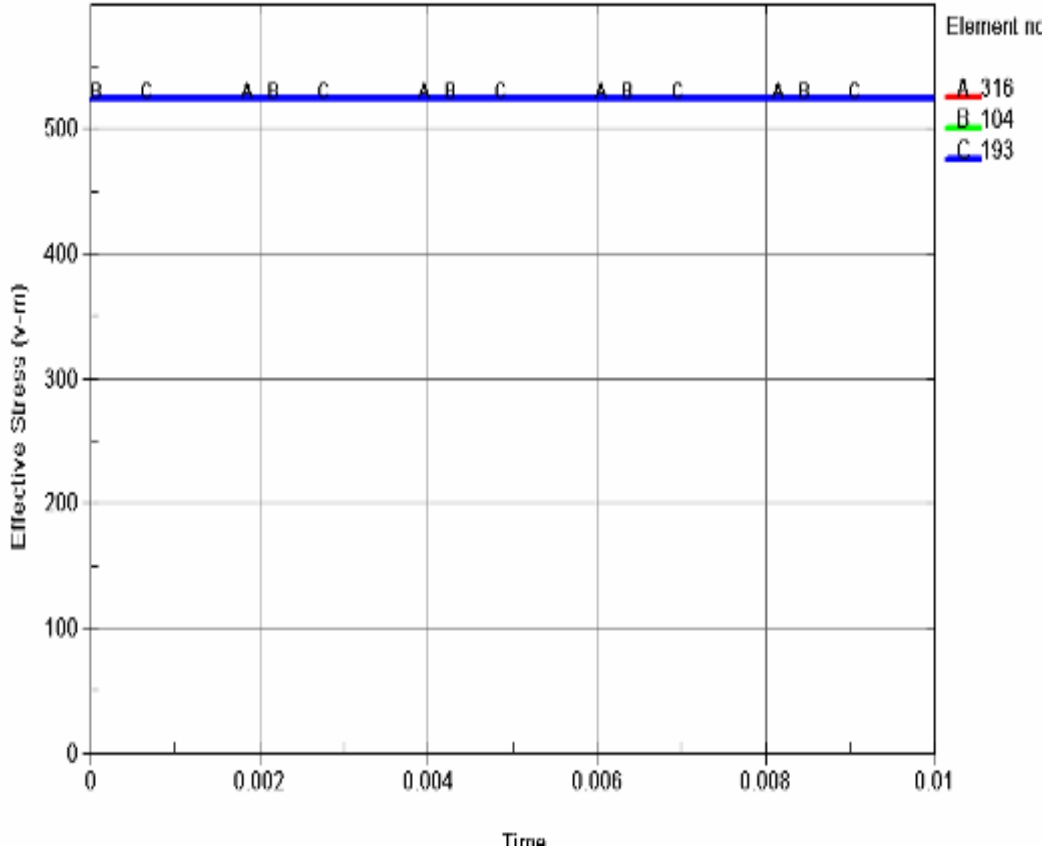


Figure 3.38 Constant stress on the beam during the transient explicit analysis

The above-mentioned procedure for modeling preload using thermal gradient technique is repeated for FE model-3 of the cantilever beam with bolted joints. For bolted joint FE model, the temperature gradient was applied on the bolt shank (between the bolt head and nut) as shown in Figure 3.39. Figure 3.40 shows the constant pre-stress (preload) on the bolt assembly at the end of the explicit FE analysis. The advantage of this method of getting pre-stress in bolted joints is that the temperature is a scalar quantity and does not depend on the direction.



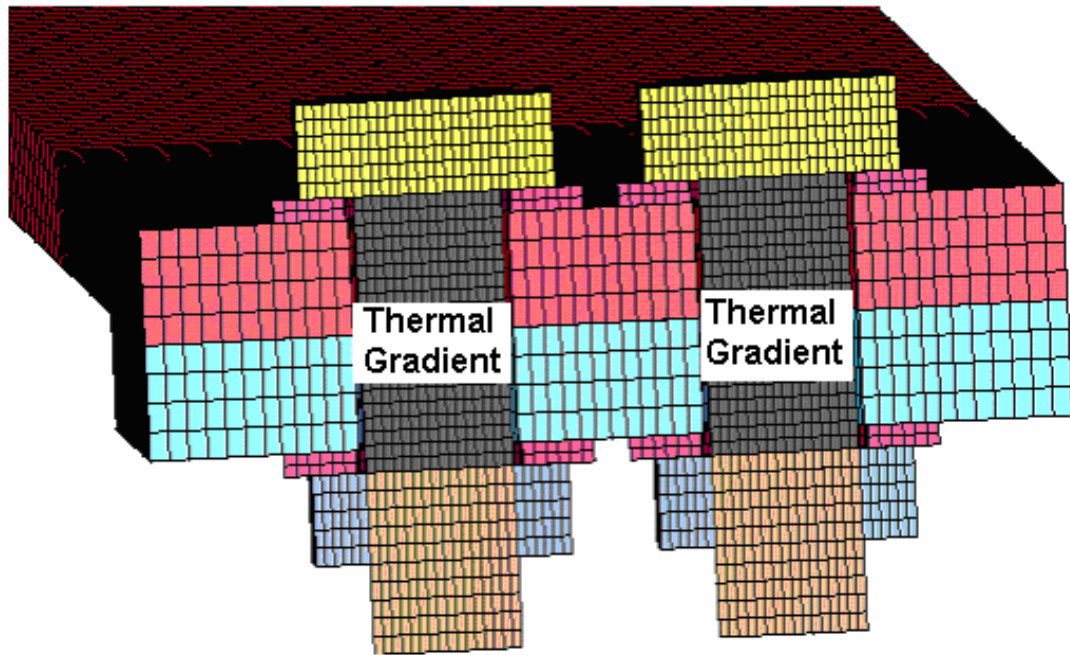


Figure 3.39 Bolt assembly with thermal gradient on the bolt shank

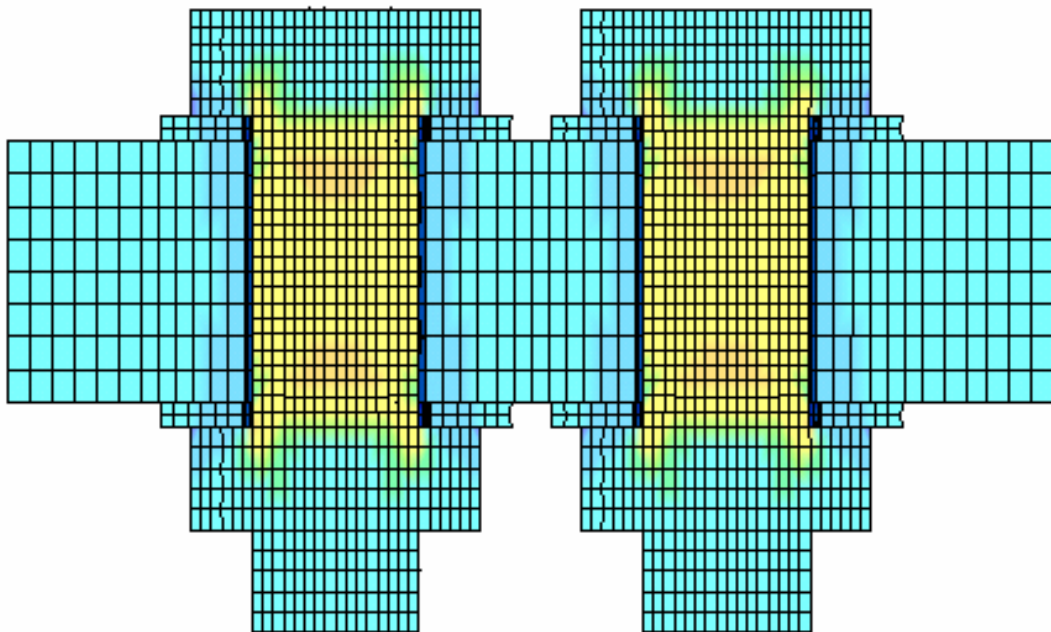


Figure 3.40 Pre-stress on the bolt assembly by thermal gradient

### 3.8.5 Using INITIAL\_STRESS\_SOLID card in LS-DYNA

LS-DYNA card, INITIAL\_STRESS\_SOLID can be used for defining the pre-stress in the bolted joints. Using this card, the initial stress and strain (Normal stress, Shear stress and plastic strain) can be explicitly defined on any solid element. These normal stresses are in global X, Y, and Z-directions.

Figure-3.41 shows the FE model-3 of cantilever beam with bolted lap joint. Initial stress (tensile axial stress) is defined on all the elements of the bolt shank. Theoretically the bolt shank will have a tensile stress when the nut is tightened on the bolt. Therefore the tensile stress (Positive stress) has to be defined for the bolt shank. The axis of bolt is in Z-direction. Therefore Z-stress is defined to all the elements in the bolt shank. Dynamic relaxation needs to be applied for this method to dampen the initial kinetic energy produced during the deformation of plates and bolt. Figure-3.41 shows the Von-Mises stress during the explicit analysis of this structure. Here is the example of the card used. Here is the example of card defined in LS-DYNA FE model.

```
*INITIAL_STRESS_SOLID  
100001 , 1  
, 0.0 , 800.0e6
```

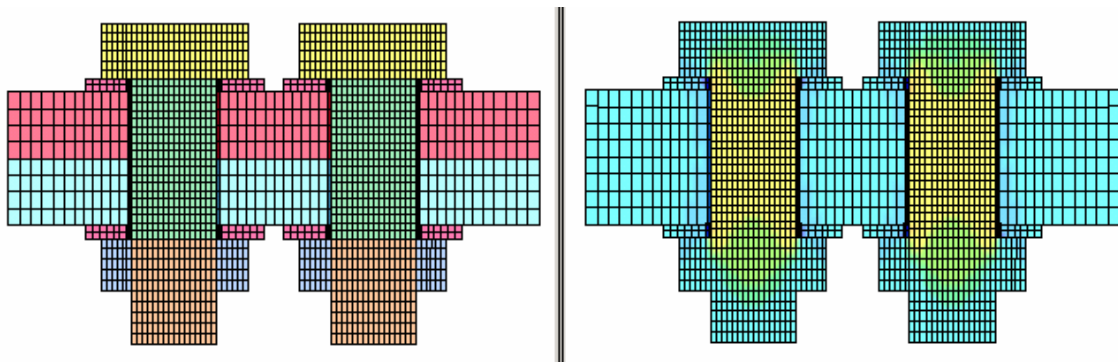


Figure 3.41 Bolt assembly with pre-stress using INITIAL\_STRESS\_SOLID card

### 3.8.6 Using INITIAL\_STRESS\_SECTION card in LS-DYNA

This method of modeling the preload in a bolt assembly is an easy and straightforward method and can be used in many applications to define pre-load. This method uses three LS-DYNA keyword cards namely - \*DATABASE\_CROSS\_SECTION\_PLANE, \*INITIAL\_STRESS\_SECTION and DEFINE\_CURVE. The DATABASE\_CROSS\_SECTION card defines the cross-section of the part where the preload need to be applied. INITIAL\_STRESS\_SECTION card assigns the stress (preload) to the part and the stresses are defined using DEFINE\_CURVE card. Figure 3.42 shows the bolt assembly with all the three cards defined. The N, L and M vector defines the cross section of the part (bolt shank) shown in black color. Dynamic relaxation technique was used to damp the initial kinetic energy, which is due to the deformation of the bolt and structure when preload is applied. Here is the example of LS-DYNA cards used in this method.

```
*DATABASE_CROSS_SECTION_PLANE_ID
$   csid   title
      1Schraube
$   psid   xct   yct   zct   xch   ych   zch
22,0.457,0.0,0.0,0.457,0.0,0.00635
$   xhev   yhev   zhev   lenl   lenm   id   itype
0.457,0.00735,0.0,1.0,1.0
*SET_PART_LIST
$^
$   SID   DA1   DA2   DA3   DA4
      22   0.0   0.0   0.0   0.0
$   PID1   PID2   PID3   PID4   PID5   PID6   PID7
PID8
      3
*INITIAL_STRESS_SECTION
$   ISSID   SECID   LCID   PSID
      1     1     41     22
$
*DEFINE_CURVE
$   LCID   SIDR   SFA   SFO   OFFA   OFFO   DATTYP
41,1
$           A1           O1
0.0,0.0
0.1e-3,432.0e6
```

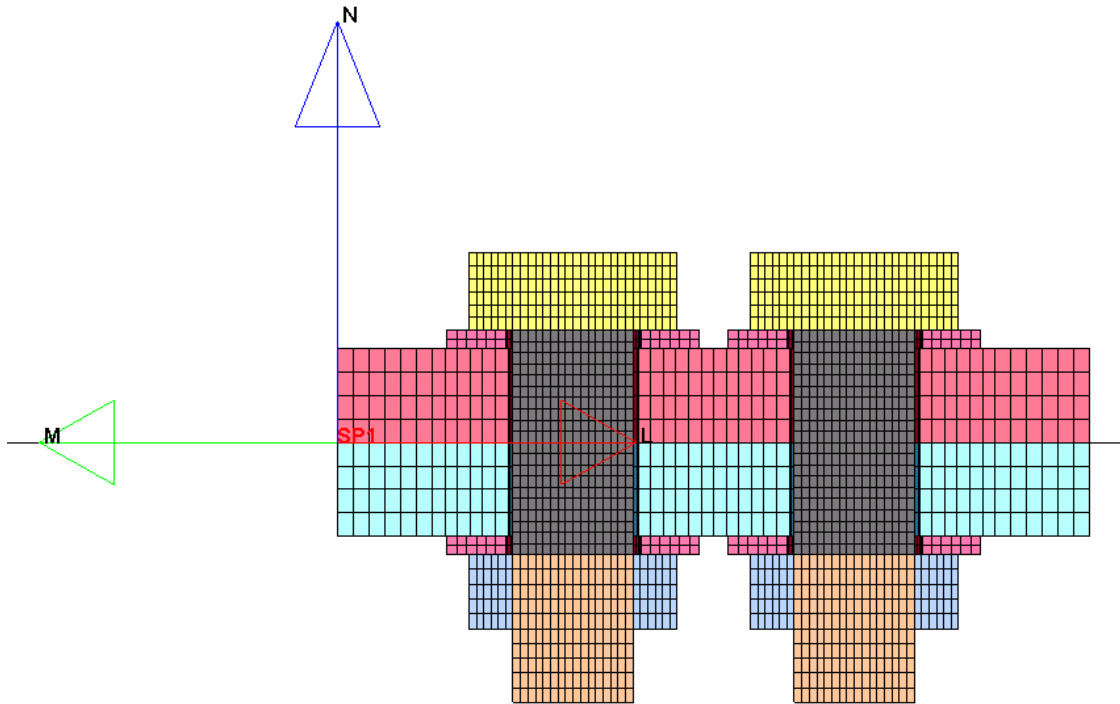


Figure 3.42 Bolt assembly with vectors for defining pre-stress

All six FE preload modeling techniques were tested for 34 Nm pre-torque case on the bolted cantilever beam. This pre-torque gives a 21 KN and 422 MPa force and axial stress in the bolt shank respectively. Figure 3.43 shows the force on the bolt shank from all the six pre-load modeling technique during the transient analysis. The preload from all the methods are constant through out the simulation except the first two methods which shows the transient part in which the preload increase from zero to 21 KN in the first millisecond. These preload modeling techniques are not unique to bolted joints, but can be used in any FE models to induce preload or pre-stress.

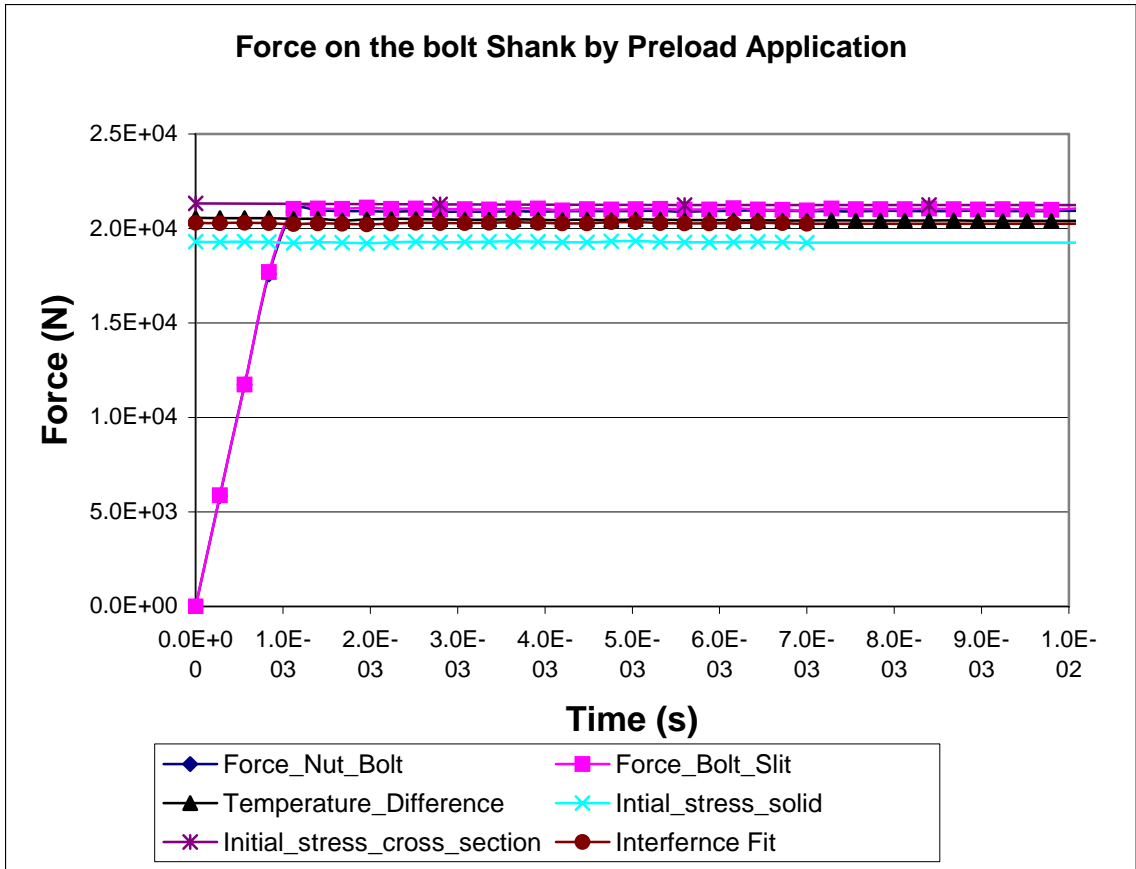


Figure 3.43 Force (preload) on the bolt shank for 34 Nm pre-torque

### 3.9 Experimental measurement of damping factors

The results of all the three FE models (Model-1, 2, & 3) of the cantilever beam with bolted joint studied in the beginning of this chapter, showed higher magnitude and frequency contents. The experimental results showed decay in the response due to damping in the bolted structure, but the FE results showed no decay in their prediction. This is due to the absence of damping in the material model used in the FE simulation. Therefore the damping needs to be explicitly defined in the FE model. The parametric study of external damping in the FE model, showed that the addition of damping factor will damp the FE response on the bolted structure. The damping factor for the FE

simulation can be calculated using the FFT response from the experiment. Comparison of FFT from the experiment and FE simulation (Figure 3.14, Figure 3.17 and Figure 3.20) showed that the FE simulation predicts high frequency response, which are absent in the experimental results. Therefore stiffness proportional damping ( $\beta$ ) factor can be used to mitigate the high frequency responses from the FE results. The stiffness proportional damping factor will be computed using half-power bandwidth method.

The damping factor for the bolted structure within elastic range is 5-7% and for plastic response is (yielding) 10-15% [56]. The damping factor can also be calculated using the FFT of the experimental time history response. Half-power bandwidth method [60] was used to measure the damping factor for the cantilever beam with bolted joints. The half-power bandwidth method is used in the frequency domain. This method is based on the observation that the shape of the frequency response is controlled by the amount of damping in the system. Therefore it is possible to estimate the damping factor from the properties of the frequency curve. Damping factor is calculated by identifying the two frequencies that neighbor the fundamental natural frequency of the system and whose magnitude is equal to  $R_d/\sqrt{2}$  (Figure 3.44). The damping factor is calculated according to the following equation:

$$\xi = \frac{f_2 - f_1}{f_2 + f_1}$$

The FFT of the cantilever beam with bolted joint for point A2 is shown in Figure 3.45. The half-power bandwidth method is applied to the first natural frequency of the beam is shown in Figure 3.46. The  $f_1$  and  $f_2$  obtained from the plot are 50.5 and 57.5, which yields a damping factor of 0.065 (6.5%). This is within the range of 5-7%. Therefore the stiffness proportional damping factor of 6.5% (0.065) was used in all the

three FE models of the cantilever beam. For high impact analysis, where the bolted structure deforms significantly (yielding), the stiffness proportional damping factor of 14.0% (0.14) was used based on the Newmark [56].

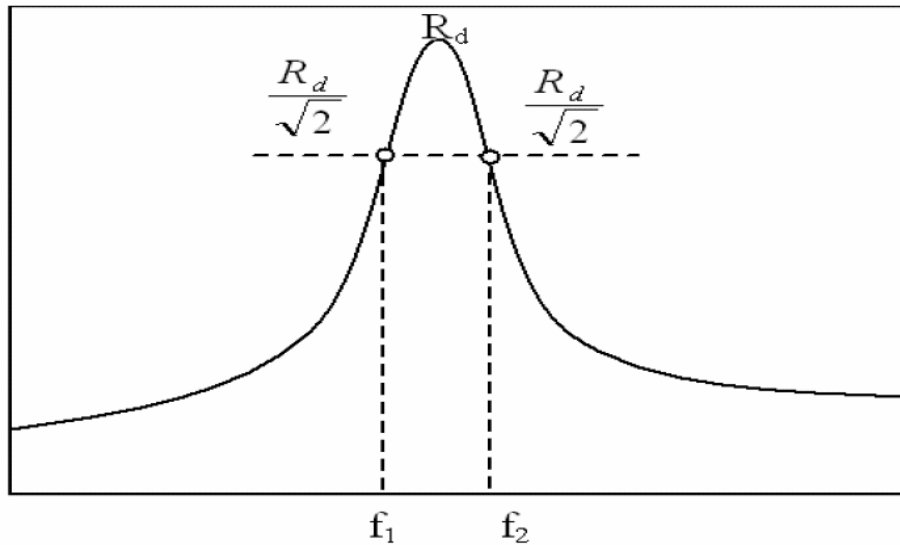


Figure 3.44 Half-power bandwidth method [60]

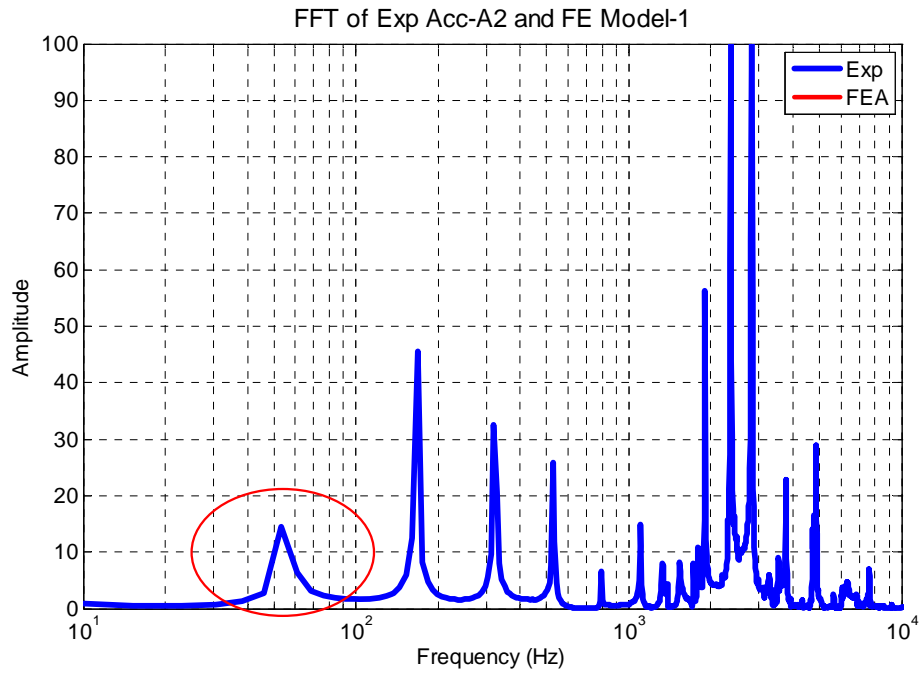


Figure 3.45 FFT from the experiment

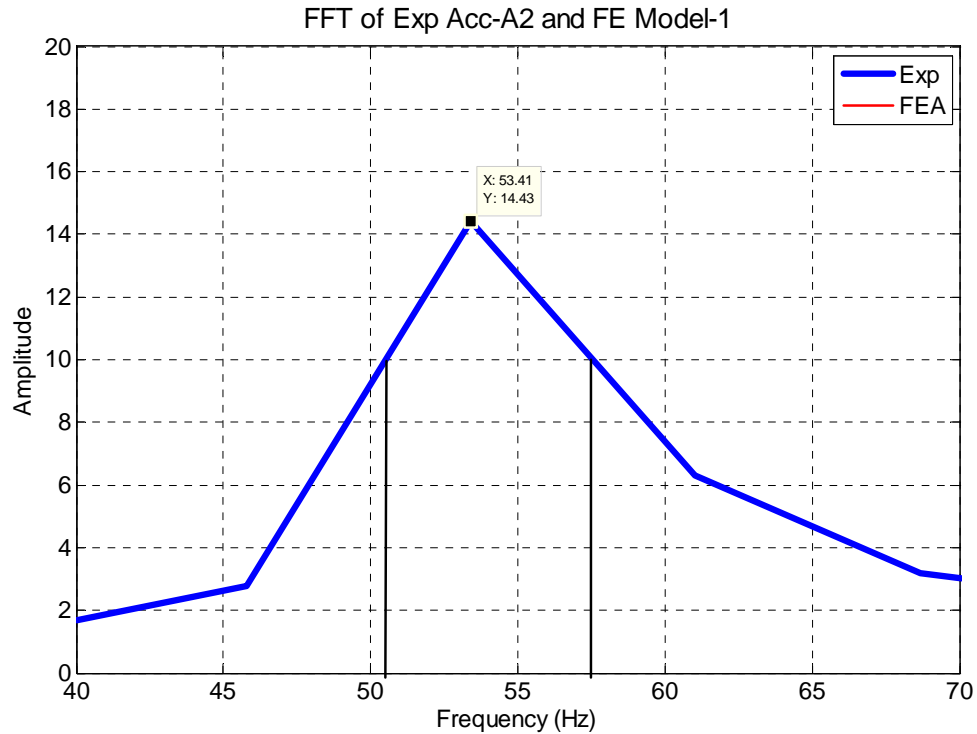


Figure 3.46 Half bandwidth method applied to first natural frequency of the cantilever beam

The addition of stiffness proportional damping in the FE model resulted in the exponential decay of the time history response similar to the experimental values. Figure 3.47 and Figure 3.48 show the FE model-1 and FE Model-2, time history response with 6.5% (0.065) stiffness proportional damping factor included in the FE model. Stiffness proportional damping was used in these FE models to mitigate the high frequency response. Table 3-6 shows the NRMSD of two FE models (with damping) prediction from the experimental values. Addition of damping in the FE model decreased the NRMSD by 50%. The modeling techniques used in FE model-1 and FE model-3 will be checked again with the high impact loading prediction.



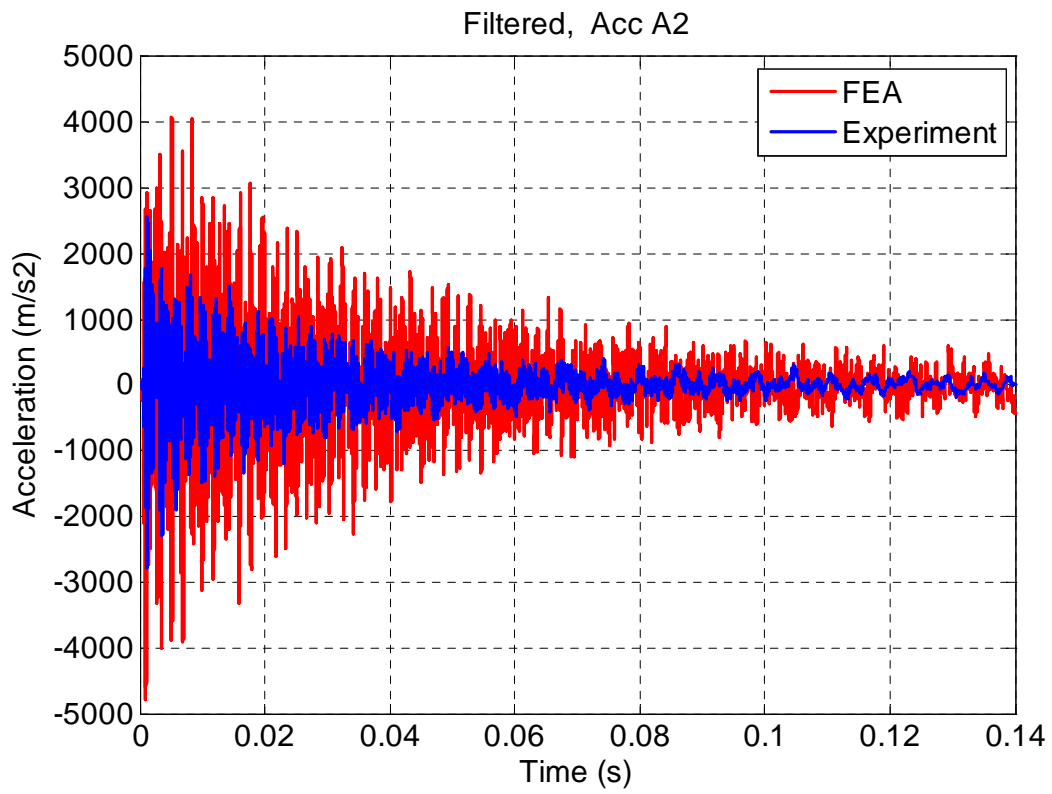
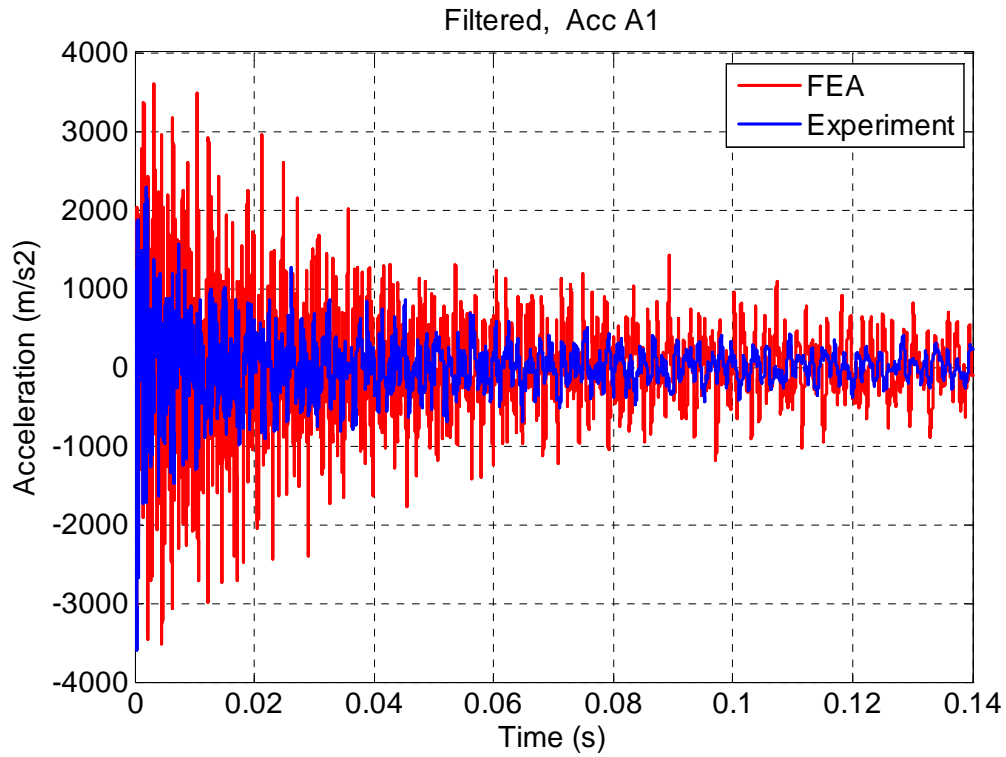


Figure 3.47 Model-1, Time history response with SPD 6.5% (0.065)

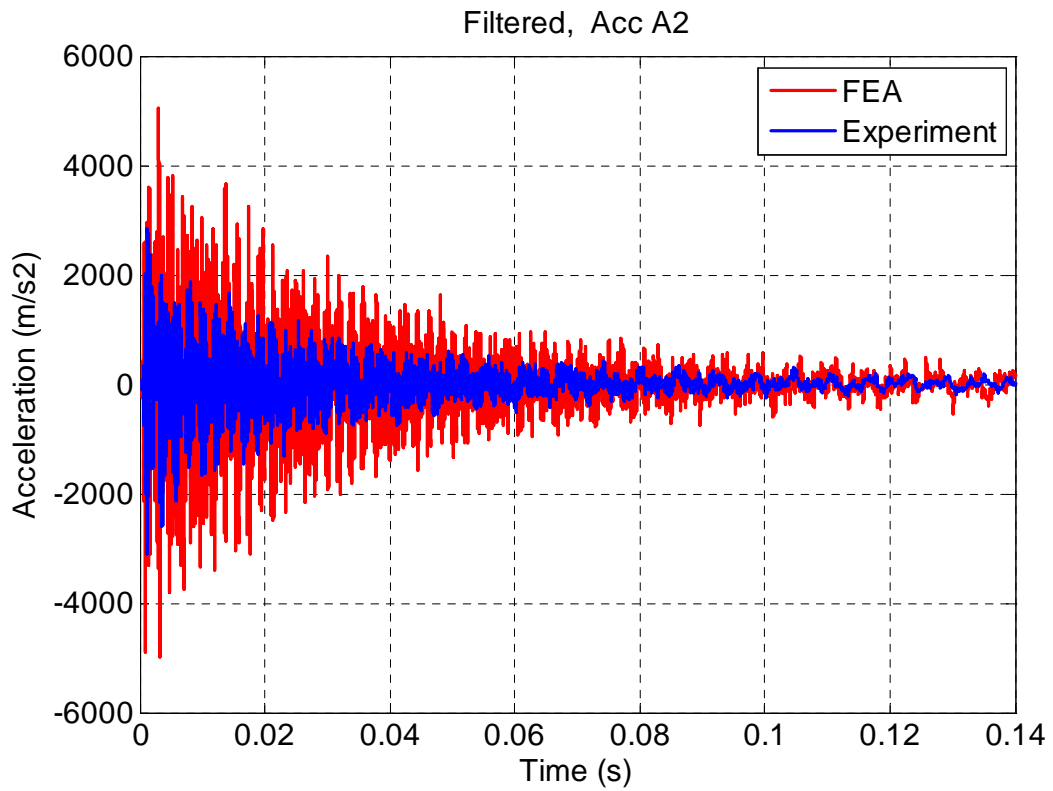
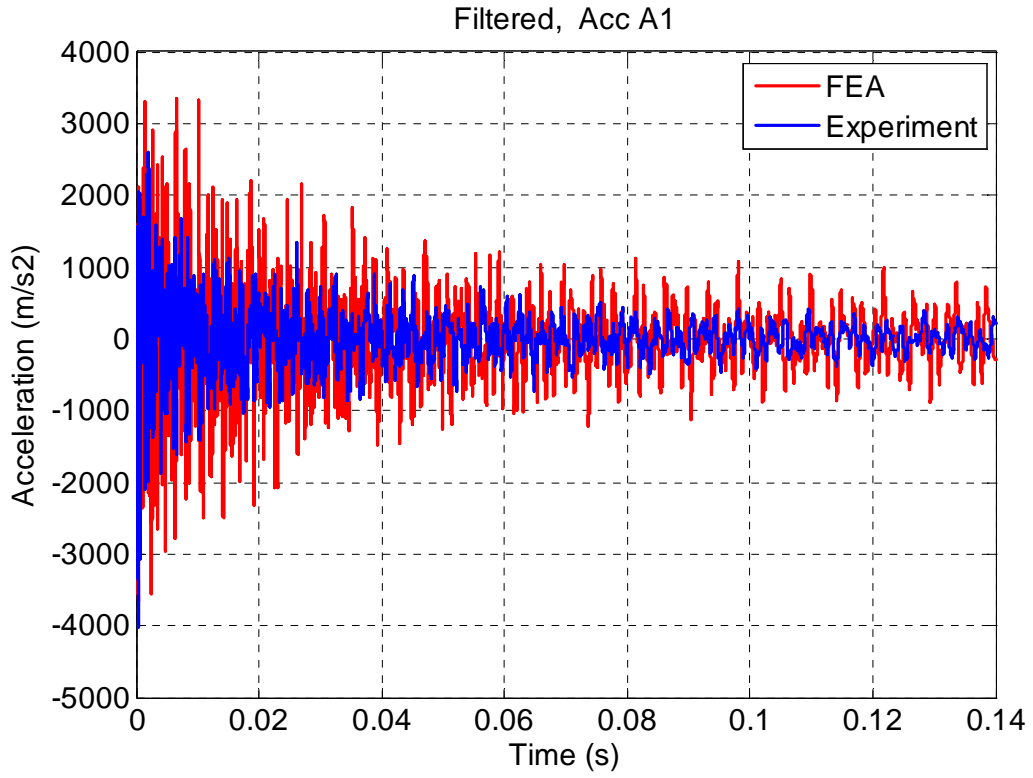


Figure 3.48 Model-2, Time history response with SPD 6.5% (0.065)

Table 3-6 NRMSD between experiment and FE model transient results

Normalized Root Mean Square deviation between Experiment and FE results		
FE Model	Experiment	
	Acceleration (A1)	Acceleration (A2)
FE Model-1 with SPD 6.5% (0.065)	0.10	0.09
FE Model-2 with SPD 6.5% (0.065)	0.09	0.09

### 3.10 Summary of results

In an explicit FE analysis, the computed results depends on many factors such as mesh size & density, damping in the FE model, element formulation and type of element, etc. These factors can be tuned to make the FE results close to the experimental (actual) values. Some of the conclusions based on the parametric study of the cantilever beam with and without bolted joint are as follows:

- The damping needs to be defined explicitly for the transient FE simulation. The Rayleigh damping is used in FE analysis to account for all kinds of damping.
- The MPD damps only low frequency response and rigid body motion whereas the SPD damps high frequency responses.
- The SPD factor of 6.5% (0.065) and 14% (0.14) can be used for elastic and plastic impact analysis.

- The fully integrated element formulation (FIEF) requires more CPU time and also predicts higher frequency values for every mode. Therefore the FIEF needs to be avoided in shock analysis.
- Interference fit, Thermal gradient, Initial stress solid and Initial stress cross-section methods can be used for defining preload on bolted joints in FE simulation.
- Preload modeling in bolted joint for transient FE analysis can be omitted in low impact analysis but is essential in high impact loading to account for joint damping.

## CHAPTER 4

### LOW IMPACT ANALYSIS ON HAT SECTION AND FLAT PLATE

One of the ways to understand the dynamic response of the bolted joints was to study the shock propagation in simple structures such as a cantilever beam with bolted lap joints. In the previous chapter the cantilever beam with bolted joint was tested for low force impact loading and the FE parametric study was carried out. Along with the FE parametric study, different preload modeling techniques for explicit FE analysis were discussed. The knowledge gained from studying the simple structure like cantilever beam can be used to understand the response of more complex bolted structures. A hat section with flat plate joined together with four-bolt assembly was selected to study the response of bolted joints subjected to impact loading. The bolted hat-plate structure was selected for study, based on numerous discussions with structural dynamic research staff at the U.S. Army Research Laboratory (ARL). This structure is representative of structures found in many military ground vehicles that are subjected to shock loads such as blasts or projectile impact.

Figures 4.1 and 4.2 show the hat-plate bolted joint structural configuration chosen for impact response analysis. The structure consists of five major parts: Hat section, spacers (washers), flat plate, bolts and nuts. While assembling the structure, the spacers were placed between the flat plate and hat section. The spacers were added so that the contact surface between hat and plate was very well defined. The hat and plate are not perfectly flat so the exact contact locations between the hat and plate are not known if the spacers are not used. Hex bolts and nuts were used to put them together. The hat section is made from 6.35 mm ( $\frac{1}{4}$  in) steel plate. These dimensions were suggested by an Army Research

Laboratory (ARL) team as a good start for joint configuration study. The metric plain washer has been used as the spacer between hat section and flat plate. The plain washer is 10 mm, narrow and zinc plated according the ANSI B18.22M-1981, R1990 [61]. The rectangular flat plate is 6.35 mm ( $\frac{1}{4}$  in) thick and is made of 1045 steel, same as hat section. Class 8.8, M10 $\times$ 1.25 hex bolts and nuts are used to connect the flat plate to the hat section. The bolts and nuts dimensions follow the ANSI B18.2.3.5M-1979, R1989 standard [61].

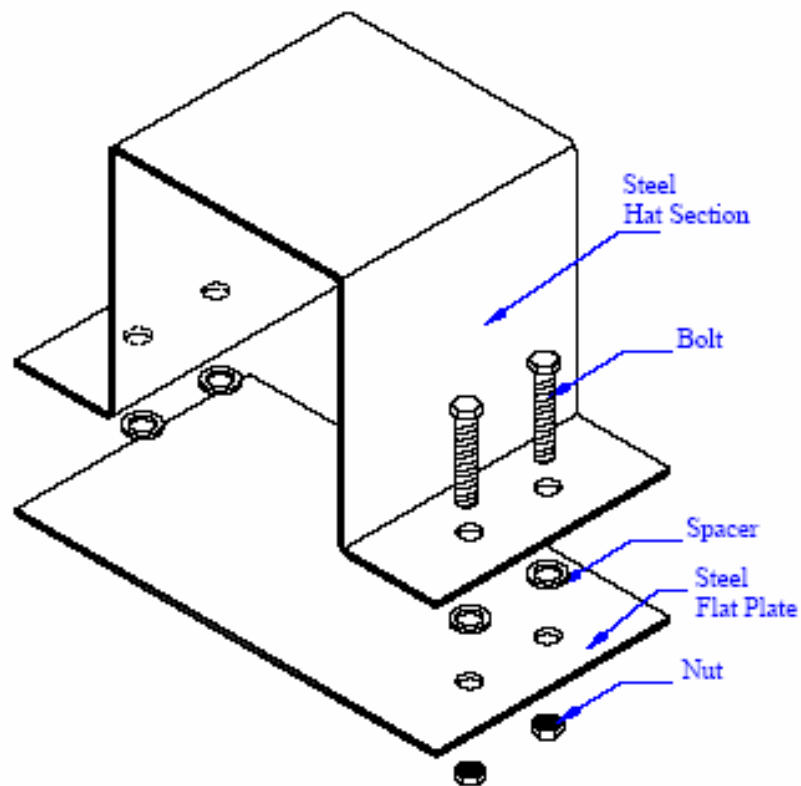


Figure 4.1 Bolted hat-plate structure configuration

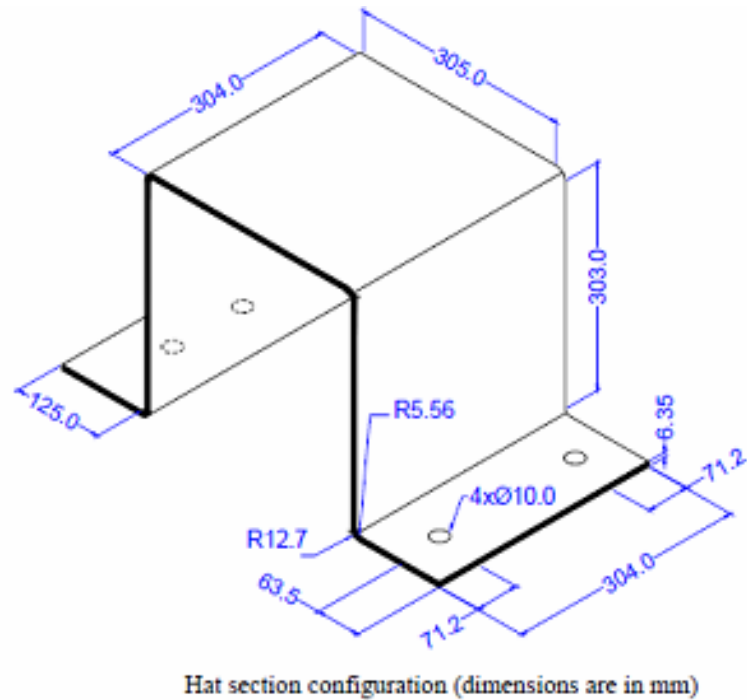


Figure 4.2 Hat section configuration

#### 4.1 Experimental setup and procedure

The test setup includes the bolted joint structure (Hat-plate structure), accelerometers, impulse hammer, signal conditioners and oscilloscope. The details of these instruments are given in Chapter 2. Figure 4.3 shows the bolted joint configuration hanging from a large steel support frame (A-Frame) by 1-m long steel wires. The instrumented impact hammer can deliver only low impact forces on the hat-plate structure (no deformation or damage to the structure) In the impact experiments, the bolts in the hat section were subjected to axial impact load (Figure 4.3) and the response of the structure was measured at two points. Two accelerometers were mounted on the hat and plate sections (one on hat section and one on the plate) as shown in Figure 4.4.

The procedure for the impact experiment on the hat-plate structure is shown in Figure 4.5. Unlike the cantilever beam impact experiment in Chapter 2, here the bolted hat-plate structure was suspended from an A-Frame during the experiment. The hanging of the hat-plate structure eliminates all boundary conditions on the FE model during simulation of the impact analysis. High strength steel wires were used for hanging the hat-plate structure. The length of the steel wires were more than one meter (3 ft), and this ensures the free boundary condition on the Hat-plate structure.

The steel tip was used in the instrumented impact hammer to strike the hat-plate structure at the center of the inside of the hat in the y-direction as shown in Figures 4.3 and 4.4. The schematic of the experimental procedure is shown in Figure 4.5. The PCB Model 352C22 accelerometers were glued to the hat-plate structure using wax adhesive. Accelerometer 1 is mounted at the center of the top side of the hat and is measuring acceleration in the x-direction, perpendicular to the loading direction. Accelerometer 2 is mounted at the center of the flat plate and is measuring acceleration in the loading, y-direction. The impact hammer and the accelerometers were connected to the oscilloscope through signal conditioner. When the impact hammer strikes the hat structure, the impact hammer and the accelerometers generate voltage proportional to the excitation. The impact hammer and accelerometer data were recorded at a sampling rate of 500,000 samples/second. The high sampling rate ensures the capture of high frequency response from the accelerometers. Figure 4.6 shows the typical force curve generated, when the instrumented impact hammer strikes the bolted hat-plate section. The impact curve shown in the Figure 4.5 has a peak force value of 20 kN.





Figure 4.3 Experimental set-up for axial loading on the bolt assembly

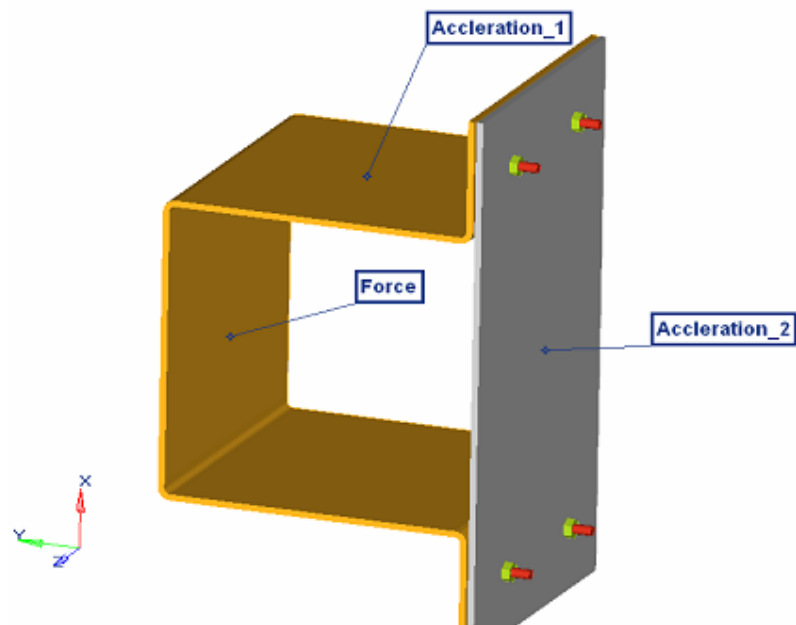


Figure 4.4 Location of impact force and acceleration measurement - The Force is applied in the y-direction, acceleration 1 is measured in the x-direction and acceleration 2 is measured in the y-direction

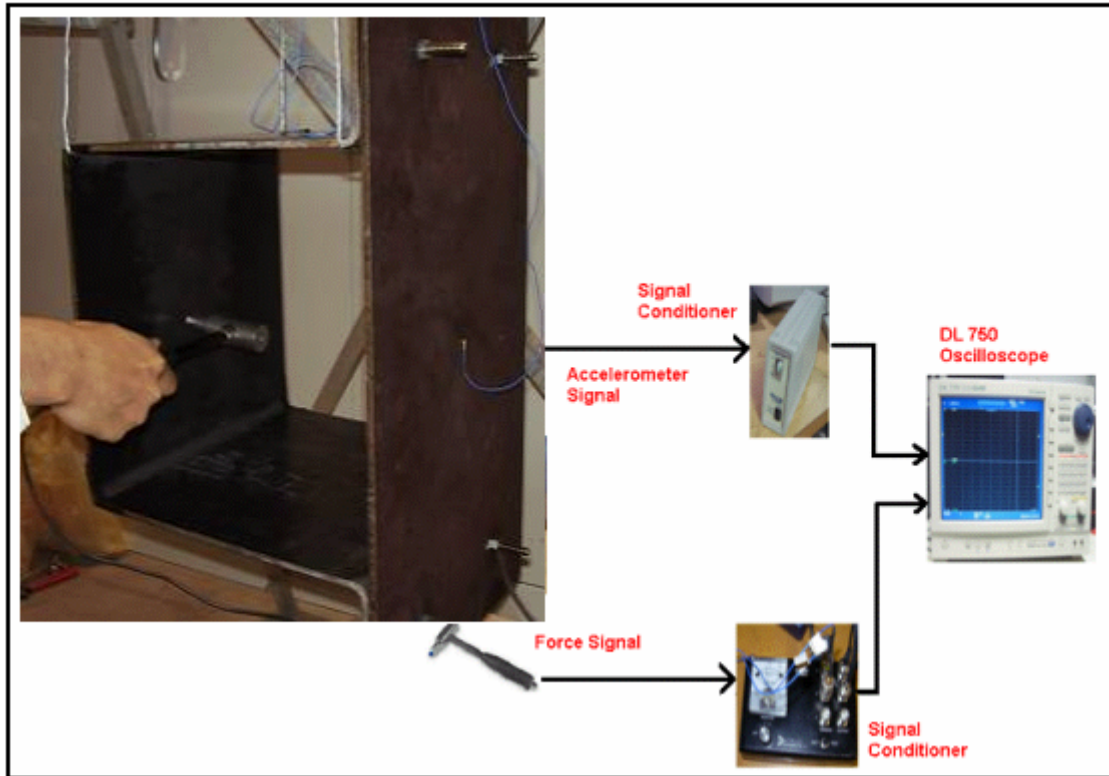


Figure 4.5 Experimental setup for impact analysis on bolted hat-plate structure

#### 4.2 Experimental and FE modal analysis of the bolted hat-plate section

The first step in any transient (dynamic) analysis is conducting the modal analysis to get the natural frequencies of the structure. The experimental modal analysis is carried out by subjecting the hat-plate structure to an impulse (Figure 4.6) and measuring the free vibration of the structure. The Fast Fourier Transform (FFT) of the free vibration response gives the natural frequency of the structure. Figure 4.7 shows the FFT of the hat-plate structure, where the frequency (abscissa) corresponding to all the peaks are the natural frequencies of the hat-plate section. Table 4.1 shows the natural frequencies of the bolted hat-plate section derived from the experimental modal analysis in ascending order. The number of natural frequencies excited on the bolted hat-plate structure is almost

twice that of the cantilever beam. The response of the structure for an impact load will be a function of number of frequencies excited. Therefore the bolted hat-plate structure will be complicated to predict compared to the cantilever beam.

The FE modal analysis is an Eigenvalue problem and the Eigenvalues and the Eigenvectors obtained represent the frequencies and the corresponding mode shapes. LS-DYNA solver was used for both modal and transient analysis. Implicit and explicit solvers were used to solve modal and transient analysis respectively. Figure 4.8 shows the FE modal analysis of the bolted hat-plate section and the first eight mode shapes along with the frequency values. The FE modal analysis predicts all the mode shapes and the frequencies: axial, bending and torsion.

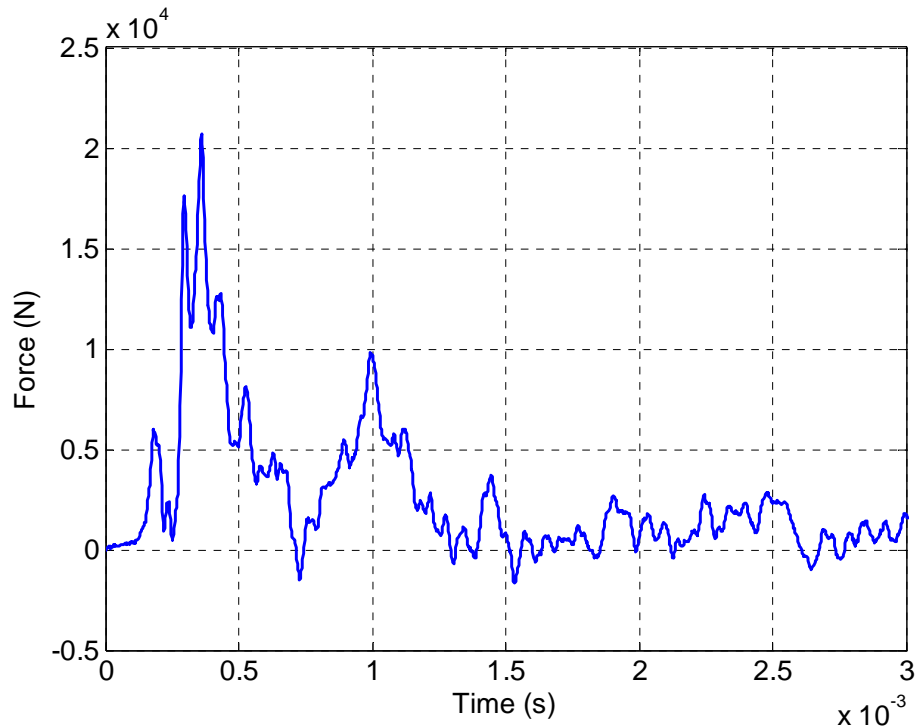


Figure 4.6 Typical impact force measured from the instrumented impact hammer

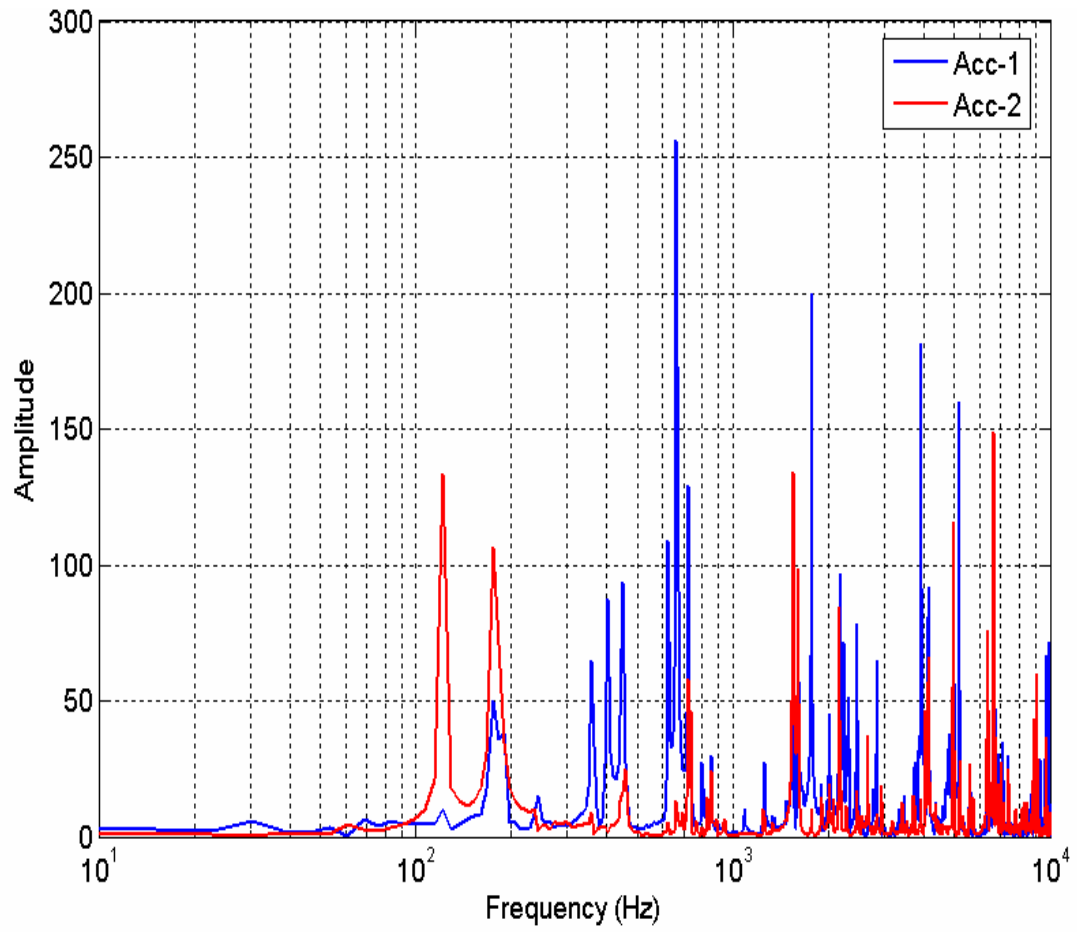


Figure 4.7 FFT of the hat and plate structure

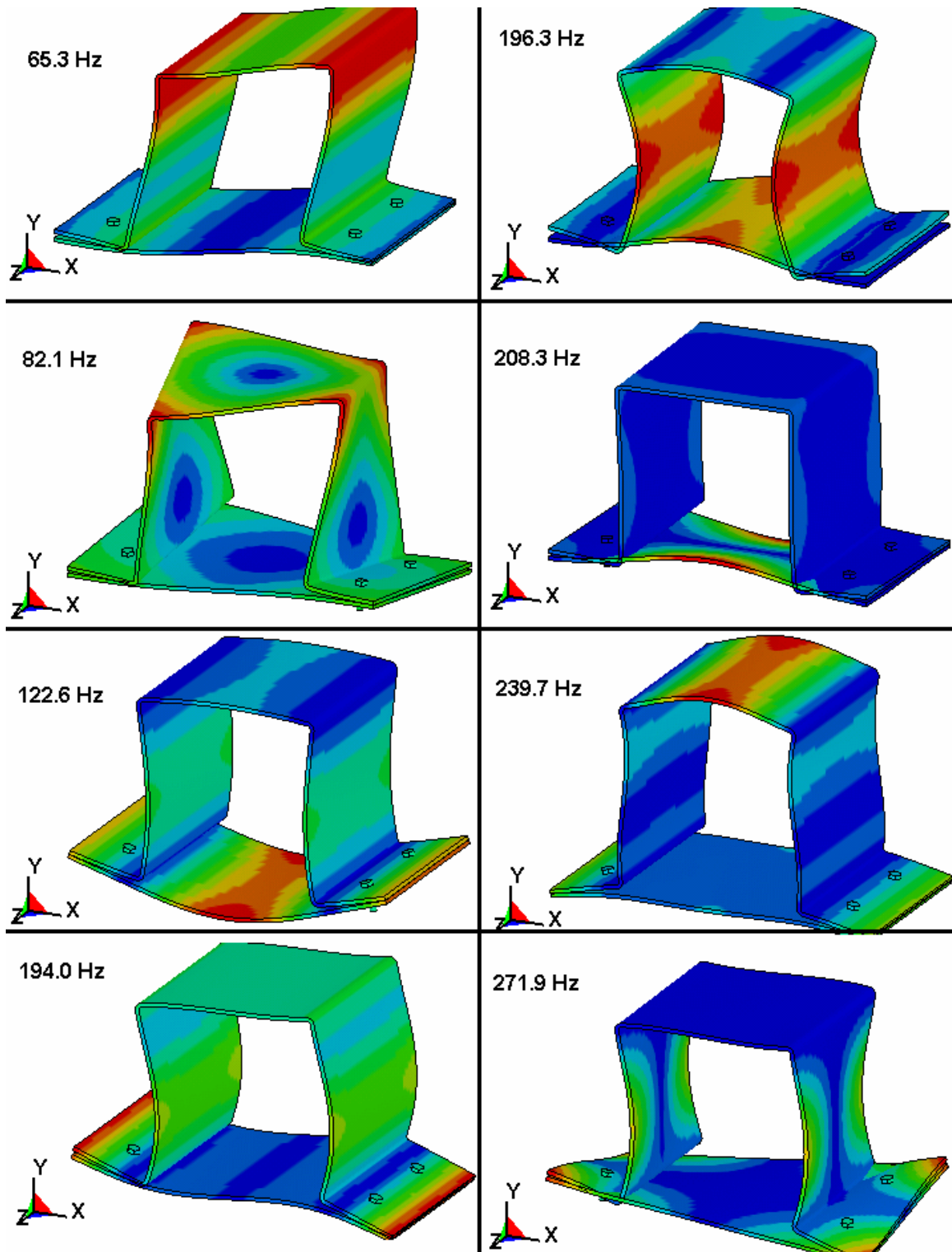


Figure 4.8 Mode shape and natural frequencies of the bolted hat-plate structure

Table 4-1 Natural frequencies of the hat-plate structure from experimental modal analysis

Mode	Natural Frequency		Mode	Natural Frequency
1	61.0		24	5652
2	122.1		25	5737
3	170.9		26	6299
4	354.0		27	6543
5	390.6		28	6714
6	451.7		29	6995
7	622.6		30	7263
8	659.2			
9	671.4			
10	720.2			
11	732.4			
12	1245			
13	1538			
14	2161			
15	2283			
16	2454			
17	2954			
18	3430			
19	4138			
20	4370			
21	4797			
22	4944			
23	4956			

### 4.3 Effect of impact hammer striking head on the transient response of structure

The instrumented hammers used in the impact experiments have an inter-changeable striking head. The striking head are usually of three types – Soft, Medium and Hard. The soft striking head is made of soft plastic, while the medium head is made of hard plastic. The hard striking head is made of hardened steel. The hard head is best suited for exciting high frequencies in the structure.

Figure 4.9 shows the impact force measured from the striking of impact hammer on the bolted hat-plate structure using three striking heads. For comparison purpose, a peak force of 3000 N was selected for all the three striking hammer cases as shown in Figure 4.10. The width ( $\Delta t$ ) of the impact force curve depends on the type of striking head. For hard, medium and soft striking head, the width of the force curve is 0.4 ms, 0.7 ms and 1.6 ms respectively. Figure 4.10 show the response (acceleration) of the hat-plate section structure, when impacted with three striking heads. Even though three striking heads induced the same peak force of 3000 N on the structure, the response of the structure is different for three cases. There is no repeatability in the response of the structure for the same input peak force. The hard striking head of the impact hammer excites the higher frequencies in the structure, compared to the medium and soft heads. Also the magnitude of the response of the structure is higher for hard striking head case. In all the impact experiment in this report, the hard striking head was used.

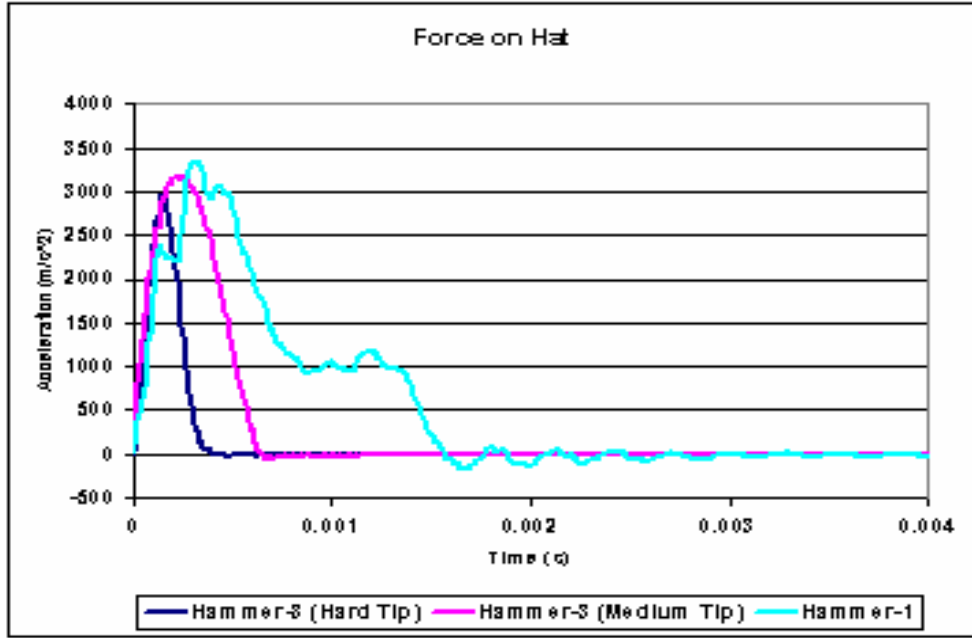


Figure 4.9 Force curve from impact hammer for hard, medium and soft striking head

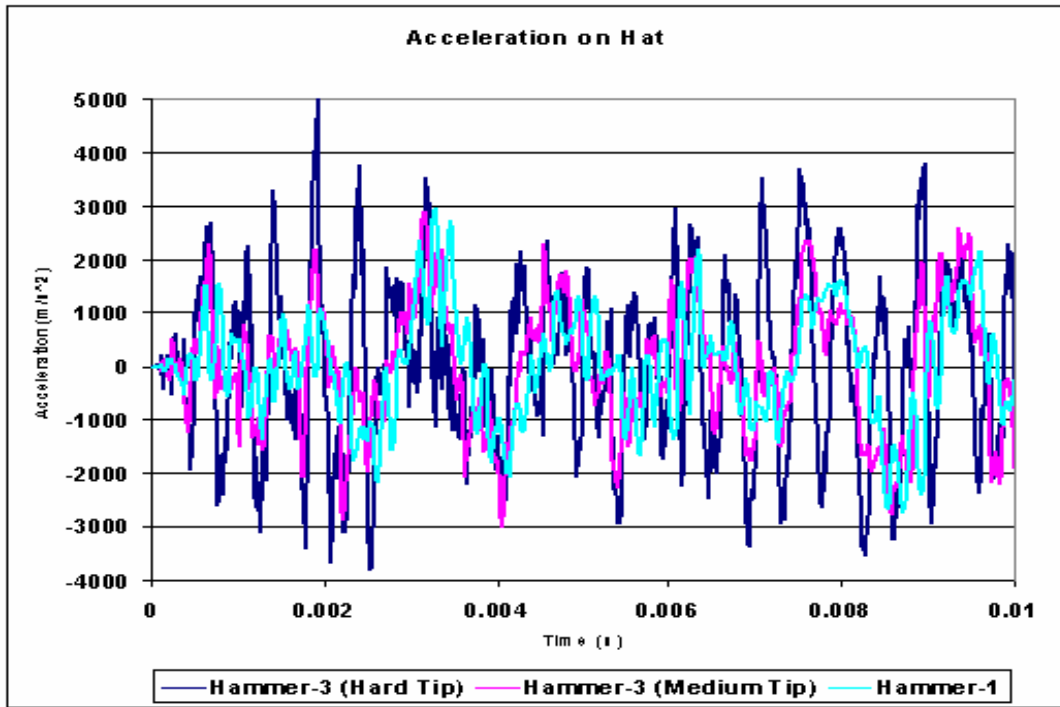


Figure 4.10 Time history response from impact hammer for hard, medium and soft striking head



#### 4.4 Transient analysis of bolted hat-plate section subjected to impact load

In chapter two and three of this report, a detailed study of simplified bolted joint (cantilever beam with bolted lap joint) subjected to low impact loading is presented. Results from that chapter are used to generate the computational FEA model of the hat-plate bolted structure. A complex bolted structure, such as hat-plate structure shown in Figure 4.1, which resembles a mounting structure in a vehicle was subjected to low impact load and its response was studied both experimentally and using FE analysis. Figure 4.11 show the FE model of the bolted hat-plate section with 3-D solid elements. The contacts are not defined between the bolt assembly and the hat-plate section. This FE model is similar to FE Model-2 in the previous chapter. The detailed view of the bolt assembly is shown in Figure 4.12. Based on the previous chapter conclusion, a stiffness proportional damping factor of 6.5% (0.065) was used in this FE model.

##### 4.4.1 Response of bolted hat-plate structure to low force impact loading

The experimental and FE responses of the bolted hat-plate structure subjected to low force impact loading are shown in Figures 4.13 and 4.14. The FFT shows the high frequency response predicted by the FE model similar to cantilever beam FE model-2, especially at higher natural frequency ( $>1000$  Hz). The experiment and FE time history response were showing same magnitude, but the FE prediction shows high frequency contents. Table-4.2 shows the NRMSD between the experiment and the FE results. The NRMSD values for the hat-plate structure are similar to the cantilever beam. Thus the FE model of the bolted hat-plate structure can be used for high impact loading simulation.

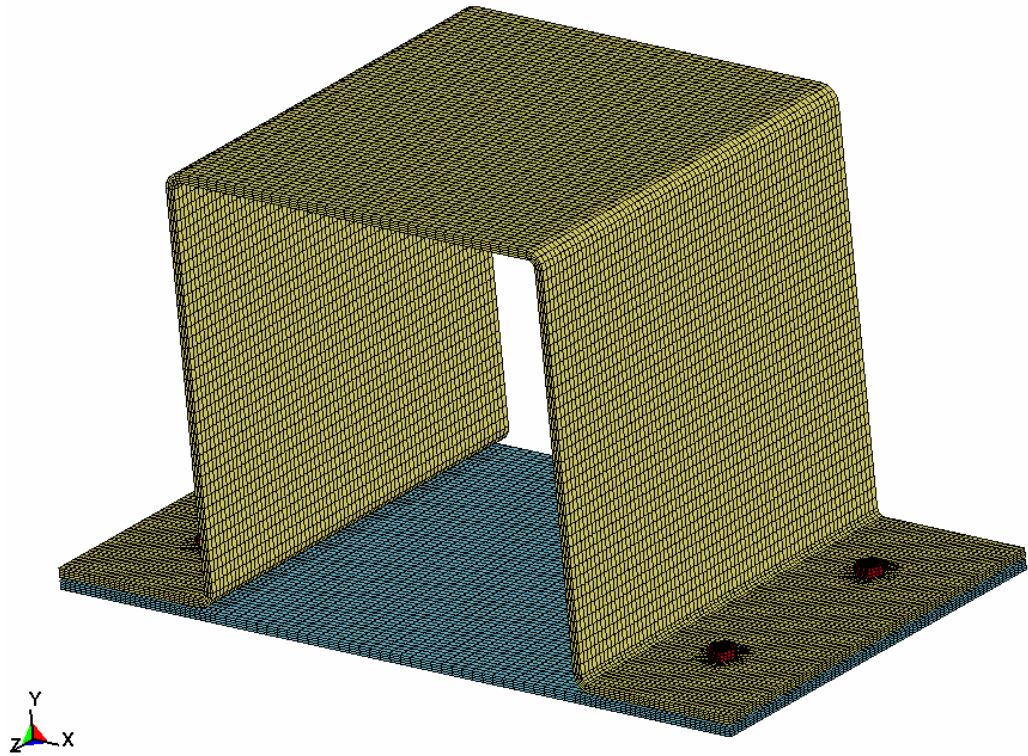


Figure 4.11 Solid element FE model of bolted hat-plate structure

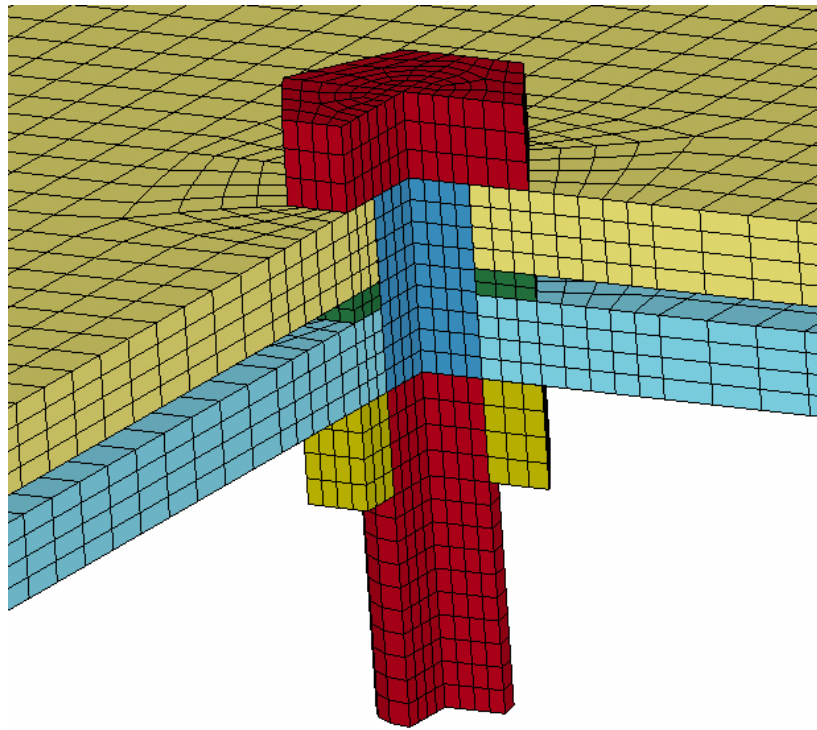


Figure 4.12 Detailed view of bolt assembly in the hat-plate structure

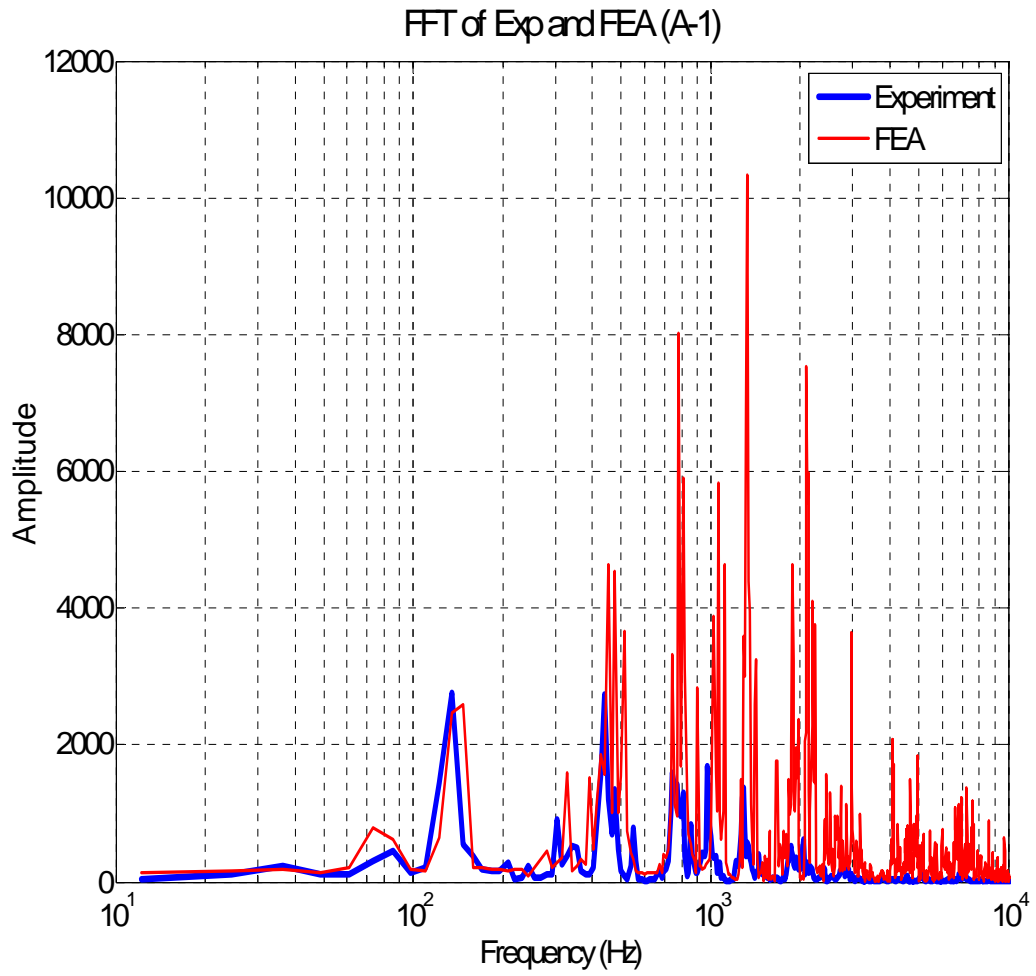


Figure 4.13 FFT of experiment and FEA

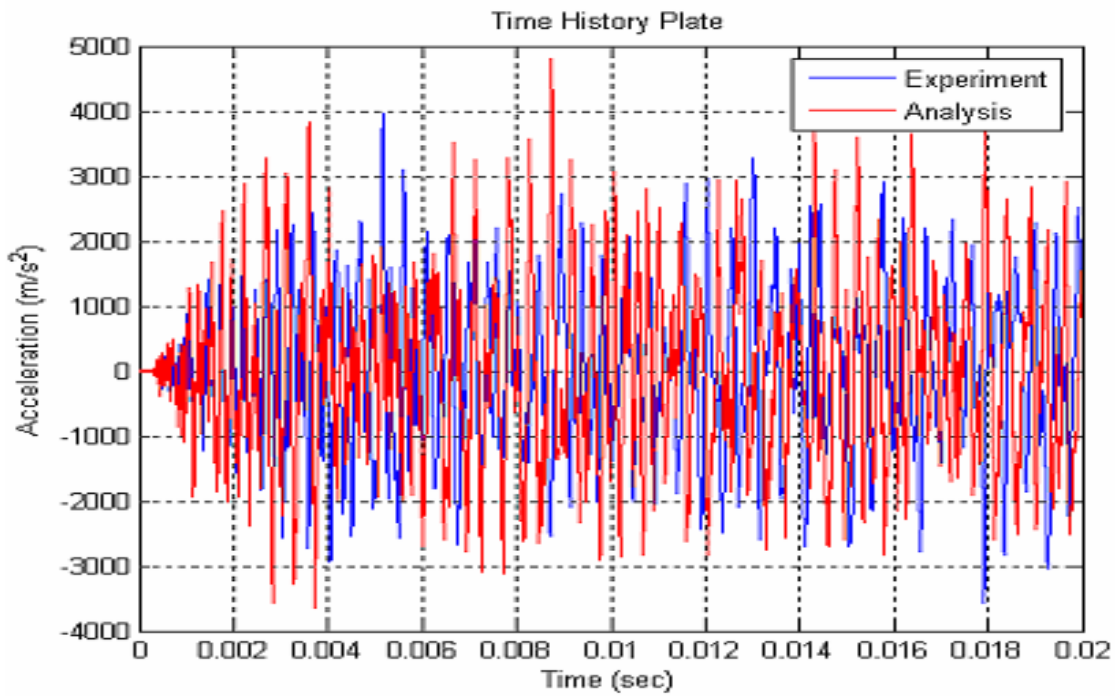
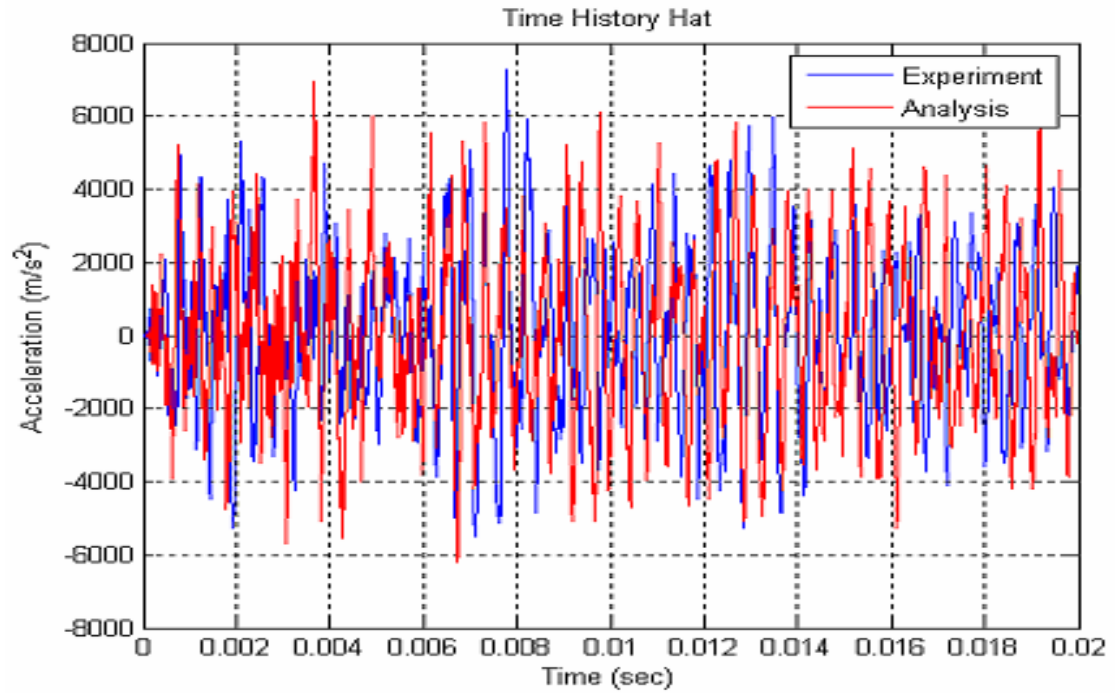


Figure 4.14 Experimental and FE time history response for bolted hat-plate structure for low impact loading

Table 4-2 NRMSD between experiment and FE model transient results

Normalized Root Mean Square deviation between Experiment and FE results		
FE Model	Experiment	
	Acceleration (A1)	Acceleration (A2)
FE Model-2	0.10	0.11

#### 4.5 Summary of results

The bolted hat-plate structure is more complex than the bolted cantilever beam with lap joint. The low impact loading experiment on the bolted hat-plate structure was carried out to study the shock propagation in complex bolted joints. For a similar impact load, a large number of natural frequencies were excited in the hat-plate structure compared to cantilever beam. The transient impact response of a structure will depend on the number of frequencies excited. Therefore simulating the impact analysis on the bolted hat-plate structure is more complicated than the simple cantilever beam. The NRMSD values for the hat-plate structure are similar to the cantilever beam. The experimental and FE analysis of low impact analysis on the bolted structures will help in studying the response of these structures to high impact loading, where the structure will permanently deform.

## CHAPTER 5

### IMPACT ANALYSIS USING AIR GUN

#### 5.1 Introduction

In combat, military vehicles undergo a high impact/shock loading such as mine blast (Figure 1.2) or projectile impact. Sometimes even the vehicle may undergo frontal or rear crash, which can damage the vehicle. In all these cases, the structure in the vehicle and the bolts used in the vehicle structure may experience large shock loading. These loads may yield or damage the structure and the bolts. There is only a limited amount of published literature describing the proper method for analyzing the transient shock propagation across bolted connections for high impact loading. To understand, model and simulate the response of the vehicle to these impact loadings is very important as this will help in designing better vehicle components. Also this will help in isolating critical components such as electronics, and the driver from the shock.

When the structures with bolted joint undergo low impact loading, there won't be any permanent deformation or failure in the structures. The only non-linearity in low impact loading is the friction in the bolted joint. It is easy to model and simulate the low impact loading on bolted structures using FEA or any other numerical techniques. In chapters two and three of this report, a simple cantilever beam with bolted lap joint subjected to low impact loading and the transient response of the cantilever beam was analyzed. Two sets of cantilever beam (monolithic beam and bolted lap joint beam) were studied for experimental and FEA modal analysis. Also the effect of preload in the bolted joint on the transient response of the cantilever beam was studied. Explicit finite element analysis was used to simulate the shock propagation in bolted joint of the cantilever beam.

Various factors that affect the finite element simulation such as damping modeling, element density, element formulation, preload modeling and contacts were studied. In chapter four, a more complex structure such as hat section with bolted plate subjected to low impact loading was studied for modal and transient analysis. The bolted joint of the hat-plate structure was subjected low impact loading and this transient phenomenon was simulated using LS-DYNA solver. The knowledge gained by analyzing bolted structures for low impact loading will be used to analyze the same structures for complex high impact loading.

When a vehicle trips a land mine or a vehicle is subjected to projectile hit in combat, the bolted joint in the vehicle undergo a large impact /shock load. To predict or model the vehicle response to the large impact loading, there is a need to understand the response of bolted joint to high impact loading. This chapter provides a detailed experimental set-up and procedure for conducting high impact loading on structure with bolted joint. An air gun was used to fire an aluminum slug at high velocity on the bolted structure to induce a medium and high shock loading. Two complex bolted structures (Hat-plate and Two-hat structures) were used to study the shock propagation in bolted joints with high impact loading. A detailed FE model was used to simulate the impact analysis of the bolted structure. The detailed FE model of bolted joint and structure, using 3-D solid elements is not practical to use it in the full vehicle FE model. Therefore a simple and practical FE model with shell elements was developed to simulate the high impact loading. This simple LS-DYNA FE model takes less than  $1/10^{\text{th}}$  the CPU time as the more detailed FE model.

## 5.2 Design of air gun experiment for high impact loading

There are many ways to induce a structure with high shock loading. Drop test, air gun test, gas gun test, split Hopkinson pressure bar test and pendulum impact are some of the widely used high impact loading experimental set-up configurations. In this project, an air gun was used to induce a high impact / shock loading in bolted structure. The air gun uses pressurized air to shoot a slug (through a barrel) into the structure. In the air gun test, the velocity of the slug is a function of length of barrel, mass of slug, the pressure in the tank, friction between slug and barrel, and cross sectional area of slug.

The air gun at the UNLV CMEST (The Center for Mechanical & Environment Systems Technology) [62] was used for this project. The UNLV CMEST air gun was modified, by adding an A-frame stand and a safety catch tube. The block diagram of the air gun test set-up is shown in Figure 5.1. The original air gun had a rocker arm and a test table at the end of the barrel, which were designed to create the desired shock into the seat system and provided a platform for measuring its responses. In the new design of the air gun test set-up, the rocker assembly and the test table were removed and in its place a sturdy A-Frame (Figure 5.2) was placed. A-Frame was used for hanging the bolted hat-plate structure.

The purpose of the air gun is to accelerate an aluminum slug to high velocity in a short distance. The slug moving at high velocity strikes the test specimen (bolted hat-plate structure). The response of the bolted structure for high velocity impact can be recorded using accelerometers. The air gun consists of a 6.1 m (20-foot) long barrel with a 5.1 cm (2 inch) diameter seamless steel pipe, large pressure vessel, catch tube, aluminum slug, A-Frame, and a ball valve.



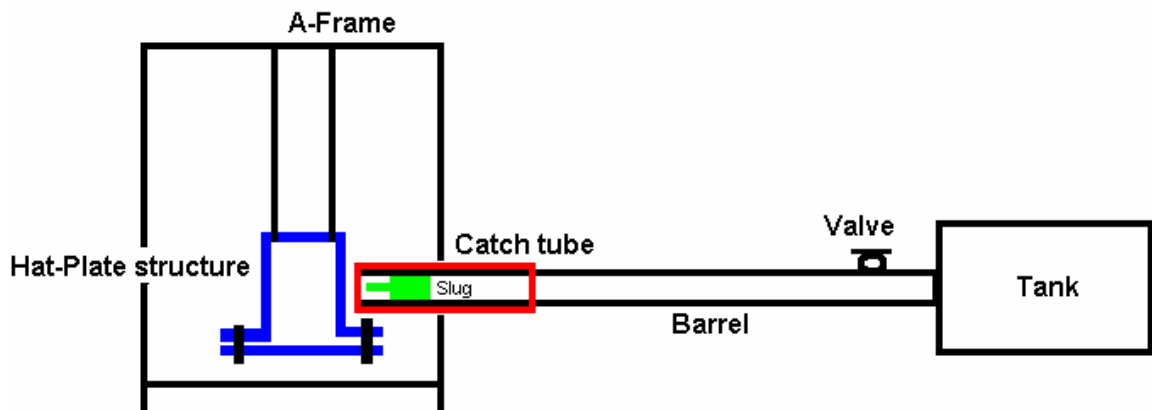


Figure 5.1 Block diagram of air gun experimental set up



Figure 5.2 A-frame used in the air gun experiment

Two 6.1 m (20-ft) I-Beams (10.2 cm x 5.1 cm cross-section) were used to provide support for the barrel and also add mass to the gun, to resist recoil. These I-beams run parallel and are joined together with four steel tubes that are welded to the beam flanges as shown in Figure 5.3. The pressure vessel (air tank) used in the air gun is 0.129 m<sup>3</sup> (7900 in<sup>3</sup>) volume and rated to 1.379 MPa (200 psi) maximum pressure. A pressure gauge mounted on the air tank (Figure 5.4) was used to read the pressure in the tank. The air tank was mounted at the end of the I-Beam using four bolts and the 5.0 cm (2 in). port on the tank faces too the other ends of the beams. A 5.0 cm (2 in), full-bore hand actuated ball valve is attached to the port with an 8 in. long pipe nipple, allowing movement of the valve handle (Figure 5.4). Both sides of the ball valve are standard 5.0 cm (2 in) female pipe threads. In order to load the cannon, a breach was added on the down streamside of the ball valve. The breach is constructed with two pipe unions and one 45.7 cm (18 in) long pipe nipple. Threaded into the downstream pipe union is the 6.1 m (20-foot) long seamless steel pipe. Supports for the steel pipe are constructed from 3.17 cm (1.25 in) unistrut and bolted to the cross supports that hold the I-beams together. The pipe is fixed to the unistrut with pipe clamps that can slide along the unistrut to adjust the height of the barrel if need [62].

The free end of the air gun barrel is fitted with a catch-tube as shown in Figure 5.5. The catch tube is a safety device designed specifically for this air gun test. The catch tube slides on the barrel end and has an opening of 3.8 cm (1.5 in) at the closed end. This opening allows the front end (striking part) of the slug to pass through. The catch tube captures the slug after the slug impacts the bolted structure as shown in Figure 5.6. The slug will stay inside the catch tube after impacting the bolted structure. Also the catch

tube will absorb any kinetic energy left in the slug after the impact. The catch tube is chained to the I-Beam as shown in Figure 5.5. This allows the catch tube to travel for 15.0 cm (~six inches) and then stops sliding on the barrel. Figure 5.7 shows the aluminum slug used in the air gun test. The total length of the slug is 15.2 cm (6 in) with the striking part of 55.7 mm (2.2 inch). The diameter of the striking part and sliding part of the slug are 27.4 mm (1.1 inch) and 50.7 mm (2 inch) respectively. The sliding part, slides in the barrel and the striking part of the slug impacts on the bolted structure as shown in Figure 5.6.



Figure 5.3 Air gun barrel and the I-Beam



Figure 5.4 Pressure tank and barrel of the air-gun test



Figure 5.5 Catch tube

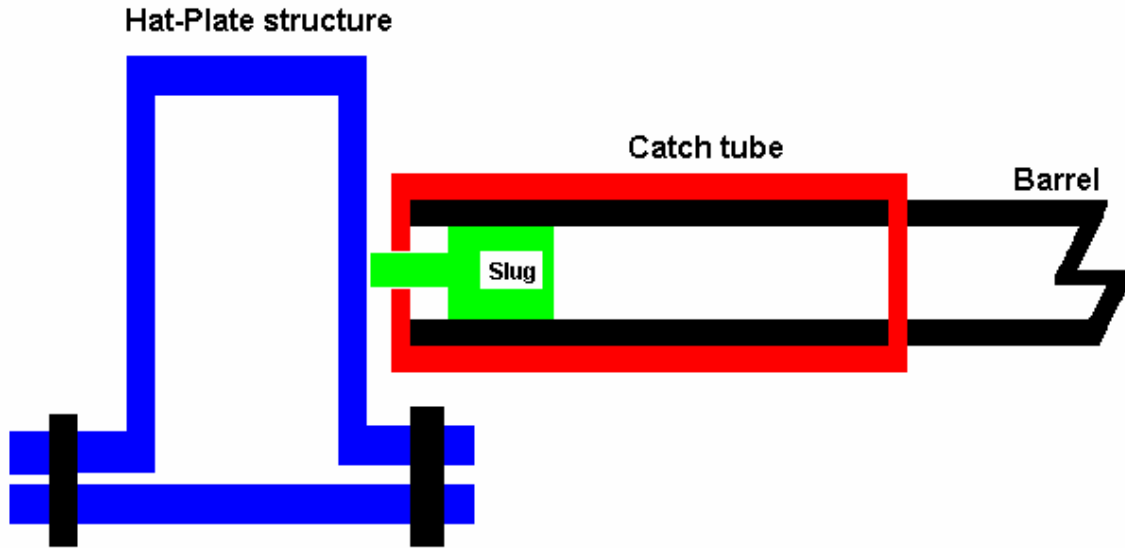


Figure 5.6 Diagram of slug impacting the hat-plate structure

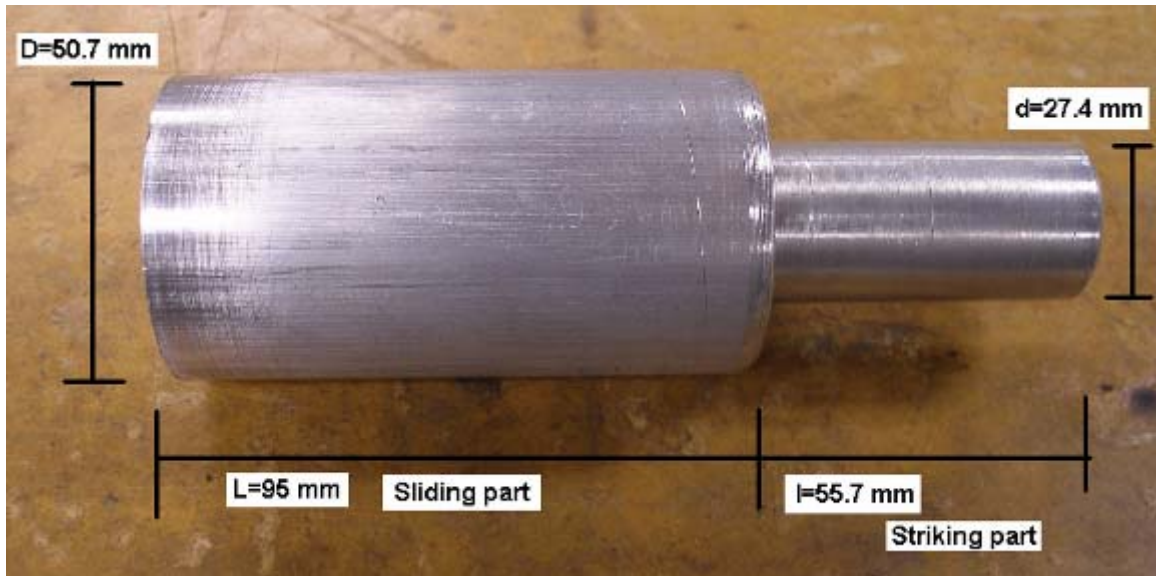


Figure 5.7 Aluminum slug used in the air gun experiment

### 5.3 Air gun experiment procedure

The UNLV CMEST air gun test was used to conduct a high impact / shock loading experiment on the bolted structures. The air gun uses pressurized air to drive an aluminum slug at high velocity on to a test structure. The velocity of the slug depends on the mass of slug, pressure in the tank and the length of the barrel. In this experiment, the length of barrel and mass of slug was kept constant and the air pressure in the tank was varied, to get the required slug velocity. The impact force on the bolted structure is proportional to velocity of impacting slug. The bolted hat-plate structure and two-hat bolted structures were used to study the high impact loading. These two structures are shown in Figure 5.8 and Figure 5.9 respectively. The details of the hat-plate structure are given in Chapter 4. The two-hat structure is 2.65 mm thick and is approximately half the size of the hat-plate structure. The low impact loading experiment on the two-hat structure was carried out by Doppola [9]. These two structures were recommended by ARL to conduct impact experiment and simulate the shock propagation in bolted joint using LS-DYNA FE solver.

The accelerometers and load cell used in the medium impact experiment (explained in Chapter 2) cannot be used for high impact loading experiments. Figure 5.10 shows the load cell and accelerometer used in the medium impact loading experiment. The load cell was mounted on the hat-section using 5/8-18 studs as shown in Figure 5.8. A protective aluminum cap was mounted on the stud nut to protect the nut from direct impact and also to distribute the impact load evenly on the load cell. The accelerometers were directly screwed to hat and plate structure. The bolted structures were freely hanging from the A-Frame during the experiment. The hanging structure eliminates all the boundary



condition, for easier simulation using FEA. Figure 5.11 shows the slug projecting out of the catch tube and striking the two-hat structure (193<sup>rd</sup> frame and 206<sup>th</sup> frame or 64.33 ms and 68.66 ms). These pictures were taken using high-speed camera with 3000 frames per second. The slug stays in the catch tube after it strikes the bolted structure. The velocity of slug used in this experiment ranges from 9 m/s to 80m/s. The catch tube helps in stopping the high velocity slug, after the slug impacts the bolted structure during experiment.



Figure 5.8 Bolted hat-plate structure with load cell and accelerometer

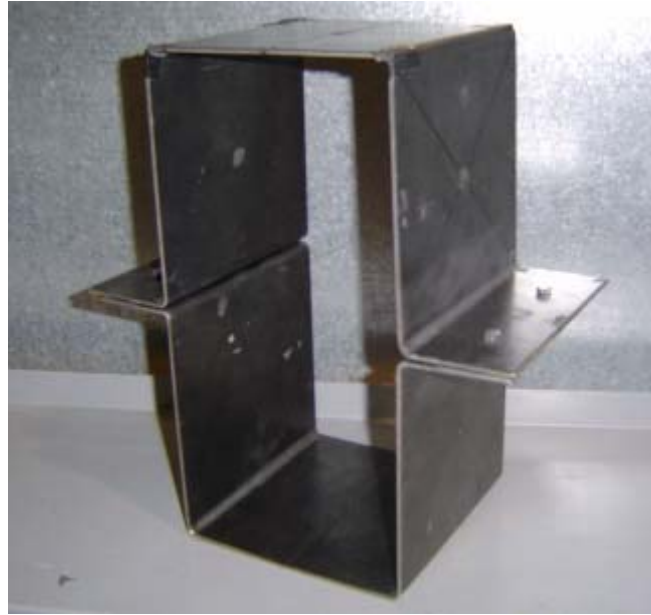




Figure 5.9 Bolted two-hat sections used in high impact loading experiment

**Model 205C**



PERFORMANCE	ENGLISH	SI
Sensitivity ( $\pm 15\%$ )	0.08 mV/lb	17.98 mV/kN
Measurement Range (Compression)	60,000 lb	266.9 kN
Maximum Static Force (Compression)	70,000 lb	311.4 kN
Broadband Resolution (1 to 10,000 Hz)	1 lb-rms	4.45 N-rms
Low Frequency Response	0.0003 Hz	0.0003 Hz
Upper Frequency Limit	50 kHz	50 kHz



**Model 350B21**

PERFORMANCE	ENGLISH	SI
Sensitivity ( $\pm 30\%$ )	0.05 mV/g	0.005 mV/(m/s <sup>2</sup> )
Measurement Range	$\pm 100,000$ g pk	$\pm 980,000$ m/s <sup>2</sup> pk
Frequency Range ( $\pm 1$ dB)	1 to 10,000 Hz	1 to 10,000 Hz
Frequency Range ( $\pm 3$ dB)	0.5 to 35,000 Hz	0.5 to 35,000 Hz
Resonant Frequency	$\geq 200$ kHz	$\geq 200$ kHz

Figure 5.10 Load cell and accelerometer specification





Figure 5.11 High speed camera image of slug impacting the two-hat structure (64.33 ms and 68.66 ms)

#### 5.4 Design and analysis of catch tube

The catch tube is a safety device, designed specifically for this air gun experiment. When the slug is fired from the air gun, the slug accelerates from the tank side towards the open end of the barrel. The catch tube is mounted at the exit side of the barrel. When the slug exits the barrel and catch-tube, it strikes the bolted structure and transmits the energy. Depending on the mass of the structure and exit velocity of the slug, the slug may rebound or try to exit the barrel and catch tube. The catch tube allows the striking part of the slug to exit the barrel and stops the sliding part of the slug (Figure 5.6). During the air gun experiment, part of the kinetic energy of the slug will be transferred to the bolted structure and the remaining part will be absorbed by the catch-tube, based on the mass of the structure. In the worst case (assuming the slug fails to impact the structure), the catch tube must absorb all the energy of the slug as shown in the Figure 5.12. The slug exit velocity was in the range of 10 m/s to 80 m/s and the mass of the slug was 600 grams.

First step in the experiment was to make sure that the catch tube is adequate to capture the slug, when the slug exits the barrel. In the initial design of the catch-tube, only four L-shaped clamps were welded at the front end of the catch-tube. The catch tube was tested, by firing slug at velocities ranging from 5 m/s to 80 m/s as shown in Figure 5.12. During this initial test, no structure was mounted and the catch tube absorbed all the energy of the slug. When the slug impacted the catch tube at the velocity of 80 m/s (air pressure in the tank = 0.17 MPa (25 psi)), the catch tube front plate along with the four L-clamps deformed as shown in Figure 5.13. Also some of the welds in the catch tube front end cracked. This design was not adequate to withstand the worst case that can be encountered during the air gun experiment.

The failure of the catch tube front end and the four L-Clamps during initial test was verified using explicit FE analysis. A LS-DYNA FE model was developed to simulate the slug impacting on the catch tube at velocity of 80 m/s. The FE model of the catch tube and the slug is shown in Figure 5.14. In this FE model, the slug was defined with an initial velocity of 80 m/s (axial direction). The slug impacts the front end of the catch tube and the deformation of front end plate and the L-Clamps are shown in Figure 5.15. The FE model confirms the inadequacy of the catch-tube in capturing the slug moving at a velocity of 80 m/s. The catch tube was modified by welding two more L-clamps at the front end and also by doubling all the welds thickness. The modified catch tube is shown in Figure 5.16. Later in all the air gun experiment, the modified catch tube was used. Figure 5.17 and Figure 5.18 shows the velocity and displacement plot of the catch tube and slug predicted by LS-DYNA FE model with a slug initial velocity of 60 m/s. The slug rebounds after impacting with the catch tube with the rebounding velocity of 5 m/s. The impact induces a forward velocity of 15 m/s for the catch tube and the velocity is in half sinusoidal form because of the reflecting stress waves traveling along the length of the catch tube.

The velocity of the catch tube and the slug can be calculated analytically by using conservation of momentum equation and collision equation.

$$m_A v_A + m_B v_B = m_A v'_A + m_B v'_B$$

$$e = \frac{v'_B - v'_A}{v_A - v_B}$$

$m_A, m_B$  = Mass of Slug and Catch tube

$v_A, v_B$  = Velocity of Slug and Catch tube before impact

$v'_A, v'_B$  = Velocity of Slug and Catch tube after impact

$e$  = Coefficient of Re stitution

Figure 5.19 shows the velocity plot of catch-tube and slug for various coefficient of restitution ( $e$ ) value. The analytically predicted velocity values of catch tube and slug, corresponding to coefficient of restitution ( $e$ ) 0.15, matches with the FE velocity values. The low value of ' $e$ ' indicates that the impact point deformed plastically.



Figure 5.12 High speed camera image of slug and catch tube



Figure 5.13 Deformed catch tube from the slug impact

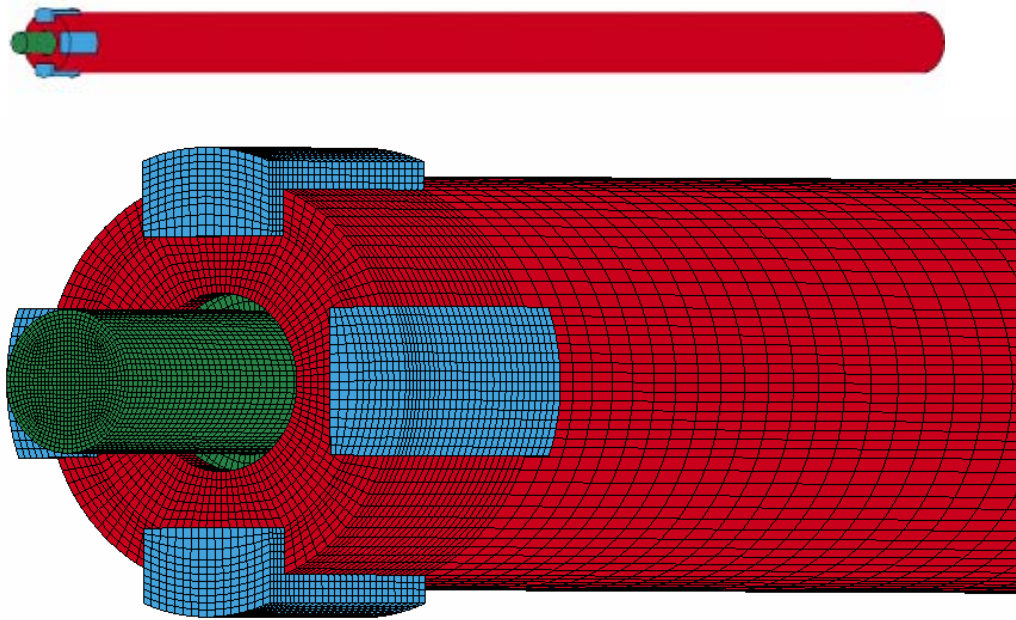


Figure 5.14 FE model of slug and the catch tube (initial design)

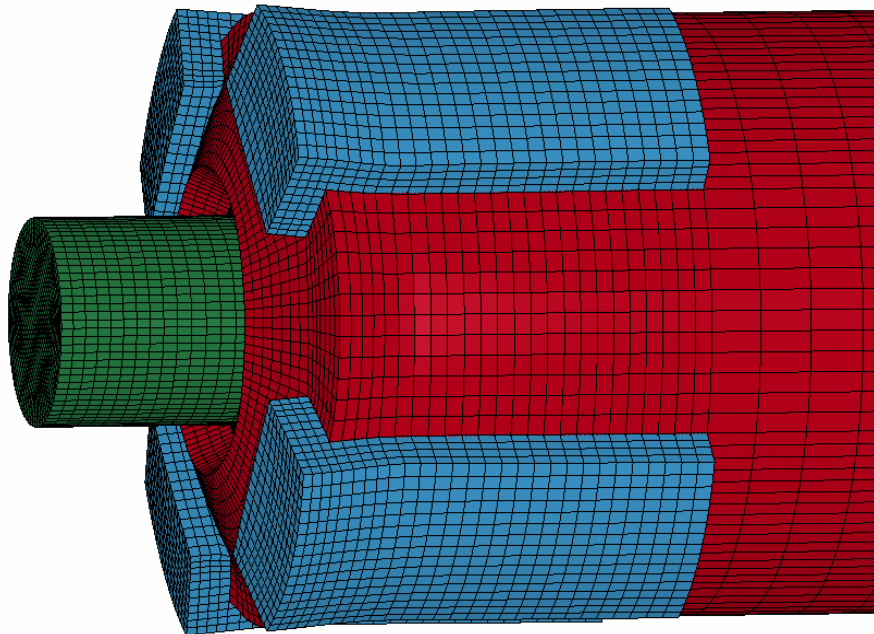


Figure 5.15 Deformed catch tube from FE analysis



Figure 5.16 Final design of catch-tube with six L-clamps

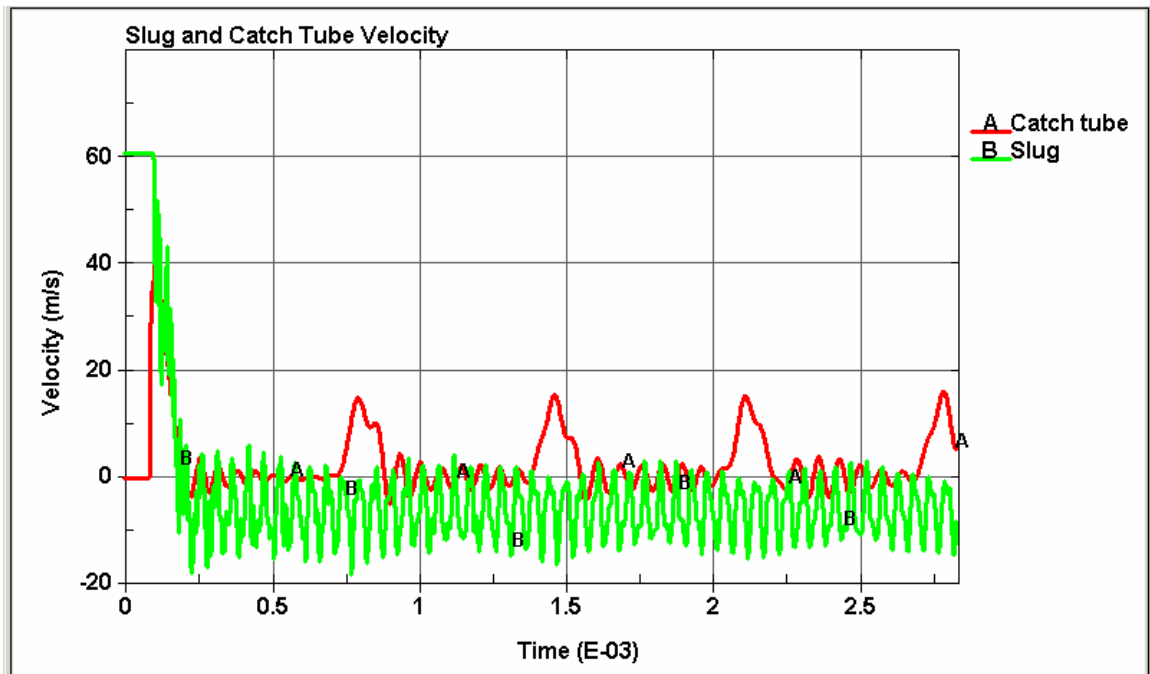


Figure 5.17 Velocity of slug and catch tube predicted by LS-DYNA FE analysis

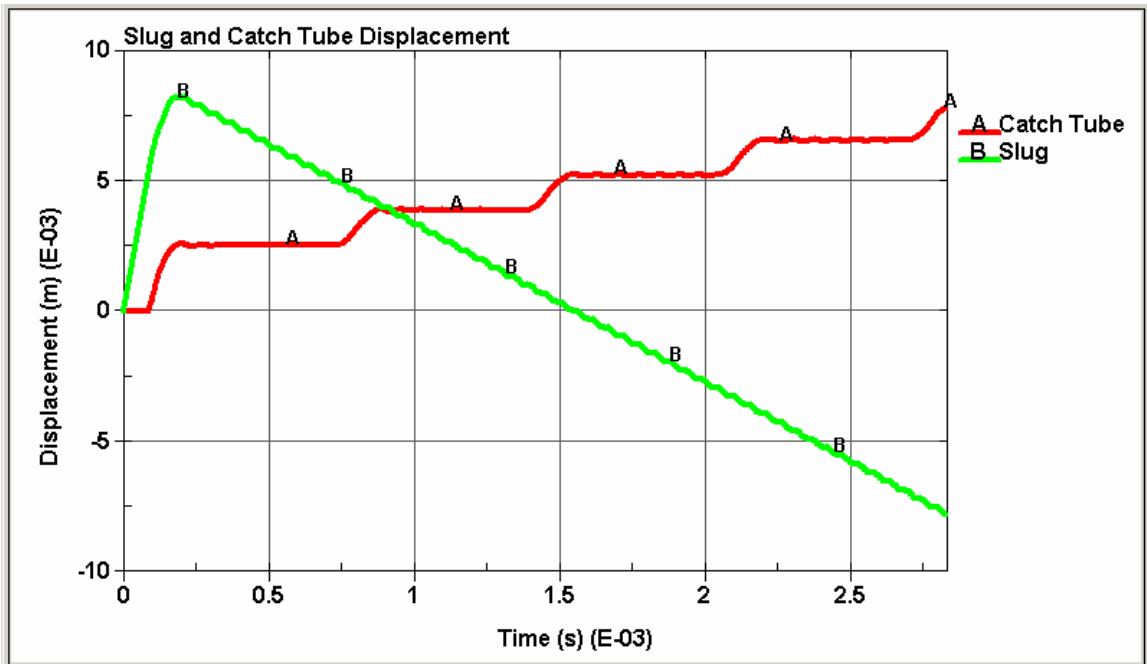


Figure 5.18 Displacement of slug and catch tube predicted by LS-DYNA FE analysis

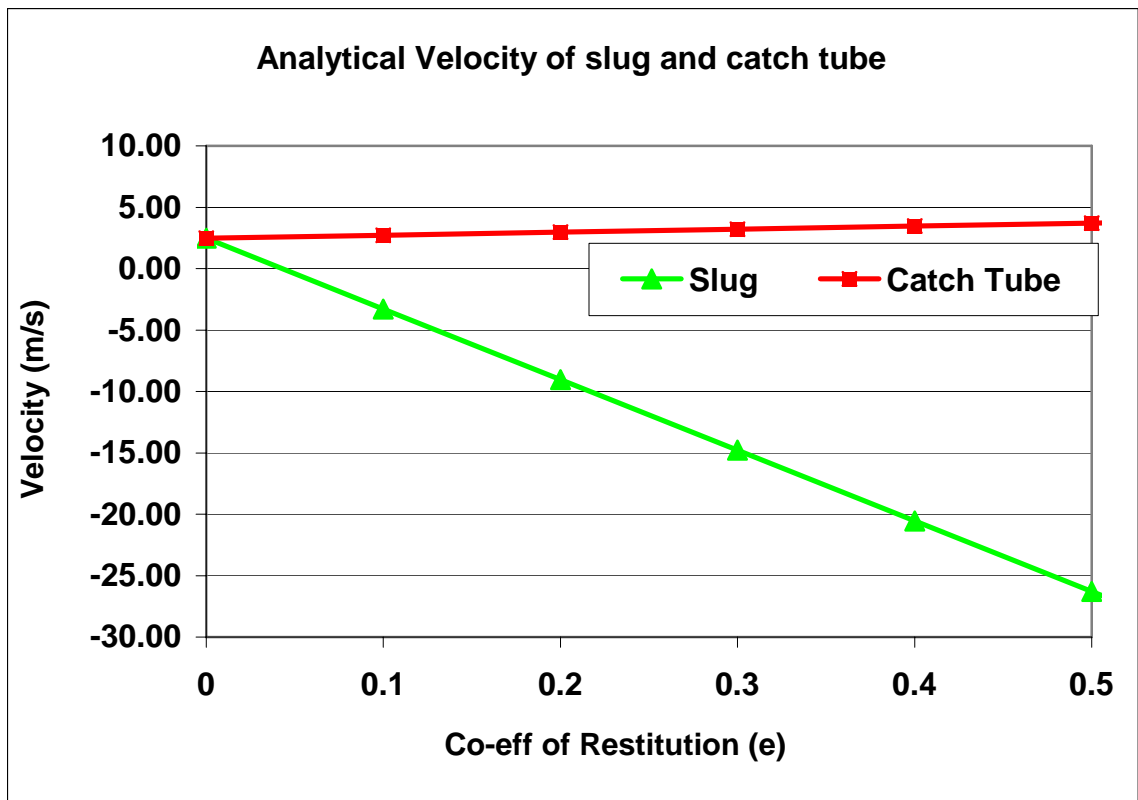


Figure 5.19 Analytical velocity of catch tube and slug for various 'e' values



## 5.5 Calibration of air gun experiment

The exit velocity of the slug in the air gun experiment depends on the pressure in the tank, length of the barrel, mass of the slug and barrel diameter. The pressure in the tank decreases (because of expansion) as the slug moves from the initial position (near valve) to the final position (near the barrel exit) as shown in Figure 5.20. The decrease in the pressure is caused by the increase in the volume (behind the slug) as the slug moves and this expands the compressed air in the tank. The slug velocity is the input for the FE model. Therefore it is very important to calculate the slug velocity accurately, as the FE results are based on the slug velocity. Slug velocity was calculated analytically based on the air gun dimensions and pressure in the tank. Also the velocity of slug was calculated using high-speed video camera.

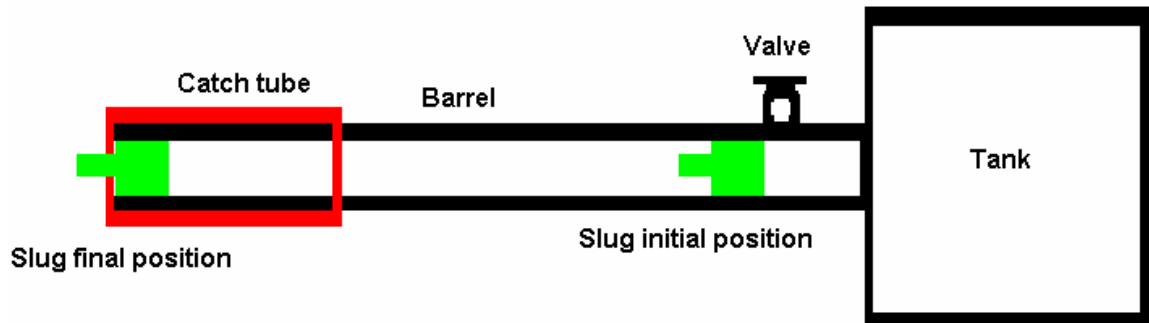


Figure 5.20 Diagram showing initial and final position of slug in the barrel

### 5.5.1 Analytical slug velocity calculation

The velocity of the slug can be calculated by using thermodynamics and dynamics equations. Boyle's law states, "For a given volume of ideal gas at constant temperature,



the product of volume and pressure is constant". [62]. The mathematical equation for Boyle's law is given as

$$PV=K \text{ (constant)}$$

$$P_1V_1= P_2V_2$$

P, V = Pressure and Volume of the closed system

Sectioning the barrel into small incremental distances and using Boyle's Law to calculate each incremental change in pressure, determines the force pushing on the back of the slug. Hundred increments of the barrel were used in calculating the velocity of the slug. Newton's second law was used to calculate the acceleration of the slug at each increment of the barrel.

We have

$$F = P \times A$$

$$a = F / M$$

where

F = Force

A=Area of barrel / slug

a = Acceleration

M = Mass of slug

The acceleration is assumed to be constant over each increment. The incremental velocity of the slug can be calculated from acceleration by using the kinematics equation.

$$V^2=V_0^2 + 2.a (x-x_0)$$

A MATLAB program based on above equations was used to calculate the velocity of the slug. The input for the program was tank volume, tank pressure, mass of slug, length

of barrel, area of barrel and number of increments on the barrel. Figure 5.21 shows the plot with the relation between the pressure in the tank and the exit velocity of the slug. All the variables except the tank pressure were kept constant throughout the experiment. Therefore the exit velocity is proportional to the tank pressure. The MATLAB program used in calculating the exit velocity of the slug is given in APPENDIX-A.

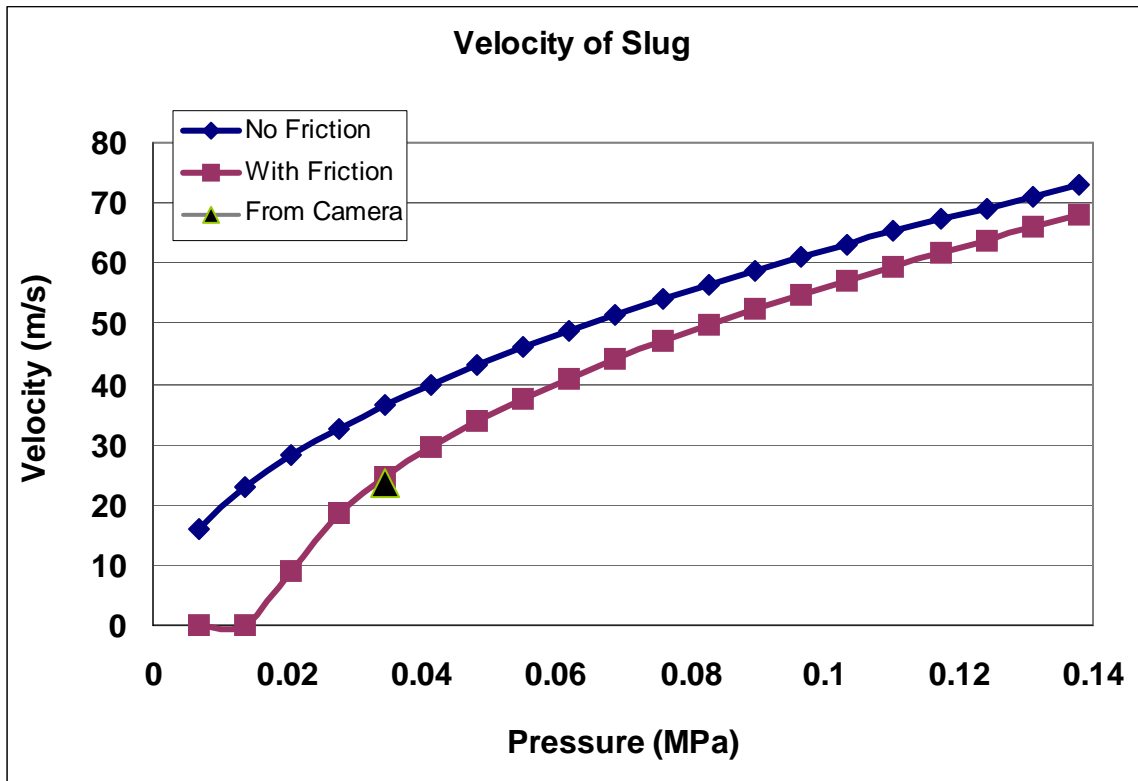


Figure 5.21 Theoretical velocity of slug with & without friction and velocity of slug obtained from the high-speed camera

### 5.5.2 Slug velocity verification using high speed camera

A high-speed camera (Phantom V 4.3, Vision Research) was used to record a slow-motion play back film of the air gun experiment. This camera allows taking 3000 frames per second, and outputs both film and pictures of every frame. Figure 5.22 shows the

three consecutive pictures, taken at every 1/3000 second. These pictures can be used to measure the slug velocity. A cardboard with vertical lines drawn for every 2.54 cm (1 in) is placed behind the catch tube as shown in Figure 5.22. The high-speed camera will capture the slug impacting the catch tube with marked cardboard in the background. The pictures shown in Figure 5.22 were used to measure the velocity of the slug by using "Get data" software [63]. This software allows measuring the distance in a digital picture by counting pixels. Each frame in Figure 5.22 is 1/3000<sup>th</sup> second apart and the distance traveled by the slug during 1/3000<sup>th</sup> second is 7.98 mm (0.31428 in), which is equal to 23.5 m/s. The corresponding pressure in the tank was 0.0344 MPa (5 psi). In other words, the slug will attain an exit velocity of 23.5 m/s for a air pressure of 0.0344 MPa (5 psi).

The theoretical exit velocity of slug for 0.0344 MPa (5 psi) air pressure in the tank is 36.7 m/s. But the high-speed camera shows that the exit velocity is only 23.5 m/s. This difference in the theoretical exit velocity of the slug is due to the absence of friction in the force equation. The friction force is given by

$$F = \mu N$$

$$F = \text{Friction Force}$$

$$\mu = \text{Friction Coefficient}$$

$$N = \text{Normal Force}$$

Friction coefficient was assumed as 0.5 [53] and then the exit velocity of the slug was calculated. The new theoretical exit velocity of the slug was 24.0 m/s. Figure 5.21 shows the velocity vs. tank pressure plots for theoretical (without and with friction added) and the high-speed camera results.

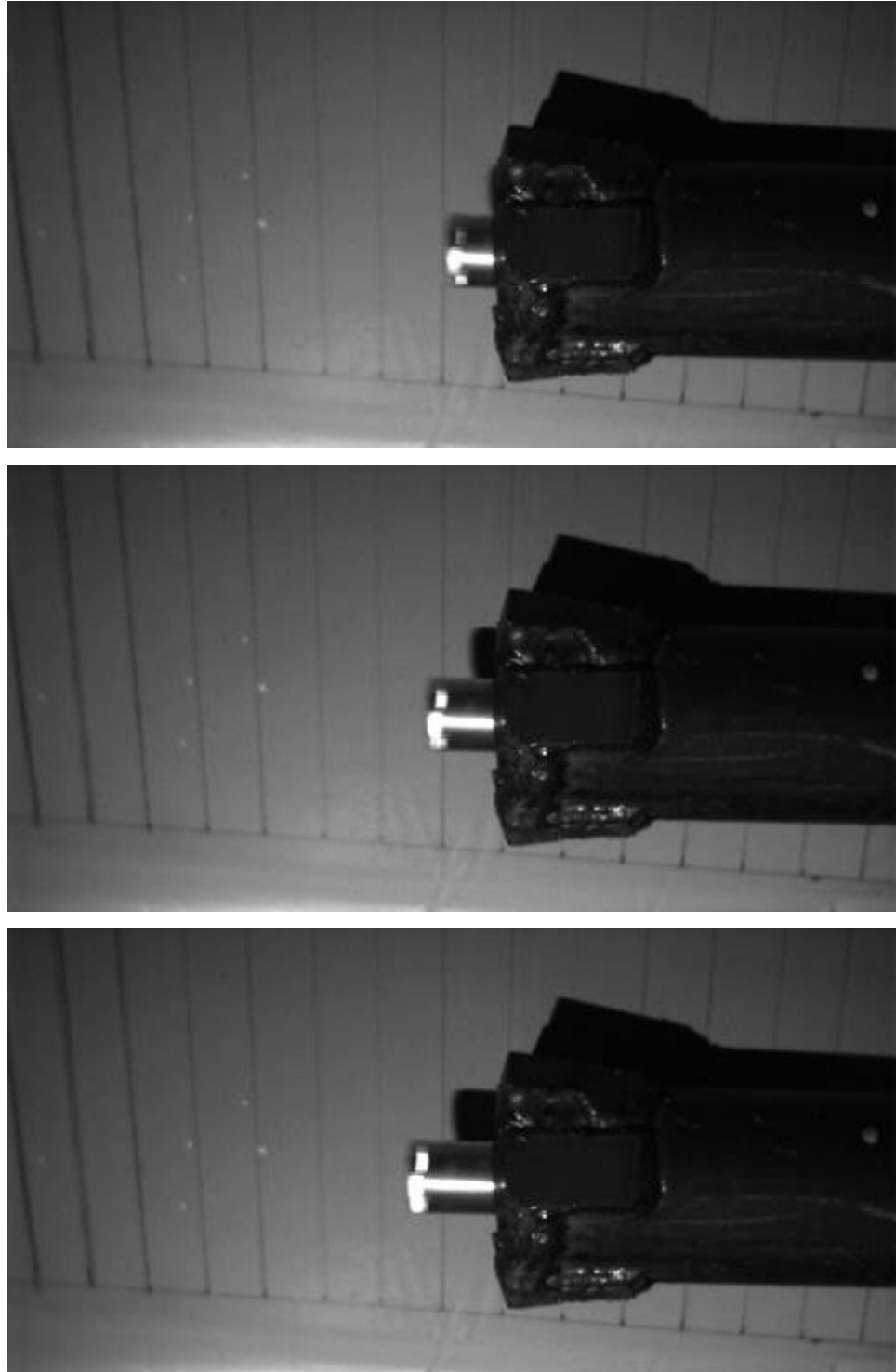


Figure 5.22 Images of slug and catch tube from high-speed camera to calculate the velocity of slug (1.66 ms, 2.0 ms and 2.33 ms)

## 5.6 High impact analysis of bolted structures using air gun

In the previous chapters, the response of the bolted structures subjected to low force impact loading was analyzed experimentally and computationally using FEA. Experimental and FE study included both modal analysis and impact analysis of a simple (cantilever beam with bolted lap joint) and a complex structure (bolted hat-plate structure). Also a parametric study of FE variables, which affect the transient response of the bolted structure, was carried out. In combat, army vehicles undergo high impact / shock loading when the vehicle trips a land mine. The army vehicle uses hundreds of bolted joints to connect different parts of the vehicle. To accurately simulate the blast on a vehicle using FE analysis, it is important to understand the response of the bolted joints and the structure to high shock loading.

Two types of bolted structure were selected to study the high impact loading. They are bolted hat-plate structure (used in previous chapters) and the bolted two-hat structure as shown in Figure 5.8 and Figure 5.9 respectively. The detailed experimental procedure for medium and high impact loading on bolted structure using air gun is explained in section 5.3. An aluminum slug weighing 600 grams was fired using pressurized air on the bolted structure. This induces a high impulse / shock on the bolted structure, which is similar to the shock experienced during blast loading. This is a controlled way of shock loading on the bolted structure.

### 5.6.1 Repeatability of the air gun experiment

The velocity of the slug is a function of air pressure in the tank. All other variables were kept constant during the experiment and only air pressure in the tank was varied to get the desired velocity of slug. In the previous section, the calibration of air gun

experiment using analytical and high-speed camera is explained. Another important aspect in the air gun experiment is the repeatability of the impact load. The experimental set-up to confirm the repeatability of the experiment using hat-plate structure is shown in Figure 5.23. A load cell (PCB-Model 205C) with an aluminum cap was mounted on the hat section of the structure (Figure 5.8). Along with this, two accelerometers were mounted on the hat-plate structure (one on hat and another one on plate) and the load cell and accelerometers were connected to oscilloscope to record the data. The accelerometers on the hat and plate structure measure the response in the loading and perpendicular to loading direction respectively. The slug was fired from the air gun, directly on to the load cell. During the two cases of repeatability experiment, the slug was fired at 24 m/s, which corresponds to 0.0344 MPa (5-psi) air pressure in the tank. Figure 5.24 is the plot of impact force between the aluminum slug and the bolted hat-plate structure when the slug was fired at 24 m/s velocity for two repeatability cases. For both the cases, the peak is around is 110 kN. Figure 5.25 and Figure 5.26 shows the acceleration plot of the hat (Acc-1) and plate (Acc-2) of two repeatability cases. The acceleration measured on the hat and plate structure during the repeatability test shows identical response. This confirms that the air gun test is deterministic and is not a random process and can be simulated using FE analysis. Figure 5.27 shows the FFT of the hat-plate structure when subjected to low impact loading (using instrumented impact hammer) and medium impact loading (slug impact). As expected, the peaks in the FFT curve for high impact loading has higher magnitude and also there is more number of peaks. This suggests that high impact loading excites more natural frequencies of the hat-plate structure.

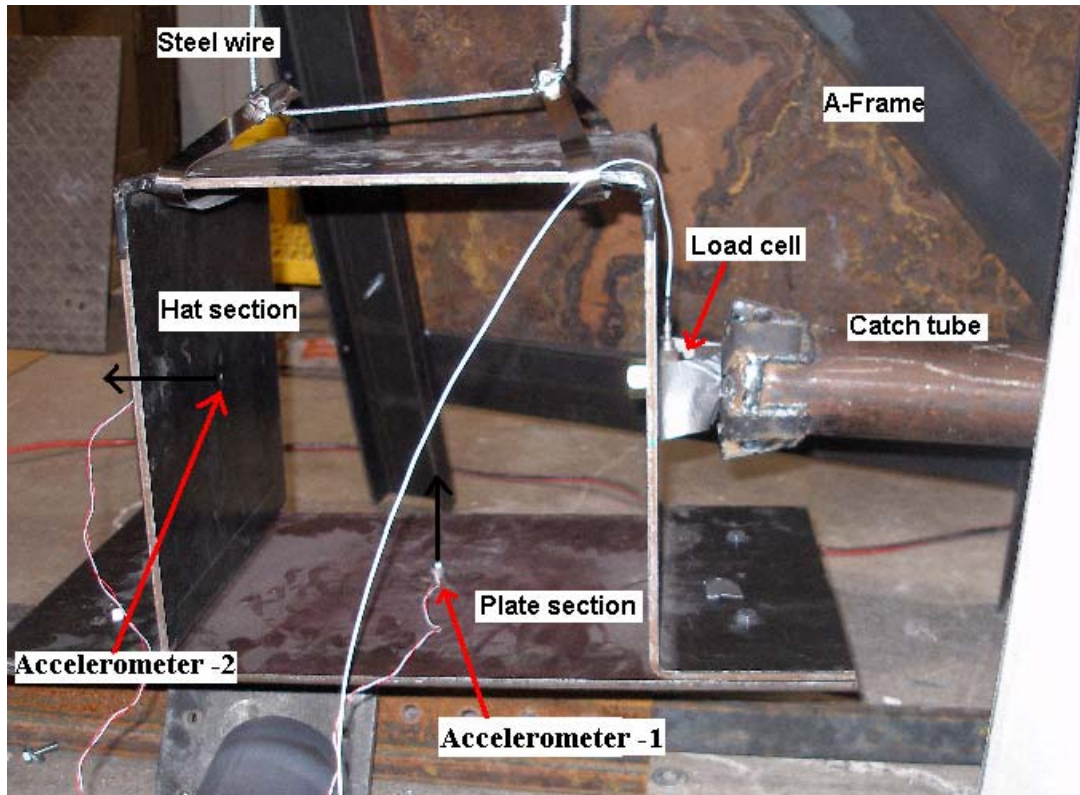


Figure 5.23 Experimental set-up of high impact loading on the hat-plate structure (Acceleration is measured in the arrow direction)

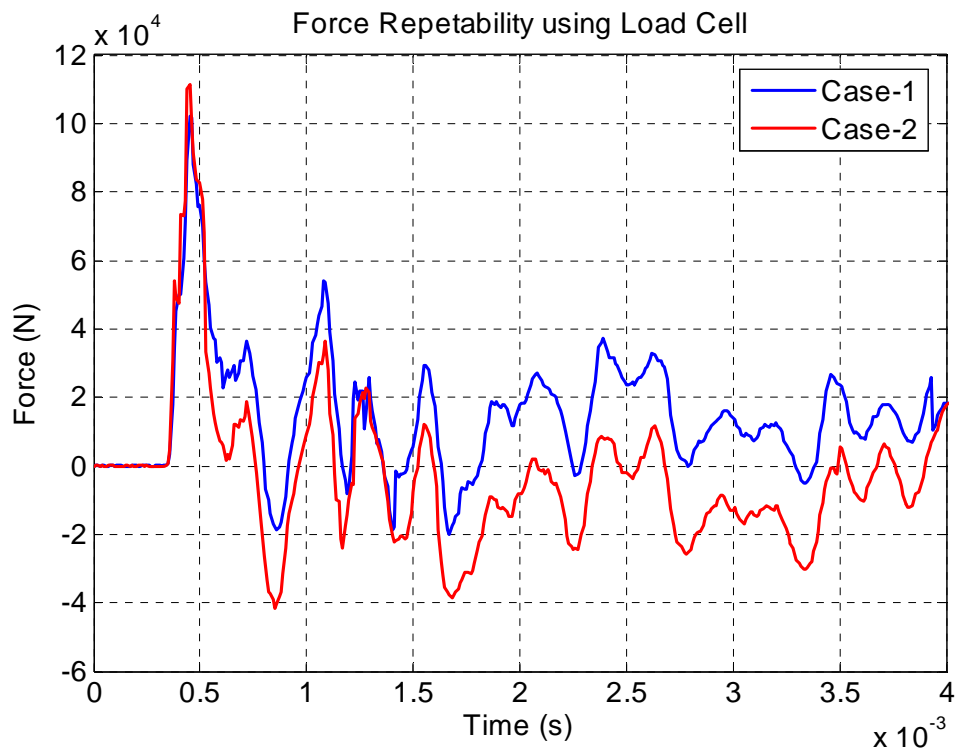


Figure 5.24 Impact force repeatability for the slug velocity of 24 m/s

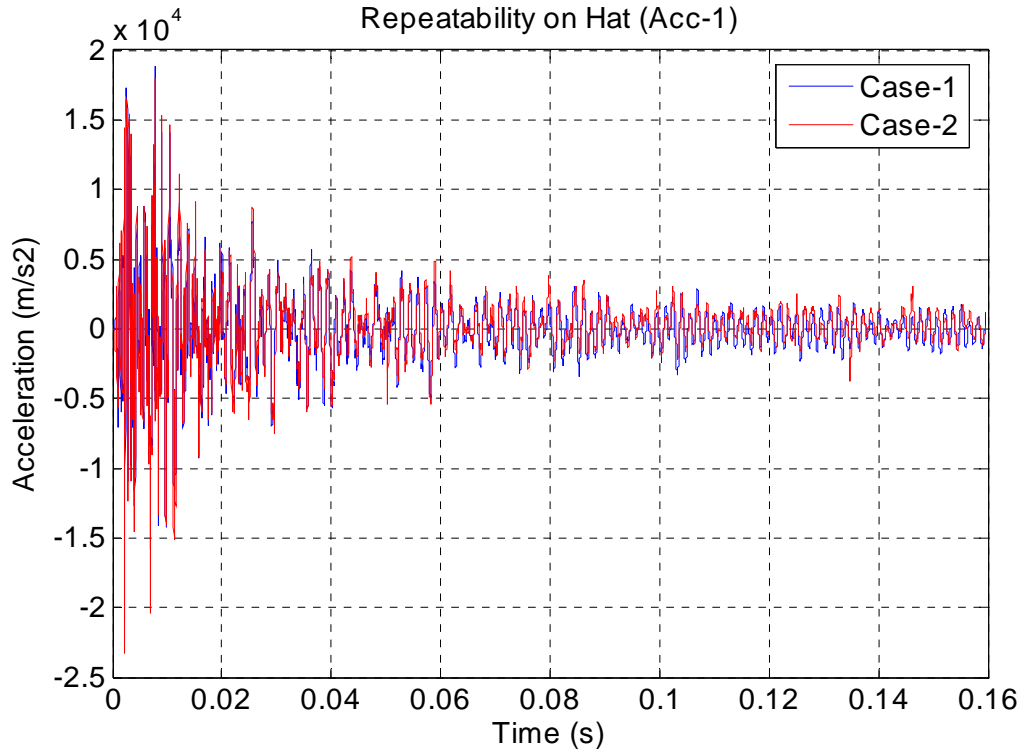


Figure 5.25 Acceleration repeatability on the hat structure

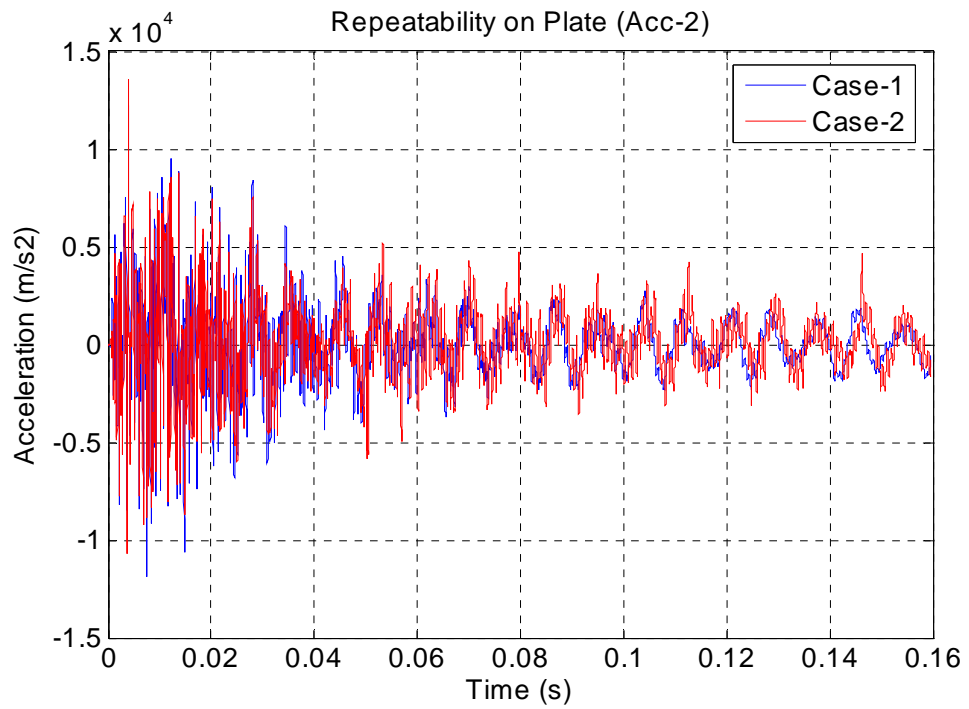


Figure 5.26 Acceleration repeatability on the plate structure



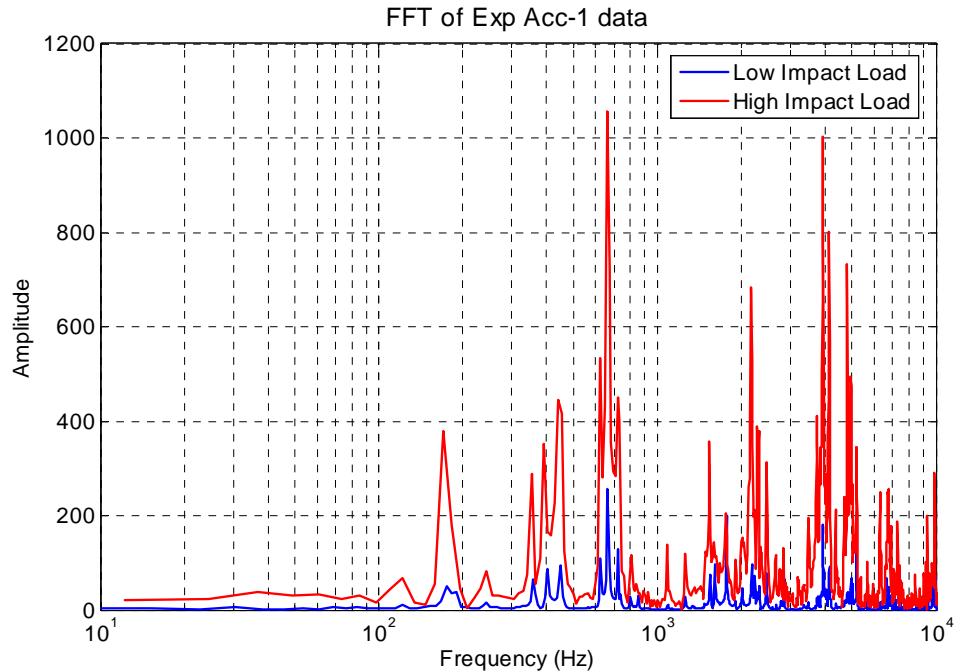


Figure 5.27 FFT of hat structure response from low and medium impact loading

### 5.6.2 FE analysis of medium impact loading on the hat-plate structure

The bolted hat-plate structure was selected to study the shock loading on bolted joint experimentally, and FE analysis was used to simulate the shock loading. The low force (20kN) impact loading analysis on the bolted hat-plate structure is explained in previous chapter. Air gun with slug was used to induce the medium force (150 kN) and high force (235 kN) impact / shock loading on the bolted hat-plate structure. LS-DYNA explicit solver was used to simulate the high impact loading on bolted hat-plate structure. Two FE models of hat-plate structure were developed to study the shock phenomenon. Figure 5.28 shows the detailed FE model (Model-1) of hat-plate structure with 3-D solid elements. Contacts were defined in the FE model between the bolt assembly and hat-plate structure, and also between the hat and plate sections. Preload was also defined on the bolt assembly using Initial\_Stress\_Section card. Slug was modeled using 3-D solid

elements and initial velocity (equal to exit velocity of slug from the barrel) was defined on all the nodes of slug FE model. Damping was not defined in the FE model because the bolted joint was modeled with contacts and friction. This FE model of hat-plate structure has all the details of air gun experiment. Figure 5.29 shows the FE Model-2 of the hat-plate structure using shell elements. In this FE model, the bolt is modeled using `Constrained_Rivet_ID` card. This card connects two structures with a rigid beam, as shown in Figure 5.29. Five rivets were modeled for each bolt and totally 20 rivets replaces four bolt assembly in the hat-plate structure. Surface contacts were defined between hat and plate structure. This FE model is similar to FE model-1 in chapter-3 with shell elements except the rivets. In medium and high impact loading, the rivets were added to the FE model instead of tied contact, so that the deformation near the bolt location can be captured. These modifications simplify the FE model to great extent and also decrease the CPU time during transient analysis. In the FE simulation of vehicles subjected to blast or crash analysis, all the bolt assemblies in the vehicle cannot be represented in detail in the FE model. Similar to a simplified FE model as in Figure 5.29, can be used to represent bolted joint in FE model of vehicle.

Stiffness proportional damping (SPD) factor of  $\beta = 6.5\%$  (0.065) were used in the FE model-2. In chapter three of this report damping factor for bolted joint structures was calculated using half-power bandwidth method. For elastic analysis, the calculated damping factor was 6.5% (0.065) and this value is within the range [5-7%] given by Newmark [56]. Also he defined damping factor of 10-15% for plastic range. Therefore a SPD factor of  $\beta = 6.5\%$  (0.065) was used in the FE model for the medium force impact loading cases where the structure deformed elastically. A SPD factor of  $\beta = 14\%$  (0.14)

was used in the FE model for the high force impact loading case where there was significant plastic deformation in the structure and a load cell was not used. The peak impact force was estimated from the FE analysis.

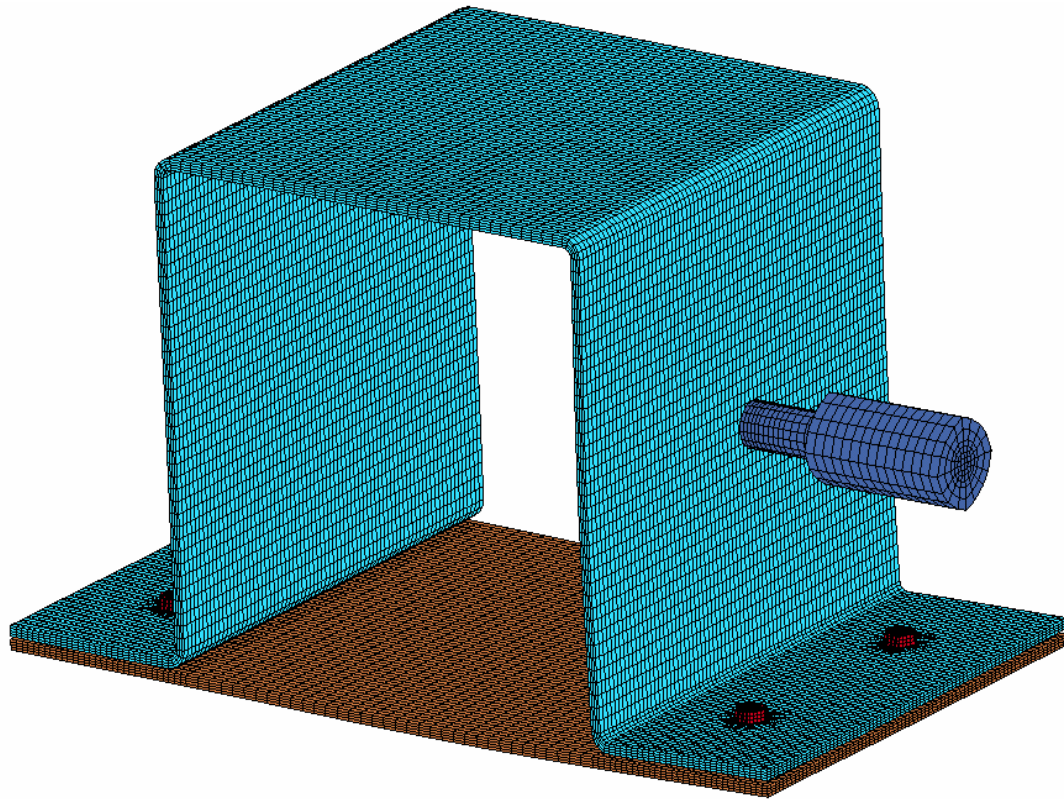


Figure 5.28 FE model-1 of bolted hat-plate structure and slug with solid elements

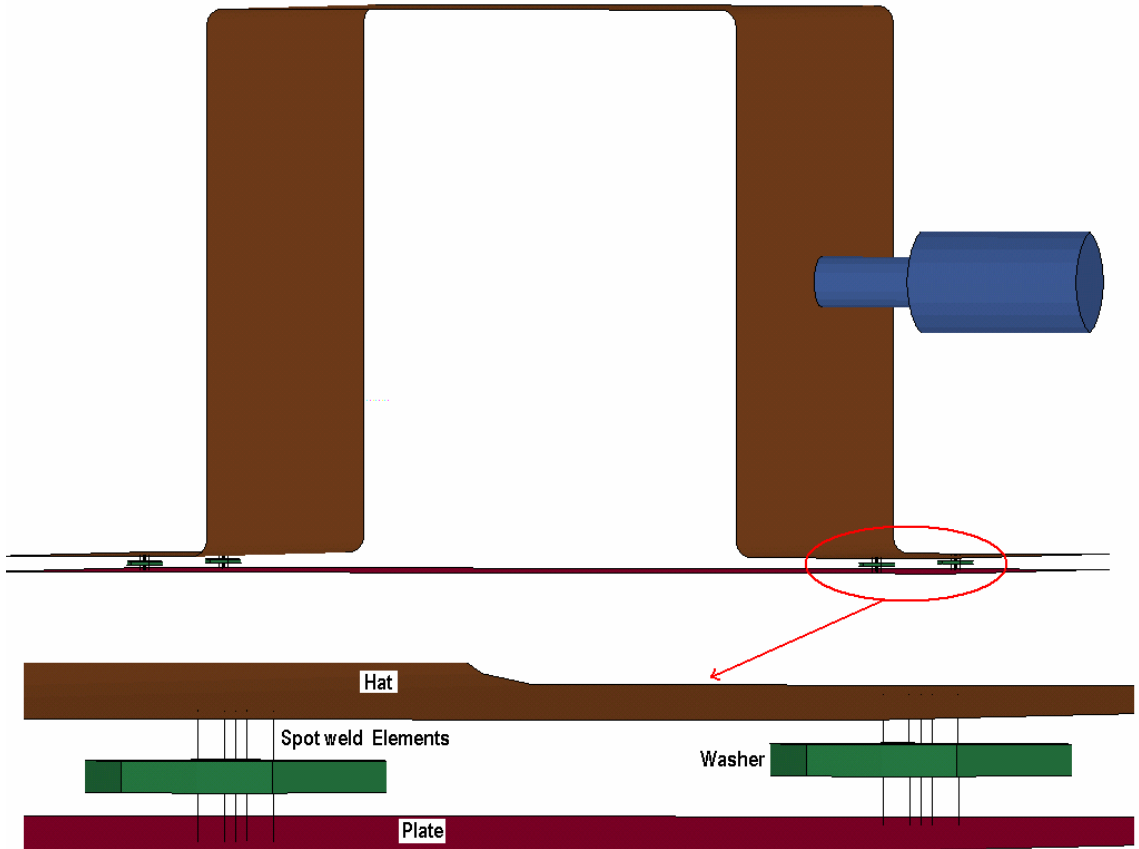


Figure 5.29 FE model-2 of hat-plate structure with shell elements and rivets

In the air gun experiment with the hat-plate structure, initially a load cell was mounted on the hat structure as shown in Figure 5.24. The slug was fired on this load cell and the force was measured along with acceleration of the structure. These are controlled experiments and the experiment was repeated for different velocity of the slug. The impact experiment was repeated with slug velocity of 9 m/s, 24 m/s and 34 m/s. These three velocities correspond to 0.020 MPa (3 psi), 0.034 MPa (5 psi) and 0.048 Mpa (7 psi) air pressure in the tank. Even though in these experiments, the slug was fired on the load cell mounted on the hat-structure, the velocity of slug was low enough to not damage load cell or structure.

The forces measured from the load cell, along with the predicted forces from the Model 1 and Model 2 FE simulations, when the slug impacts at velocity of 9 m/s, 24 m/s and 34 m/s (0.020 MPa (3 psi), 0.034 MPa (5 psi) and 0.048 (7 psi) air pressure) on the hat-plate structure are shown in Figures 5.30 - 5.32. The peak force recorded on the load cell for 9 m/s, 24 m/s and 34 m/s slug velocity impact is 45 kN, 105 kN and 150 kN respectively. Both the FE models predict the peak force with good accuracy.

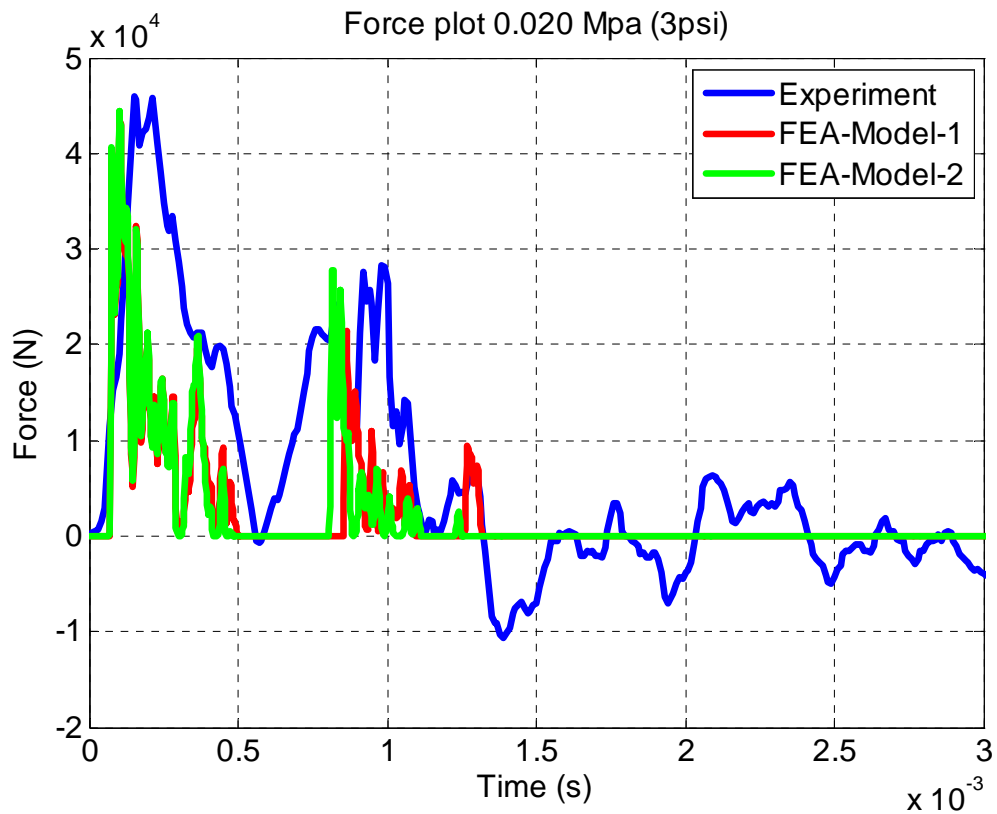


Figure 5.30 Impact force plots from experiment and FEA for velocity of 9 m/s slug

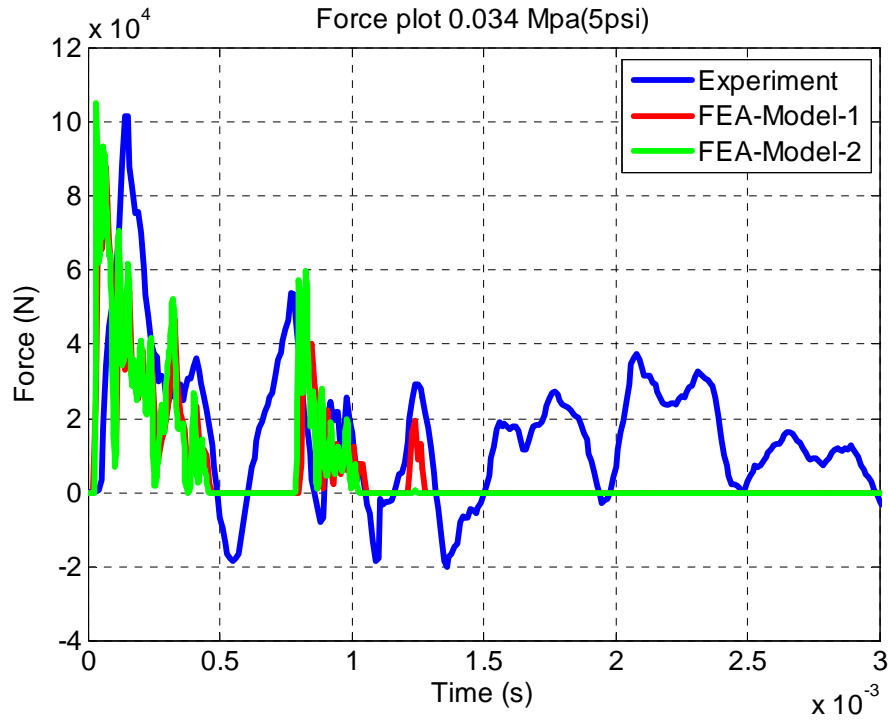


Figure 5.31 Impact force plots from experiment and FEA for velocity of 24 m/s slug

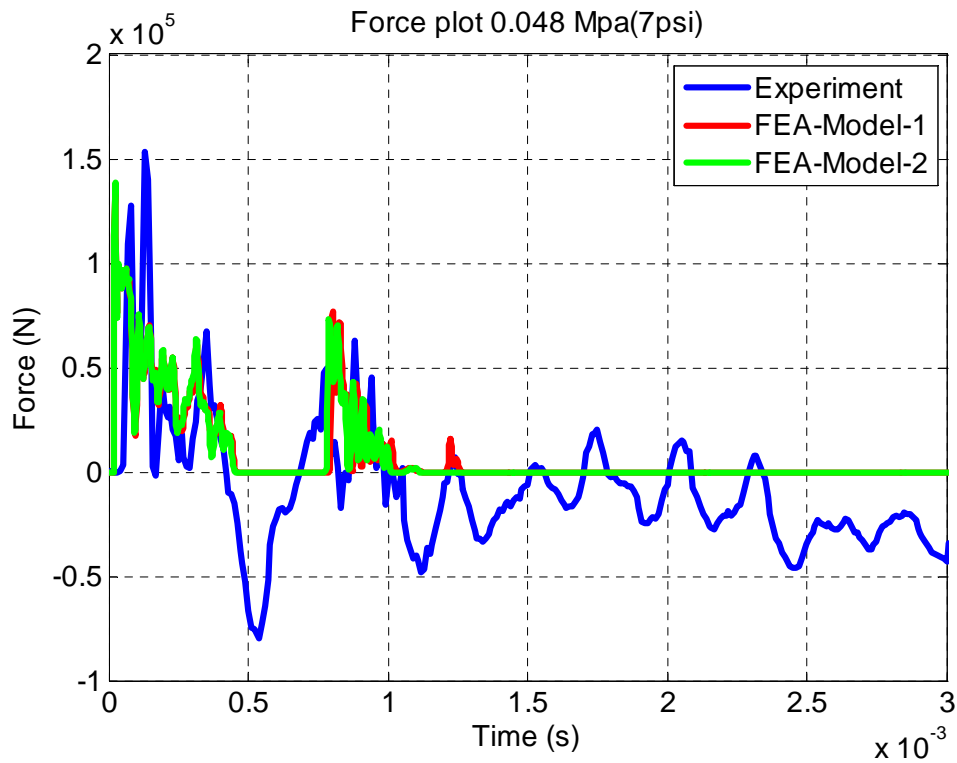


Figure 5.32 Impact force plots from experiment and FEA for velocity of 34 m/s slug

During the air gun experiment, the response (acceleration) of the hat-plate structure was measured at two points: one on the hat structure and another one on plate structure as shown in Figure 5.33. In the medium force impact load experiment, the load cell was mounted on the hat structure and the velocity of slug was low enough not to damage load cell or the structure. Figure 5.34 and Figure 5.35 show FFT and the experimental and FE Model-1 prediction of acceleration, for the slug impacting the hat-plate structure at velocity of 24-m/s. The frequency of FE prediction of hat section is in good agreement with the experimental results, but the magnitudes are higher. Also the FE prediction shows the shock wave reflection similar to experimental results. The FE model prediction on the plate (Acc-2) is in good agreement with the experiment. The damping was not included in the FE Model-1 because the contacts and friction were modeled in the FE model. Here the assumption is that the contacts and friction in the FE model will account for the joint damping. Similarly Figures 5.36 and Figure 5.37 show the FFT and the experimental and FE Model-2 acceleration results. The responses predicted by FE Model-2 are showing high magnitudes than the experimental results. Even though both the FE models predicted the impact force with good accuracy, the acceleration predicted from the FE Model-2 is having high magnitudes.

Table 5.1 shows the Normalized root mean square deviation (NRMSD) of the FE time history response (acceleration) from the experiment values. Here the experimental time history values are taken as basis and the deviation of FE results from the experimental values are measured. The NRMSD between the experimental and FE Model-1 are 0.13 and 0.14 for hat and plate structures respectively. Three-dimensional solid elements were used in the FE Model-1 and all the contacts with friction were

defined in this model. Preload on the bolt assembly was also defined in the FE Model-1. In other words, the FE Model-1 includes all the details of the experimental air gun experiment.

The FE Model-2 of hat-plate structure uses shell elements, and the bolts were defined as beams using \*Control\_Rivet\_ID card. This is a simplified FE model, and can be practically implemented in the full vehicle FE model to represent the bolted joints. This FE model gives NRMSD values of 0.14 and 0.18 for hat and plate structure acceleration response. The FE Model-2 reduced the CPU time by one order. The simplified FE Model-2 successfully predicted the impact force and the acceleration response for high impact loading on the bolted structures. The simplified model was capable of predicting the medium velocity slug impact and this same model will be used with same parameters for high impact loading. The high impact loading simulation will be highly non-linear and includes geometric, material and contact non-linearity.

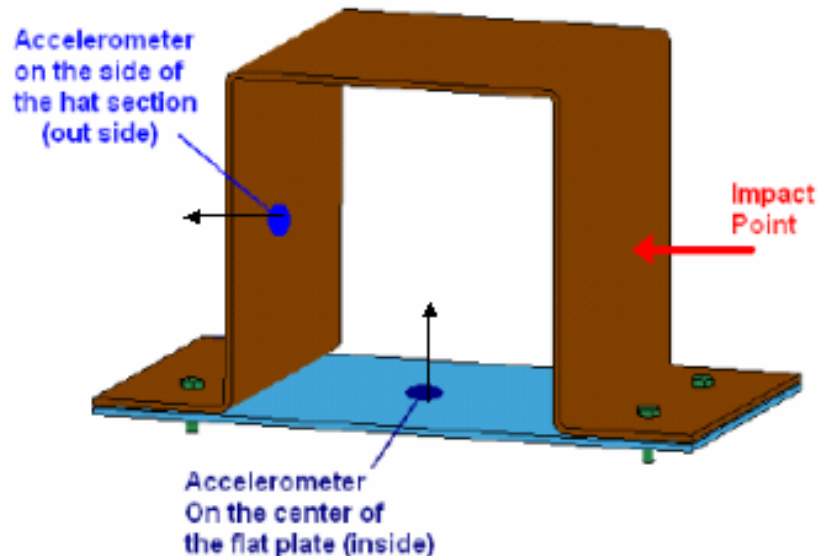


Figure 5.33 Hat-plate structure showing impact point and accelerometer locations



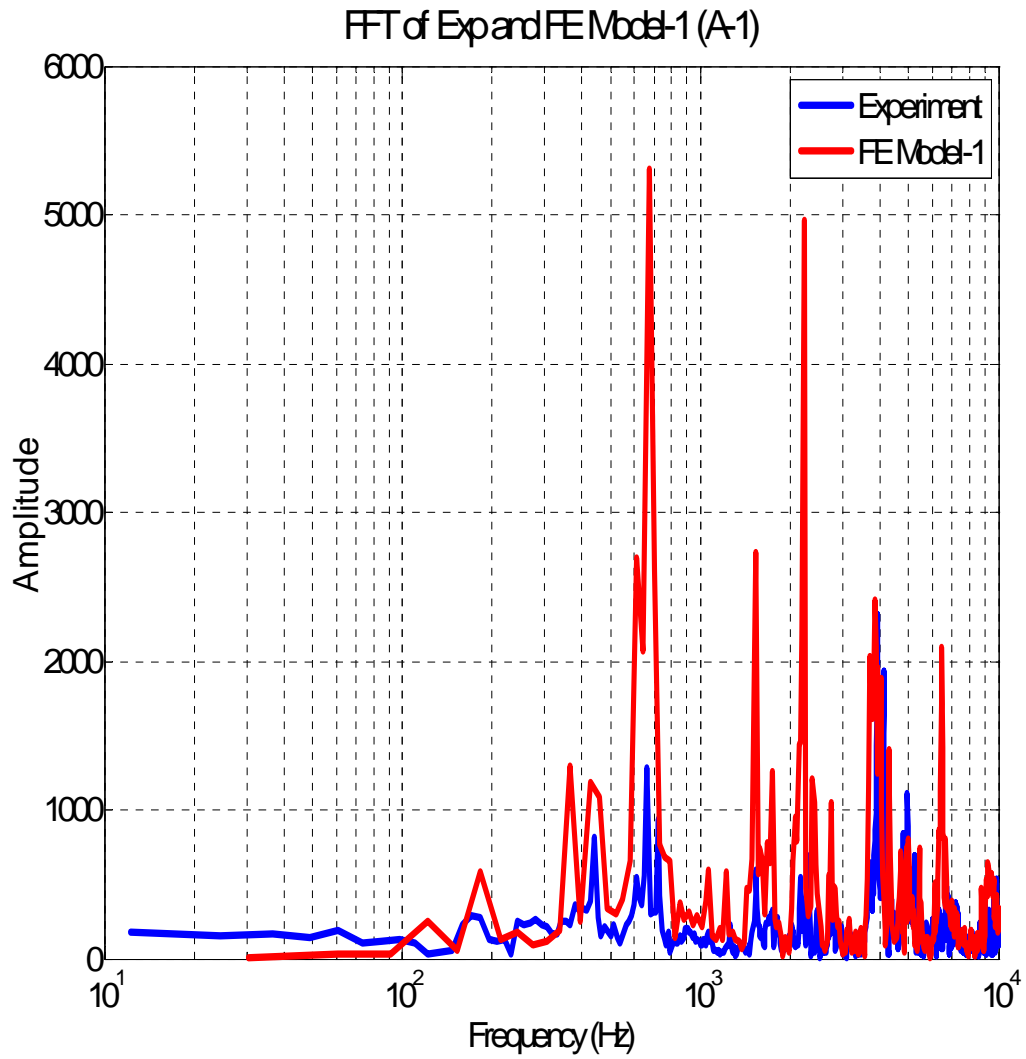


Figure 5.34 FFT of the experiment and FE model-1 for medium force impact loading

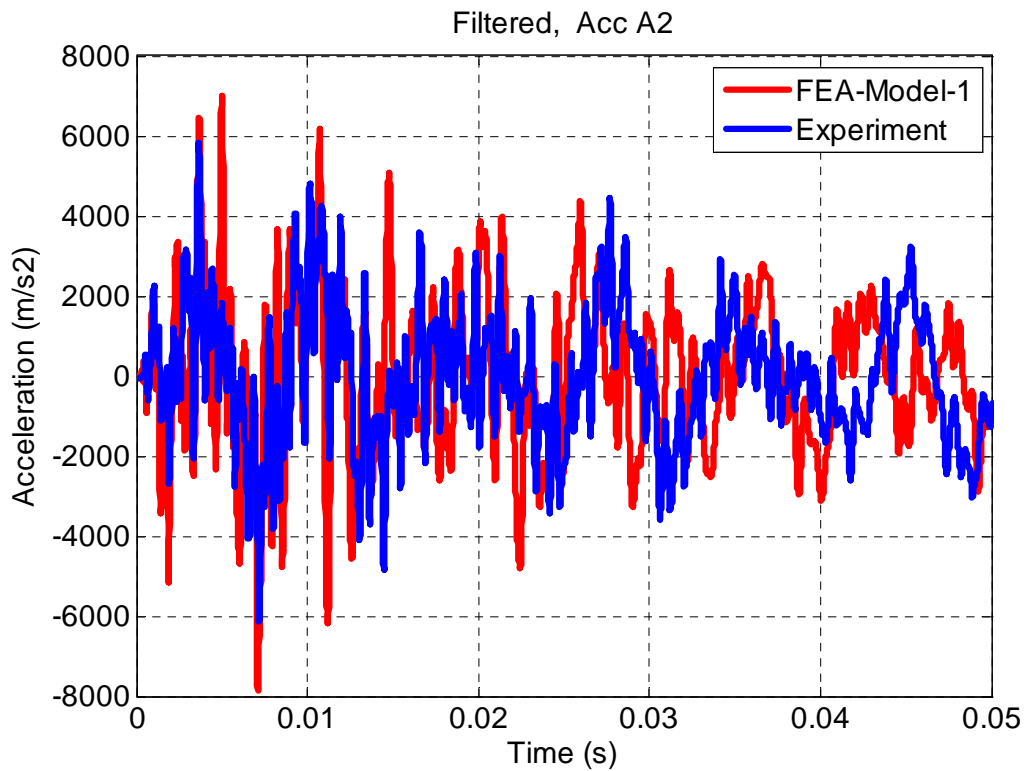
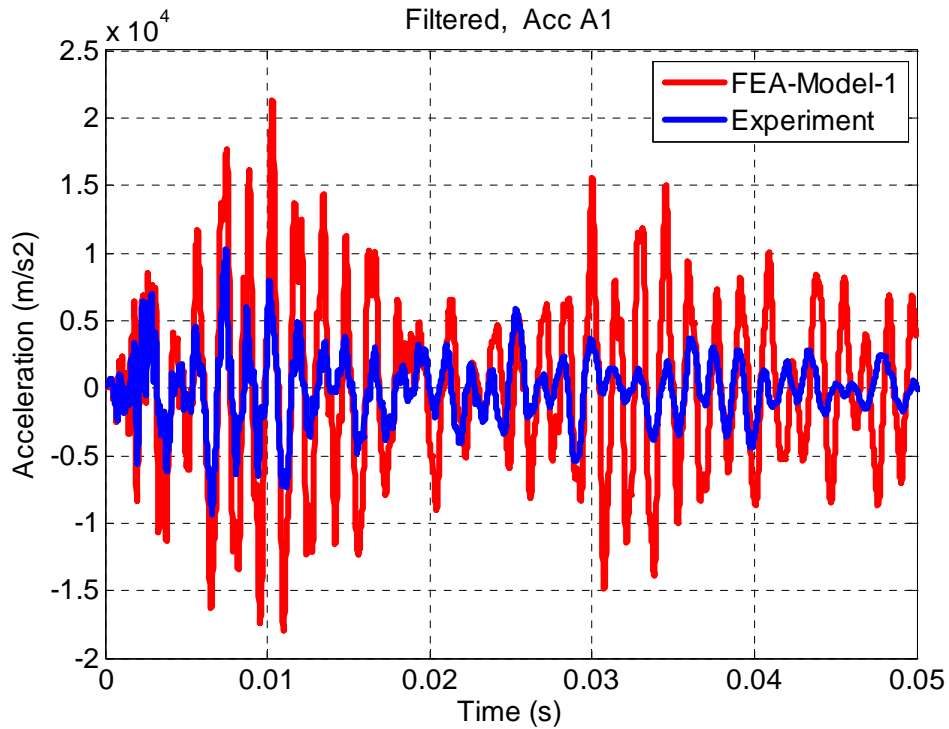


Figure 5.35 Acceleration on hat (Acc-1) and plate (Acc-2) structure for 24 m/s slug impact (medium force impact load)

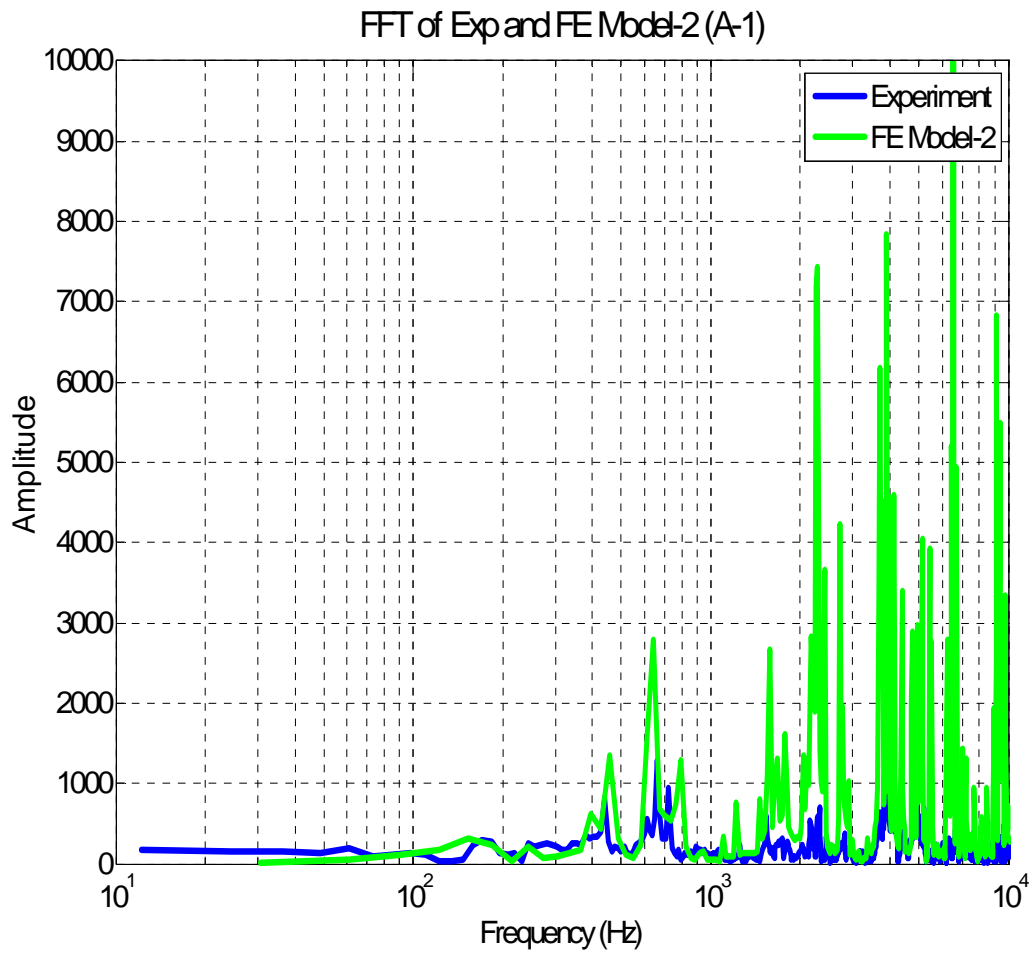


Figure 5.36 FFT of the experiment and FE model-2 for medium force impact loading

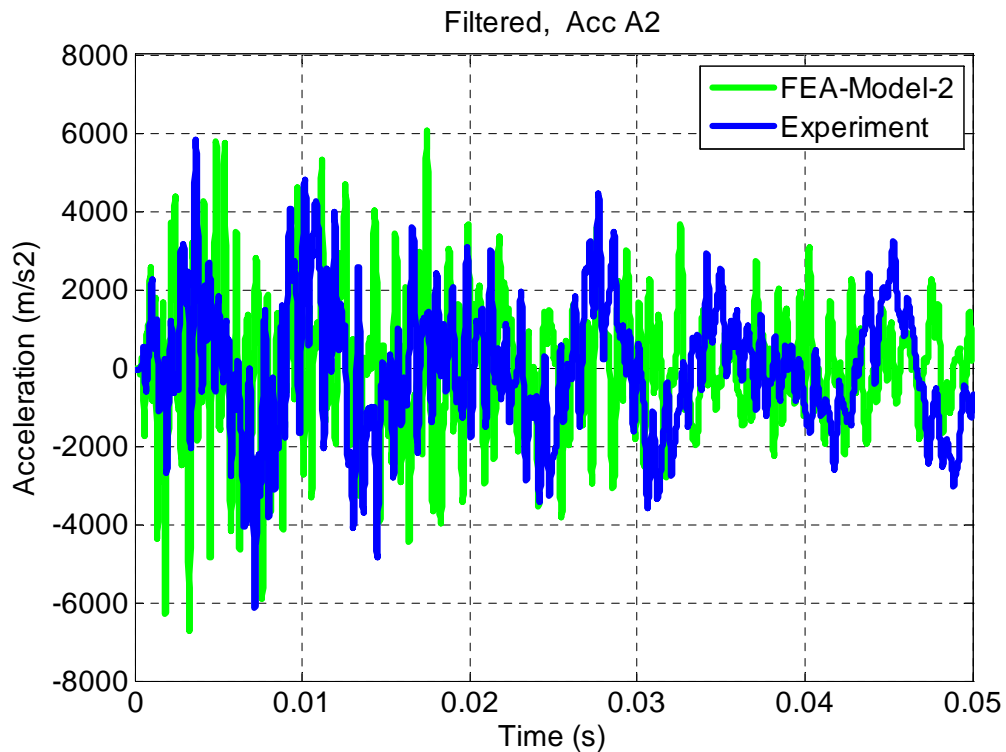
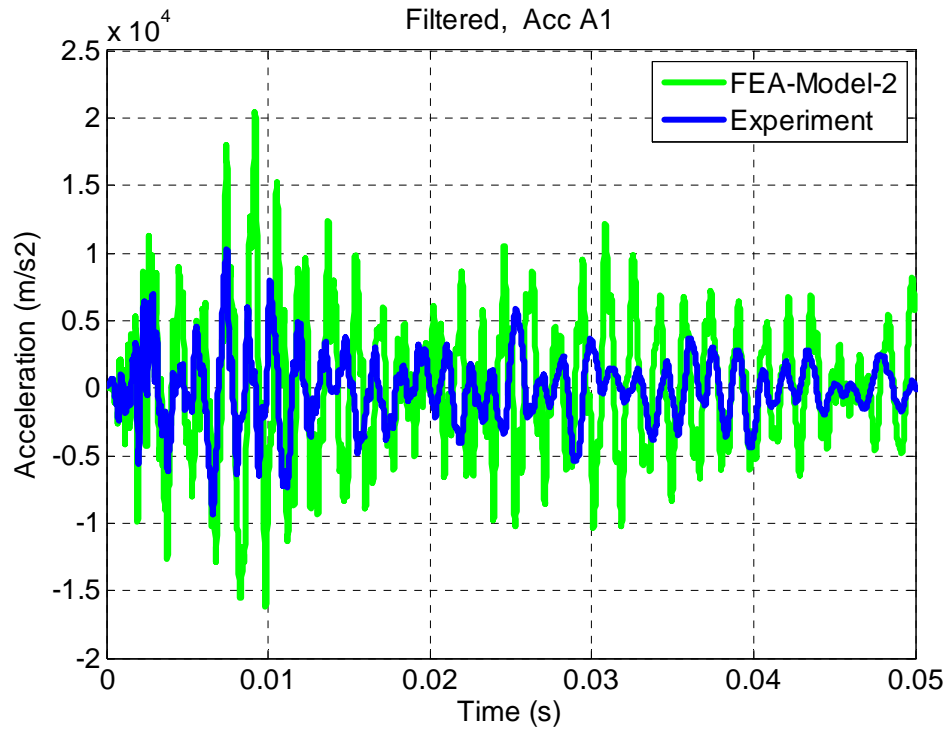


Figure 5.37 Acceleration on hat (Acc-1) and plate (Acc-2) plate structure for 24 m/s slug impact (medium force impact load)

Table 5-1 NRMSD between experiment and FE Model 1 &2

Normalized Root Mean Square Deviation between Experiment and FE results		
FE Model	Experiment	
	Acc-1 Hat Section	Acc-2 Plate Section
Model-1 (Solid Elements)	0.13	0.14
Model-2 (Shell Elements)	0.14	0.18

### 5.6.3 Response of hat-plate structure to high force impact loading

In the medium force impact loading experiment, the load cell was mounted on the hat structure and the slug was fired on the load cell, so that the impact load can be measured. This allowed verifying the impact load obtained by the FE analysis. The controlled air gun experiment was non-destructive because the impact load was small. Another batch of air gun experiments were conducted on bolted hat-plate structure without mounting load cell on the hat section. In these destructive air gun experiments, the slug was fired at velocity of 44 m/s and 68 m/s, which correspond to 0.068 MPa (10 psi) and 0.137 MPa (20 psi) air pressure in the tank. The FE analysis of these load cases indicated a peak impact force of 160 kN and 235 kN for these two impact velocities. For the slug velocity of 68 m/s, the hat section deformed significantly (plastic deformation) at the impact point. For safety reasons, the air gun tests were stopped at this slug velocity (68 m/s).

Figure 5.38 shows the experimental and FE Model-2 of the deformed bolted hat-plate structure. The FE Model-2 used in the medium force impact load air gun experiment

simulation was used in this case. The SPD factor ( $\beta$ ) of 14% (0.014) [56] was used in the FE model-2 for high force impact loading, because this analysis involves yielding (plasticity) of the hat structure. The plastic deformation predicted by the FE model-2 matches with the experimental prediction at the impact point. Figure 5.39 shows the plastic strain contours, where the maximum plastic strain is 0.152. Accelerometers were mounted on the hat-plate structure during the high impact air gun experiment. The cable on the accelerometer mounted on the plate structure, was accidentally snapped during the experiment and only the response of the hat structure was recorded. Figures 5.40 shows the impact force (peak force is 235 kN) on the hat-plate structure for the slug impacting at 68 m/s. Figures 5.41 and 5.42 show the FFT and experimental and FE Model-2 response of the hat-plate structure for the slug impacting at velocity of 68 m/s. The acceleration predicted by FE Model-2 is in good agreement with the experimental response. To quantify the response from experiment and FE model-2, the NRMSD criteria was used and is shown in the Table 5-2. The NRMSD for controlled impact analysis (elastic range) and for the high impact analysis (plastic range) is identical (0.14). Therefore the simplified FE model-2 can be used successfully to predict the high impact / shock loading on the bolted structure. This FE model also can be used in the larger army vehicle FE model with damping.

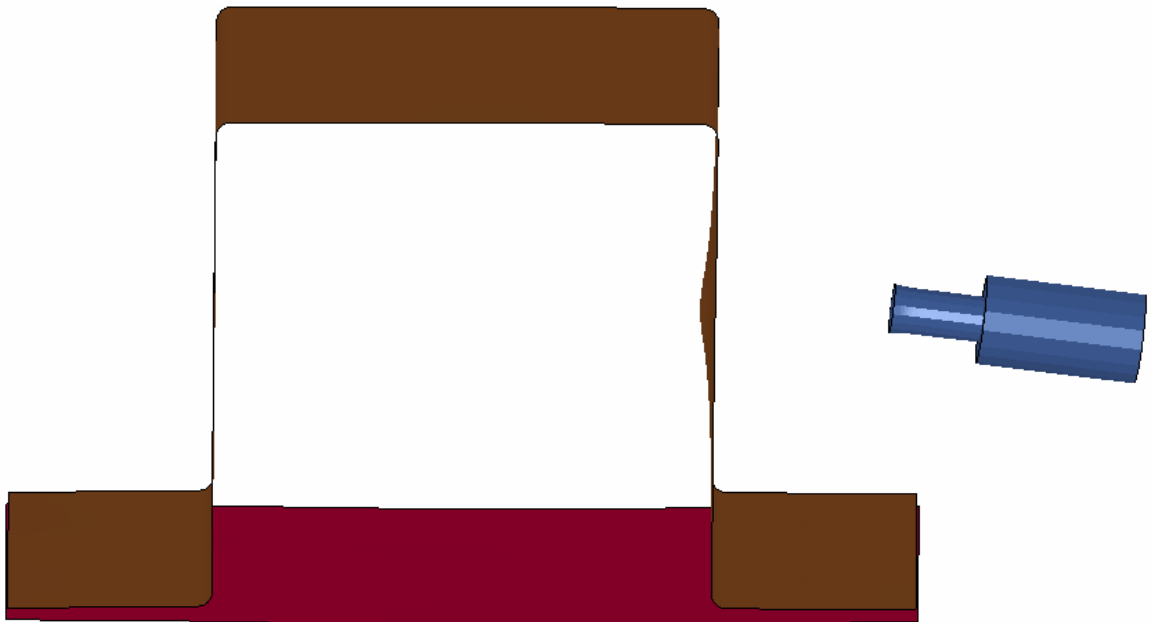
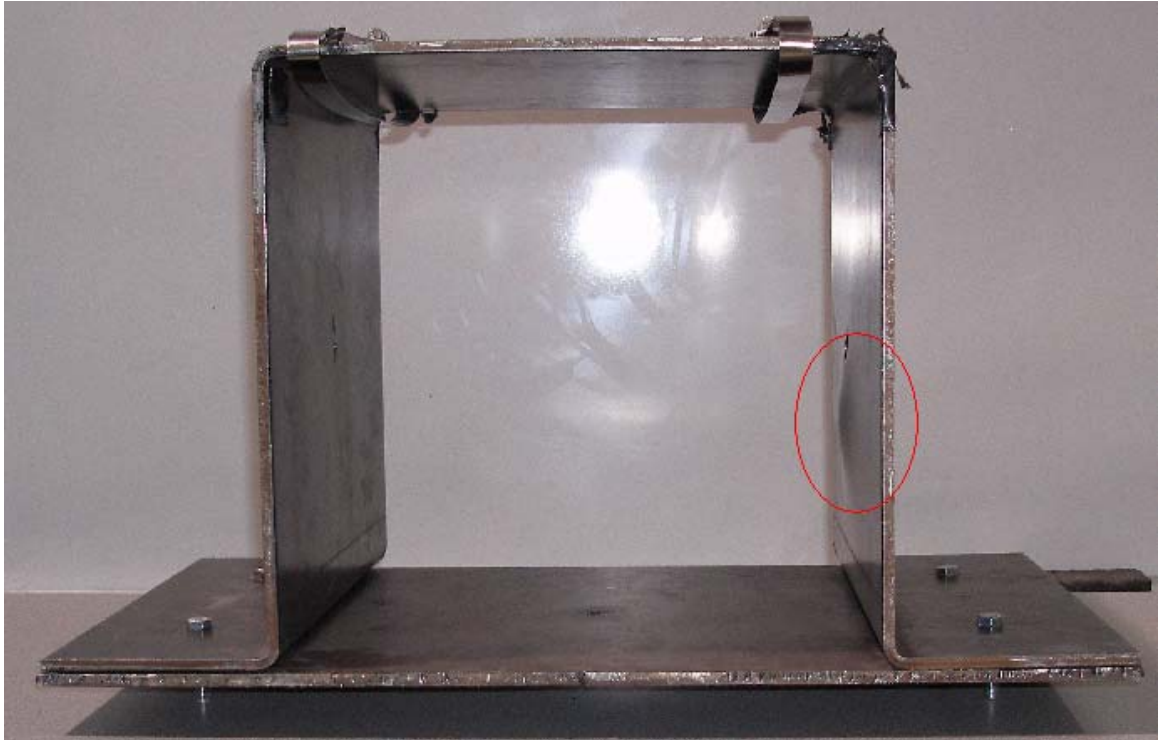


Figure 5.38 Experimental and FE model-2 showing deformed hat structure for slug impacting at velocity of 68 m/s

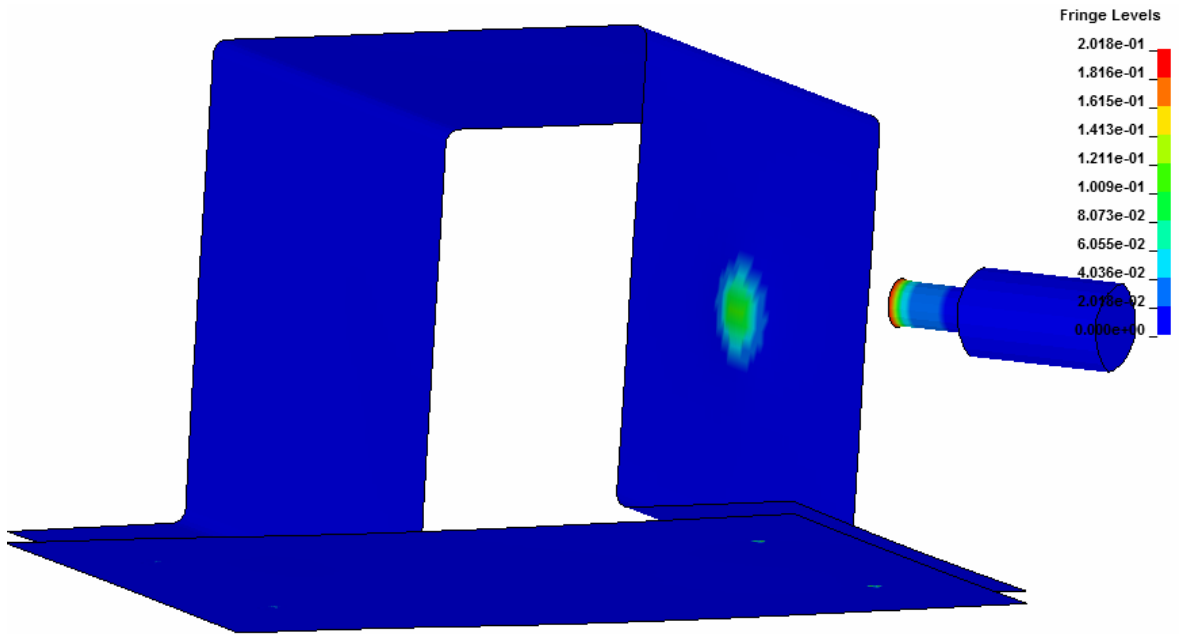


Figure 5.39 Plastic strain contours on FE model-2 for slug impacting at velocity of 68 m/s

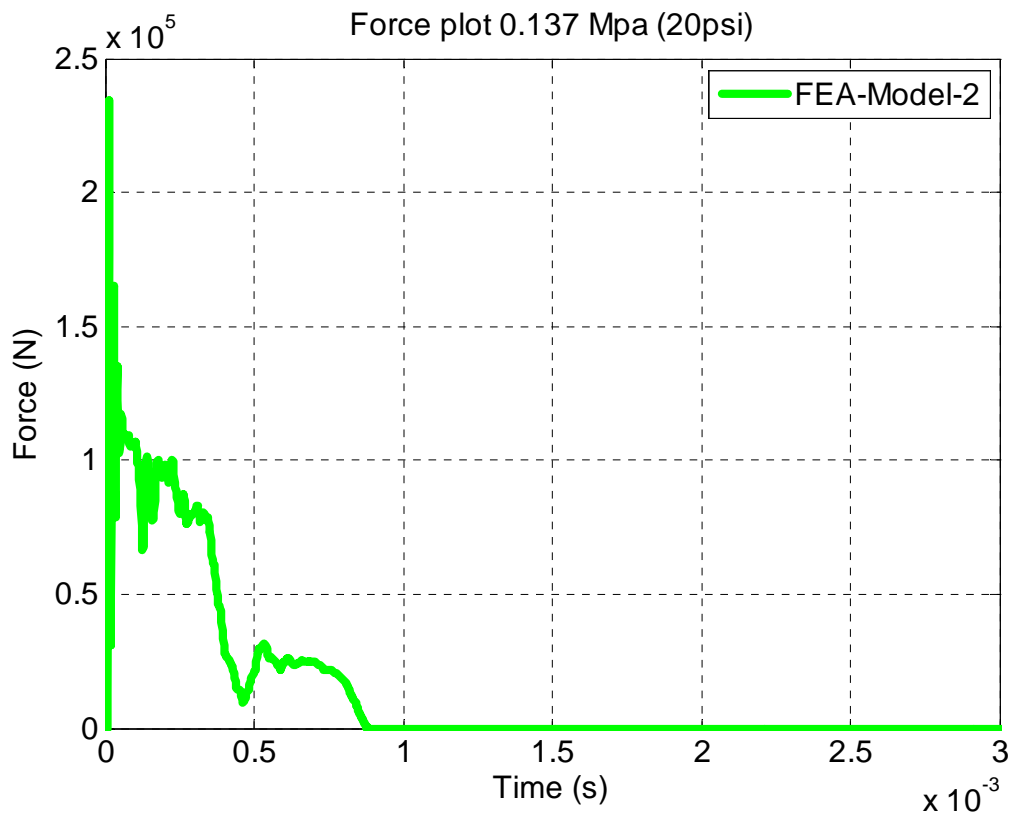


Figure 5.40 FE model-2 impact force curve for 68 m/s slug impact velocity



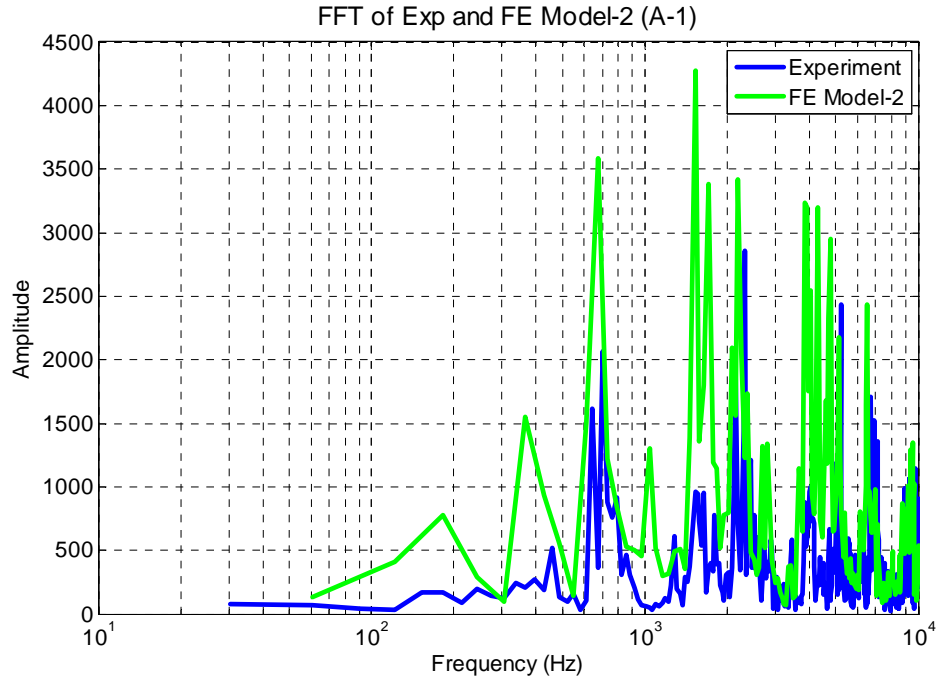


Figure 5.41 FFT from experiment and FE model-2 for slug velocity of 68 m/s

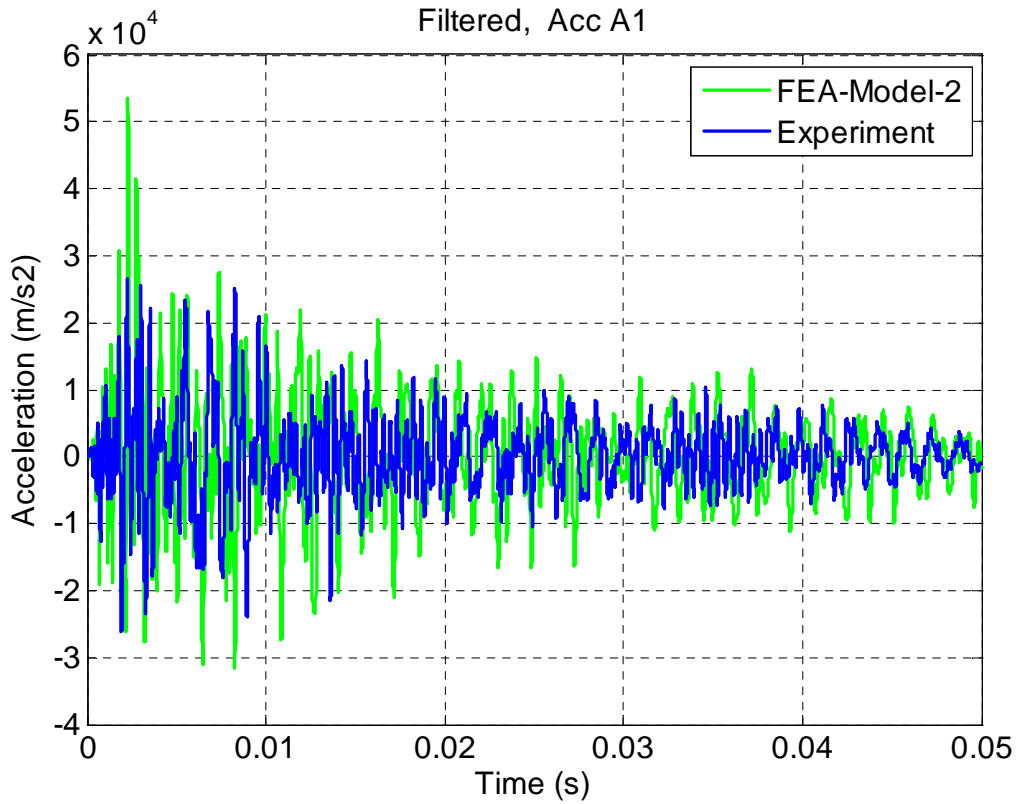


Figure 5.42 Acceleration plots on hat structure for slug impacting at 68 m/s

Table 5-2 NRMSD between Experiment and FE Model-2 for slug impacting at 68 m/s velocity

Normalized Root Mean Square Deviation between Experiment and FE results		
FE Model	Experiment 20psi	
	Acc-1 Hat Section	Acc-2 Plate Section
Model-2 (Shell Elements Damping)	0.137	NA

### 5.7 Response of bolted two-hat structure to high force impact loading: FE analysis and experiments

The previous section explains a high impact experiment on the bolted hat-plate structure using air gun and slug. The hat-plate structure was recommended by ARL for studying the shock propagation in bolted joints. A simplified FE Model-2 with shell elements was developed to simulate the high impact loading and the prediction from this model is similar to the detailed FE Model-1. The modeling technique used in FE model-2 will be tested on another complex bolted structure. This bolted structure also resembles many bolted joints in the combat vehicle is the two-hat structure shown in Figure 5.43. Doppala [9] conducted the low force impact loading study on this structure with bolted and adhesive joints. The two-hat structure is 2.65 mm thick and is approximately half the size of the hat-plate structure. Four M5 bolts were used to connect two hat structures together and the bolts were tightened using the torque wrench to 8.69 Nm pre-torque. This pre-torque induces a preload of 8.69 kN on the bolt shank, which is approximately

442 MPa pre-stress. The SPD factor ( $\beta$ ) of 14% (0.014) was used in the FE model as this simulation involves yielding (plasticity) of the hat structure.

High impact / shock loading on the bolted two-hat structure was induced using air gun and the slug as explained in the previous section. The experimental set-up is shown in Figure 5.43. Two accelerometers were mounted on the two-hat structure: one on the top hat and the other one on the bottom hat structure. The slug from the air gun barrel, striking the two-hat structure was captured using high-speed camera as shown in Figure 5.44 (4.33 ms after impact). This figure shows the slug striking the two-hat structure, and the deformed structure-accelerating forward. The experiment was conducted for slug velocity of 24 m/s and 34 m/s, which correspond to 0.034 MPa (5 psi) and 0.048 MPa (7 psi) air pressure in the tank.

The simplified FE model-2 that uses shell elements and Constrained\_Rivet\_ID card was used to simulate the impact loading on the bolted two-hat structure. The simplified model (Model-2) uses less CPU time compared to solid element FE model and can be implemented in the full vehicle FE model to represent bolted joints. Figure 5.45 shows the impact force from the FE model-2 for the slug impacting at velocity of 24 m/s and 34 m/s. The slug impact produces a peak force of 92.5 kN and 130.0 kN respectively.

Figure 5.46 (front view) and Figure 5.47 (side view) shows the deformed two-hat structure for the slug impacting at velocity of 34 m/s. The top hat structure bends at the impact point due to slug impact and this is successfully predicted by the FE model-2. Figure 5.48 - 5.50 are the comparison of the FFT and the experimental and FE response of the two-hat structure for the slug impacting at velocity of 34 m/s. The FE acceleration plots match with good accuracy to the experimental plots. NRMSD criteria were used to

compare the results between the experiment and FE analysis. The NRMSD for the top and bottom hat structures are 0.10 and 0.16 respectively. The NRMSD from the FE Model-2 for the two-hat structure is similar to the hat-plate structure. Hence the simplified FE model-2 can be successfully used to simulate the impact or shock loading on the bolted structures. The FE model-2 reduces the CPU time by one order compared to similar detailed FE Model-1 with solid elements.

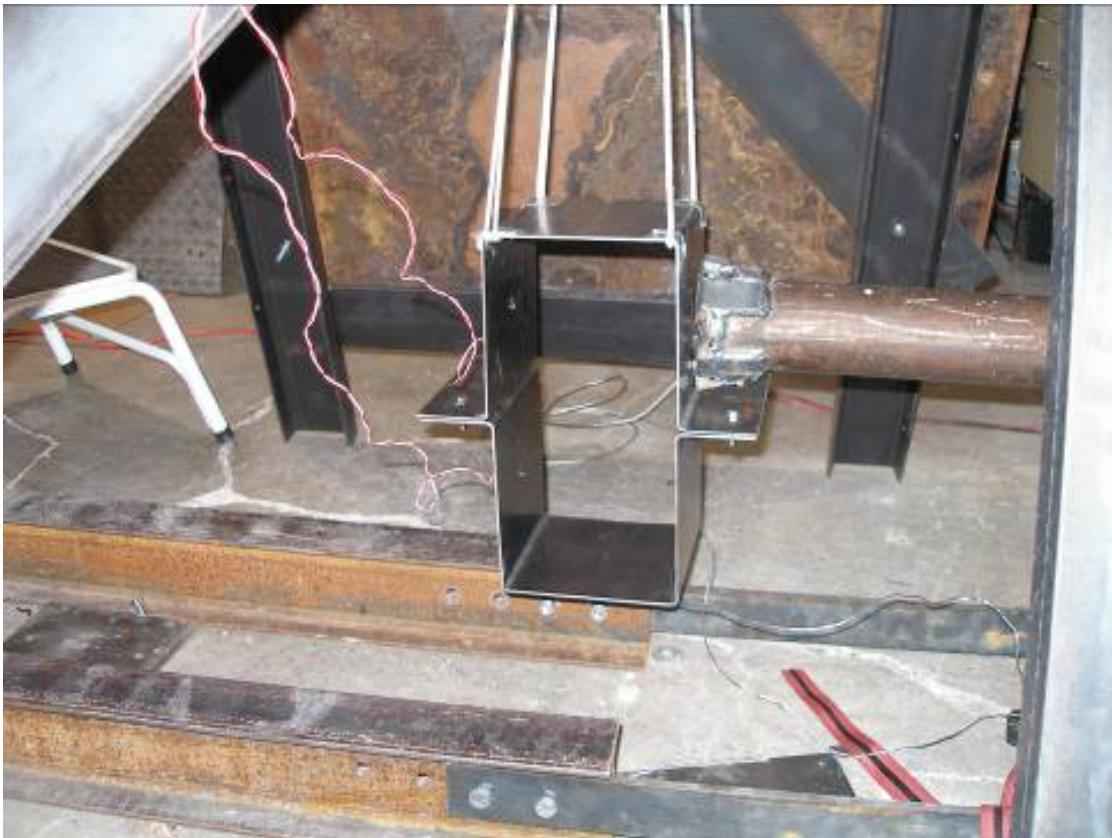


Figure 5.43 High impact loading experimental set-up for two hat structure



Figure 5.44 High speed camera image showing slug impacting the structure (4.33 ms after impact)

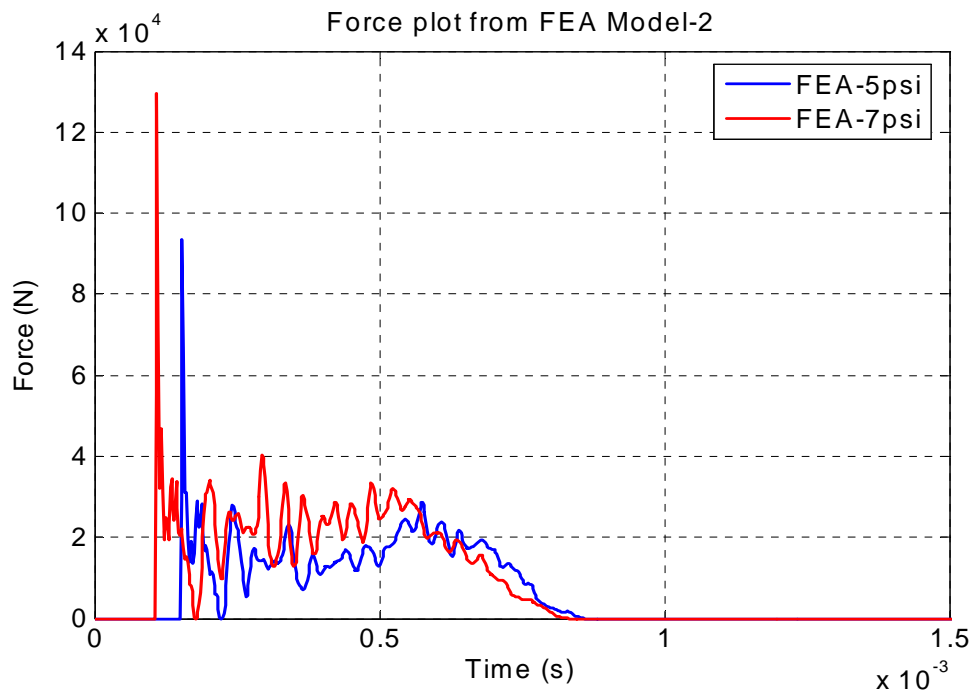


Figure 5.45 Impact force from FE Mode-2 for slug impacting at velocity of 24 and 34 m/s on two-hat structure

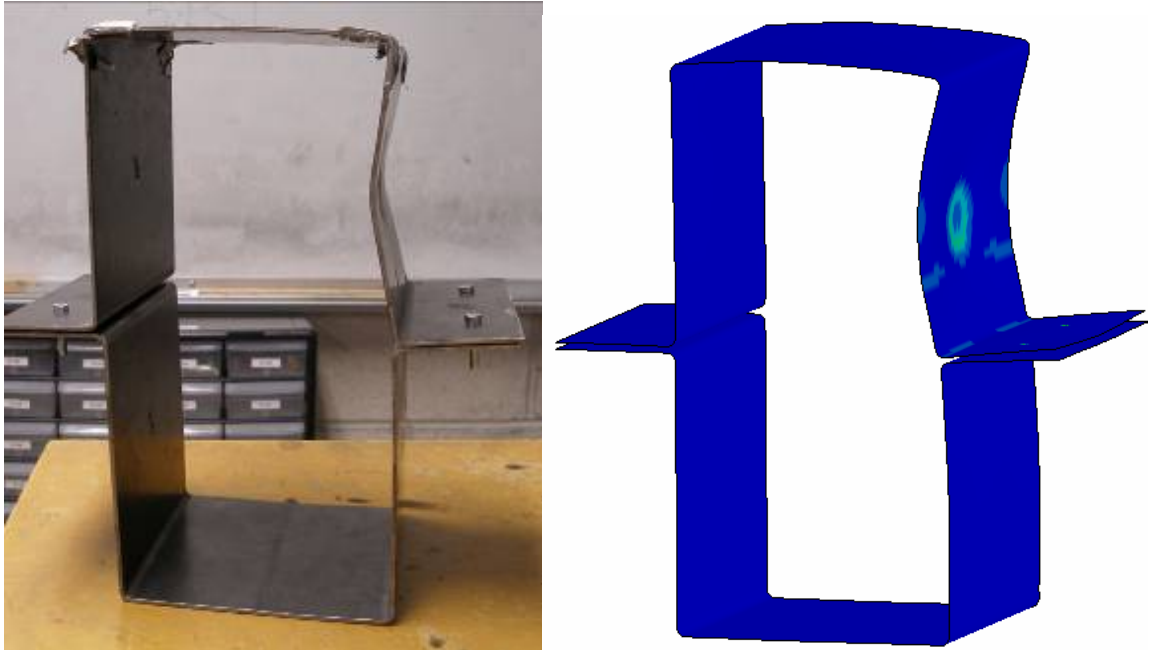


Figure 5.46 Experiment and FE Model-2 showing deformed shape of two-hat structure for slug impacting at 34 m/s (front view)

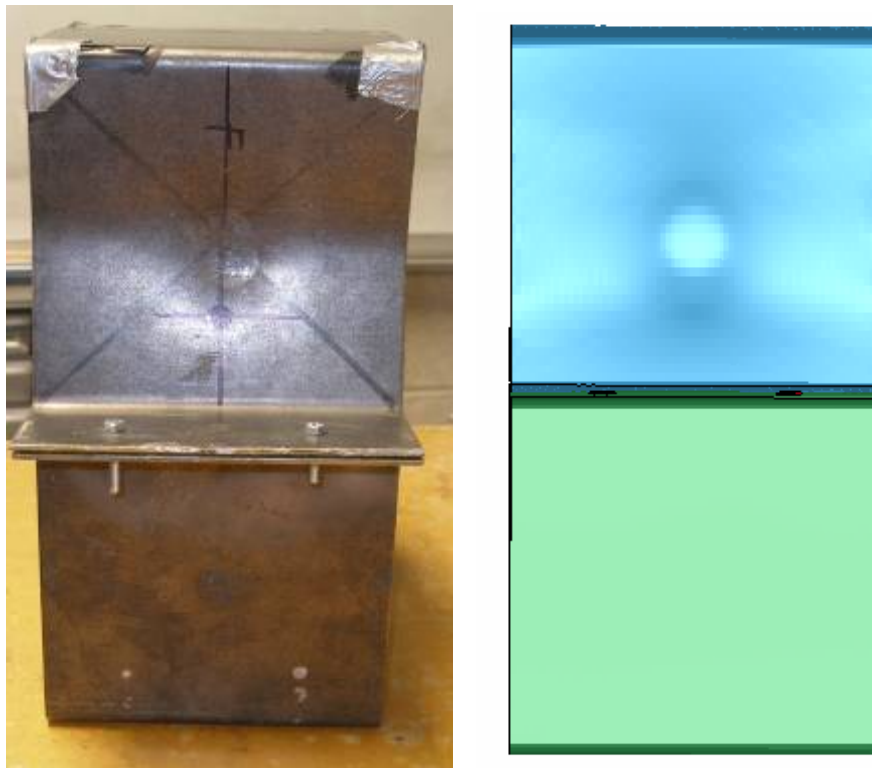


Figure 5.47 Experiment and FE Model-2 showing deformed shape of two-hat structure for slug impacting at 34 m/s (side view)

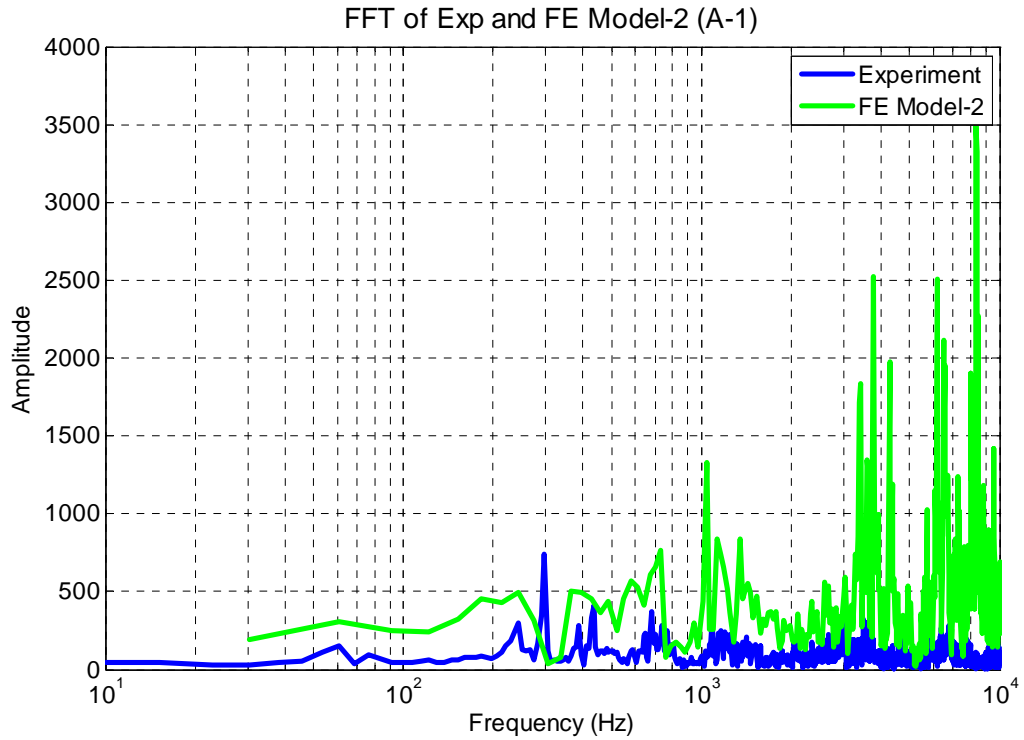


Figure 5.48 FFT from experiment and FE model-2 for slug velocity of 34 m/s

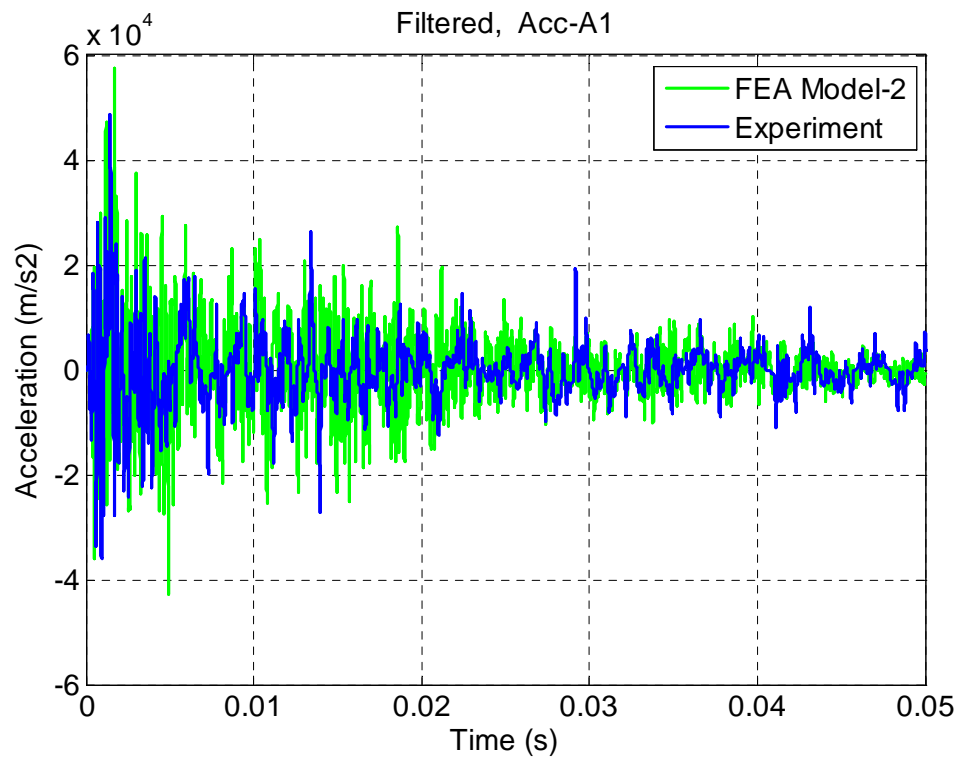


Figure 5.49 Experimental and FE Model-2 results of top hat structure for slug impacting at 34 m/s velocity

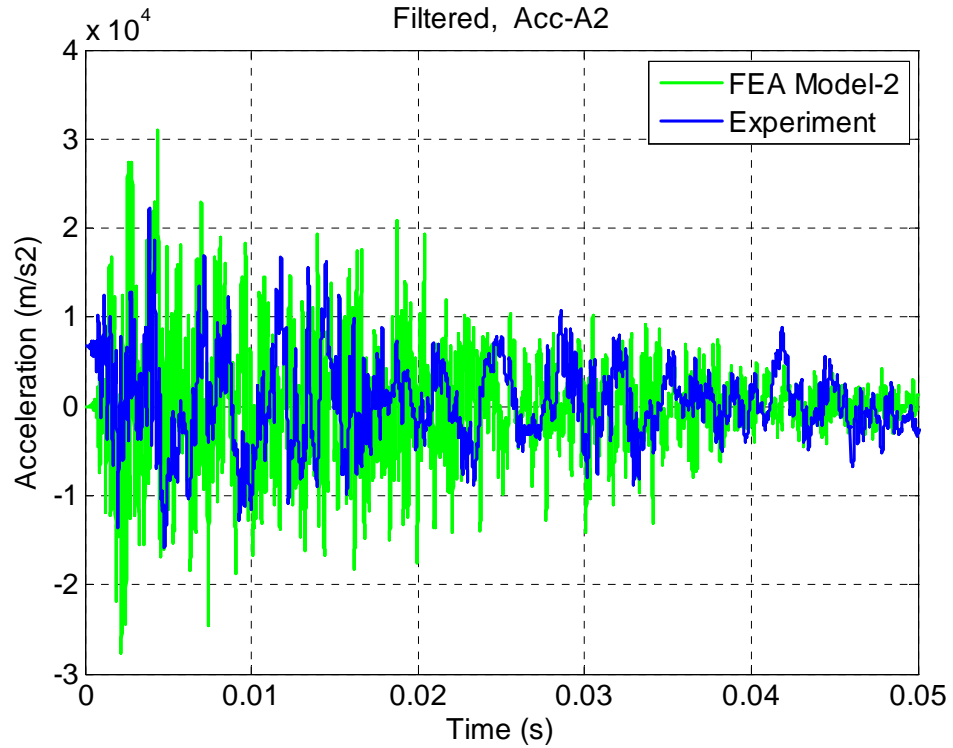


Figure 5.50 Experimental and FE Model-2 results of bottom hat structure for slug impacting at 34 m/s velocity

Table 5-3 NRMSD between the experiment and FE mode-2 for two hat structure

Normalized Root Mean Square Deviation between Experiment and FE results		
FE Model	Experiment 0.048 Mpa (7 psi)	
	Acc-1 Hat Section	Acc-2 Plate Section
Model-2 (Shell Elements SPD-0.14)	0.10	0.16



## 5.8 Summary of results

The air gun experiments were designed to study the high impact / shock loading on the bolted structures. Air gun and the slug were adequate to input high shock loading on the bolted structures and also deform the structure significantly. The catch tube designed specifically for the air gun experiment was capable of stopping the slug. Two bolted structures were tested for high impact loading and the shock propagation through bolted joints were successfully simulated using LS-DYNA FE solver. The FE Model-1 of the bolted structure was complex and used 3-D solid elements and was capable of predicting the high impact response with good accuracy. Contacts and friction were included in this FE model, which accounts for joint damping. This FE model needs significantly more CPU time as this a fully defined model. A simplified FE Model-2 was developed with shell elements and without bolts modeled explicitly on the FE model. In this FE model, the joint damping was modeled using Rayleigh stiffness proportional damping. The damping factor was calculated using half bandwidth method. An NRMSD criterion was used to quantify the FE results. The NRMSD for FE model-2 is 0.14, which is similar to the NRMSD of the detailed FE model-1. The CPU time for FE model-1 is 30 hours and for FE model-2 is less than 3.0 hours. Thus the CPU time reduced by one order when FE model-2 was used to simulate the impact analysis. Hence the simplified FE model-2 can be successfully used to simulate the impact or shock loading on the bolted structures and can be used in the larger army vehicle FE models.

## CHAPTER 6

### CONCLUSIONS AND FUTURE WORK

An extensive literature survey showed that there is little work done on the shock transmission through bolted joints. Most of the available articles on structural dynamic analysis rely on modal analysis for comparing transient responses and only a few references compare the transient response or time histories. None of the published articles investigate the transient shock transmission through bolted joint in detail for high impact loading.

A simple cantilever beam with bolted lap joint was selected to study the shock propagation in bolted joints. Then a more complex bolted hat-plate structure was selected to study the response of bolted structure to low, medium and high impact loading. Experimental and numerical analysis of an impact load on the cantilever beam with bolted lap joint is conducted to understand the dynamic characteristics. The instrumented impact hammer and accelerometer were used to excite the structure and measure the acceleration respectively. The experimental repeatability and consistency test confirmed that the response of the structure was deterministic and are not random. This enables us to simulate the experiment using commercial FE software. The low impact experiment on the cantilever beam was conducted using three pre-torques on the bolt: 21 Nm, 34 Nm and 47 Nm. The bolt preload effect on the cantilever structure confirms that the increase in bolt preload increases the natural frequency of the structure at higher mode.

Three LS-DYNA FE models were developed to simulate the transient response of the cantilever beam with bolted lap joint to impact load. These three models were FE model with shell elements (FE Model-1), solid element model with no preload (FE Model-2)

and solid FE model with preload and contacts (FE Model-3). All the three FE models predicted higher magnitude response compared to experimental results. The FE model-3 with all the details predicted high frequency and magnitude response. Two parameters, which affect the simulation results, are identified and their effects are studied. These parameters are damping, and element formulation. The LS-DYNA FE model uses Rayleigh damping, which includes mass and stiffness proportional damping. Mass proportional damping can damp rigid body and low frequencies response, and stiffness proportional damping damps high frequency response. The predictions from under-integration and fully integration element formulation very almost identical, but the fully integrated element formulation needs more CPU time.

All six preload modeling techniques explained in this report can be used for implicit and explicit FE analysis. But the thermal, initial stress solid and initial stress cross-section methods are suitable for non-linear dynamic problems especially for geometrically non-linear problems. These methods are simple and easy to model.

Stiffness proportional damping factor was calculated using half-power bandwidth method and for the elastic analysis the damping factor is 6.5% (0.065). This value is within the range (5-7%) prescribed by Newmark [56]. For plastic analysis the damping factor is 10-15% [56]. An NRMSD criterion was used to calculate the deviation of FE results from the experimental values. Addition of damping in the cantilever beam FE model-1 and FE model-2 decreased the NRMSD by 50%.

Bolted hat-plate structure is a complex joint section found in army vehicles and was used to study the shock propagation in bolted joints. This structure was subjected to the low impact loading and the response of the structure was measured. The acceleration was

measured at two points – one on hat section and one on plate section. The impact experiment was simulated using LS-DYNA explicit analysis and the response from experiment and FE were compared. The damping factor of 6.5 was used in this FE model. There is a fairly good match between the experiment and analysis on the hat section acceleration. The experience gained in studying the bolted structures subjected to low impact loading was used in high impact or shock loading on bolted structures.

Air gun at the UNLV CMEST was modified, to induce high shock loading on the bolted structures. The air gun fires an aluminum slug on the freely hanging bolted structures. Bolted hat-plate and two hat structures were used in the high impact loading experiments. The velocity of the slug fired from the air gun was calibrated using high-speed camera. LS-DYNA solver was successfully used to simulate the high impact loading on the bolted structures. A detailed FE Model-1 of bolted structures with 3-D solid elements with all the details was used to simulate the transient analysis. Another simplified FE Model-2 with shell elements and without any complexity was successfully developed and used in the transient analysis. The NRMSD for FE model-2 is 0.14, which is similar to the detailed FE model-1. The CPU time for FE model-1 is 30 hours and for FE model-2 is less than 3.0 hours. Thus the CPU time reduced by one order when FE model-2 was used to simulate the impact analysis. Hence the simplified FE model-2 can be successfully used to simulate the impact or shock loading on the bolted structures and can be used in the larger army vehicle FE models.

## Future work

- The future work in this project includes testing the simplified FE model in the actual FE model of the army vehicle.
- Another important aspect in the impact experiment is the measurement of strain. In the future impact experiments, the strain can be measured using strain gauges and this strain can be compared with the strain predicted from the FE analysis.
- Because for the safety reason, the slug from the Air gun experiment was fired up to velocity of 68 m/s. The velocity of the slug can be increased by increasing the air pressure in the tank. This will allow using bigger bolted structures.
- The study of impact loading can be extended to other kinds of joints in the vehicle such as welded joints and bonded joints.
- All the bolted structures used in this project are steel. The study of impact analysis can also be extended to bolted composite structures. Nowadays, the composite structures replace a lot of steel structures in the army vehicle.

## APPENDIX-A

Mat-Lab code for calculating the slug velocity in the air gun experiment.

```

% Kumar Karpanan PhD Disseratation
clc;
clear;
%This program calculates the velocity of the slug from the airgun
%The velocity of the slug is a function of mass of slug, pressure
%in the tank and length of the barrel
%Friction between the slug and barrel are included
%SI Units: Kg, m, s, N

%Slug shape
%-----\
%          -----
%   A1          A2      !
%          -----
%-----/
%-----
PR=20*6894.75; %Pressure in the tank 5,10,,psi |
%-----

VT=7900*1.6e-5; %Volume of the Tank 7900 in^3
RHO=2700; %Density of Aluminum
LB=20*0.3048; %Length of the Barrel 20 feet
AB=3.1416*(2*25.4*1e-3)^2/4; %Area of the barrel (Dia=2in)

NI=100; % Number of iteration
D1=50.76*1e-3; D2=27.4*1e-3; % diameter of slug
L1=95.1*1e-3; L2=55.7*1e-3; % Length of slug
A1=3.1416*D1^2/4; A2=3.1416*D2^2/4 ; %Area of slug
V1=A1*L1; V2=A2*L2; V12=V1+V2; % Volume of slug
MS=RHO*V12; %Total Mass of the slug

x_inc=LB/NI; % Increments
x(1,:)=0;
veloc(1,:)=0; % Initial Velocity
timel(1,:)=0;
p(1,:)=PR;
for i=1:NI
%sections the barrel into incremental distances
x(i+1,:)=(x_inc)+x(i,:);
%calculates the incremental change in volume due to the slug traveling
down the barrel
v(i+1,:)=VT+(AB*x(i+1,:));
%calculates the incremental change in pressure using Boyle's Law (P1V1
= P2V2)
p(i+1,:)=(PR*VT)/v(i+1,:);
%Calculates incremental acceleration From Newton's Second Law acc
a=F/m=p.A/m
a(i+1,:)=((p(i+1,))*A1)/MS; % No Friction
% With friction force added F=uN u=0.15 to 0.6 N=weight of slug=60 N
%a(i+1,:)=((p(i+1,))*A1)-(0.6*60))/MS;

%Calculates incremental velocities with v2=u2+2as

```

```

veloc(i+1,:)=(veloc(i,:)^2+2*a(i+1,:)*x_inc)^0.5;

%Calculates incremental time v=u+at
time(i+1,:)=(veloc(i+1,:)-veloc(i,:))/(a(i+1,:));%time per step
time1(i+1,:)=time1(i,:)+ time(i+1,:);%total time

end
% figure('position',[50 100 600 500],'Color',[1 1 1]);
% plot (time1,p,'b-','linewidth',2);
% xlabel('Time (s)','fontsize',14);
% ylabel('Pressure (MPa)','fontsize',14);
% grid on;
% title('Pressure drop in the tank','fontsize',16);
% ylim([0 7e4]);
%
% figure('position',[150 200 600 500],'Color',[1 1 1]);
% plot (time1,veloc,'r-','linewidth',2);
% xlabel('Time (s)','fontsize',14);
% ylabel('Velocity (m/s)','fontsize',14);
% grid on;
% title('Velocity of slug wrt time','fontsize',16);
% %xlim([10 100000]);

%plot (time1,p)
Pressure_in_the_tank_Psi = PR/6894.75
Mass_of_the_slug_Kg = MS
Final_Velocity_of_Slug_mps=max(veloc)

```

## REFERENCES

1. Livermore Software Technology Co, "LS-DYNA Keyword User's Manual," 9.70, Livermore: Livermore Software Technology Co, 2003.
2. J.O. Hallquist, Livermore Software Technology Co, "LS-DYNA Theoretical Manual", Livermore Software Technology Co, May 1998.
3. Aaron Das Gupta, Joseph. M. Santiago and Henry. L. Wisniewski, "Shock Damage to Sensitive Components in an Armored Vehicle", Computers in Engineering- Volume- 2, ASME 1982.
4. R.A. Ibrahim, C.L. Pettit, "Uncertainties and Dynamic Problems of Bolted Joints and other Fasteners", Journal of Sound and Vibration 279 (2005) 857-936.
5. Mohammed R. Bahaari and Archibald N. Sherbourne, " Structural Behavior of End-Plate Bolted Connections to Stiffened Columns", Journal of Structural Engineering, Vol 122, No. 8 August 1996.
6. S H Ju, C.Y. Fan and G.H. Wu, "Three-Dimensional Finite Elements of Steel Bolted Connection", Engineering Structures, 26 (2004) 403-413.
7. Y.I. Maggi, R.M. Goncalves, R.T. Leon and L.F.L. Ribeiro, "Parametric Analysis of Steel Bolted End Plate Connections Using Finite Element Modeling", Journal of Constructional Steel Research, 61 (2005) 689-708.
8. Patton Mallory, M. Smith, and Pellicane P. J., " Modeling Bolted Connections in Wood: A Three Dimensional Finite Element Approach", Journal of Testing and Evaluation, Vol 26, No. 2, March 1998, pp115-124.



9. Karthik Doppala, "Experimental and Finite Element Studies of Shock Transmission Through Jointed Hat Sections", M.S. Thesis, University of Nevada, Las Vegas, United States, 2005.
10. Masoud Fegghi, "Experimental and Finite Element Studies of Shock Transmission Through Bolted Joints", PhD. Dissertation, University of Nevada, Las Vegas, United States, 2007.
11. Steffen Mattern, Karl Schweizerhof, "Wave Propagation in Automotive Structures Induced by Impact Events", Universitat Karlsruhe, Institut fur Mechanik.
12. W. H. Semke, G. D. Bibel, S. Jerath, S. B. Gurav, and A. L. Webster, "Efficient Dynamic Structural Response Modeling of a Bolted Flange Piping Systems", International Journal of Pressure Vessels and Piping, Vol 83, 2006, pp 767-776.
13. Young Doo Kwon, Hyun Wook Kwon, Ji-Hoon Hwangbo and Suck Ho Jang, "Finite Element Modeling for Static and Dynamic Analysis of Structures with Bolted Joint", Key Engineering Materials, Vol 306-308 (2006) pp 547-552.
14. John D. Pratt and Gerard Pardoen, "Comparative Behavior of Single and Dual Bolted Lap Joints", Journal of Aerospace Engineering, Vol.15, No 2, April 2002.
15. A. Eskandarian, D. Marzougui, and N. E. Bedewi, "Impact Finite-Element Analysis of Slip-Base Sign Support Mechanism", Journal of Transportation Engineering, vol. 126, pp. 143-153, 2000.
16. J. D. Reid and N. R. Hiser, "Detailed Modeling of Bolted Joints With Slippage", Finite Elements in Analysis and Design, vol. 41, pp. 547-562, 2005.

17. Jeong Kim, Joo-Cheol Yoon, Beom-Soo Kang, "Finite Element Analysis and Modeling of Structure with Bolted Joints", *Applied Mathematical Modeling* Vol-31, 2007, pp 895–911.
18. Richard B. Englund, David H. Johnson and Shannon K. Sweeney, "Mechanical Engineering Design Education: Issues and Case Studies, DE-Vol.102, ASME 1999.
19. L. Gaul and J. Lenz, "Nonlinear Dynamics Of Structures Assembled By Bolted Joints", *Acta Mechanica*, vol. 125, pp. 169-181, 1997.
20. Danny L. Gregory, David O. Smallwood, Ronald G. Coleman and Michael A. Nusser, "Experimental Studies to Investigate Damping in Frictional Shear Joints", Sandia National Laboratories, Albuquerque.
21. Jaime Esteban and Craig A. Rogers, "Energy Dissipation Through Joints: Theory and Experiments", *Computers and Structures*, Vol. 75, 2000, pp 347-359.
22. H. R. Kess, N. J. Rosnow, and B. C. Sidle, "Effects Of Bearing Surfaces on Lap Joint Energy Dissipation", *Proceedings of Proceedings of International Modal Analysis Conference (IMAC)-XX*, Los Angeles, CA, United States, pp. 603-610, 2002.
23. D. W. Lobitz, D. L. Gregory, and D. O. Smallwood, "Comparison of Finite Element Predictions to Measurements from the Sandia Microslip Experiment", *Proceedings of International Modal Analysis Conference (IMAC)-XIX*, Kissimmee, FL, United States, vol. 2, pp. 1388-1394, 2001.
24. Henrik Wentzel, "Modeling of Frictional Joints in Dynamically Loaded Structures- A Review", Dept of Solid Mechanics, Royal Institute of Technology (KTH) Sweden.
25. L. Gaul and R. Nitsche, "The Role of Friction on Mechanical Joints," *Applied Mechanics Reviews*, vol. 54, pp. 93-106, 2001.

26. Henrik Wentzel and Marten Olsson, "Mechanisms of Dissipation in Frictional Joints- Influence of Sharp Contact Edges and Plastic Deformation", *Wear* (2008), doi:10.1016/j.wear.2008.04.026.
27. Clarence W. de Silva, "Vibration Fundamentals and Practice," CRC Press.
28. Paul Jacob and Lee Goulding, "An Explicit Finite Element Primer," NAFEMS.
29. D. J. Segalman, "Modeling Joint Friction in Structural Dynamics", *Structural Control and Health Monitoring*, Vol. 13, 2006, pp430-453.
30. Liu Man and J. M. Wilson, "On the Damping Ratio of Multi-Degree-of-Freedom Systems", *Communications in Applied Numerical Methods*, Vol. 8, 265-271, 1992.
31. T. A. Duffey, B. B. Lewis, and S. M. Bowers, "Bolt Preload Selection for Pulse-Loaded Vessel Closures", *Proceedings of the Joint ASME/JSME Pressure Vessels and Piping Conference*, Honolulu, HI, United States, vol. 301, pp. 167-174, 1995.
32. E. Esmailzadeh, M. Chorashi, and A. R. Ohadi, "Analysis of Preloaded Bolted Joints Under Exponentially Decaying Pressure", *Journal of Pressure Vessel Technology*, *Transactions of the ASME*, vol. 118, pp. 393-398, 1996.
33. E. Kerekes, B. Szabo, and B. Unger, "Prestressed Bolt Joints Under Dynamical Load", Presented at 6th Mini Conference on Vehicle System Dynamics, Identification and Anomalies (VSDIA'98), Budapest, Hungary, pp. 545-555, 1998.
34. K. Schiffner and C. Droste, "Simulation of Prestressed Screw Joints in Complex Structures", *Computers and Structures*, Vol.64, No. 5/6, 995-1003, 1997.
35. Sae U. Park, Madhu R. Koka, Kevin R. Thomson and Jeffery L. Robbins, "A FE Modeling and Validation of Vehicle Rubber Mount Preloading and Impact Response", 8<sup>th</sup> International LS-DYNA Users Conference, Crash/Safety, pp 5-23.

36. B. O'Toole, K. Karpanan, and M. Feghhi, "Experimental and Finite Element Analysis of Preloaded Bolted Joints Under Impact Loading", Presented at 47th AIAA/ASME/ASCE/AHS/ASC Structures, Structural Dynamics, and Materials Conference, Newport, RI, United States, vol. 3, pp. 2024-2032, 2006.
37. D. Szwedowicz, E. Martinez, J. Bedolla, and J. M. Rodriguez, "Experimental and Numerical Free Vibration Analysis of Bolted Connections with Respect to Mechanical Clearances", ASME Design Engineering Technical Conference and Computers and Information in Engineering Conference, Chicago, IL, United States, vol. 3, pp. 991-998, 2003.
38. Z. Tao, R. J. Zhao, and G. Q. Yao, "Analysis and Study on the Static and Dynamic Behaviors of Jointed Parts", Proceedings of the Twenty-fifth International Machine Tool Design and Research Conference, Birmingham, England, pp. 363-367, 1985.
39. Ala Tabiei and Martin Lambrecht, "Structural Analysis in the Frequency Domain and Understanding Impact Data", Short Course given by Ala Tabiei.
40. D. F. Pilkey, G. Park, and D. J. Inman, "Damping Matrix Identification and Experimental Verification", Proceedings of SPIE on Passive Damping and Isolation - The International Society for Optical Engineering, vol. 3672, pp. 350-357, 1999.
41. W. H. Semke, G. D. Bibel, S. Jerath, S. B. Gurav, and A. L. Webster, "A Dynamic Investigation of Piping Systems with a Bolted Flange", Presented at Design and Analysis of Piping, Vessels and Components (2002 ASME Pressure Vessels and Piping Conference), Vancouver, BC, Canada, vol. 440, pp. 121-128, 2002.

42. T. Sabuwala, D. Linzell, and T. Krauthammer, "Finite Element Analysis of Steel Beam to Column Connections Subjected to Blast Loads", *International Journal of Impact Engineering*, vol. 31, pp. 861-876, 2005.
43. X. Ma, L. Bergman and A. Vakakis, "Identification of Bolted Joints Through Laser Vibrometry," *Journal of Sound and Vibration* Vol. 246(3), pp 441-460, 2001.
44. A. Tabiei and J. Wu, "Validated Crash Simulation of the Most Common Guardrail System in the USA", *International Journal of Crashworthiness*, vol. 5, pp. 153-168, 2000.
45. J. D. Reid, "New Breakaway Mailbox Designed Using Nonlinear Finite Element Analysis", *Finite Elements in Analysis and Design*, vol. 32, pp. 37-49, 1999.
46. Matthew Oldfield, Huajiang Ouyang and John E. Mottershead, "Simplified Models of Bolted Joints Under Harmonic Loading," *Computers and Structures*, Vol. 84, pp 25-33, 2005.
47. H. Ouyang, M. J. Oldfield and J. E. Mottershead, "Experimental and Theoretical Studies of a Bolted Joint Excited by a Torsional Dynamic Load," *International Journal of Mechanical Sciences*, Vol. 48, pp 1447-1455.
48. C. J. Hartwigsen, Y. Song, D. M. McFarland, L. A. Bergman and A. F. Vakakis, "Experimental Study of Non-Linear Effects in a Typical Shear Lap joint Configuration," *Journal of Sound and Vibration*, Vol. 277, pp 327-351, 2004.
49. Y. Song, C.J. Hartwigsen, D.M. McFarland, A.F. Vakakis, L.A. Bergman, "Simulation of Dynamics of Beam Structures with Bolted Joints Using Adjusted Iwan Beam Elements", *Journal of Sound and Vibration* 273 (2004) 249–276.

50. M.A. McCarthy, C.T. McCarthy, V.P. Lawlor and W.F. Stanley, "Three Dimensional Finite Element Analysis of Single-Bolt, Single-Lap Composite Bolted Joints: Part 1- Model Development and Validation", *Composite Structures*, Vol. 71, pp-140-158, 2005.
51. Richard Figliola and Donald Bearley, "Theory and Design for Mechanical Measurements", 4<sup>th</sup> Edition.
52. Bendat & Piersol, "Random Data Analysis and Measurement Procedures", 3rd Edition, Wiley, 2000.
53. Robert C. Juvinall and Kurt M. Marshek, "Fundamentals of Machine Component Design", Third edition, John Wiley and sons, Inc.
54. American Society of Materials, "Engineering Properties of Steel", 7<sup>th</sup> Edition.
55. C.F. Beards, "The Damping of Structural Vibration by Controlled interfacial Slip in Joints", *Journal of Vibration, Acoustics, Stress and Reliability in Design* 105, pp-369-372, 1983.
56. Newmark N.M. and Hall W.J., "Earthquake Spectra and Design", Earthquake Engineering Research Institute, 1982.
57. De Groot, Morris H., "Probability and Statistics", 2<sup>nd</sup> edition, Addison-Wesley, 1980.
58. Ray W. Clough and Joseph Penzien, "Dynamics of Structures", Third Edition, Computers and Structures, Inc.
59. Robert D. Cook, David S. Malkus, Michael E. Plesha, and Robert J. Witt, "Concepts and Applications of Finite Element Analysis", Fourth Edition.
60. Lazan, B. J. "Damping of Materials and Members in Structural Mechanics", Pergamon, Oxford, U.K, 1968.

61. E. A. Avallone and T. Baumeister, "Marks Standard Handbook for Mechanical Engineers, 10th ed, McGraw-Hill Professional, 1996.
62. Christopher Ransel, "Seat Shock Test Stand Development", M.S. Thesis, University of Nevada, Las Vegas, United States, 2005.
63. Levine, Ira. N. "Physical Chemistry", McGraw-Hill Publishing, 1978.
64. Get Data Graph Digitizer, <http://www.getdata.com.ru/>

## VITA

Graduate College  
University of Nevada, Las Vegas

Kumarswamy, Karpanan Nakalswamy

### Degrees:

Bachelor of Science in Mechanical Engineering, 2001  
Kuvempu University  
Karnataka, India.

Master of Science in Mechanical Engineering, 2005  
University of Nevada, Las Vegas  
Las Vegas, Nevada.

### Special Honors and Awards:

- Phi Kappa Phi, Fall 2007.
- Tau Beta Pi, Fall 2004.

### Publications:

#### Journal Articles:

- B. O'Toole, M. Trabia, J. Thota, T. Wilcox, K. Kumar, "Structural response of blast loaded composite containment vessels", SAMPE Journal, Volume 42, No. 4, July/August 2006

#### Selected Conference Presentations:

- O'Toole, Kumar K, M Fegghi, "Experimental and finite element analysis of preloaded bolted joints under impact loading" 47<sup>th</sup> AIAA/ASME/ASCE/AHS/ASC Structures, Structural Dynamics and Materials Conference, 1-4 May 2006, Newport, Rhode Island.
- B. O'Toole, M. Trabia, J. Thota, T. Wilcox, K. Kumar, "Structural response of blast loaded composite containment vessels", International SAMPE Symposium and Exhibition,
- K Karpanan, B O'Toole, Sachiko Sueki, M Fegghi, S Ladkany, "Simulation and Measurement of Shock Transmission Across Bolted Joints", Proceedings of the 78th Shock and Vibration Symposium Nov. 4-8, 2007, Philadelphia, PA.
- Sachiko Sueki, S Ladkany, K Karpanan, B O'Toole, "Material Wave Speed Mismatch for High-G Acceleration Mismatch", Proceedings of the 78th Shock and Vibration Symposium Nov. 4-8, 2007, Philadelphia, PA.

Dissertation Title: "Experimental and Numerical Analysis of Structures with Bolted Joints Subjected to Impact Load Fracture".



Dissertation Examination Committee:

Chairperson, Brendan O'Toole, Ph.D.

Committee Member, Woosoon Yim, Ph.D.

Committee Member, Mohamed Trabia, Ph. D.

Committee Member, Daniel Cook, Ph. D.

Graduate Faculty Representative, Samman Ladkany, Ph.D.